



This work is protected by copyright and other intellectual property rights and duplication or sale of all or part is not permitted, except that material may be duplicated by you for research, private study, criticism/review or educational purposes. Electronic or print copies are for your own personal, non-commercial use and shall not be passed to any other individual. No quotation may be published without proper acknowledgement. For any other use, or to quote extensively from the work, permission must be obtained from the copyright holder/s.



Keele
University

This work is protected by copyright and other intellectual property rights and duplication or sale of all or part is not permitted, except that material may be duplicated by you for research, private study, criticism/review or educational purposes. Electronic or print copies are for your own personal, non-commercial use and shall not be passed to any other individual. No quotation may be published without proper acknowledgement. For any other use, or to quote extensively from the work, permission must be obtained from the copyright holder/s.



**Hydroxypropylmethacrylamide based
thermoreponsive magnetomicelles for
controllable drug delivery in pancreatic
cancer**

Ali Taha Yassen Alsuraifi

**A thesis submitted in partial fulfilment of the requirements of
Keele University for the degree of Doctor of Philosophy at the
School of Pharmacy**

December 2018

Abstract

Thermo-responsive polymers are a class of smart polymers that respond to change in temperature. This property makes this type of polymers useful materials in a wide range of applications especially, in the field of drug delivery system. Polymers, which have primary amino groups, such as N-(3-aminopropyl) methacrylamide hydrochloride (APMA), have been used for post-polymerization modification reactions for the development of new materials for biomedical applications. Here I aim to fabricate an amphiphilic monomers composed of APMA by substituting (palmitoyl, dansyl, cholesteryl and oxadiazole) groups onto the primary amine in the APMA monomer.

These monomers were then copolymerized with N-(2-hydroxypropyl)methacrylamide (HPMA) in six different monomer feed ratios in order to characterise the effect of hydrophobic pendants on the copolymer properties including lower critical solution temperature (LCST), solubility, drug loading and drug release.

In this study drug loading and release properties of HPMA-co-APMA copolymers were studied by using four model hydrophobic drugs, propofol, griseofulvin, prednisolone and paclitaxel. High performance liquid chromatography (HPLC) measurements were performed in order to compare drug loading properties of the copolymer formulas. The most potent carrier candidate was loaded in order to carry out thermo-responsive release study. The results showed that all the copolymer formulations in this study possessed the ability to encapsulate practically poor-soluble drugs within their hydrophobic core. HPLC measurement has demonstrated that HPMA-co-(APMA-Oxadiazole 1%) (O-1) and HPMA-co-(APMA-Dansyl 2%) (D-2) have a higher drug solubilisation capacity than other copolymer formulations.

In vitro release profiles of different model drugs of the optimal formulation of copolymers were investigated at four different temperatures. Unfortunately, these copolymers showed uncontrolled release of all of the loaded drugs. To set-up thermo-responsive copolymers for controlled drug release, approaches based on introducing poly ethylene glycol (PEG) block as a part of O-1 and D-2 amphiphilic copolymers. A significant enhancement in response to the change in temperature as the drug release across the membrane was seen when PEG was present for the three hydrophobic drugs models. Then hybrid nanoparticles (HNPs) were prepared and attached to O-1 as localised nano-heaters to accelerate drug release in responded to temperature change.

Finally, the optimal formulation of (O-1)-*b*-(PEG) and (O-1)-*b*-(PEG)-HNPs loaded with paclitaxel (PTX) were tested for their cytotoxicity *in vitro* on BxPC-3 cells. *In-vitro* MTT assay results established the ability of (O-1)-*b*-(PEG)-PTX and (O-1)-*b*-(PEG)-HNPs-PTX novel formulations to accumulate and kill pancreatic cancer cells more effectively, compared to the free PTX.

Key words: Thermo-responsive drug delivery, Iron oxide-gold nanoparticles, smart polymers.

“This thesis is the result of the author's original research. The copyright of this thesis belongs to the author under the terms of the United Kingdom Copyright Acts as qualified by Keele University. Due acknowledgement must always be made of the use of any material contained in, or derived from, this thesis.”

ACKNOWLEDGEMENTS

First and foremost I would like to thank Allah for this guidance in this journey of life. His continuous grace and mercy was with me throughout my life and ever more during the tenure of my research.

During the journey of my graduate study, I have been very fortunate of meeting and collaborating with some outstanding people who I would like to acknowledge for their invaluable contribution.

Firstly, I would like to express my sincere gratitude to Dr Clare Hoskins, for being such a wonderful supervisor. Her deep passion for research and commitment to excellence are some of the many traits that have deeply motivated me. I would also like to express my sincere gratitude towards my co-supervisor Dr Tony Curtis for his supportive manner and advice, and I am honoured to have worked with such an intelligent and accomplished man.

I am also very grateful to all former and current members of the Nanopharmaceutics group, for their various forms of support during my graduate studies. Special thanks to Mark, Neil and Karen for the help and training they imparted to me on some of the characterization instruments actively used in this research.

Words are inadequate to express my feeling and deepest gratitude to my parents, siblings, for their moral support, loves and cares throughout. My gratitude and abundance of love to my wife, Najlaa you are my inspiration and motivators as without you I would not have been able to overcome the most difficult times of my life. Thank you Hussein and Fatimah (my children), for your smiling and calming support at all times!

Thank you so much for always being there to help raise my self-confidence and motivation to fulfil my dreams. I love you all!

Finally, I would like to express my gratitude to the Ministry of Higher Education and Scientific Research in Iraq (MOHESR) and University of Basrah for the financial support during my studies.

Ali

Contents

Chapter One: Introduction	1
1.1- Introduction.....	2
1.2- Micelles	2
1.2.1- Polymeric micelles	5
1.3- Copolymers	7
1.3.1- Block copolymers.....	9
1.3.2- Graft copolymers	11
1.4- Smart polymers	12
1.4.1- pH-Responsive polymers.....	14
1.4.2- Bio-responsive polymers.....	16
1.4.3- Light Responsive polymers	17
1.4.4- Thermo-responsive polymers.....	18
1.4.5- Multi-responsive polymer	23
1.5- Combination of stimuli-responsive polymers and magnetic nanoparticles properties.	23
1.6- Aims and Objectives.....	25
Chapter Two: Synthesis and Characterisation of modified monomers and copolymers .	26
2.1- Introduction.....	27
2.1.1- Thin Layer Chromatography (TLC)	29
2.1.2- Fourier Transform Infrared Spectroscopy (FTIR)	30
2.1.3- Nuclear Magnetic Resonance Spectroscopy (NMR).....	31
2.1.4- Aims and Objectives.....	32
2.2- Materials and Methods	33
2.2.1- Materials.....	33
2.2.2- Methods.....	34
2.2.2.1- Chemical modification reactions	34
2.2.2.1.1- Substitution of palmitoyl chloride onto the n-(3-aminopropyl) methacrylamide hydrochloride monomer (P-APMA).....	34
2.2.2.1.2- Substitution of dansyl chloride onto the n-(3-aminopropyl) methacrylamide hydrochloride monomer (D-APMA).....	35
2.2.2.1.3- Substitution of cholesteryl chloroformate onto the n-(3-aminopropyl) methacrylamide hydrochloride monomer (C-APMA).....	35
2.2.2.1.4- Synthesis of 5-(4-Aminophenyl)-1,3,4-oxadiazole-2-thiol (D1).....	36

2.2.2.1.5- Synthesis of 4-oxo-4-[[4-(5-sulfanyl-1,3,4-oxadiazol-2 yl) phenyl] amino]butanoic acid (D2).....	37
2.2.2.1.6- Synthesis of 4-[(2,5-dioxopyrrolidin-1-yl)oxy]-4-oxo-N-[4-(5-sulfanyl-1,3,4-oxadiazol-2-yl)phenyl]butanamide (D3).....	37
2.2.2.1.7- Substitution of 4-oxo-4-[[4-(5-sulfanyl-1,3,4-oxadiazol-2 yl) phenyl] amino]butanoic acid onto the n-(3-aminopropyl) methacrylamide hydrochloride monomer (O-APMA).....	38
2.2.2.2- RAFT polymerization of HPMA with modified APMA	39
2.2.2.3- Synthesis of block copolymer	40
2.3- Characterisation of modified monomer	40
2.3.1- Melting point.....	40
2.3.2- Thin layer chromatography	40
2.3.3- Fourier transform infrared spectroscopy (FTIR)	41
2.3.4- Nuclear magnetic resonance spectroscopy (NMR).....	41
2.4- Results	41
2.4.1- Physical properties	41
2.4.2 - Characterization of Modified Monomers	42
2.4.2.1 - Characterization of (P-APMA).....	42
2.4.2.2- Characterization of (D-APMA).....	45
2.4.2.3- Characterization of (C-APMA).....	48
2.4.2.4- Characterization of 5-(4-Aminophenyl)-1,3,4-oxadiazole-2-thiol (D1).....	51
2.4.2.5- Characterization of 4-oxo-4-[[4-(5-sulfanyl-1,3,4-oxadiazol-2 yl) phenyl] amino]butanoic acid (D2).....	53
2.4.2.6- Characterization of 4-[(2,5-dioxopyrrolidin-1-yl)oxy]-4-oxo-N-[4-(5-sulfanyl-1,3,4-oxadiazol-2-yl)phenyl]butanamide (D3)	56
2.4.2.7- Characterization of (O-APMA).....	59
2.4.2.8- Characterization of RAFT polymerization of HPMA with modified APMA.....	62
2.4.2.9- Characterization of block copolymerization.....	70
2.5- Discussion.....	74
2.6- Conclusion	79
Chapter Three: Synthesis and characterisation of hybrid nanoparticles	80
3.1- Introduction.....	81
3.1.1- Inductively Coupled Plasma – Optical Emission Spectroscopy (ICP-OES)	83
3.1.2- Transmission electron microscopy TEM	84

3.1.3- Photon correlation spectroscopy	85
3.1.4- Ultraviolet- visible spectroscopy	86
3.1.5- Aims and Objectives.....	87
3.2- Materials and Methods	88
3.2.1- Materials.....	88
3.2.2- Methods.....	88
3.2.2.1- Synthesis of iron oxide nanoparticles	88
3.2.2.2- Polymer coating of iron oxide nanoparticles.....	89
3.2.2.3- Gold seeding	89
3.3- Hybrid nanoparticles Characterisation.....	91
3.3.1- Inductively Coupled Plasma - Optical Emission Spectroscopy (ICP-OES).....	91
3.3.2- Transmission electron microscopy TEM	91
3.3.3- Photon correlation spectroscopy	91
3.3.4- Ultraviolet- visible spectroscopy	91
3.4- Results.....	92
3.4.1- Inductively Coupled Plasma-Optical Emission Spectrometry (ICP-OES).....	92
3.4.2- Transmission electron microscopy imaging	92
3.4.3- Photon correlation spectroscopy	94
3.4.4- UV/Visible spectroscopy	95
3.5- Discussion.....	96
3.6- Conclusion	98
Chapter Four: Drug loading and release kinetics from polymeric aggregates	99
4.1- Introduction.....	100
4.1.1- Model Drugs	101
4.1.2- High performance liquid chromatography (HPLC)	103
4.1.3- Aims and Objectives.....	105
4.2- Materials and Methods	105
4.2.1- Materials.....	105
4.2.2- Methods.....	106
4.2.2.1- Copolymer Solubility Study	106
4.2.2.2- (HPMACO-AMPA-Oxadiazole)-b-PEG-HNP Conjugation.....	106
4.2.2.3- Drug Loading.....	106
4.2.2.4- Solubility Study	107

4.2.2.4.1- Determination of Propofol.....	107
4.2.2.4.2- Determination of Griseofulvin	107
4.2.2.4.3- Determination of Prednisolone.....	107
4.2.2.4.4- Determination of Paclitaxel.....	107
4.2.2.5-Particle size and size distribution measurements	108
4.2.2.6- Transition electron microscopy	108
4.2.2.7- In vitro drug release	108
4.3- Results.....	109
4.3.1- Copolymer Solubility Study.....	109
4.3.2- Solubility Study	109
4.3.2.1- Determination of Propofol Solubility in HPMA-co-APMA-R	109
4.3.2.2- Determination of Griseofulvin Solubility in HPMA-co-APMA-R.....	113
4.3.2.3- Determination of Prednisolone Solubility in HPMA-co-APMA-R	118
4.3.2.4- Determination of Propofol, Griseofulvin and Prednisolone Solubility in (O-1)-b-(PEG) and (D-2)-b-(PEG)	122
4.3.2.4- Determination of Propofol, Griseofulvin and Prednisolone Solubility in (O-1)-b-(PEG)-HNPs.....	124
4.3.3-Particle size and size distribution.....	127
4.3.5- In vitro drug release.....	131
4.4- Discussion.....	142
4.5- Conclusion	147
Chapter Five: Biological Characterisation of the Novel Thermo-responsive Amphiphilic Copolymer Formulations	148
5.1- Introduction.....	149
5.1.1- Bioavailability Investigation.....	149
5.1.1.1- Cytotoxicity evaluation	149
5.1.1.1.1- MTT Assay	150
5.1.1.1.2- Trypan blue exclusion assay.....	150
5.1.1.2- Intracellular drug uptake.....	151
5.1.2- Aims and Objectives.....	151
5.2.1- Materials.....	152
5.2.2- Methods.....	152
5.2.2.1- Cell culture preparation	152
5.2.2.2- Cytotoxicity evaluation	153

5.2.2.2.1- <i>MTT assay procedure</i>	153
5.2.2.3- <i>Determine intracellular drug concentrations in cellular uptake</i>	155
5.2.2.4- <i>In vitro thermoresponsive cytotoxicity assay</i>	156
5.3- <i>Results</i>	157
5.3.1- <i>MTT Assay</i>	157
5.3.2- <i>Determine intracellular drug concentrations in cellular uptake</i>	159
5.3.3- <i>In vitro thermoresponsive cytotoxicity assay</i>	160
5.4- <i>Discussion</i>	162
5.5- <i>Conclusion</i>	166
Chapter Six: General Conclusions and Future Work	167
6.1- <i>General conclusion</i>	168
6.2- <i>Future work</i>	171
References	172
Appendix	203

List of Figures

Figure 1- Schematic representation of direct and reverse micelle formation dependent upon surrounding media.	3
Figure 2- Detection of critical micelle formation concentration (CMC) by measuring the surface tension as a function of the surfactant concentration.	4
Figure 3- Schematic representation of (a) star micelle (b) crew-cut micelle.	5
Figure 4- Schematic representation of copolymer types.	8
Figure 5- Chemical structure of ABS copolymer.	8
Figure 6- Chemical structure of hydrophilic polymers commonly used in block copolymers A) poly (ethylene oxide), B) poly (acrylic acid), C) poly (2-hydroxyethyl methacrylate) and D) poly (2-methyl-2-oxazoline).	9
Figure 7- Chemical structure of hydrophobic polymers commonly used in block copolymers A) poly (propyleneoxide), B) polystyrene, C) poly (L-lactic acid) and D) poly (diethylaminoethyl methacrylate).	10
Figure 8- Schematic illustration of drug incorporation into amphiphilic copolymer in aqueous medium.	11
Figure 9- Different types of smart polymeric drug delivery systems for controlling drug release.	14
Figure 10- Representation of the switch between a neutral and charged state of pH-responsive polymer particles.	15
Figure 11- Representation of the glucose-responsive controlled release of insulin.	17
Figure 12- Schematic illustration of the LCST-type phase transition.	19
Figure 13- Chemical Structure of pHPMA.	27
Figure 14- Chemical Structure of APMA.	28
Figure 15- Chemical Structure of (A) palmitoyl chloride (B) 5-(4-aminophenyl)-1,3,4-oxadiazole-2-thiol (c) dansyl chloride (D) cholesteryl.	28
Figure 16- Schematic design of a basic TLC plate for monitoring reaction progress.	30
Figure 17- Schematic diagram illustrate the essential features of FTIR spectrometer.	31
Figure 18- Schematic diagram illustrate the essential features of NMR spectrometer.	32
Figure 19- Chemical synthesis of P-APMA.	34
Figure 20- Chemical synthesis of D-APMA.	35
Figure 21- Chemical synthesis of D-APMA.	36
Figure 22- Chemical synthesis of D1.	36

Figure 23- Chemical synthesis of D2.	37
Figure 24- Chemical synthesis of D3.	38
Figure 25- Chemical synthesis of O-APMA.	38
Figure 26- Synthesis of poly (HPMA-co-APMA-R).	39
Figure 27- Synthetic scheme for (HPMA-co-APMA-R)-b-PEG diblock copolymers.	40
Figure 28- Chromatogram of TLC plate (p-APMA).	42
Figure 29- FTIR spectra of P-APMA.	43
Figure 30- ¹ H NMR spectra of P-APMA in CDCl ₃ carried out using 300MHz NMR at 25 °C.	44
Figure 31- ¹³ C NMR spectra of P-APMA in CDCl ₃ carried out using 300MHz NMR at 25 °C.	44
Figure 32- Chromatogram of TLC plate (D-APMA).	45
Figure 33- FTIR spectrum of D-APMA.	45
Figure 34- ¹ H NMR spectra of D-APMA in CDCl ₃ carried out using 300MHz NMR at 25 °C.	47
Figure 35- ¹³ C NMR spectra of D-APMA in CDCl ₃ carried out using 300MHz NMR at 25 °C.	47
Figure 36- Chromatogram of TLC plate (C-APMA).	48
Figure 37- FTIR spectrum of C-APMA.	48
Figure 38- ¹ H NMR spectra of C-APMA in CDCl ₃ carried out using 300MHz NMR at 25 °C.	50
Figure 39- ¹³ C NMR spectra of C-APMA in CDCl ₃ carried out using 300MHz NMR at 25 °C.	50
Figure 40- Chromatogram of TLC plate D1.	51
Figure 41- FTIR spectrum of D1.	51
Figure 42- ¹ H-NMR spectra of D1 in DMSO carried out using 300MHz NMR at 25 °C.	52
Figure 43- ¹³ C NMR spectra of D1 in DMSO carried out using 300MHz NMR at 25 °C.	53
Figure 44- Chromatogram of TLC plate D2.	53
Figure 45- FTIR spectrum of D2.	54
Figure 46- ¹ H NMR spectra of D2 in DMSO carried out using 300MHz NMR at 25 °C.	55
Figure 47- ¹³ C NMR spectra of D2 in DMSO carried out using 300MHz NMR at 25 °C.	56
Figure 48- Chromatogram of TLC plate D3.	56
Figure 49- FTIR spectrum of D3.	57

Figure 50- ^1H NMR spectra of D3 in DMSO carried out using 300MHz NMR at 25 °C.	58
Figure 51- ^{13}C NMR spectra of D3 in DMSO carried out using 300MHz NMR at 25 °C.	58
Figure 52- Chromatogram of TLC plate (O-APMA).	59
Figure 53- FTIR spectrum of O-APMA.	59
Figure 54- ^1H NMR spectra of O-APMA in DMSO carried out using 300MHz NMR at 25 °C.	61
Figure 55- ^{13}C NMR spectra of O-APMA in DMSO carried out using 300MHz NMR at 25 °C.	61
Figure 56- FTIR spectrum of poly(HPMA-co-HPMA-P).	62
Figure 57- ^1H NMR spectra of poly(HPMA-co-HPMA-P) in DMSO carried out using 300MHz NMR at 25 °C.	63
Figure 58- FTIR spectrum of poly(HPMA-co-HPMA-D).	64
Figure 59- ^1H NMR spectra of poly(HPMA-co-HPMA-D) in DMSO carried out using 300MHz NMR at 25 °C.	65
Figure 60- FTIR spectrum of poly(HPMA-co-HPMA-C).	66
Figure 61- ^1H NMR spectra of poly(HPMA-co-HPMA-C) in DMSO carried out using 300MHz NMR at 25 °C.	67
Figure 62- FTIR spectrum of poly(HPMA-co-HPMA-O).	68
Figure 63- ^1H NMR spectra of poly(HPMA-co-HPMA-O) in DMSO carried out using 300MHz NMR at 25 °C.	69
Figure 64- FTIR spectrum of poly(HPMA-co-HPMA-O)-co-PEG.	70
Figure 65 - ^1H NMR spectra of poly(HPMA-co-HPMA-O)-co-PEG in DMSO carried out using 300MHz NMR at 25 °C.	71
Figure 66- FTIR spectrum of poly(HPMA-co-HPMA-D)-co-PEG.	72
Figure 67- ^1H NMR spectra of poly(HPMA-co-HPMA-D)-co-PEG in DMSO carried out using 300MHz NMR at 25 °C.	73
Figure 68- Disproportionation termination routes.	78
Figure 69- Schematic of MNP-gold core-shell NPs.	83
Figure 70- Schematic diagram illustrate the essential features of ICP-OES.	84
Figure 71- Schematic diagram illustrate the essential features of TEM.	85
Figure 72- Schematic diagram illustrate the essential features of PCS.	86
Figure 73- Particles size effect on their movement.	86

Figure 74- Schematic diagram illustrate the essential features of UV-Vis spectrophotometer.	87
Figure 75- Schematic diagram of iron oxide nanoparticles coating by PEI.	89
Figure 76- Schematic diagram of gold seeding process.	90
Figure 77- Schematic diagram of gold coating process.	90
Figure 78- A graph showing the concentrations of Fe and Au in HNPs detected by ICP-OES.	92
Figure 79- TEM images of (A) Fe ₃ O ₄ nanoparticles, (B) Fe ₃ O ₄ -PEI nanoparticles, (C) Fe ₃ O ₄ -PEI-Au seed and (D) HNPs.....	93
Figure 80- shows the absorbance spectra of HNP particles.	96
Figure 81- Chemical structure of propofol.	101
Figure 82- Chemical structure of griseofulvin.	102
Figure 83- Chemical structure of prednisolone.	102
Figure 84- Chemical structure of paclitaxel.	103
Figure 85- Schematic diagram illustrate the essential features of HPLC.	104
Figure 86- Maximum concentration of propofol solubilised by each copolymer formula (6 mgmL ⁻¹) at 1:1, 1:5 or 1:10 initial polymer:drug loading ratios (n=3, ave ± SD). 110	110
Figure 87- Drug loading of propofol onto a) HPMA-co-APMA-P and b) HPMA-co-APMA-D at varied grafting ratio and different initial drug:polymer loading ratios (n=3, ave ± SD).....	111
Figure 88- Drug loading of propofol onto a) HPMA-co-APMA-C and b) HPMA-co-APMA-O at varied grafting ratio and different initial drug:polymer loading ratios (n=3, ave ± SD).....	113
Figure 89- Maximum concentration of griseofulvin solubilised by each copolymer formula (6 mgmL ⁻¹) at 1:1, 1:5 or 1:10 initial polymer:drug loading ratios (n=3, ave ± SD). 114	114
Figure 90- Drug loading of griseofulvin onto a) HPMA-co-APMA-P and b) HPMA-co- APMA-D at varied grafting ratio and different initial drug:polymer loading ratios (n=3, ave ± SD).....	115
Figure 91- Drug loading of griseofulvin onto a) HPMA-co-APMA-C and b) HPMA-co- APMA-O at varied grafting ratio and different initial drug:polymer loading ratios (n=3, ave ± SD).....	117

Figure 92- Maximum concentration of prednisolone solubilised by each copolymer formula (6 mgmL ⁻¹) at 1:1, 1:5 or 1:10 initial polymer:drug loading ratios (n=3, ave ± SD).	118
Figure 93- Drug loading of prednisolone onto a) HPMA-co-APMA-P and b) HPMA-co-APMA-D at varied grafting ratio and different initial drug:polymer loading ratios (n=3, ave ± SD).	119
Figure 94- Drug loading of prednisolone onto a) HPMA-co-APMA-C and b) HPMA-co-APMA-O at varied grafting ratio and different initial drug:polymer loading ratios (n=3, ave ± SD).	121
Figure 95- Drug loading of propofol onto (O-1)-b-(PEG) and (D-2)-b-(PEG) at different initial drug:polymer loading ratios (n=3, ave ± SD).	122
Figure 96- Drug loading of griseofulvin onto (O-1)-b-(PEG) and (D-2)-b-(PEG) at different initial drug:polymer loading ratios (n=3, ave ± SD).	123
Figure 97- Drug loading of prednisolone onto (O-1)-b-(PEG) and (D-2)-b-(PEG) at different initial drug:polymer loading ratios (n=3, ave ± SD).	123
Figure 98- Maximum concentration of propofol, griseofulvin and prednisolone solubilised by (O-1)-b-(PEG)-HNPs copolymer formula (6 mgmL ⁻¹) at 1:10 initial polymer:drug loading ratios (n=3, ave ± SD).	124
Figure 99- Maximum concentration of paclitaxel solubilised by (O-1)-b-(PEG)-HNPs copolymer formula (6 mgmL ⁻¹) at 1:1 initial polymer:drug loading ratios (n=3, ave ± SD).	125
Figure 100- TEM micrographs of optimal formulations nano-aggregates of (O-1)-b-(PEG) 6 mgmL ⁻¹ sample a) in the absence of HNPs, b) in the presence of HNPs.	129
Figure 101- Representation of the (O-1)-b-(PEG) conjugation to gold surface of HNPs via oxadiazole pendant group.	130
Figure 102- Representation a) size and zeta potential of optimal formulations nano-aggregates of (O-1)-b-(PEG) 6 mgmL ⁻¹ sample in the absence and in the presence of HNPs.	131
Figure 103- In vitro release of propofol from P-0.25 formulation at different temperatures.	132
Figure 104- In vitro release of propofol from D-2 formulation at different temperatures. ..	132
Figure 105- In vitro release of propofol from C-0.25 formulation at different temperatures.	133

Figure 106- <i>In vitro</i> release of propofol from O-1 formulation at different temperatures. ...	133
Figure 107- <i>In vitro</i> release of propofol from (D-2)-b-(PEG) formulation at different temperatures.	134
Figure 108- <i>In vitro</i> release of propofol from (O-1)-b-(PEG) formulation at different temperatures.	135
Figure 109- <i>In vitro</i> release of griseofulvin from (D-2)-b-(PEG) formulation at different temperatures.	136
Figure 110- <i>In vitro</i> release of griseofulvin from (O-1)-b-(PEG) formulation at different temperatures.	136
Figure 111- <i>In vitro</i> release of prednisolone from (D-2)-b-(PEG) formulation at different temperatures.	137
Figure 112- <i>In vitro</i> release of Prednisolone from (O-1)-b-(PEG) formulation at different temperatures.	138
Figure 113- Propofol entrapped in the interior layers of the membrane.	139
Figure 114- <i>In vitro</i> release of propofol from (O-1)-b-(PEG)-HNPs formulation at different temperatures.	139
Figure 115- <i>In vitro</i> release of griseofulvin from (O-1)-b-(PEG)-HNPs formulation at different temperatures.	140
Figure 116- <i>In vitro</i> release of prednisolone from (O-1)-b-(PEG)-HNPs formulation at different temperatures.	141
Figure 117- The ionisation of phenols.	146
Figure 118- Mechanism of MTT reduction into formazan.	150
Figure 119- Illustration the 96-well plate assembly for the MTT assay.	154
Figure 120- Illustration the 6-well plate assembly for the drug uptake study.	156
Figure 121- BxPC-3 cell viability (%) as determined by MTT assay after 24 h exposure to varied concentrations of PTX and polymer formulations (n=3, ave ± SD).	158
Figure 122- IC ₅₀ (µg/ml) of PTX and polymer formulas as determined by MTT assay, after 24 h (n=3, ave ± SD).	158
Figure 123- Cellular uptake study on BxPC-3 cell line after 1 h, 4 h and 24 h exposure with PTX, (O-1)-b-(PEG)-PTX and (O-1)-b-(PEG)-HNPs-PTX (n=3, ave ± SD).	159
Figure 124- <i>In vitro</i> thermoresponsive cytotoxicity test on BxPC-3 cell line as determined by MTT assay after exposure to varied concentrations of PTX and polymer formulations (n=3, ave ± SD).	160

Figure 125- IC_{50} (μgmL^{-1}) of heat-treated PTX and polymer formulations as determined by MTT assay, after 24 h ($n=3$, ave \pm SD)..... 161

List of Tables

TABLE 1- Tumour-targeting selectivity of anticancer-incorporated polymeric micelle	6
TABLE 2- Various stimuli and responsive materials.....	13
TABLE 3- Examples of thermos-responsive polymers.....	20
TABLE 4- Monomer feeding ratio.....	39
TABLE 5- Physical properties of the modified monomers.....	42
TABLE 6- Summary of functional P-APMA.....	43
TABLE 7- Summary of functional D-APMA.....	46
TABLE 8- Summary of functional C-APMA.....	49
TABLE 9- Summary of functional D1.....	52
TABLE 10- Summary of functional D2.....	54
TABLE 11- Summary of functional D3.....	57
TABLE 12- Summary of functional O-APMA.....	60
TABLE 13- Summary of functional poly(HPMA-co-HPMA-P).....	62
TABLE 14- Summary of functional poly(HPMA-co-HPMA-D).....	64
TABLE 15- Summary of functional poly(HPMA-co-HPMA-C).....	66
TABLE 16- Summary of functional poly(HPMA-co-HPMA-O).....	68
TABLE 17- Summary of functional poly(HPMA-co-HPMA-O)-co-PEG.....	70
TABLE 18 - Summary of functional poly(HPMA-co-HPMA-D)-co-PEG.....	72
TABLE 19- Size, polydispersity index and zeta potential analysis for 1 mgmL^{-1} aqueous polymer solutions $n=3$, ave (SD).....	95
TABLE 20- Effect of grafted hydrophobic groups onto copolymer solubility.....	109
TABLE 21- Summary of polymer-drug formulation conditions and encapsulation properties (encapsulation efficiency (EE) and loading capacity (LC)), results shown as average, $n=3$	126
TABLE 22- Photon correlation spectrometry size analysis of optimal Copolymers formulations at 6 mg/ml with initial polymer:drug feed ratio of 10:1, ($n=3$, ave).....	128
TABLE 23- Preparation of Excipient Solutions for MTT assay.....	153

List of Abbreviations

^{13}C NMR	13 carbon nuclear magnetic resonance
^1H NMR	Proton nuclear magnetic resonance
AAPBA	3-acrylamidophenylboronic acid
ABS	Poly Acrylonitrile-Butadiene-Styrene
AIBN	Azobisisobutyronitrile
AOT	Sodium bis(2-ethylhexyl) sulfosuccinate
APMA	N-(3-aminopropyl) methacrylamide hydrochloride
ASP	Aspartic acid
AspPBA	Aspartamidophenylboronic acid
AuNPs	Gold nanoparticles
BCS	Biopharmaceutics Classification System
BNIPDaoct	Bisnaphthalimidopropylidiaminooctane
CDCl_3	Chloroform
CLC	Column liquid chromatography
CMC	Critical Micellar Concentration
CPM	Complex polymeric micelle
CPT	Camptothecin
CT	Computed tomography
CTAB	Cetyl trimethylammonium bromide
CTAC	Cetyltrimethylammonium chloride
DCC	N,N'-Dicyclohexylcarbodiimide
DCM	Dichloromethane
DDSs	Drug delivery systems
DLS	Dynamic light scattering
DMAEMC	N-dimethylaminoethyl methacrylate hydrochloride
DMF	Dimethylformamide
DMSO	Dimethyl sulfoxide
DOX	Doxorubicin
EE	Encapsulation efficiency
FBS	Foetal bovine serum
FTIR	Fourier Transform Infrared Spectroscopy

GC	Gas chromatography
GOD	Glucose oxidase
HNPs	Hybrid nanoparticles
HPLC	High performance chromatography
HPMA	N-(2-hydroxypropyl) methacrylamide
ICP-OES	Inductively Coupled Plasma Optical Emission Spectroscopy
IE	Ion exchange
LC	Loading capacity
LCST	Lower critical solution temperature
LMWC	Low molecular weight chitosan
LMWPC	Low molecular weight palmitoyl chitosan
LSPR	Localised surface plasmon resonance
MAA	Methacrylic acid
MBCSP	magnetic-based core-shell particles
MMA	Methyl methacrylate
MNPs	Magnetic nanoparticles
MOFs	Metal-organic frameworks
MP	Melting point
MPC	Poly(2-methacryloyloxyethyl phosphorylcholine)
MRI	Magnetic resonance imaging
mV	Millivolt
NaDS	Sodium decyl sulfate
NanoPM	Nanophotomedicine
NHS	N-Hydroxysuccinimide
NIPAAm	N-isopropylacrylamide
NMR	Nuclear Magnetic Resonance
NR	Natural rubber
OX	Oxadiazole
P4VP	poly (4-vinylpyridine)
PAA	Poly (acrylic acid)
PAA	Poly allylamine
PAPBA	Poly N-3-acrylamido phenylboronic acid
PCL	Poly (ϵ -caprolactone)

PCS	photon correlation spectroscopy
PDEA	Poly (diethylaminoethyl methacrylate)
PDI	Polydispersity index
PEG	Poly(ethylene glycol)
PEI	Poly(ethylenimine)
PEO	poly(ethylene oxide)
PHPA	Poly(2-hydroxypropylacrylate)
pHPMA	Poly(N-(2-hydroxypropyl) methacrylamide)
PiPO _x	Poly(2-isopropyl-2-oxazoline)
PLA	Poly lactide
PLGA	Poly (D,L-lactide-co-glycolide)
PLLA	Poly (L-lactic acid
PMOXA	Poly (2-methyl-2-oxazoline)
PNIPAAm	Poly (N-isopropylacrylamide)
PNNPAM	Poly(N-n-propylacrylamide)
ppm	Part per million
PPO	Poly(propyleneoxide)
PPV _s	poly(phenylene vinylene)s
PPy	Pyrene pendant groups
PS	Polystyrene
PS/SAN	Poly(styrene)/poly(styrene-co-acrylonitrile)
PTX	Paclitaxel
PVA	poly (vinyl alcohol)
PVA-co-PEG	Polyvinyl alcohol- polyethylene glycol
PVME	Poly (vinyl methyl ether)
PVP	poly (N-vinylpyrrolidone)
RBF	Round bottom flask
R_f	Retention factor
RP	Reversed-phase
SCF	Supercritical fluid technology
SDS	Sodium dodecyl sulfate
SE	Size exclusion
SH	Thiol group

TB	Trypan blue
TEM	Transmission electron microscopy
TLC	Thin layer chromatography
TMAEMC	N-trimethylaminoethyl methacrylate chloride
UCST	Upper critical solution temperature
UHMWPE	Ultra-high molecular weight polyethylene
X-UHMWPE	Cross-linked ultra-high molecular weight polyethylene

Chapter One

Introduction

1.1- Introduction

The search for new drugs in disease management is expensive and time consuming. Improvement in the safety and biological relevance of “old” drugs has been attempted using formulation strategies in order to exert much greater control over drug fate. These strategies include controlling the drug release rate as well as targeting to specific diseased tissues (Kshirsagar, 2000). Drug delivery systems (DDSs) have been widely applied in order to avoid the main limitations of traditional formulations that usually occur when a bolus injection is administered resulting from the high plasma drug concentration (Censi *et al.*, 2010). The main aim of any targeted DDS is to deliver specific amounts of the drug to the targeted site at an appropriate rate, in addition to minimize local and systemic toxic effects to healthy tissues (Balmayor *et al.*, 2011). Moreover, DDSs can act as a protectant for drug molecules against physiological degradation and elimination, resulting in prolonged circulation times.

The water solubility of a drug is an important factor in relation to its ability to be administered either intravenously or orally (Khadka *et al.*, 2014). More than 40% of new drugs under investigation are poorly water-soluble (Hoskins *et al.*, 2016). Hence, careful formulation strategies are required in order to improve aqueous solubility of lipophilic drug candidates. One of the major technologies arising within the past two decades for hydrophobic drug solubilisation is the use of polymeric micelles.

1.2- Micelles

Micelles are aggregates or supramolecular assemblies of amphiphilic molecules dispersed in aqueous solution with a size usually between 5 nm and 100 nm (Mitra *et al.*, 2017). Typically, amphiphilic molecules consist of two regions; a hydrophilic (polar or charged) region and a hydrophobic (non-polar) region. In aqueous solution, amphiphilic molecules arrange themselves in a spherical form, in which the polar part (head) is outward facing toward the surrounding water molecules while the non-polar parts (tail) are driven to an interior structure away from the water (Mancin *et al.*, 2016, Dhembre *et al.*, 2009).

In general, there are two types of micelle system; 1) ionic which include ionic or zwitterionic, and 2) neutral. Traditionally, micelles formed from surfactant molecules have been used as excipients for drug solubilisation and delivery. When surfactant molecules have a negative or positive charge on the polar head they are classified as anionic surfactants e.g. sodium decyl sulfate (NaDS), sodium dodecyl sulfate (SDS), cetyltrimethylammonium chloride (CTAC)

and Cetyl trimethylammonium bromide (CTAB) while neutral surfactants don't have any charge on their polar head groups such as poly (oxyethylene glycol tert-octylphenol) ethers and poly (oxyethylene glycol octylphenol) ethers. Depending on the polarity of the surrounding media, micelles can form into different conformations (Figure 1):

- (i) Direct Micelles: when formed in water or polar solvent, the polar head moieties of the surfactant molecules arrange themselves toward water while the hydrophobic groups are buried from water.
- (ii) Reverse Micelles: when the media is of low polarity this will lead to the surfactant to become orientated in such a way that the hydrophilic moieties are towards the interior of the micelle, leaving the hydrophobic part in contact with the organic solvent, a common example of this type is sodium bis(2-ethylhexyl) sulfosuccinate (AOT) (Facchin *et al.*, 2017, Thomas *et al.*, 2010, Fenn *et al.*, 2009).

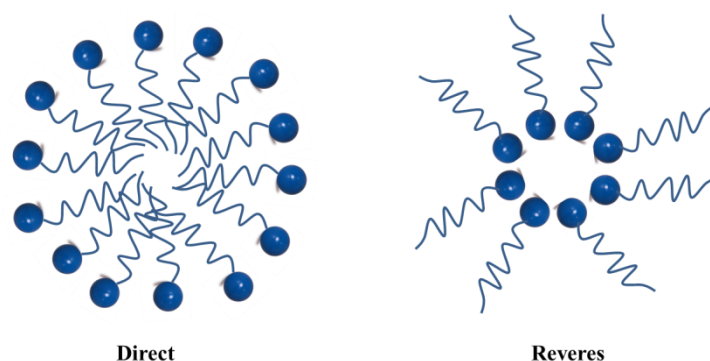


Figure 1- Schematic representation of direct and reverse micelle formation dependent upon surrounding media.

Surfactant concentration, pH, ionic strength and temperature have an important impact on the size and shape of micelles. In addition to spherical shapes, micelles can be found as cylinders, bilayers and ellipsoids (Santos *et al.*, 2016, Lombardo *et al.*, 2015). Micellar formation occurs spontaneously at a specific concentration which is dependent on molecular make-up. This concentration is known as the Critical Micellar Concentration (CMC). Below the CMC, surfactant molecules exist as single entities, occupying the surface of the bulk liquid, at and

above the CMC, spontaneous aggregation occurs and micellar structures form. Further increase in concentration can result in an increased number of micelles, but will not impact the micellar size (Figure 2) (Wijaya *et al.*, 2016, Chakraborty *et al.*, 2011, Holmberg *et al.*, 2002).

The mechanism driving spontaneous aggregation and micellar formation is due to a reduction in Gibbs' free energy. It is energetically more favourable for the hydrophobic moieties to shield themselves from the aqueous environment and cluster together forming the hydrophobic core (Dhembre *et al.*, 2009).

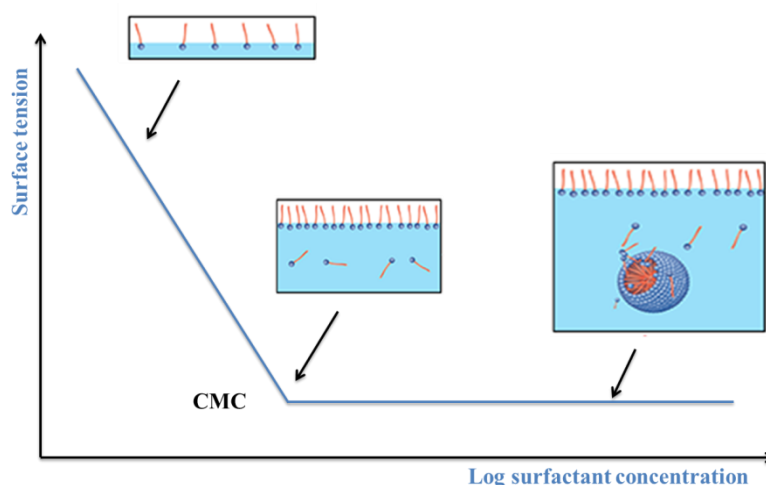


Figure 2- Detection of critical micelle formation concentration (CMC) by measuring the surface tension as a function of the surfactant concentration

Micellar technology has been widely used in technologies such as surfactants, soaps, lubricants and detergents, cosmetics etc. (Cornwel, 2018, Zheng *et al.*, 2009). However, surfactant micelles suffer from great instability upon dilution in bloodstream following dosing, which hinders their usage for medical application. Additionally, a large amount of surfactant excipient is required in order to solubilise some of the excessively hydrophobic drug molecules, this result in more viscous formulations which are not very efficient or cost effective and may carry an increased toxicity due to the large excipient concentration. Advances in knowledge have led to the development of polymeric micelles. These systems overcome some of the challenges faced by surfactant micelles and are proving to play a key part in the field of cancer therapy and drug delivery, particularly in the solubilisation of poorly soluble anticancer agents in aqueous solution (Svenson and Prud'homme , 2012).

1.2.1- Polymeric micelles

Polymer micelles are generally more stable than low molecular weight surfactants, possessing lower CMC values (as much as 1000 times lower), greater solubilising potential, slower dissociation, prolonged retention of loaded drugs, and higher drug accumulation at the target site (Movassaghian *et al.*, 2015). In order to form polymeric micelles, amphiphilic polymers have to be constructed, composing of hydrophilic and hydrophobic monomer units. These types of amphiphiles can be formed by either block copolymers or grafted comb shaped polymers. Poly(ethylene glycol) (PEG) also known as poly(ethylene oxide) (PEO) has been widely used as the hydrophilic moiety in many amphiphilic polymers because of their desirable properties, including high solubility in water and low toxicity (Grallert *et al.*, 2012) while the hydrophobic moiety often consists of hydrocarbon chains of varied length e.g. alkyl, acyl or sterol-like groups (Hoskins *et al.*, 2012a).

Depending on the relative length of the blocks of diblock copolymers, micellar structures are commonly distinguished into two types: ‘star-micelles’ when the insoluble block is smaller than soluble one, in this case, the micelle core will be small and the corona very large; and ‘crew-cut micelles’ when the micelles have a short soluble corona and large insoluble moieties (Rodri’ *et al.*, 2005, Karayianni and Pispas, 2016) (See Figure 3).

Polymeric micelles have been reported to have several features including: very small size 10-100 nm, high structural stability (static and dynamic) which plays an essential role in their *in vivo* application, ability to encapsulate a high amount of hydrophobic drug, maintaining their aqueous dissolution, bioavailability enhancement and reduction in the toxicity of poorly soluble drugs in water (Movassaghian *et al.*, 2015).

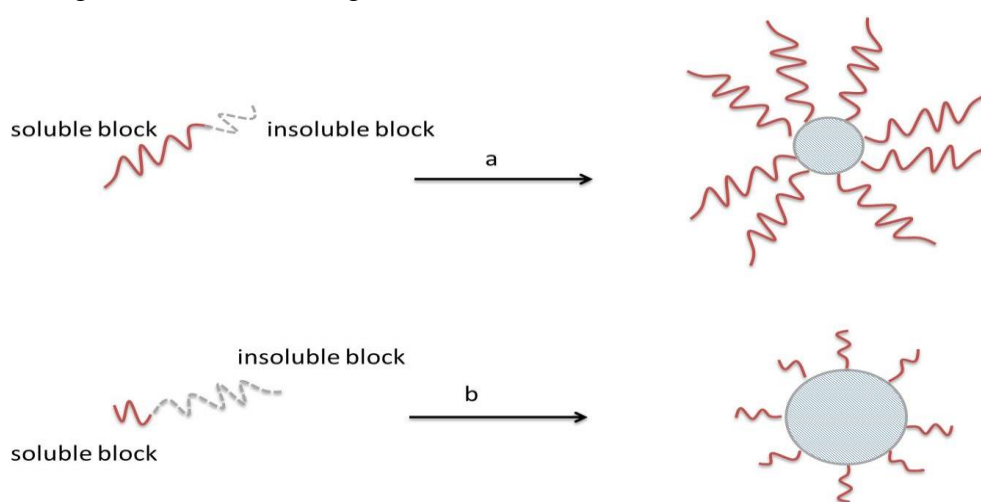


Figure 3-Schematic representation of (a) star micelle (b) crew-cut micelle.

Japanese researchers have had precedence to use polymeric micelle carriers in drug tumour targeting and clinical trials as well. Yokoyama and colleagues identified that polymeric micelles forming from poly(ethylene glycol)-*b*-poly(aspartic acid) PEG-*b*-poly(ASP) could be used as successful polymeric micelle carriers for platinum chelate cisplatin via a reaction between a carboxylic acid ligand exchange reaction between a chloride ion of cisplatin and a carboxylic acid residue of the poly(ASP) chain (Yokoyama., 2011, Yokoyama *et al.*, 1996).

The poor-soluble anticancer drug can be also incorporated physically into polymeric micelles. Li and colleagues reported using a dialysis method to encapsulate ethaselen anticancer drug into polymeric micelles fabricated from monomethoxy poly(ethylene glycol)-poly(lactide) (mPEG-PLA) diblock copolymers. They mention a remarkable increase in ethaselen solubility in water up to 82 µg/mL before freeze-drying (Li *et al.*, 2009). More examples are shown in Table 1.

Table 1- Tumour-targeting selectivity of anticancer-incorporated polymeric micelle.

Polymeric micelle	Block Copolymer	Drug	Micelle Size (diameter)	Indication	Reference
Genexol PM	PEG-P(D,L-lactide)	Paclitaxel	20-50 nm	Breast cancer, Pancreatic cancer, Small cell lung cancer	Kim <i>et al.</i> , 2004 Wilson <i>et al.</i> , 2008
NK012	PEG-PGL(SN-38)	SN-38	20 nm	Breast cancer	Matsumura <i>et al.</i> , 2009
NC-6004	PEGPGL (Cisplatin)	Cisplatin	30 nm	Solid tumours	Matsumura, 2008 Wilson <i>et al.</i> , 2008
SP1049C	Pluronic L61 and F127	Doxorubicin	22-27 nm	Adenocarcinoma of oesophagus	Sutton <i>et al.</i> , 2007
NK105	PEG-(aspartate)	Paclitaxel	85 nm	Advanced stomach cancer	Matsumura, 2008 Hamaguchi <i>et al.</i> , 2007

Various types of amphiphilic copolymers have been designed for this matter included grafted and block copolymers, dendrimers, comb and star shaped polymers.

1.3- Copolymers

Polymer alteration with the goal of getting specific properties to the final product has given a considerable push to macromolecular science. Copolymerization reactions are used to enhance the desirable and targeted properties of some polymers to meet the requirements of the special application. A copolymer is a macromolecule composed of two or more monomeric repeating subunits linked together to control the resulting material properties. A copolymerization reaction of a mixture of vinyl esters was first revealed in 1914 by Klatte F. The intensive applied research in the subsequent period showed that the copolymers have desirable physical properties as compared to polymers of single monomers (Mayo and Walling, 1950).

Copolymers can be sorted into four general classes (see Figure 4)

- 1- Alternating copolymers.
- 2- Random copolymers.
- 3- Block copolymers.
- 4- Graft copolymer.

The majority of the commercial polymer blends consist of 2-3 polymers as a block or graft copolymer. This technology is widely used because it's cheap and reduces the time that is consumed to develop new monomers and new polymerization methods to create new polymeric materials (Cor *et al.*, 1998). One of the most commonly used copolymer is Acrylonitrile-Butadiene-Styrene (ABS). Copolymerization of these three polymers together shows an enhancement in chemical and thermal resistance; good dimensional stability; and increased toughness and impact strength to the copolymer (Figure 5) (Kulich *et al.*, 2001).

Many commercial copolymers are used in medical and pharmaceutical sectors including burn wound care such as polyvinyl alcohol-polyethylene glycol (PVA-co-PEG), sutures such as Polyglactin 910, artificial hip joints made by grafting poly(2-methacryloyloxyethyl phosphorylcholine) (MPC) onto a highly cross-linked UHMWPE (X-UHMWPE)...etc. (Madaghiale *et al.*, 2014, Sharp *et al.*, 1989, Kazuhiko, 2015).

Amphiphilic graft copolymers have gained much attention because of their sensitivity to the outer chemical and physical stimuli include pH, temperature, light and electric field (Zhang *et al.*, 2007).

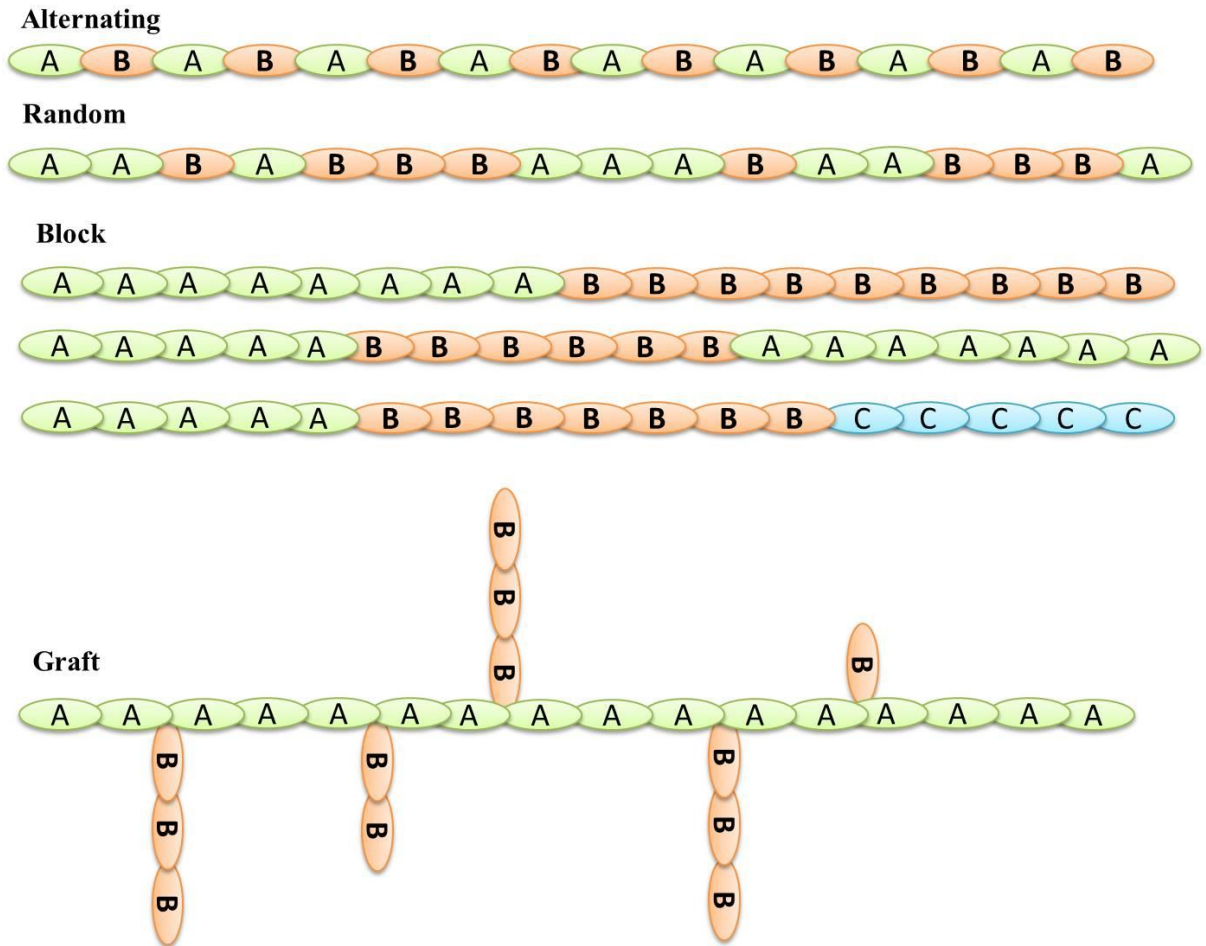


Figure 4-Schematic representation of copolymer types.

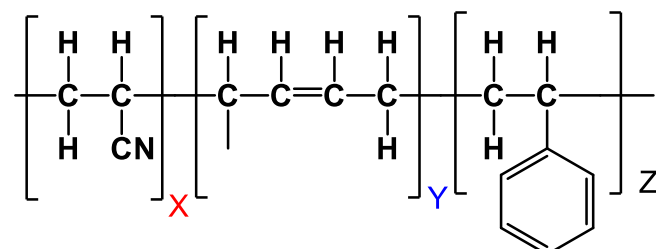


Figure 5-Chemical structure of ABS copolymer.

1.3.1- Block copolymers

Block copolymers are one of most widely used materials for self-assembly studies in nanomedicine (Cabral and Kataoka, 2010). Block copolymers are macromolecules that consist of different monomer clusters formed together in continuous blocks. In general, block copolymers are sorted into three categories depending on the types and numbers of polymer blocks AB, ABA or BAB and ABC (Tharmavaram *et al.*, 2017). Typically, amphiphilic block copolymers are made-up from the polymerization of one hydrophobic segment and one hydrophilic segment. The most popular application of amphiphilic diblock copolymers in the pharmaceutical and biomedical sector is their use as drug and gene delivery vehicles.

Polymers such as poly (ethylene oxide) (PEO), poly (acrylic acid) (PAA), poly (2-hydroxyethyl methacrylate) (pHEMA) and poly (2-methyl-2-oxazoline) (PMOXA) are examples of the hydrophilic polymer. Among the many hydrophilic polymers, poly (ethylene oxide) (PEO) is still particularly interesting compared to fabricated amphiphilic block copolymers due to its high solubility in water and its biocompatibility. Moreover, PEG blocks protein and cell surface interactions which lead to reduce nanoparticle uptake (Yue and Ian, 2016, Ulbrich *et al.*, 2016, Dehbari *et al.*, 2017, Achilias and Sifaka, 2017, Zhang and Zhang, 2017)

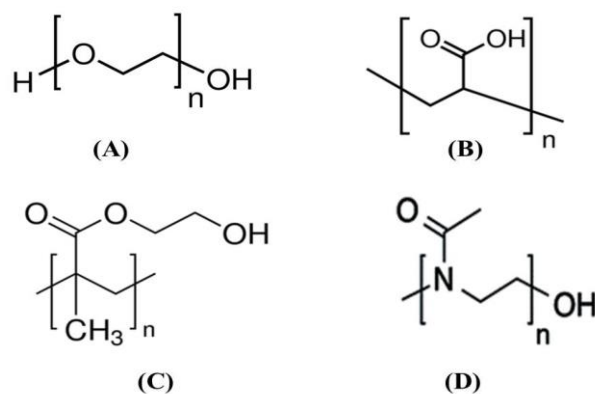


Figure 6- Chemical structure of hydrophilic polymers commonly used in block copolymers A) poly (ethylene oxide), B) poly (acrylic acid), C) poly (2-hydroxyethyl methacrylate) and D) poly (2-methyl-2-oxazoline).

There is a plethora of hydrophobic polymer moieties that have been described in the literature such as poly(propyleneoxide) (PPO), polystyrene (PS), poly (L-lactic acid) (PLLA) and poly (diethylaminoethyl methacrylate) (PDEA) (Figure 7).

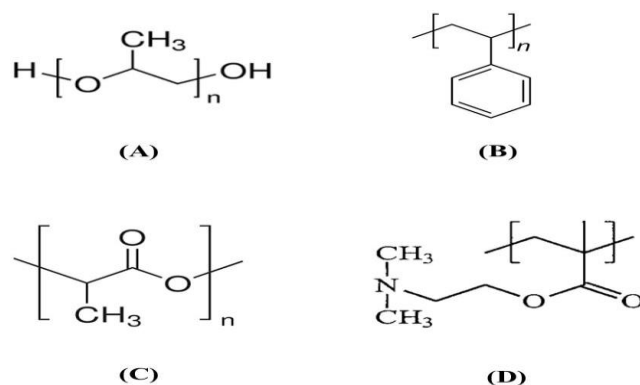


Figure 7- Chemical structure of hydrophobic polymers commonly used in block copolymers A) poly (propyleneoxide), B) polystyrene, C) poly (L-lactic acid) and D) poly (diethylaminoethyl methacrylate).

Polymers for the preparation of self-assembled polymer micelles for drug delivery can either be di-block (hydrophilic-hydrophobic) or tri-block (hydrophilic-hydrophobic-hydrophilic) in common (Torchilin, 2006).

One of the common tri-block (ABA) systems is Poloxamers also known by the trade name Pluronics® which consists of poly (ethylene oxide)-block-poly (propylene oxide)-block-poly (ethylene oxide) PEO-PPO-PEO. It is highly biocompatible and resistant to protein adsorption and cellular adhesion due to its amphiphilic nature (Yue and Ian, 2016, Elena and Alexander, 2008).

Most other amphiphilic block copolymers have been formulated from, poly(N-isopropylacrylamide), Poly(E-caprolactone), poly(methyl methacrylate), and poly(l-lactide) as a hydrophobic polymer segment and Poly(ethylene glycol) (PEG) as a hydrophilic polymer segment which is considered as a gold standard in the field of drug delivery among other hydrophilic polymers (Xinru *et al.*, 2009, Grossen *et al.*, 2017, Shalgunov *et al.*, 2017, Jiang *et al.*, 2017)

1.3.2- Graft copolymers

Generally, graft copolymers are easier to synthesize than block copolymers and offer all its properties. Graft copolymers can be made by attaching polymeric side groups onto the linear polymer backbone, where the grafted side groups have different properties than the backbone and depending on the nature of these two parts, graft copolymers have found a wide range of applications (Sebastian and Axel, 1999). In this respect, Rieger and colleges reported the use of ring-opening copolymerization to prepare novel biodegradable and biocompatible poly (ϵ -caprolactone)-graft-poly(ethylene oxide), PCL-*g*-PEO. These amphiphilic graft copolymers have similar surfactant properties of PEO-*b*-PCL diblock copolymers (Rieger *et al.*, 2006).

Graft copolymers have shown promising potential in drug, proteins and gene delivery application. Several monomers have been used for this purpose such as methyl methacrylate (MMA), N-dimethylaminoethyl methacrylate hydrochloride (DMAEMC), methacrylic acid (MAA) and N-trimethylaminoethyl methacrylate chloride (TMAEMC) (Sadeghi and Heidari, 2011, Qian *et al.*, 2006). In the aqueous medium, the hydrophobic moieties form the inner core of the structure, and the bioactive material molecules are incorporated into the hydrophobic inner core, particularly for hydrophobic drugs (Figure 8).

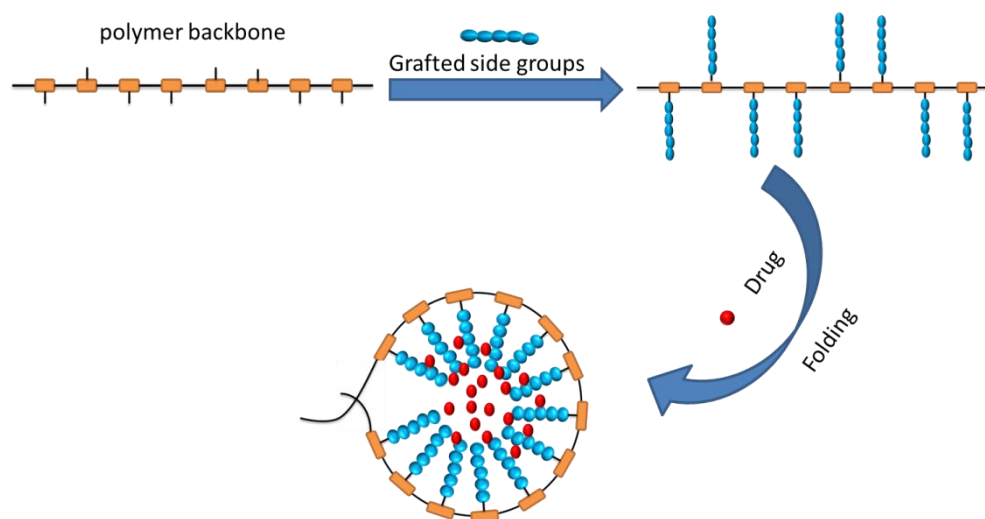


Figure 8- Schematic illustration of drug incorporation into amphiphilic copolymer in aqueous medium.

Grafting copolymerization has also been used to graft synthetic polymers onto natural polymers to add some new properties, in the meanwhile reduce the initial properties loss due to change in the original structure. Natural polymers such as chitosan, alginate, starch,

gelatine and cellulose seem attractive raw materials in this respect due to their structural variety and water solubility. Mochalova and his co-workers performed graft copolymerization of acrylamide in water-acetic acid solutions of chitosan. The graft copolymerization of acrylamide with chitosan using ammonium persulfate as an initiator has also been reported. The studies showed that the copolymer films show better mechanical properties as compared with those of polysaccharide (Mochalova *et al.*, 2006). In another study by Sadeghi and Heidari, a pH-sensitive gelatine-based hydrogel was synthesized through cross-linking graft copolymerization of methacrylic acid (MAA) onto gelatine. They concluded that the gelatine-g-PMAA hydrogel demonstrated a pH-responsiveness character at pH between 2 to 8; give the synthesized hydrogels great potential as a good candidate for controlled delivery of bioactive agents (Sadeghi and Heidari, 2011).

Smart polymers or stimuli-responsive polymers have been extensively used for responsive drug delivery. The following outline is provided as an overview of smart polymers with some examples.

1.4- Smart polymers

Smart polymers or so-called “Stimuli-responsive polymers” are an exciting and emerging class of macromolecule materials which respond to an internal or external stimulus by changing their dimension, structure, or aggregation state (Menglian *et al.*, 2017, Qi *et al.*, 2017). Many Stimuli-responsive polymers are found in nature, including proteins, polysaccharides and nucleic acids (Pasparakisa and Vamvakaki, 2011).

In general, the stimuli can be either physical, chemical or biochemical. Typical physical stimuli are temperature, ultrasound, light, and magnetic and electrical fields whereas chemical stimuli comprise the solution pH and the addition of salt or metals, while biochemical stimuli include the occurrence of biomolecules and bioactive molecules such as proteins, polysaccharides, amino acids and glucose (Manourasa and Vamvakaki, 2017). Table 2 below provides examples of various stimuli and responsive materials. Sophisticated polymeric systems, that respond to combinations of two or more of the various stimuli, which are known as dual or multi-stimuli-responsive polymers, can be even smarter than their mono-responsive counterparts and further enhance the loading efficiency and prolonged sustained release times (Karimi *et al.*, 2015).

Table 2- Various stimuli and responsive materials.

Environmental stimulus	Responsive material	Reference
Temperature	N-(2-hydroxypropyl) methacrylamide (HPMA), Poly (N-isopropylacrylamide) (PNIPAAm), Poly(2-isopropyl-2-oxazoline) (PiPOx)	Tang <i>et al.</i> , 2017 Škvarla <i>et al.</i> , 2017 Kim <i>et al.</i> , 2016 Alfurhood <i>et al.</i> , 2016
pH	Poly (acrylic acid), poly (methacrylic acid) (PMAA), poly (ethylene imine), poly(L-lysine), and poly(N,N-dimethyl aminoethyl methacrylamide)	Karolewicz <i>et al.</i> , 2016
Temperature and Light	Modified poly(acrylamide)s	Kawatani <i>et al.</i> , 2017
Electric field	poly(vinyl alcohol) and poly(acrylic acid-co-2-acrylamido-2-methyl propyl sulfonic acid)	Song-Bai <i>et al.</i> , 2008
Ultrasound	poly(lactic acid-co-glycolic acid)	Zhang <i>et al.</i> , 2014
Temperature and electric field	Poly(pyrrole)	Jun Ge <i>et al.</i> , 2012
Temperature and pH	poly(β -amino ester)	Lu <i>et al.</i> , 2017

Researchers have used these stimuli-responsive polymeric systems to endorse the drug loading and to modulate the rate and site of drug release. The use of these polymers has shown enhanced drug release behaviour depending on the type of stimulus and rate of response (Figure 9). In this section, some specific stimuli-responsive polymer systems will be discussed. Special emphasis is placed on thermo-responsive polymers.

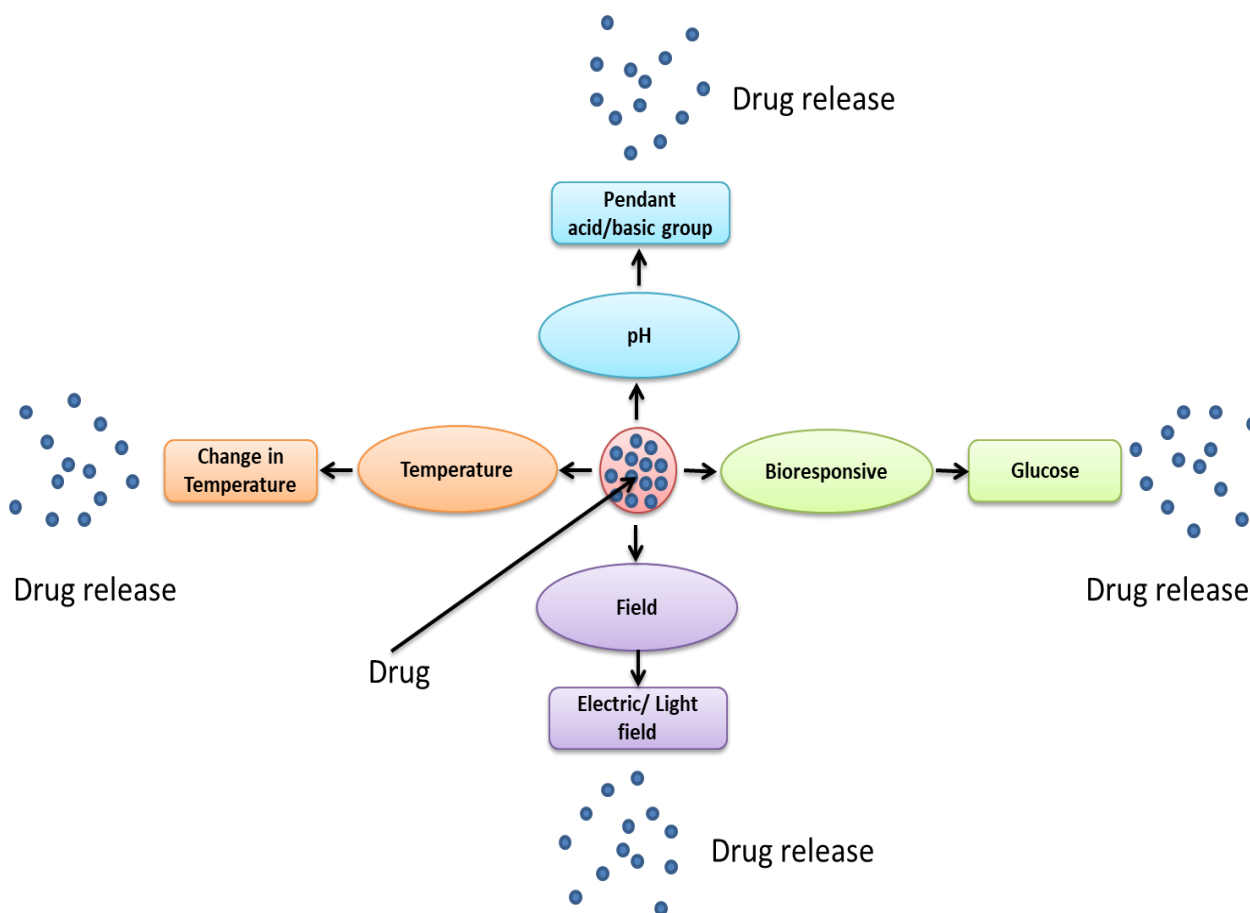


Figure 9- Different types of smart polymeric drug delivery systems for controlling drug release.

1.4.1- pH-Responsive polymers

pH-responsive polymers are polyelectrolytes that endure in their structure ionisable groups (weak acidic or basic groups) with pKa values 3 to 10. These groups either accept or donate protons in response to changes in environmental pH. The pendant acidic or basic groups such as carboxylic, sulfonate and primary or tertiary amino groups on polyelectrolytes demonstrate a change in ionization state as a function of pH. The alterations in structural and properties such as solubility, surface activity, and chain conformation have been explained by changes in the ionization, where specific polymer groups switch between a neutral and charged state (Figure 10) (Mihai *et al.*, 2011). These unique properties of pH-responsive polymers have sparked particular interest in their use in drug delivery applications based on the fact that the human body presents a range of pH along the gastrointestinal tract and also in some specific segments of tumours, which provide environmental stimuli for responsive drug release.

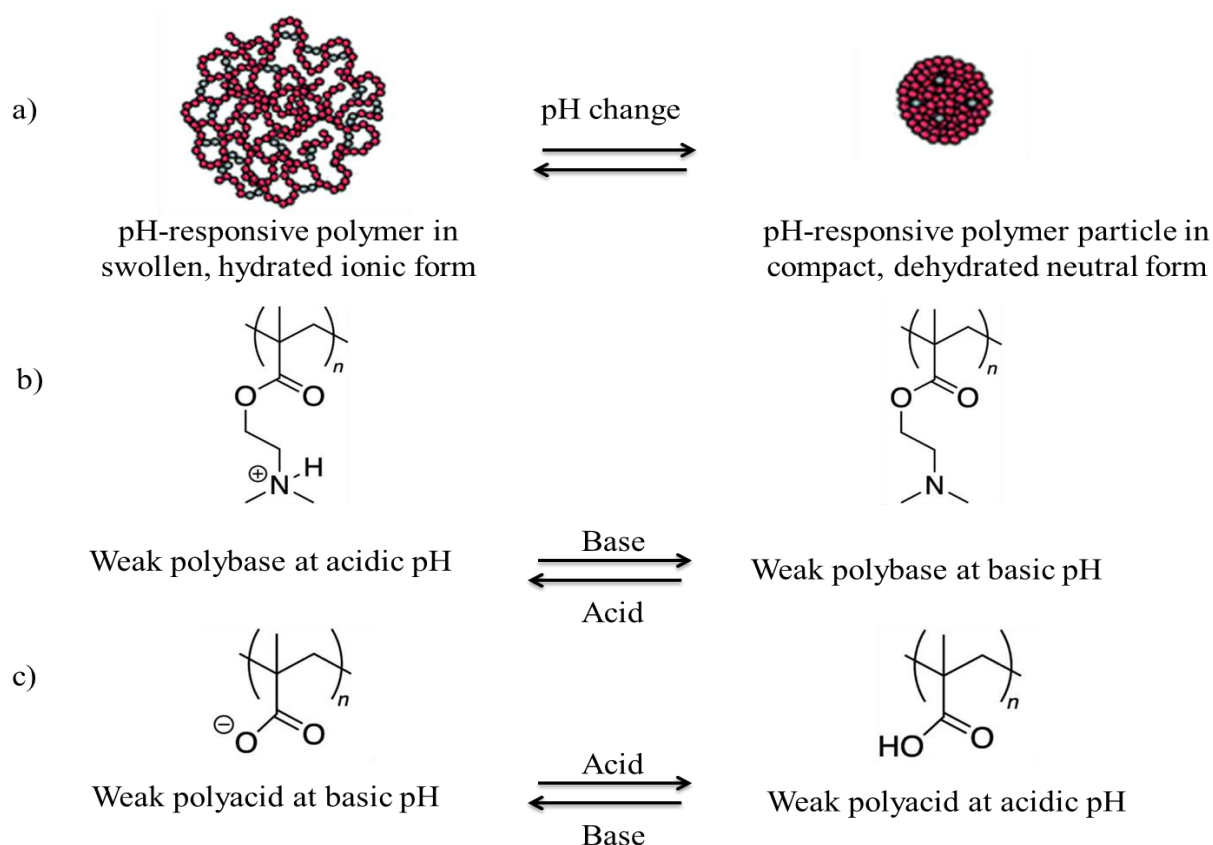


Figure 10- Representation of the switch between a neutral and charged state of pH-responsive polymer particles.

There are a number of different mechanisms which control the release of entrapped/encapsulated drug from a pH-responsive polymer including diffusion controlled, swelling controlled, and chemically controlled mechanisms (Muhammad *et al.*, 2017).

Recently, pH-responsive crosslinked natural rubber (NR) and poly (4-vinylpyridine) (P4VP) via free radical crosslinking reaction have been synthesised (Chanon *et al.*, 2017). It was reported that the P4VP-crosslinked NR was found to be pH-responsive in acidic solution. The release of dye from the P4VP-crosslinked NR could happen upon increasing the pH of solution above 4 (Chanon *et al.*, 2017).

Mitra and Kamyar fabricated magnetic nanoparticles grafted pH-responsive poly (methacrylic acid-co-acrylic acid)-grafted poly(vinylpyrrolidone). They found that at pH 1.2 the cumulative release of the drug from nano-carrier was 78% compared with 5 and 31% at

pH 5.5 and 7.2 respectively. They concluded that the drug release kinetics and mechanism follows a Fickian diffusion controlled and Fickian pattern (Mitra and Kamyar, 2017).

An acidic tumour pH-responsive nanophotomedicine (pH-NanoPM) was synthesised by Park and colleagues for targeted photodynamic therapy (PDT). It was reported that the pH-NanoPM was fabricated by self-assembly of a pH-responsive polymeric photosensitizer (pH-PPS) containing pH-cleavable methoxypolyethylene glycol (pH-C-mPEG) with a size of ~110 nm. They also reported that pH-NanoPM showed improved cellular internalisation at acidic tumour pH compared to normal pH when exposing HeLa human cervical cancer cells, which led to a remarkable cancer cell killing effect (Park *et al.*, 2016).

1.4.2- Bio-responsive polymers

Bio-responsive polymers present an interesting option for the delivery of some hormones and drugs. Glucose-responsive hydrogels, one of the bio-responsive polymers, are a powerful approach for the treatment of diabetes (Dong *et al.*, 2016, Matsumoto *et al.*, 2017). The approach is based on delivering appropriate amounts of insulin in response to changing glucose levels. As glucose diffuses within the hydrogel, it converts to gluconic acid by glucose oxidase (GOD) catalyses leading to decrease in the pH of the environment resulting in swelling or collapsing the gel depending on its characteristics and the subsequent release of insulin (Nicholas and Christie, 2006) (Figure 11).

Kataoka and colleagues have previously reported that a gel composed of N-isopropylacrylamide (NIPAAm) and 3-acrylamidophenylboronic acid (AAPBA), demonstrates a reversible volume change in response to glucose concentration. Kataoka found that adequately controlled and pulse-shaped release of insulin can be achieved at pH 9 and 28 °C (Kataoka *et al.*, 1998).

In another interesting piece of research, the self-assembly of two types of diblock copolymers, poly(ethylene glycol)-*b*-poly(aspartic acid-co-aspartamidophenylboronic acid) (PEG-*b*-Poly(Asp-co-AspPBA)) and poly(N-isopropylacrylamide)-*b*-poly(aspartic acid-co-aspartamidophenylboronic acid) (PNIPAM-*b*-Poly(Asp-co-AspPBA)) have been used to develop a glucose-responsive complex polymeric micelle (CPM). The block copolymers form complex micelles with a novel core-shell-corona structure by controlling the weight ratio between PNIPAM and the PEG ($W_{\text{PNIPAM}}/W_{\text{PEG}} = 6/4$). The CPM shows reversible glucose-induced swelling changes in response to a stepwise change in the glucose

concentration, facilitating the repeated on-off release of insulin controlled by glucose level. It was also reported that the CPM provides effective protection for the encapsulated insulin against protease degradation (Liu *et al.*, 2013).

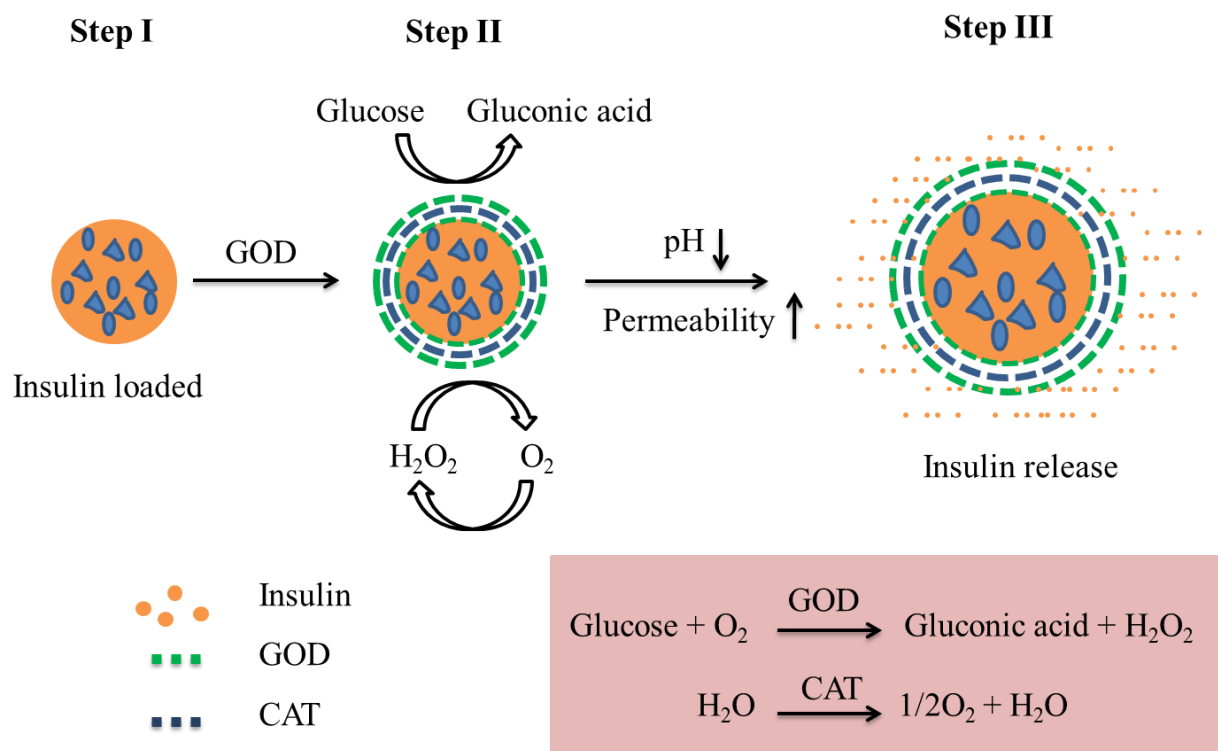


Figure 11- Representation of the glucose-responsive controlled release of insulin.

1.4.3- Light Responsive polymers

Inexpensive and easily controlled are the main advantages that make light (ultraviolet or visible) represent as one of the most important external stimuli for drug delivery systems (Thakur and Thakur, 2016). When a light source with appropriate wavelength is applied to the hydrogels, which employs photosensitizers such as azobenzene, stilbene, and triphenylmethane, the chromophore absorbs the light, resulting in an increase in local temperature of the hydrogel. As a result, the hydrogel changes its degree of swelling behaviour in response to temperature change (Jin *et al.*, 2010).

One of the major limitations in the use of light stimuli-responsive polymers in drug delivery systems is leakage of non-covalently-bound chromophores during swelling or shrinking of the system which leads to an inconsistent and slow response of the hydrogel towards the stimulus. A second drawback from the point of view of the researchers is dark toxicity (Honey *et al.*, 2014).

Jiang and co-workers described the synthesis of diblock copolymers containing hydrophilic poly (ethylene oxide) (PEO) and a hydrophobic poly(methacrylate) bearing pyrene pendant groups (PPy). The self-assembly of amphiphilic block copolymers bearing these groups in water led to the formation of micelles, which can be dissociated by light. UV light irradiation of the micellar solution triggers the cleavage of the photo-responsive pyrene moieties, generating a hydrophilic poly (methacrylic acid). As a result of the cleavage, the polymer micelles will be completely dissociated (Jiang *et al.*, 2005).

Recently, a photo-responsive lipid-polymer hybrid nanoparticle system consisting of three distinct functional components has been reported. This comprised of (i) a poly (D,L-lactide-co-glycolide) (PLGA); (ii) a soybean lecithin monolayer and (iii) a photo-responsive polymeric shell with anti-biofouling properties have been synthesised. It was reported that the poly (D,L-lactide-co-glycolide) (PLGA) used to encapsulate doxorubicin while soybean lecithin monolayer acts as an active barrier to prevent drug leakage. Furthermore, the nanoparticle stability under light irradiation was enhanced by the photo-responsive polymeric shell with anti-biofouling properties. The *in vitro* result indicated that 76 % of the encapsulating drug was released upon light irradiation against 10% release without light irradiation. The results obtained from the confocal microscopy and flow cytometry support the light-controlled drug release behaviour inside the cancer cells (Yao *et al.*, 2017).

1.4.4- Thermo-responsive polymers

Generally, the solubility of most substance will increase with increased temperature. However, smart polymers have been developed which exhibit thermo-responsive solubility changes (increase or decrease) in response to a change in temperature. This unique property has resulted in a great focus on thermo-responsive polymers as modern, highly controllable drug delivery systems.

In general, thermo-responsive polymers can be categorised into two groups according to either their lower critical solution temperature (LCST) or their upper critical solution temperature (UCST) properties. Some of the thermo-responsive polymers have been recorded in Table 3.

Almost all applications of these polymers rely on sudden solubility changes in aqueous environments at the lower critical solution temperature (LCST). The rapid change in solubility of thermo-responsive polymers around LCST can be attributed to the considerable

hydrogen bonding interactions with neighbouring water molecules, and limited intra/inter-molecular hydrogen bonding between polymer molecules (Figure 12). At increased temperatures, hydrogen bonding between the polymer and water breaks down and intra-and intermolecular hydrogen bonding / hydrophobic interactions dominate above the LCST, which results in a transition in solubility (Roy *et al.*, 2013).

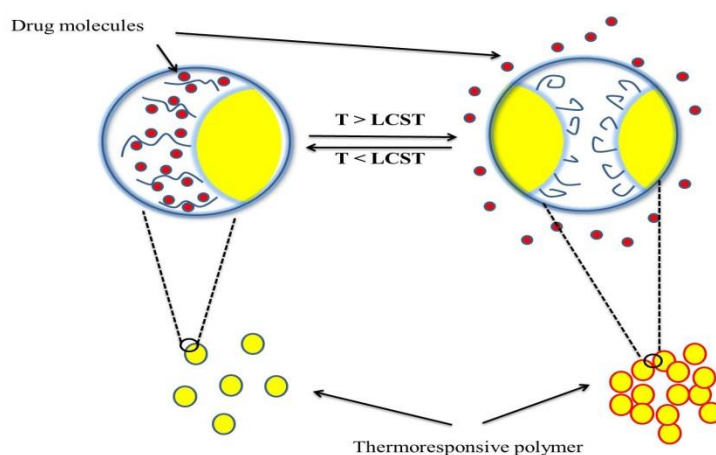
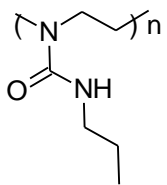
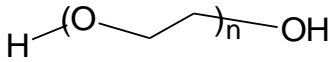
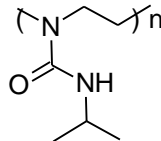
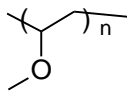
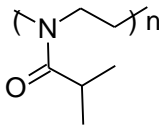
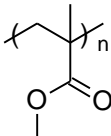


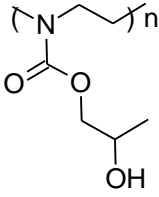
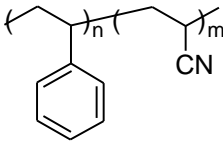
Figure 12- Schematic illustration of the LCST-type phase transition.

There are two important characteristics of thermo-responsive polymers: 1) tunability of their LCST and 2) sharp phase transitions in both heating and cooling processes. Dehydration and rehydration of the polymer chains are effected by the sharpness in phase transitions, which rely on the interaction balance among polymer chains and between polymer chains and the solvent water as well (Yan *et al.*, (2012).

One of the most successful polymeric systems which have been used for passive drug targeting purposes, is N-(2-hydroxypropyl) methacrylamide (HPMA) based copolymers (Kadajji and Betageri, 2011). Poly(N-(2-hydroxypropyl) methacrylamide) (pHPMA) possesses desirable properties as drug carriers such as non-immunogenicity, biocompatibility, and the possibility for functionalisation. These properties have resulted in a wide range of pharmaceutical and biomedical applications as well as in the micelle technology research (Talelli *et al.*, 2010). pHPMA self-assemblies have also been used in the design of hybrid block and grafted HPMA copolymers that self-assemble into smart hydrogels (Kopeček and Kopečková, 2010).

Table 3- Examples of thermo-responsive polymers.

Polymer	Type	CST	Reference
Poly(N-n-propylacrylamide) (PNNPAM) 	LCST	10	Ito and Kubota, 1997
Poly(ethylene oxide) (PEO) 	UCST	296	Bae <i>et al.</i> , 1991
Poly(N-isopropylacrylamide) (PNIPAM) 	LCST	32	Klaus <i>et al.</i> , 2009
Poly(vinyl methyl ether) (PVME) 	LCST	-15, -25	Van <i>et al.</i> , 2007 Assche <i>et al.</i> , 2011
Poly(2-isopropyl-2-oxazoline) (PiPOx) 	LCST	36	Uyama and Kobayashi, 1992
Poly(methyl methacrylate) (PMMA) 	UCST	87 or above	Cowie <i>et al.</i> , 1986

<p>Poly(2-hydroxypropylacrylate) (PHPA)</p> 	LCST	30-60	Vo <i>et al.</i> , 2010
<p>Poly(styrene)/poly(styrene-co-acrylonitrile) (PS/SAN)</p> 	UCST	171	Qi <i>et al.</i> , 2004

There are many examples of HPMA based copolymers being used for drug and gene delivery applications (Burke and Pun, 2010, Tang *et al.*, 2017, Abd Ellah *et al.*, 2015, Johnson *et al.*, 2011). Qin *et al.*, prepared and evaluated co-polymers consisting of N-3-aminopropyl methacrylamide (APMA) and N-2-hydroxypropyl methacrylamide (HPMA) to develop novel non-viral gene transfection carriers. They used free radical synthesis in order to fabricate the copolymers followed by total guanidination of amino groups. They found that parent cytotoxicity and efficient transfection decreased significantly at relative low charge ratios (Qin *et al.*, 2012).

Recently, Chu *et al.*, reported the use of HPMA-co-APMA polymer backbone grafted by BM9 peptide, which included bivalirudin fused to a protease substrate sequence. This copolymer formula was used for localized and prolonged bivalirudin delivery following spinal cord injuries. The results show decreased proliferation and reduced gliosis in rats treated with these bivalirudin-release depots (Chu *et al.*, 2015).

Another example of the most widely thermo-responsive polymer (amide type) is poly (N-isopropyl acrylamide) (PNIPAM). It has a sharp and reversible phase transition at a temperature near to body temperature because of the secondary amide group and a hydrophobic isopropyl group, this behaviour can reveal that some hydrogen bonds between C=O and H₂O decreased, while another type of hydrogen bonding formed between C=O and NH groups throughout the coil-globule transition (Lai *et al.*, 2012).

Contreras-García *et al.*, grafted polypropylene (pp) by N-isopropylacrylamide (NIPAAm) and N-(3-aminopropyl) methacrylamide hydrochloride (APMA) by using γ -irradiation to obtain interfaces polymers that are stimuli-responsive under physiological conditions. The scientific team reported that when they used 1 M NIPAAm/0.5 M APMA the copolymer around the physiological temperature showed rapid and reversible transitions showing a LCST, while with higher content of APMA the hydrophilicity of PP-g-(1NIPAAm-r-1APMA) becomes higher and that prevented the grafted polymer from shrinking (Contreras-García *et al.*, 2010).

Another report done by Yuting *et al.*, refer to using reversible addition fragmentation chain-transfer polymerization to prepare hydrophilic block copolymers, poly(N-(3-aminopropyl)methacrylamide hydrochloride)-block-(N-isopropylacrylamide) (PAMPA-*b*-PNIPAM). The researcher found when the solution temperature is increased that these block copolymers will self-assemble into vesicles, with the size and size distribution of the vesicles influence by the heating rate and the solution concentration (Yuting *et al.*, 2006).

Thermo-responsive polymeric materials can elicit potentially a therapeutically effective dose without unacceptable adverse effects. More recently, a number of studies have confirmed the ability of the thermo-responsive polymeric micelle to release its payload into the surrounding environment by relatively small differences in temperature.

In one of these studies (Sun *et al.*, 2014) they used methotrexate as an anticancer model. Methotrexate is a poorly soluble anticancer drug that introduces severe side effects, and thus imposes major restrictions on both clinical efficacy and therapeutic safety. To address these problems, Sun and colleagues loaded the methotrexate drug into poly(N-isopropylacrylamide-co-acrylamide)-*b*-poly(n-butyl methacrylate) block copolymer micelles. The ultimate goal was to produce a polymer formulation which could be stimuli-responsive on/off release and spatial specificity. Sun's group reported that the thermally triggered release of methotrexate was observed *in vitro*. Also, this work showed that the cytotoxicity activity of methotrexate-loaded micelles, on Lewis lung carcinoma cells, was considerably increased in combination with hyperthermia (Sun *et al.*, 2014).

In another study, doxorubicin (DOX) and camptothecin (CPT) were loaded into shape transformable amphiphilic scaffolds by Kashyap and Jayakannan. The *in vitro* drug release studies revealed that the DOX loaded scaffolds showed a selective release to deliver 90% of loaded drug at the cancer tissue temperature (40-43 °C) as compared to that of normal body

temperature (37 °C, <10%). The kinetics of DOX release at the cancer tissue temperature indicated that the formulation followed non-Fickian diffusion kinetics (Kashyap and Jayakannan, 2014).

1.4.5- Multi-responsive polymer

Some smart polymer systems have been devised to respond to more than one stimulus. These polymer systems could present a unique opportunity to fine tune their response to each incentive individually.

Ryskulova *et al.*, investigated the pH and temperature dual responsive system comprised of poly(phenylene vinylene)s (PPVs) having both carboxylic acid and methoxyoligoethylene glycol pendant groups. The fluorescence intensity is affected by pH change in a range from 3 to 10 and temperatures from 10 °C to 85 °C (Ryskulova *et al.*, 2016). In another interesting piece of research, an amphiphilic copolymer containing PEO and poly N-3-acrylamido phenylboronic acid (PAPBA) linked by a disulfide bond (PEO-SS-PAPBA) was fabricated by Yuan and co-workers. This copolymer showed glucose, pH and redox triple responses. They also reported that the controlled release of insulin could be achieved via adding glucose or glutathione (GSH) (Yuan *et al.*, 2014).

Zhou and colleagues reported that selenium-containing polymer with the drug could be used as successful multi-responsive drug release. They prepared micelles of the selenium-containing PEG with redox-triggered property and the metal-organic frameworks (MOFs) with pH-triggered property in drug delivery systems. They concluded that the cores easily collapsed in the presence of redox agents and that the shell can breakdown only under low pH conditions (Zhou *et al.*, 2017).

1.5- Combination of stimuli-responsive polymers and magnetic nanoparticles properties.

In recent years, the combination of stimuli-responsive polymers and magnetic nanoparticles into a single platform has attracted much consideration due to their unique properties. Magnetic nanoparticles (MNPs) can be triggered by internal or external stimulus which leads to internally stimulate changes to the polymeric network, allowing for a versatile stimuli-responsive system. Many of the MNPs types have been used for this purpose including hybrid nanoparticles (Jalili *et al.*, 2016, Song *et al.*, 2015).

Hybrid nanoparticles (HNPs) that are composed of iron oxide cores coated with gold have received increased interest in terms of using these nanostructures for image-guided drug delivery (Barnett *et al.*, 2013). Moreover, the introduction of HNPs between the polymer structures provide localized trigger of heating, when irradiated with a short laser burst, they lead to remote control of bulk polymer shrinkage (Roach *et al.*, 2013).

Using laser irradiation for medical applications has helped researchers to achieve specific targeting, in addition to, reduce the energy level to be compatible with medical safety standards. This phenomenon has been confirmed by using the targeting agents to diminish the laser power needed to reach therapeutic effects in cancers (Kirui *et al.*, 2010). Additionally, the magnetic properties of the iron oxide core confer imaging capability using magnetic resonance imaging (MRI) and hence real time tracking *in vivo* is possible.

Recently Hoskins *et al.*, reported the fabrication of Fe₃O₄-PEI-Au-PEG (HNPs) using poly(ethylenimine) as an intermediate separating the core and shell. The gold surface was functionalized via coating by poly(ethylene glycol) (PEG) which consist of the thiol group (-SH). The HNPs seemed to reduce T2 values in line with previously clinically utilized MRI contrast agent Feridex[®] (Hoskins *et al.*, 2012b). Roach and co-workers reported the *in vitro* release of methylene blue (as a model drug) from smart scaffolds based on thermo-responsive poly(N-isopropylacrylamide) (pNiPAM). They reported that the incorporation of HNPs resulted in scaffold deformation after very short times (seconds) of laser irradiation which lead the model drug to be released during a remote structural change of the scaffold (Roach *et al.*, 2013).

Conjugation of HNPs and polymers to the thiol-containing oxadiazole (Ox) groups is an attractive method to fabricate bi-functional imaging and as a drug delivery platform. In this respect, a new class of poly (allylamine) (PAA) polymer containing rigid oxadiazole (Ox) groups has been prepared by Barnett and colleagues. *In vitro* results showed that polymer-drug conjugates had significantly higher drug uptake in BxPC-3 cells with decreased IC₅₀ compared with free drug (Barnett *et al.*, 2013). On the other hand, the nano size and negative charge of the gold nanoparticles (AuNPs) could help to penetrate deeply inside the cells (Sonavane *et al.*, 2008). This finding helped considerably in delivering different biomaterials to target cells via conjugation with AuNPs. Moreover, AuNPs are now being developed to improve imaging with MRI and CT due to their ability to be conjugated to molecular proteins on the contrary of the iodine. In this respect, Popovtzer and co-workers reported the ability to

detect head and neck cancer at the cellular and molecular level with standard clinical CT by conjugated UM-A9 antibodies to HNPs (Popovtzer *et al.*, 2008).

1.6- Aims and Objectives

The inclusion of hybrid iron oxide-gold nanoparticles (HNPs) into thermo-responsive copolymer micelles was studied here towards the development of a targeted, thermally-triggered drug delivery system for cancer therapy. Herein, we aim to synthesis of HNPs and an amphiphilic graft polymer composed of a poly(N-(2-hydroxypropyl) methacrylamide) pHPMA backbone, and experimental verification of laser heating of the HNPs, self-assembly of the copolymers to form magnetic micelles, and thermally-enhanced drug release at target cells, in the meantime; enhance solubility of hydrophobic drugs, reduce side effects/toxicities of loaded drugs, which are key factors affecting anticancer drug developments.

Hydrophobic groups of palmitoyl, dansyl, cholesteryl and 5-(4-chlorophenyl)-1,3,4-oxadiazole were grafted onto the primary amine group of APMA monomers. These monomers were polymerised with water-soluble thermo-responsive HPMA. Optimal substitution onto the backbone of both hydrophobic and hydrophilic groups onto the primary amines of the polymer was determined. HNPs were synthesized and incorporated into the intrinsic amphiphiles structure in the oxadiazole modified polymers.

Characterisation of the novel amphiphiles was carried out using various techniques to determine the success of synthesis and physical properties of the system including aggregate formation, the magnetic potential for imaging and potential for heating via laser irradiation. Drug loading studies were carried out in order to determine optimal loading parameters such as initial drug:polymer feed, polymer concentration etc. Drug release studies were performed highlighting the capability of the system to act in a thermo-responsive manner. The structure of the oxadiazole pendant allows for further conjugation of hybrid iron oxide-gold nanoparticles (HNPs) *via* dative covalent linkage between the thiol (-SH) group in the oxadiazole structure and the gold surface of the HNP. This was realised by using heating plates. Biological investigations into drug uptake, cytotoxicity and cellular localisation were realised *in vitro* using simple assays.

Chapter Two

Synthesis and Characterisation of modified monomers and copolymers

2.1- Introduction

Intelligent polymer systems have been attracting wide interest in recent years from the scientific community. Thermo-responsive polymers are a class of smart polymers that respond to change in temperature. The characteristic feature to respond to very slight changes in the environmental conditions has actually made this class of polymers very promising for many applications especially in the field of nanomedicine (Jochum and Theato, 2013).

Here a thermo-responsive polymer was synthesised by introducing hydrophobic groups onto the primary amine group N-(3-aminopropyl) methacrylamide hydrochloride (APMA) then polymerizing with a water soluble N-(2-hydroxypropyl) methacrylamide (HPMA) monomer followed by block copolymerization with poly(ethylene glycol) (PEG).

p(HPMA) (Figure 13) is a thermo-responsive polymer which undergoes a conformational change at its lower critical solution temperature (LCST); this change results in the shrinkage of the polymer structure and disruption of the aggregates leading to drug release (Cunningham *et al.*, 2014).

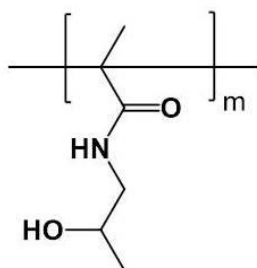


Figure 13- Chemical Structure of pHPMA.

Polymers, which have primary amino groups, such as N-(3-aminopropyl) methacrylamide hydrochloride (APMA) (Figure 14), have been used for post-polymerization modification reactions for the development of new materials for biomedical applications.

N-(3-aminopropyl)methacrylamide, a monomer that contains primary amine, has been used to prepare copolymers and cross-linked micelles for drug and gene delivery (Mendonça *et al.*, 2014). APMA can be modified via its primary amine functional group allowing attachment of various hydrophobic groups by a simple nucleophilic substitution reaction.

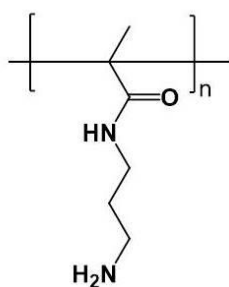


Figure 14- Chemical Structure of APMA.

In this study we grafted hydrophobic groups onto the primary amine group of APMA using palmitoyl, dansyl, cholesteryl and 5-(4-aminophenyl)-1,3,4-oxadiazole (Figure 15). These monomers will ultimately be polymerised with water-soluble thermo-responsive HPMA to form an amphiphilic polymer system to be exploited for drug solubilisation and heat activated release.

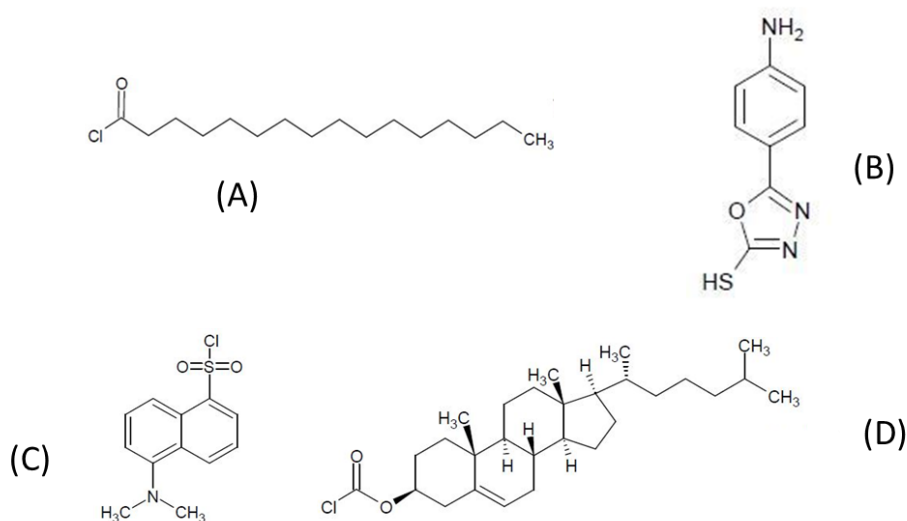


Figure 15- Chemical Structure of (A) palmitoyl chloride (B) 5-(4-aminophenyl)-1 3 4-oxadiazole-2-thiol (c) dansyl chloride (D) cholesteryl chloroformate.

The main purposes of using these hydrophobic moieties are: to develop the self- assembly of amphiphilic block copolymers, improve drug loading, enhance solubility and bioavailability of poorly soluble drugs (Trivedi and Kompella, 2010, Mourya *et al.*, 2011).

Grafted polymers based on poly(allylamine) with 5% and 10% molar substitution of cholesterol and dansyl have been previously reported. These systems have been shown to successfully form self-assemblies by probe sonication in water, demonstrated universal drug solubiliser property and had significantly enhanced propofol, griseofulvin, prednisolone, and Bisnaphthalimidopropylidiaminooctane (BNIPDaoc) solubility (Hoskins *et al.*, 2012, Hoskins *et al.*, 2012a, Hoskins *et al.*, 2010) .

Furthermore, cholesterol is able to regulate the membrane permeability during uptake and intracellular trafficking (Wanga *et al.*, 2015). Zheng *et al.*, showed that cholesterol derivatives like cholesteryl chloroformate can enhance the grafting ratio and drug loading of alginates (Zheng *et al.*, 2014).

Additionally, the use of oxadiazole as a hydrophobic pendant group has also been reported by Barnett *et al.* Barnett exploited the strong dative covalent binding between the thiol in the oxadiazole pendant and the colloidal gold surface of hybrid nanoparticles HNPs (Barnett *et al.*, 2013). They reported that the system was capable of image guided drug delivery for the solubilisation of hydrophobic compounds.

In this work we will employ oxadiazole pendants to confer amphiphilic properties into our polymeric system, subsequently incorporate HNPs into the structure and utilise these HNPs as localised triggers for heat initiated polymer shrinkage and ultimately drug release. In order to develop such a system, a wide range of techniques are required in order to fully characterise the system before drug loading and release studies can be performed. The main methods of characterisation are described below.

2.1.1- Thin Layer Chromatography (TLC)

Chromatography in general is a technique used to separate several different kinds of chemical mixtures. Chromatographic methods included many of the processes that rely on different distributions of the components of the substance to be separated between two phases: one remains constant and called the stationary phase which can be either solid or liquid, and the second phase is called the mobile phase which can be either liquid or a gas (Coskun, 2016).

There are many types of the chromatography such as: Thin layer chromatography (TLC), Gas chromatography (GC), Column liquid chromatography (CLC) and high performance liquid chromatography (HPLC) (Thammana, 2016).

TLC is a simple method that can be used in the laboratory to: monitor reactions by checking whether the reaction is complete or not, determine the number of components in a mixture, identify compounds and purity, in addition to quantification, an ability especially used in pharmaceutical industry etc. (Coskun, 2016, Yua *et al.*, 2016).

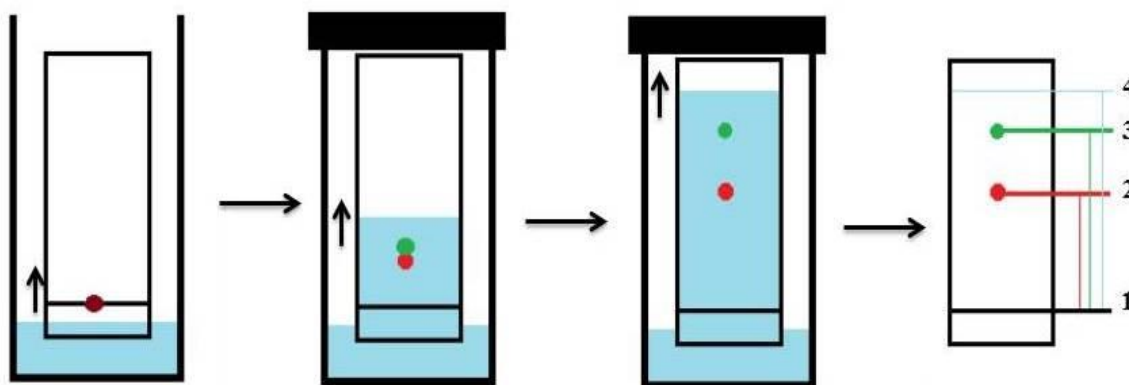


Figure 16- Schematic design of a basic TLC plate for monitoring reaction progress.

In this technique, a sample mixture is introduced in a certain amount about 1 cm from the bottom of the TLC plate and then the plate is placed in a container of solvent (Figure 16). The solvent front travels up the plate by capillary action and draws the compounds up at different speeds, thus separating the components of a mixture. Each component has a retention factor (R_f) which can be calculated by dividing the distance travelled by the sample over the distance travelled by the mobile phase. The R_f value is unique for each compound and it can be used in the qualitative analysis (Yua *et al.*, 2016).

2.1.2- Fourier Transform Infrared Spectroscopy (FTIR)

Fourier Transform Infrared Spectroscopy (FTIR) is a well-known system which has been widely used by chemists to identify the presence of certain functional groups in a sample that can be in the solid, liquid or gaseous state. FTIR spectroscopy offers qualitative and quantitative analysis for organic and inorganic compounds, polymers and polymer blends (Shaikh and Agrawal, 2014).

Infrared spectroscopy is a technique that involves the interaction of infrared radiation with sample molecules. It is based on the fact that most chemical functional groups are absorbing in the infra-red light in a region between $4000\text{-}600\text{ cm}^{-1}$ which led to the change of dipole moment of sample molecule bonds. These regions involve a biochemical fingerprint of the structure and functional groups of each sample (Matthew *et al.*, 2014). FTIR represents the

third generation of infrared spectroscopy. The main idea is based on using an interferometry technique to collect the interferogram of the sample signal followed by performing a Fourier Transform (FT) on the interferogram to get the spectrum.

FTIR spectroscopy has several advantages over the old version IR such as: very fast scan, high resolution, very useful for examining small samples and the digital form in which the data are handled in the computer allows for adjustment and refinement (Williams and Fleming, 2008).

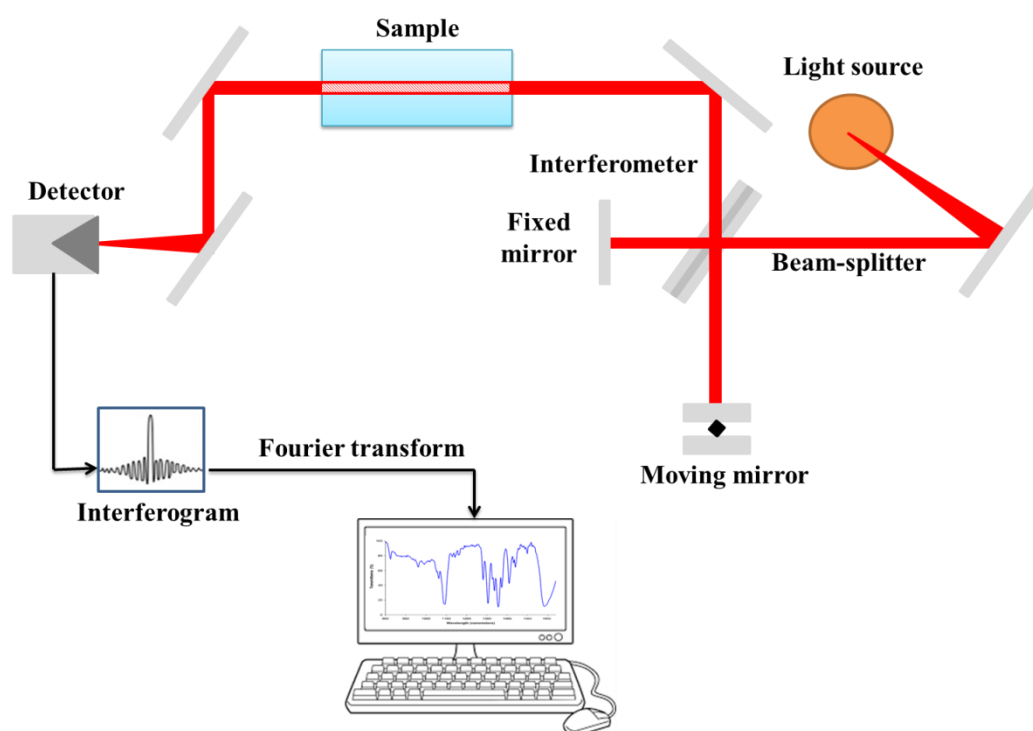


Figure 17- Schematic diagram illustrate the essential features of FTIR spectrometer.

2.1.3- Nuclear Magnetic Resonance Spectroscopy (NMR)

NMR spectroscopy is one of the most important techniques used in chemistry to investigate the structure and chemical environment of unknown compounds (Equbal *et al.*, 2015). In fact there are two common types of NMR spectroscopy are used to characterise organic structures: ^1H NMR and ^{13}C NMR.

Principles of these techniques are based on the fact that nuclei of atoms have magnetic properties that can be used to get chemical information. When these atoms are placed inside a

strong magnetic field there will be splitting of the energies one with the external field, while the other against the field (Gerothanassis *et al.*, 2012).

When an external radio-frequency signal is applied, nuclei at the lower energy level will excite into the higher energy level, when the nuclei returns to its lower level again, energy is released at the same frequency. This phenomenon is called the nuclear magnetic resonance. The absorption of energy can be detected and enlarged as a linear spectrum called the magnetic resonance signal. The applied field can be shield by the electron(s) surrounding the proton leading to a slight different between the externally applied magnetic field and the field at the nucleus. The level of shielding is influenced by several structural properties within the molecule, leading to diverse chemical shift in the NMR spectrum. The common unit to express the chemical shift is part per million (ppm) (Shoolery, 2008, Ashbrook and McKay, 2016).

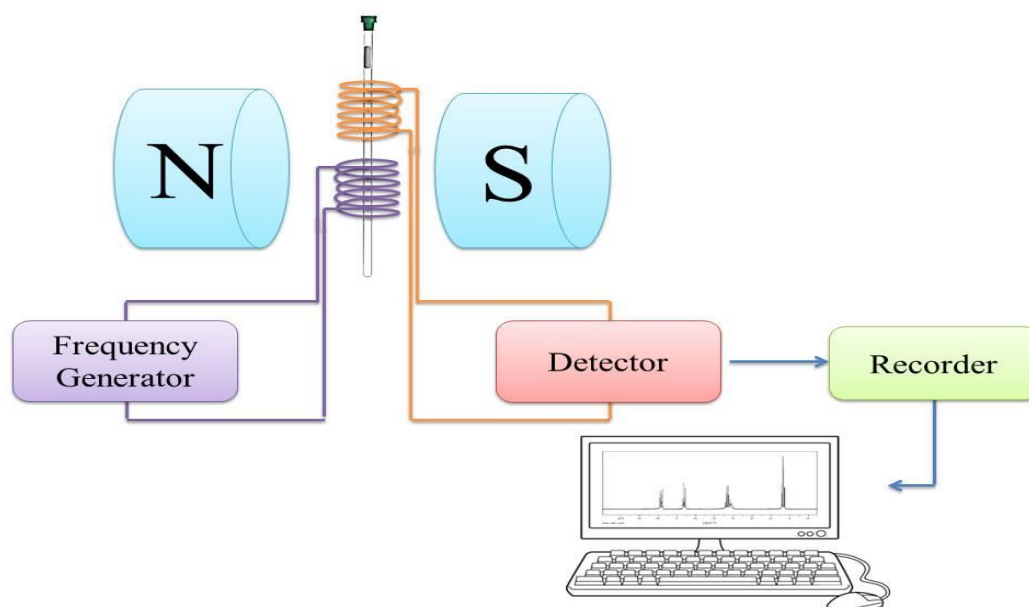


Figure 18- Schematic diagram illustrate the essential features of NMR spectrometer.

2.1.4- Aims and Objectives

The aim of this chapter is to fabricate an amphiphilic monomer composed of N-(3-aminopropyl) methacrylamide (APMA) by substituting (palmitoyl, dansyl, cholesteryl and oxadiazole) groups onto the primary amine in the APMA monomer and then polymerizing with HPMA monomer. All the products were characterized by thin layer chromatography (TLC), melting point (MP), Fourier transform infrared spectroscopy (FTIR) and nuclear magnetic resonance (NMR).

2.2- Materials and Methods

2.2.1- Materials

Item No	Material	Supplier
1	N-(3-aminopropyl) methacrylamide hydrochloride, $\geq 98\%$	Polysciences, Inc.
2	Palmitoyl chloride, 98%	Alfa Aesar
3	Dansyl chloride, 97+%	Alfa Aesar
4	5-(4-chlorophenyl)-1,3,4-oxadiazole-2-thiol, 96%	Alfa Aesar
5	Cholesterol Chloroformate, 95%	Sigma-Aldrich Co.
6	Triethylamine, 99%	Acros organics
7	4-Aminobenzhydrazide, 98%	Alfa Aesar
8	Carbon disulphide, $\geq 99\%$	Sigma-Aldrich Co.
9	Sodium hydroxide, 98%	Fisher Scientific, UK
10	Hydrochloric acid, 37%	Fisher Scientific, UK
11	Succinic anhydride, $\geq 99\%$	Sigma-Aldrich Co.
12	4-dimethyl amino pyridine, $\geq 99\%$	Fluka
13	N-Hydroxysuccinimide, $\geq 98\%$	Alfa Aesar
14	N,N'-Dicyclohexylcarbodiimide, 99%	Acros organics
15	N-(2-hydroxypropyl) methacrylamide	Polysciences, Inc.
16	Azobisisobutyronitrile, 98%	Sigma-Aldrich Co.
17	Dichloromethane, 99%	Fisher Scientific, UK
18	Anhydrous dimethylformamide, 99.8%	Alfa Aesar
19	Anhydrous diethyl ether, $\geq 99\%$	Fisher Scientific, UK
20	Methanol, reagent grade	Fisher Scientific, UK
21	Acetone, $\geq 99\%$	VWR chemicals
22	Deuterated chloroform-D (D, 9.98%)	Cambridge isotope laboratories, Inc.
23	Deuterated dimethyl sulfoxide-D6 (D, min.99.8%)	Apollo scientific limited
24	Deuterated methanol-D4 (D, 9.98%)	Cambridge isotope laboratories, Inc.
25	Ethanol, absolute $\geq 99.8\%$	VWR chemicals

26	Potassium hydroxide, ≥ 99.97	Sigma-Aldrich Co.
27	Poly(ethylene glycol) average mol wt 200	Sigma-Aldrich Co.

2.2.2- Methods

2.2.2.1- Chemical modification reactions

2.2.2.1.1- Substitution of palmitoyl chloride onto the n-(3-aminopropyl) methacrylamide hydrochloride monomer (P-APMA)

P-APMA was synthesized as follows: in a 100 cm³ round bottom flask (RBF), N-(3-aminopropyl) methacrylamide hydrochloride (1.79 g, 10 mmol) and (2.12 g, 10 mmol) palmitoyl chloride were dissolved in 50 mL of anhydrous dimethylformamide (DMF). The reaction was stirred at 0°C under argon atmosphere. After that, (2.92 mL, 21 mmol) of triethylamine was added to the mixture drop wise. The reaction was monitored by TLC plate and the reaction was carried out under stirring at 0°C for 3 h (Figure 19).

The reaction mixture was colourless until the triethylamine was added. A white precipitate was produced as soon as the triethylamine was added.

After evaporation of DMF, the residue was dissolved in DCM and extracted with water to remove all the triethylamine hydrochloride. The organic phase was evaporated to yield a white solid with a yield of 79%.

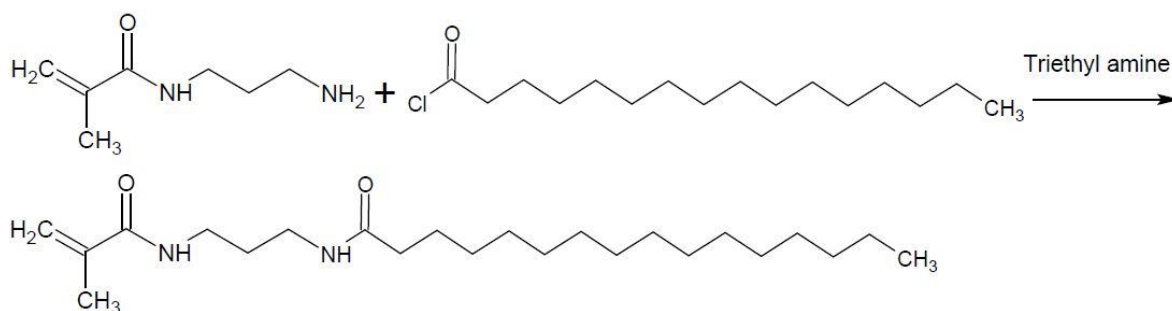


Figure 19- Chemical synthesis of P-APMA.

2.2.2.1.2- Substitution of dansyl chloride onto the n-(3-aminopropyl) methacrylamide hydrochloride monomer (D-APMA)

D-APMA was prepared from a mixture of (1.79 g, 10 mmol) of n-(3-aminopropyl) methacrylamide hydrochloride and (2.69 g, 10 mmol) of dansyl chloride were dissolved in (50 mL) anhydrous dimethylformamide. To this mixture (2.92 mL, 21 mmol) of triethylamine drop wise was added. The reaction has kept on a stirrer for 24 h at 0°C under an argon environment (Figure 20).

The reaction mixture was orange until the triethylamine was added. A white precipitate was produced as soon as the triethylamine was added and the solution colour became yellow.

The reaction solvent (DMF) was evaporated by rotary evaporation, the crude product was re-dissolved in DCM and washed by water to remove the triethylamine hydrochloride and the organic phase was dried under reduced pressure to obtain D-APMA as a dark yellow thick liquid. The yield was 65 %.

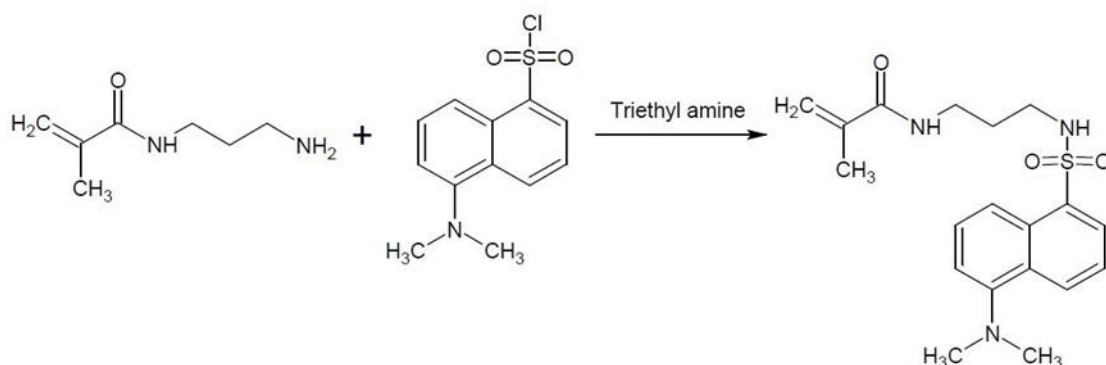


Figure 20- Chemical synthesis of D-APMA.

2.2.2.1.3- Substitution of cholesteryl chloroformate onto the n-(3-aminopropyl) methacrylamide hydrochloride monomer (C-APMA)

C-APMA was synthesized via the reaction of N-(3-aminopropyl) methacrylamide hydrochloride (1.79 g, 10 mmol) and (4.41 g, 10 mmol) of cholesteryl chloroformate in (50 ml) of anhydrous DMF at 0 °C. After that, (2.92 mL, 21 mmol) of triethylamine was added drop wise. A magnetic stirrer and bar was used to stir the suspension. After 24 h stirring at 0°C under argon, the mixture was evaporated to remove the DMF. Then the residue was dissolved in DCM and washed with water. The DCM layer then evaporated by rotary evaporation, C-APMA (75% yield) was obtained as a white solid after dried.

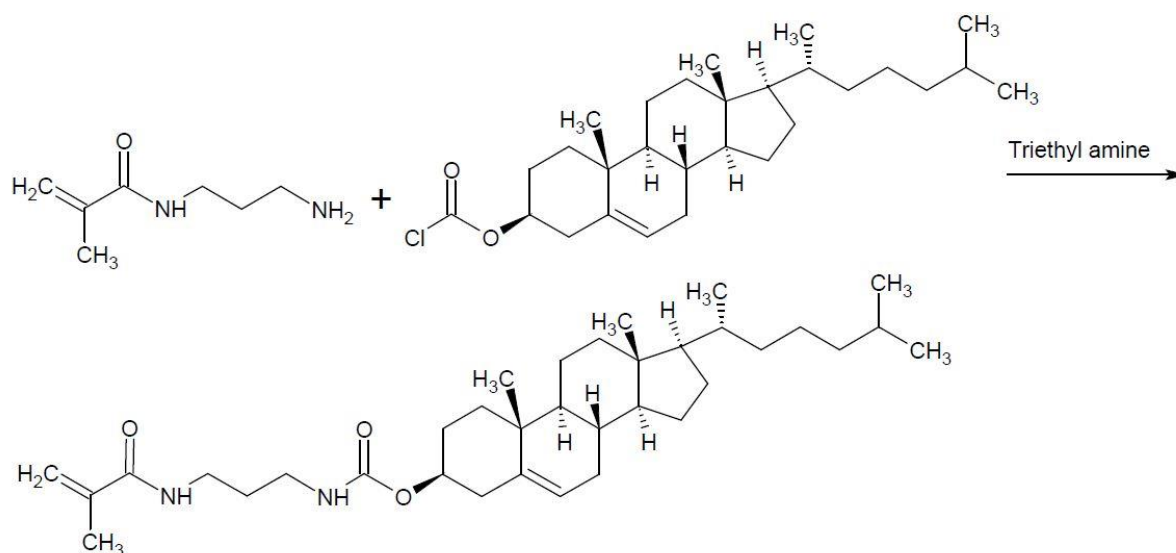


Figure 21- Chemical synthesis of D-APMA.

2.2.2.1.4- Synthesis of 5-(4-Aminophenyl)-1,3,4-oxadiazole-2-thiol (D1)

In 20 mL of 95% ethanol, potassium hydroxide (0.28 g, 5 mmol) and 4-aminobenzhydrazide (0.75 g, 5 mmol) were dissolved. The mixture was stirred at room temperature for several minutes, followed by adding carbon disulphide (0.38 g, 0.3 mL, 7.5 mmol) dropwise to the reaction mixture. The reaction was carried out under reflux for 24 h. After evaporation of the solvent, the residue was dissolved in 50 mL water; the aqueous solution was acidified with diluted hydrochloric acid to pH 6.0. Subsequently, then the precipitate was separated by filtration and washed with water for several times (Figure 22). The yield was 81.9 %.

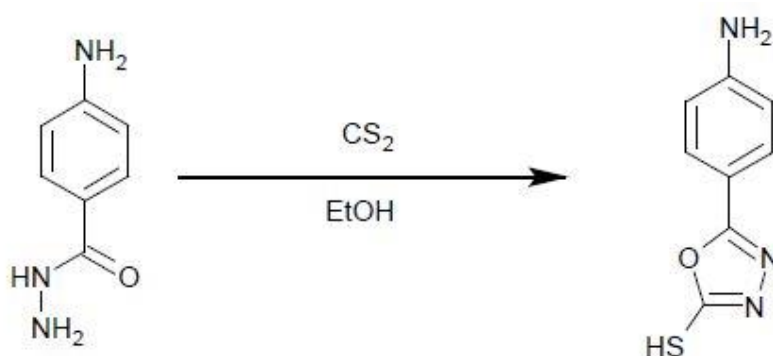


Figure 22- Chemical synthesis of D1.

2.2.2.1.5- Synthesis of 4-oxo-4-{[4-(5-sulfanyl-1,3,4-oxadiazol-2-yl) phenyl] amino}butanoic acid (D2)

Under inert atmosphere 5-(4-Aminophenyl)-1,3,4-oxadiazole-2-thiol (D1) (1.93 g, 10 mmol) and succinic anhydride (2 g, 20 mmol) were dissolved in 50 mL dichloromethane, stirring the mixture at room temperature. 4-dimethyl amino pyridine (1.2 g, 10 mmol) was dissolved in 5 mL DMF and added dropwise. After 2 h reaction at room temperature, the solution was poured into cooled anhydrous diethyl ether to isolate the product as pile yellow powder after washing it with diethyl ether (Figure 23). The yield was 70.54 %.

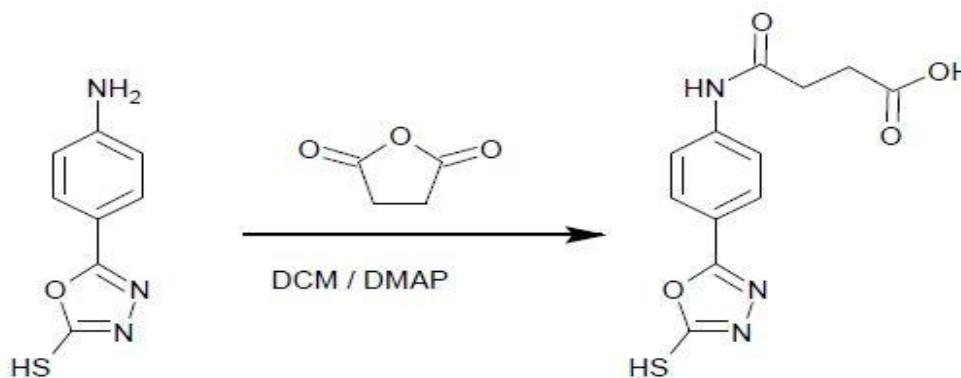


Figure 23- Chemical synthesis of D2.

2.2.2.1.6- Synthesis of 4-[(2,5-dioxopyrrolidin-1-yl)oxy]-4-oxo-N-[4-(5-sulfanyl-1,3,4-oxadiazol-2-yl)phenyl]butanamide (D3)

In a dry RBF, 4-oxo-4-{[4-(5-sulfanyl-1,3,4-oxadiazol-2-yl) phenyl] amino}butanoic acid (1.46 g, 5 mmol), N-Hydroxysuccinimide (0.57 g, 5 mmol) and N,N'-Dicyclohexylcarbodiimide (1.03 g, 5 mmol) were dissolved in 50 mL dichloromethane. After reaction at room temperature for 24 h, the mixture was filtered to remove the reaction side product and the active product was obtained as powder by precipitating in cold anhydrous diethyl ether and then washed several times with anhydrous diethyl ether (Figure 24). The yield was 71.4 %.

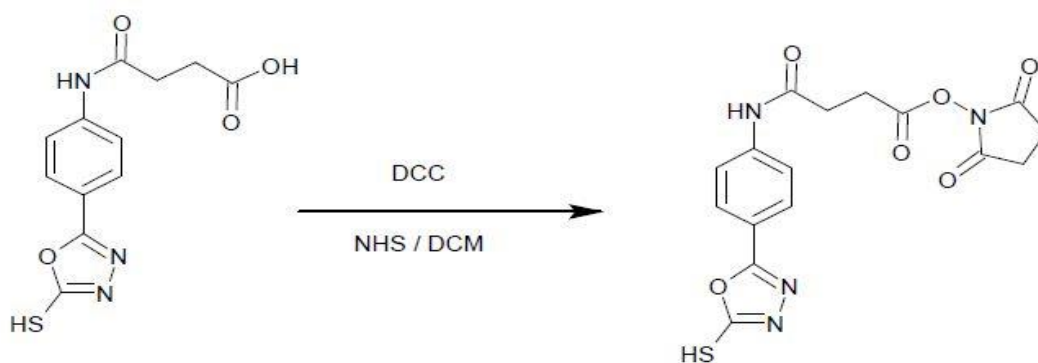


Figure 24- Chemical synthesis of D3.

2.2.2.1.7- Substitution of 4-oxo-4-[(4-(5-sulfanyl-1,3,4-oxadiazol-2-yl)phenyl) amino]butanoic acid onto the n-(3-aminopropyl) methacrylamide hydrochloride monomer (O-APMA)

Under inert atmosphere, 4-[(2,5-dioxopyrrolidin-1-yl)oxy]-4-oxo-N-[4-(5-sulfanyl-1,3,4-oxadiazol-2-yl)phenyl]butanamide (1.17 g, 3 mmol) and N-(3-aminopropyl) methacrylamide hydrochloride (0.53 g, 3 mmol) were dissolved in 30 mL DMF in a 100 mL RBF. The reaction mixture was stirred at room temperature followed by adding 1.6 mL of triethylamine drop wise and the reaction stirred overnight. After removal of DMF with the rotatory evaporator, the crude was washed by anhydrous diethyl ether (Figure 25). The yield was 78%.

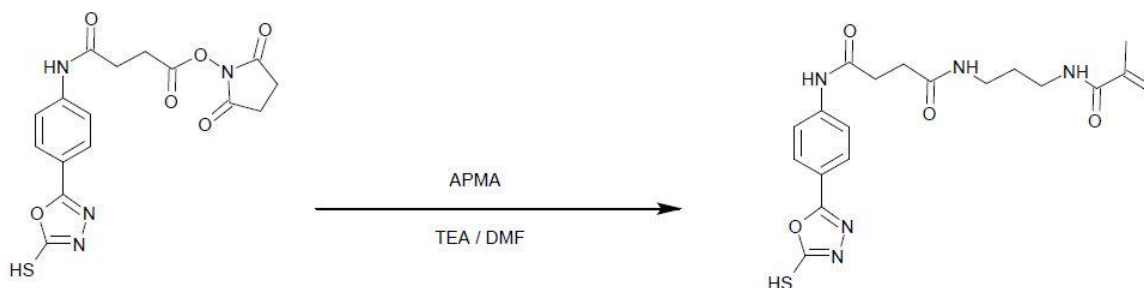


Figure 25- Chemical synthesis of O-APMA.

2.2.2.2- RAFT polymerization of HPMA with modified APMA

HPMA- modified APMA copolymerization (Figure 26) was performed in methanol at 60 °C by using azobisisobutyronitrile (AIBN) as the initiator as follows: An ampoule containing HPMA and modified APMA was attached to the Schlenk-line. After three vacuum-nitrogen cycles to remove oxygen in the ampoule, 5 mL degassed methanol was added, followed by addition of AIBN solution in methanol (0.55 mg in 1 mL) via syringe (Table 4).

The ampoule was sealed and polymerization was performed at 60 °C for 24 h. The polymer was obtained by precipitation into acetone and purified by re-dissolving in methanol and precipitation in acetone two more times.

Table 4- Monomer feeding Ratio.

Copolymerisation ratio	Mole fraction of HPMA, M1	Mole fraction of APMA-R, M2	Monomer feeding ratio (APMA-R / HPMA) per gram				AIBN per gram
			APMA-P	APMA-D	APMA-C	APMA-O	
0.25 %	99.75	0.25	0.0035/0.5000	0.0033/0.5000	0.0049/0.5000	0.0037/0.5000	0.0055
1 %	99	1	0.0236/0.8448	0.0224/0.8448	0.0340/0.8448	0.0249/0.8448	0.0055
2 %	98	2	0.0476/0.8448	0.0453/0.8448	0.0669/0.8448	0.0503/0.8448	0.0055
5 %	95	5	0.1202/0.8202	0.1144/0.8202	0.1690/0.8202	0.1271/0.8202	0.0055
10 %	90	10	0.2380/0.7770	0.2264/0.7770	0.3346/0.7770	0.2518/0.7770	0.0055

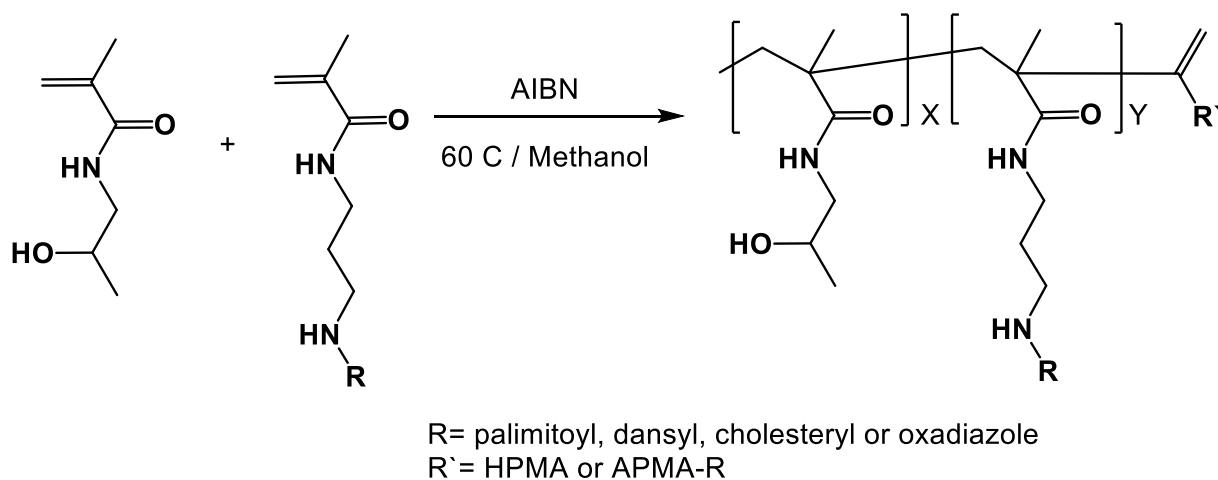


Figure 26- Synthesis of poly (HPMA-co-APMA-R).

2.2.2.3- Synthesis of block copolymer

(HPMA-co-APMA-R)-*b*-PEG diblock copolymer (Figure 27) was synthesized in the presence of a free radical source in methanol. A tube was charged with 10% : 90% or 20% : 80% PEG : HPMA-co-APMA-R molar ratios respectively, and AIBN under nitrogen atmosphere. Reaction was carried out at 60 °C for 24 h with continuous stirring. After the polymerizations were completed, block copolymers were precipitated in methanol.

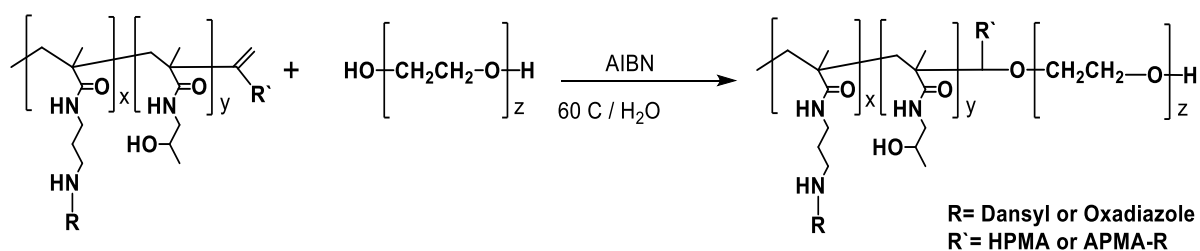


Figure 27- Synthetic scheme for (HPMA-co-APMA-R)-*b*-PEG diblock copolymers.

2.3- Characterisation of modified monomer

2.3.1- Melting point

The melting point for all modified monomers was measured by using Advanced, Digital, Melting Point / SMP3 (Bibby sterilin LTD, UK). Determination of the melting point of each compound consisted of using pre-sealed (one end) capillary tubes to hold samples, filled with 0.1-0.2 g of dry compound. The sample tubes were then placed in the melting point apparatus. Hence, slowly increasing the temperature of the heating block, the melting process was observed through the magnifying lens.

2.3.2- Thin layer chromatography

Thin-layer chromatography (TLC) analyses were carried out using Merck KGaA silica gel 60 F254 using UV detection and ethyl acetate, petroleum ether, dichloromethane and methanol as eluent solvents. A tiny amount of diluted sample was applied to TLC plate (3× 8 cm) using a clean capillary. The TLC plate then placed inside a sealed developing chamber containing the mobile phase (eluent solvents) until the solvent front is close to the top of the plate.

Hence, the R_F of products being compared to starting materials in order to ensure reactions had gone to completion.

2.3.3- Fourier transform infrared spectroscopy (FTIR)

Infrared spectra of all samples were determined on a Nicolet iS 10 FT-IR (Thermo scientific LTD, USA, at room temperature over the range 400 to 4000 cm^{-1} using a BOMEM DA-8 Fourier Transform Spectrometer (FTS) in 16 scan mode (background noise reduction) with a resolution of 4 cm^{-1} .

2.3.4- Nuclear magnetic resonance spectroscopy (NMR)

NMR ^1H and ^{13}C spectra were recorded on a 300 MHz Bruker spectrometer-Avance 300 by using deuterated chloroform (CDCl_3) and deuterated dimethyl sulfoxide (DMSO) as a solvent. The temperature of the measurements was 25 °C.

2.4- Results

2.4.1- Physical properties

Modified monomers synthesis was performed in accordance to Table 5. The table shows the physical properties of each modified monomer.

The yield of all reactions was calculated using the following formula:

$$\text{Yield} = \frac{\text{Moles of products obtained}}{\text{Moles of limiting reagent used}} * 100\%$$

Table 5- Physical properties of the modified monomers.

Compound code	Molecular formula	Molecular mass	Colour	Physical state	MP	R_f	Yield %
P-APMA	$C_{16}H_{44}N_2O_2$	394.63	White	Powder	91.5	0.39	79 %
D-APMA	$C_{19}H_{25}N_3O_3S$	375.48	Yellow	Thick liquid	-----	0.66	65%
C-APMA	$C_{35}H_{58}N_2O_3$	554.84	White	Powder	154.5	0.74	75 %
D1	$C_8H_7N_3OS$	193.22	Yellow	Powder	235	0.92	81.9 %
D2	$C_{12}H_{11}N_3O_4S$	293.29	Yellow	Powder	171	0.43	70.54%
D3	$C_{16}H_{14}N_4O_6S$	390.37	Yellow	Powder	195	0.89	71.4%
O-APMA	$C_{20}H_{24}N_4O_4S$	417.48	Yellow	Thick liquid	-----	0.8	78%

2.4.2 - Characterization of Modified Monomers

2.4.2.1 - Characterization of (P-APMA)

TLC analysis (Figure 28) revealed a new product single spot with $R_f = 0.39$. The purity of P-APMA is about 100% as established by analytical TLC.

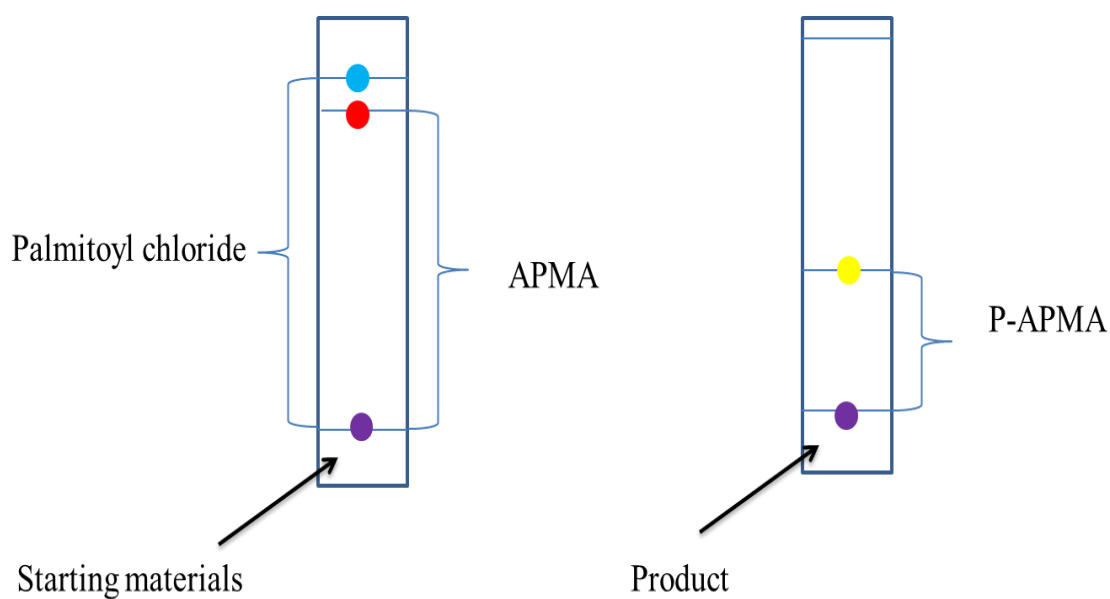


Figure 28- Chromatogram of TLC plate (P-APMA).

The FTIR spectra of P-APMA are shown in (Figure 29). The sharp intense peak at 3294 cm^{-1} was attributed to the -NH stretching vibration of APMA while the sharp band at 2916 cm^{-1} was assigned to the C-H Stretch. The peak at 1637 cm^{-1} is due to carbonyl groups. Other peaks bandwidth of the principle bands are shown in Table 6.

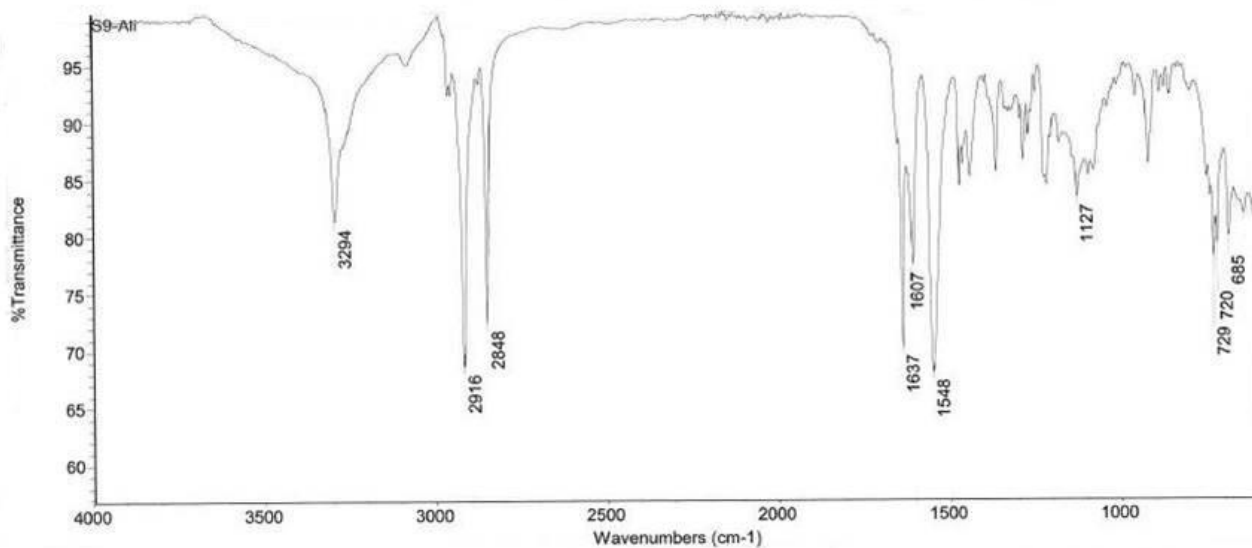


Figure 29- FTIR spectra of P-APMA.

Table 6- Summary of functional P-APMA.

Compound code	Frequency, cm^{-1}	Bond	Functional group
P-APMA	3294	N-H Stretch	Secondary amines
	2916, 2848	C-H Stretch	Alkane
	1637	C=O Stretch	Carbonyls (general)
	1607	-C=C- stretch	Alkene
	1548	N-H bend	Secondary amines
	1127	C-N stretch	Aliphatic amines
	729, 720, 685	=C-H bend	Alkene

The ^1H NMR spectrum (Figure 30) of compound P-APMA shows the palmitoyl group at the following position: 0.75 ppm (t, $\text{CH}_2\text{-CH}_2\text{-CH}_3$, 3H), 1.27 ppm (m, $\text{CH}_3(\text{CH}_2)_{12}$, 24H), 1.65 ppm (m, $\text{CO-CH}_2\text{-CH}_2\text{-CH}_2$, 2H), 2.2 ppm (t, $\text{CO-CH}_2\text{-CH}_2$, 2H) and APMA at: 1.65 ppm (m, $\text{NH-CH}_2\text{-CH}_2\text{-CH}_2\text{-NH}$, 2H), 2 ppm (s, $\text{CH}_3\text{-C}(\text{CH}_2)\text{-CO}$, 3H), 3.1 ppm (t, $\text{NH-CH}_2\text{-CH}_2\text{-CH}_2\text{-NH}$, 2H), 5.36 ppm, 5.8 ppm (s, $\text{CO-C}(\text{CH}_3)\text{-CH}_2$, 2H), 6.12 ppm (s, C-CO-NH-CH_2 , 1H), 6.75 ppm (s, $\text{CH}_2\text{-CO-NH-CH}_2$, 1H).

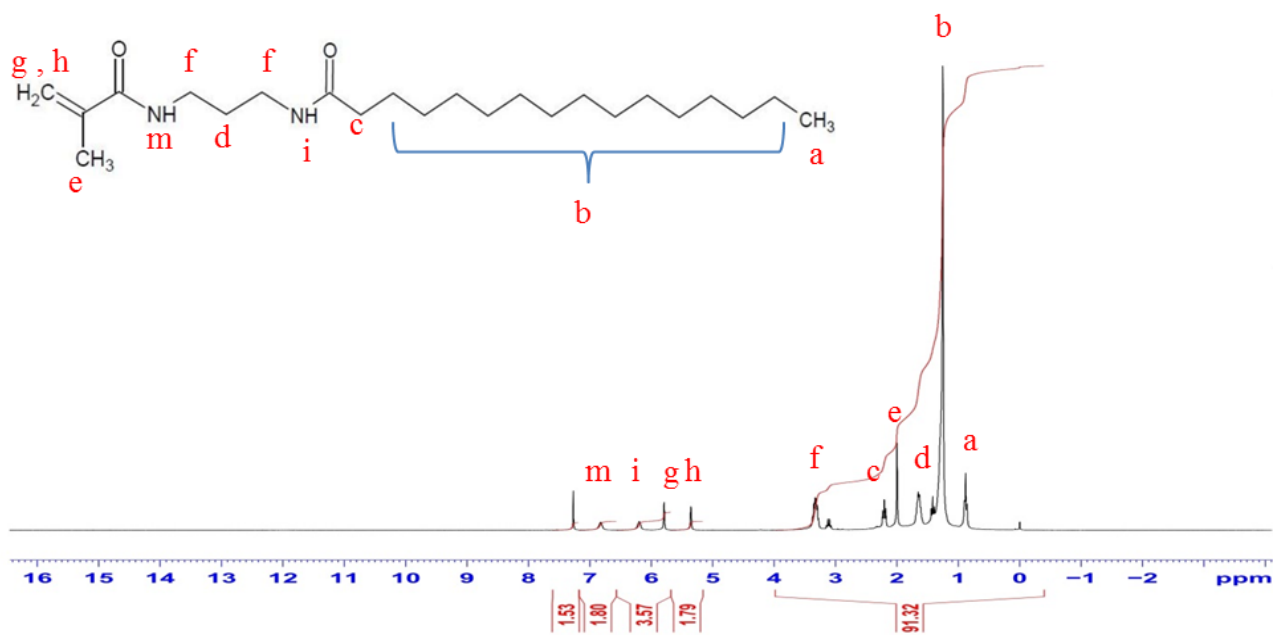


Figure 30- ^1H NMR spectra of P-APMA in CDCl_3 carried out using 300MHz NMR at 25 °C.

The ^{13}C -NMR spectrum (Figure 31) show peaks at 174 ppm and 168 ppm due to the $\text{C}=\text{O}$ bonds of palmitoyl and APMA respectively, the peaks at 139.7 ppm and 119.9 ppm due to the vinyl group and the peaks of methyl groups of palmitoyl and APMA at 14.15 ppm for the former and 18.67 ppm for the latter, the rest of band are related to CH_2 groups in palmitoyl.

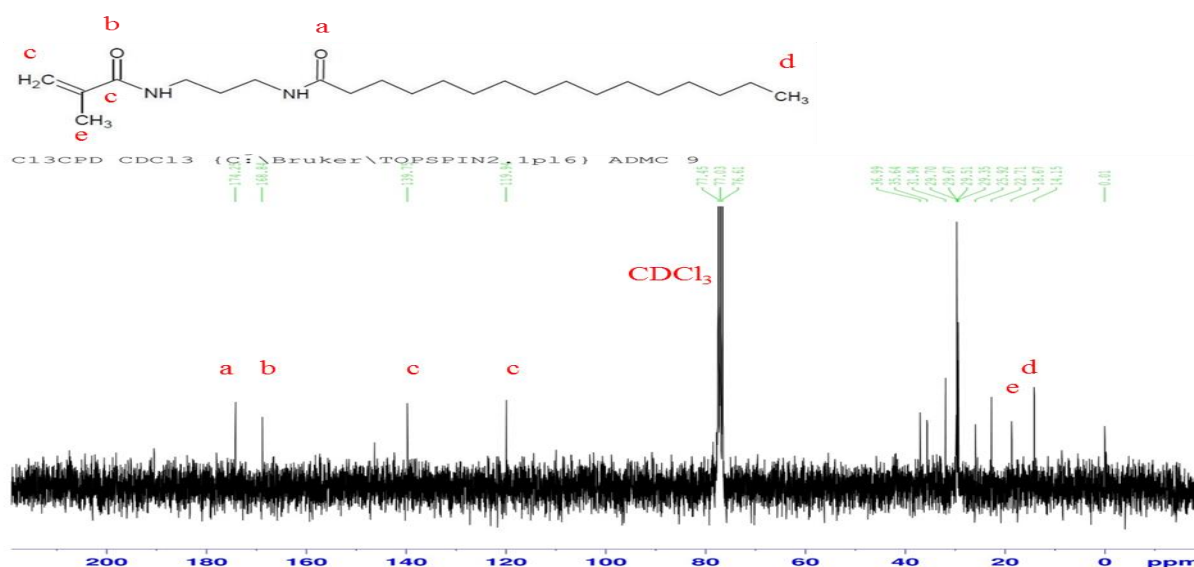


Figure 31- ^{13}C NMR spectra of P-APMA in CDCl_3 carried out using 300MHz NMR at 25 °C.

2.4.2.2- Characterization of (D-APMA)

TLC analysis (Figure 32) indicated the formation of D-APMA ($R_f = 0.66$) with around 100% purity.

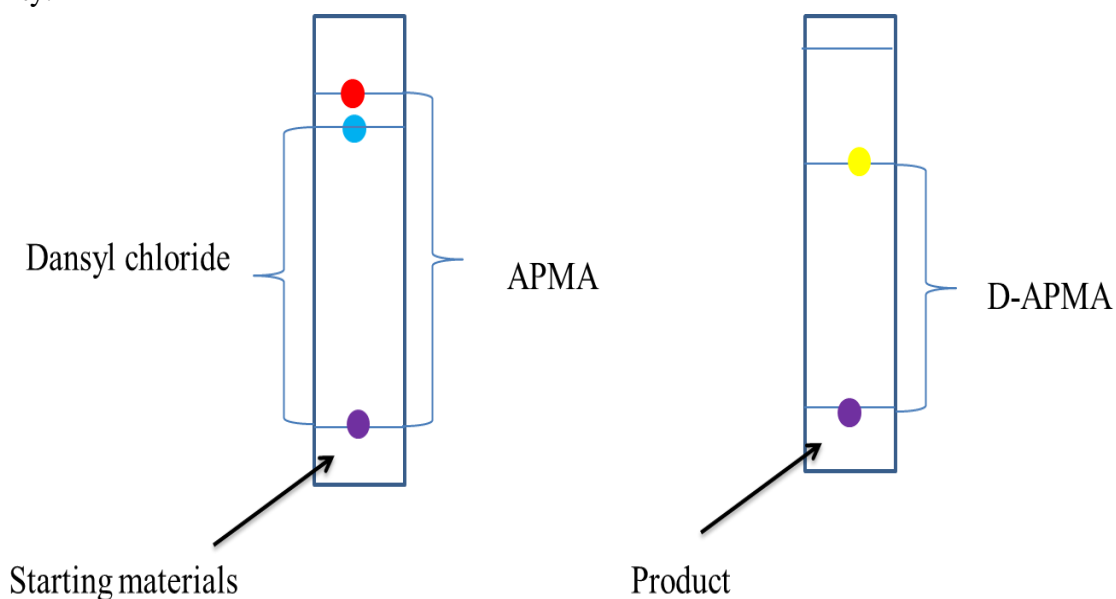


Figure 32- Chromatogram of TLC plate (D-APMA).

The FT-IR spectra of the D-APMA are shown in (Figure 33) and the main functional groups bands of the spectra are listed in table 7.

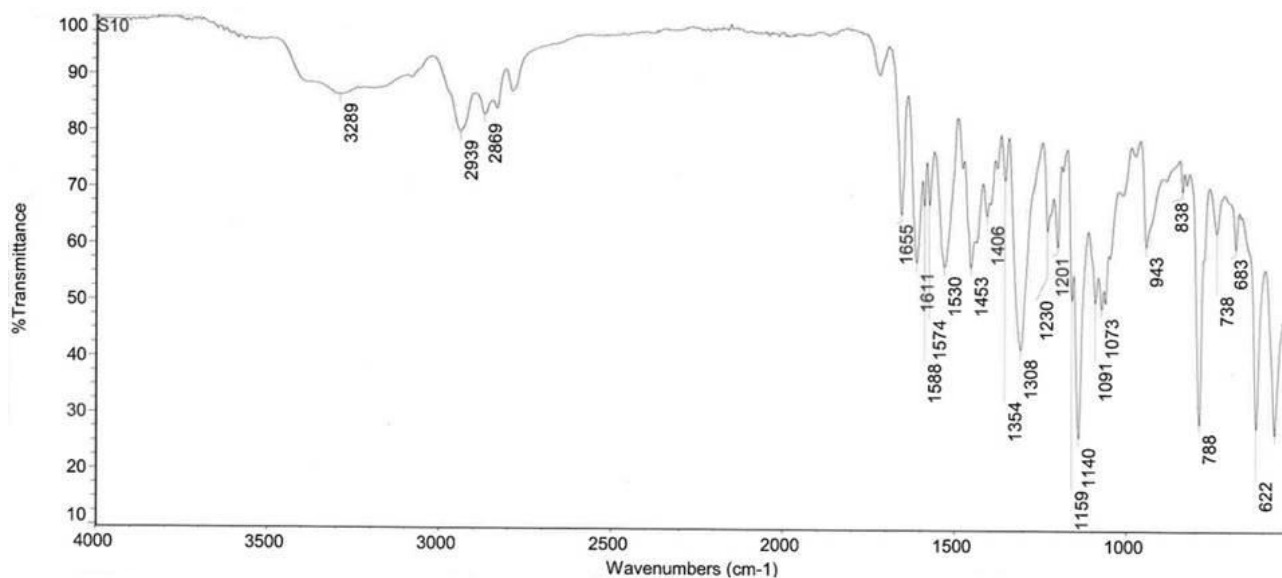


Figure 33- FTIR spectrum of D-APMA.

The FT-IR spectrum (Figure 33) indicate the presence of a broad band of N-H at 3289 cm^{-1} , sulphonyl group 1712 cm^{-1} , C=O group at 1655 cm^{-1} and C-C aromatic 1530 cm^{-1} - 1406 cm^{-1} peaks confirming the combination of the APMA with dansyl group.

Table 7- Summary of functional D-APMA.

Compound code	Frequency, cm^{-1}	Bond	Functional group
D-APMA	3289	N-H Stretch	Secondary amines
	2939, 2869	C-H Stretch	Alkane
	1712	S=O Stretch	Sulphonyl
	1655	C=O Stretch	Carbonyl
	1611	-C=C- stretch	Alkene
	1574, 1588	N-H bend	Secondary amines
	1530, 1453, 1406	C-C stretch (in-ring)	Aromatic
	1354	=C-H bend	Alkenes
	1308	S=O	Sulphonyl
	1230	C-N stretch	Aromatic amines
	1201	C-H bend	Alkanes
	1140, 1091, 1073	C-N stretch	Aliphatic amine
	943, 788, 738, 683, 622	=C-H bend	Alkene

The ^1H NMR spectrum (Figure 34) of compound P-APMA (CDCl_3) shows the dansyl group at the following position: 2.88 ppm (s, N- CH_3 , 6H), 7.2 ppm (d, naphthalene proton in position 6, 1H), 7.57 ppm (q, naphthalene protons in position 3 and 8, 2H), 8.13 ppm (d, naphthalene protons in position 4, 1H), 8.3 ppm (d, naphthalene protons in position 7, 1H), 8.32 ppm (d, naphthalene proton in position 2, 1H) and APMA at: 1.6 ppm (m, NH- CH_2 - CH_2 -NH, 2H), 1.9 ppm (s, CH_3 -C(CH_2)-CO, 3H), 3.38 ppm (t, NH- CH_2 - CH_2 -NH, 2H), 5.33 ppm, 5.67 ppm (s, CO -C(CH_3) - CH_2 , 2H), 6.14 ppm (s, C-CO-NH- CH_2 , 1H), 7.27 ppm (s, CH_2 -CO-NH- CH_2 , 1H) .

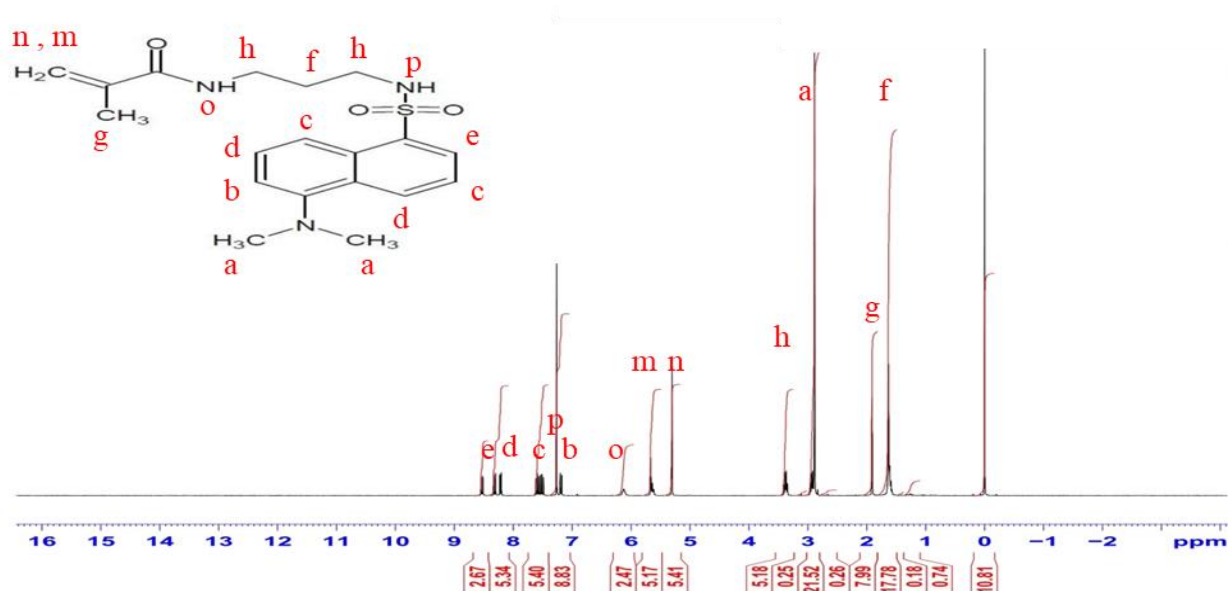


Figure 34- ^1H NMR spectra of D-APMA in CDCl_3 carried out using 300MHz NMR at 25 $^\circ\text{C}$.

The ^{13}C -NMR spectrum (Figure 35) shows the peaks of vinyl group at 123.19 ppm and 139.42 ppm, peaks at 45.44 ppm and 18.62 ppm, which are characteristics of the methyl groups in dansyl and APMA respectively. The spectrum displays the peak at 169 ppm, corresponding to carbonyl groups in APMA. The spectrum also indicates signals at 115.24 ppm, 118.88 ppm, 120.16 ppm, 128.45 ppm, 129.18 ppm, 129.52 ppm, 129.85 ppm, 130.34 ppm, 135.07 ppm and 151.9 ppm, which belong to dansyl aromatic carbons.

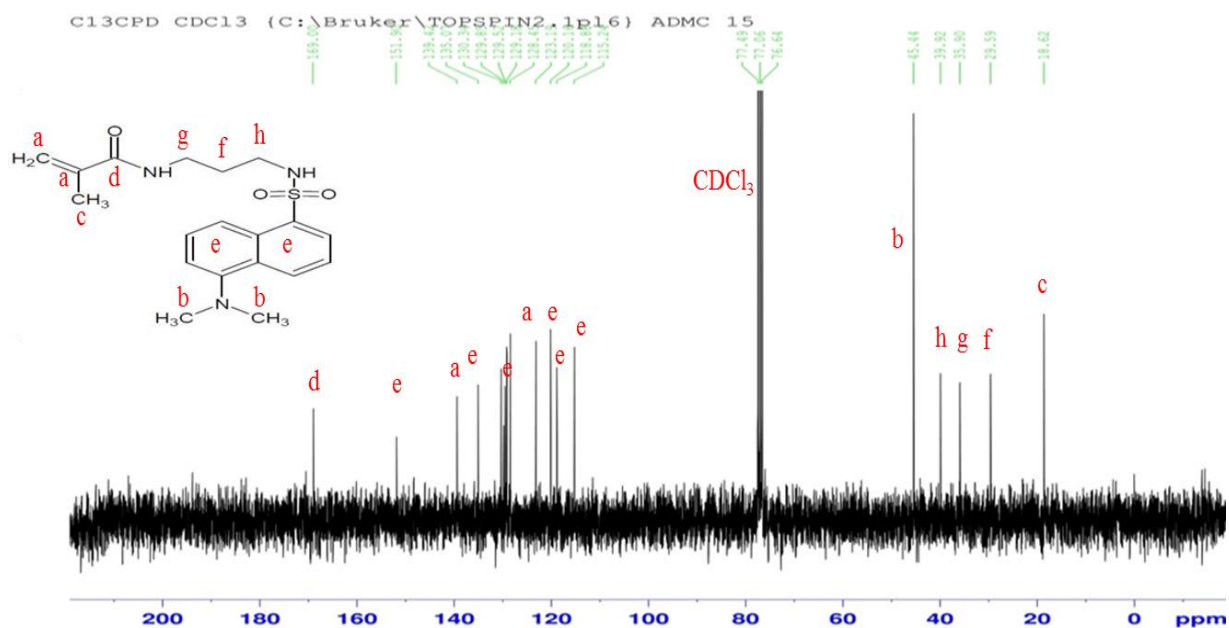


Figure 35- ^{13}C NMR spectra of D-APMA in CDCl_3 carried out using 300MHz NMR at 25 $^\circ\text{C}$.

2.4.2.3- Characterization of (C-APMA)

TLC analysis (Figure 36) shows a new product single spot with $R_f = 0.74$. C-APMA is high-purity as established by analytical TLC.

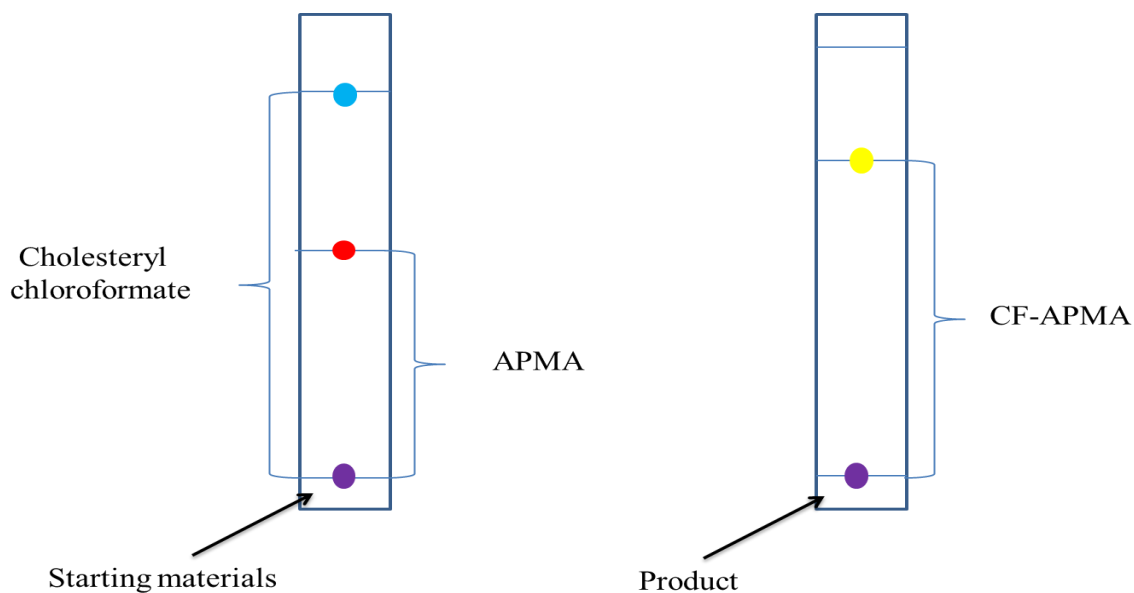


Figure 36- Chromatogram of TLC plate (C-APMA).

The FTIR spectrum of C-APMA is shown in Figure 37.

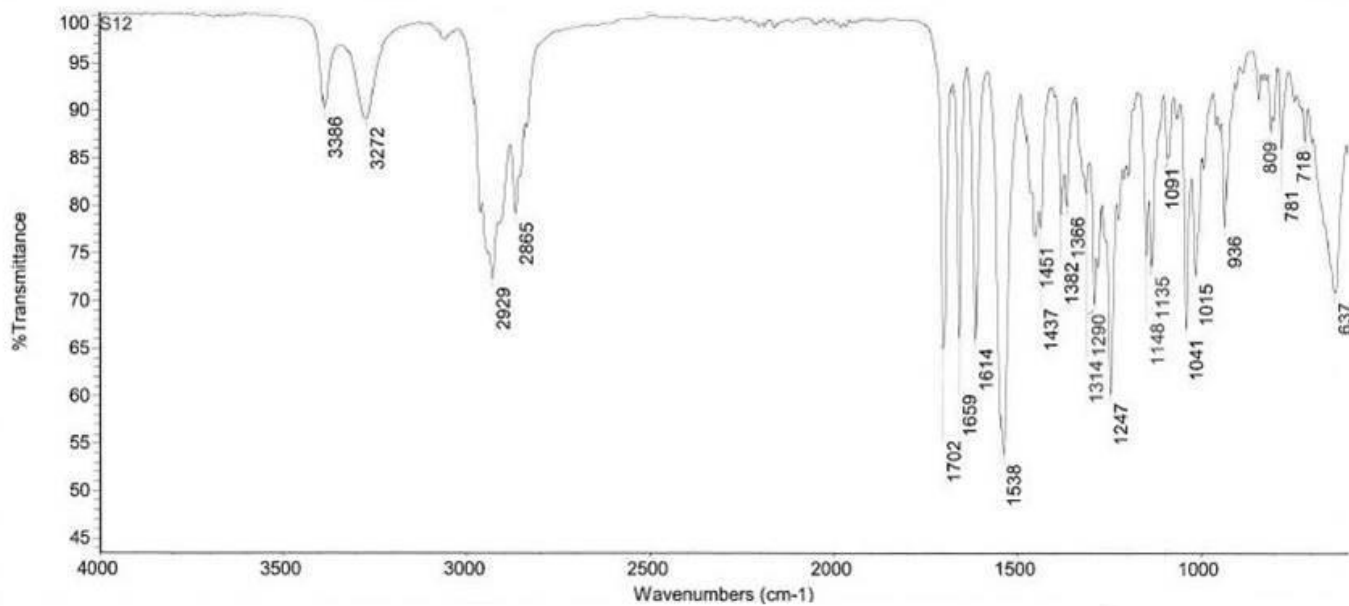


Figure 37- FTIR spectrum of C-APMA.

The FTIR spectrum indicates two peaks appeared at 3386 cm^{-1} and 3272 cm^{-1} due to the presence of NH group. The peak at 1659 cm^{-1} is assigned to C=C stretching while the peak at 1702 cm^{-1} due to C=O stretching. Other peaks bandwidth of the principle bands are shown in Table 8.

Table 8- Summary of functional C-APMA.

Compound code	Frequency, cm^{-1}	Bond	Functional group
C-APMA	3386, 3272	N-H Stretch	Secondary amines
	2929, 2865	C-H Stretch	Alkane
	1702	C=O Stretch	Carbonyls (general)
	1659	-C=C- stretch	Alkenes
	1614, 1538	N-H bend	Secondary amines
	1451, 1437, 1382, 1366	C-C bend	Alkane
	1314	C-O stretch	Esters
	1290, 1247	C-N stretch	Aliphatic amines
	1148, 1135	C-O Bend	Carbonyl
	1091, 1041	C-O stretch	Esters
	1015	C-N stretch	Aliphatic amines
	936	C-O Bend	Carbonyl
	809, 781, 718, 637	=C-H bend	Alkenes

The ^1H NMR spectrum (Figure 38) of compound C-APMA shows the cholesteryl group at the following position: 0.87 ppm ($(\text{CH}_3)_2\text{-CH-CH}_2$, 6H), 0.67ppm -2 ppm (m, cholesteryl protons, 38H), 2.37 ppm (m, CH_2 , 2H), 4.5 ppm (b, oxycyclohexyl, 1H), 5.35 ppm (b, alkenyl, 1H), and APMA at: 1.68 ppm (m, $\text{NH-CH}_2\text{-CH}_2\text{-CH}_2\text{-NH}$, 2H), 1.98 ppm (s, $\text{CH}_3\text{-C(CH}_2\text{)-CO}$, 3H), 3.24 ppm (t, $\text{NH-CH}_2\text{-CH}_2\text{-CH}_2\text{-NH}$, 2H), 5.3 ppm, 5.76 ppm (s, $\text{CO - C(CH}_3\text{) -CH}_2$, 2H), 6.67 ppm (s, C-CO-NH-CH_2 , 1H), 7.26 ppm (s, $\text{CH}_2\text{-CO-NH-CH}_2$, 1H).

2.4.2.4- Characterization of 5-(4-Aminophenyl)-1,3,4-oxadiazole-2-thiol (D1)

TLC analysis (Figure 40) (ethyl acetate: petroleum ether 1:1) indicated formation of D1 ($R_f = 0.92$). The purity of D1 is about 100% as established by analytical TLC.

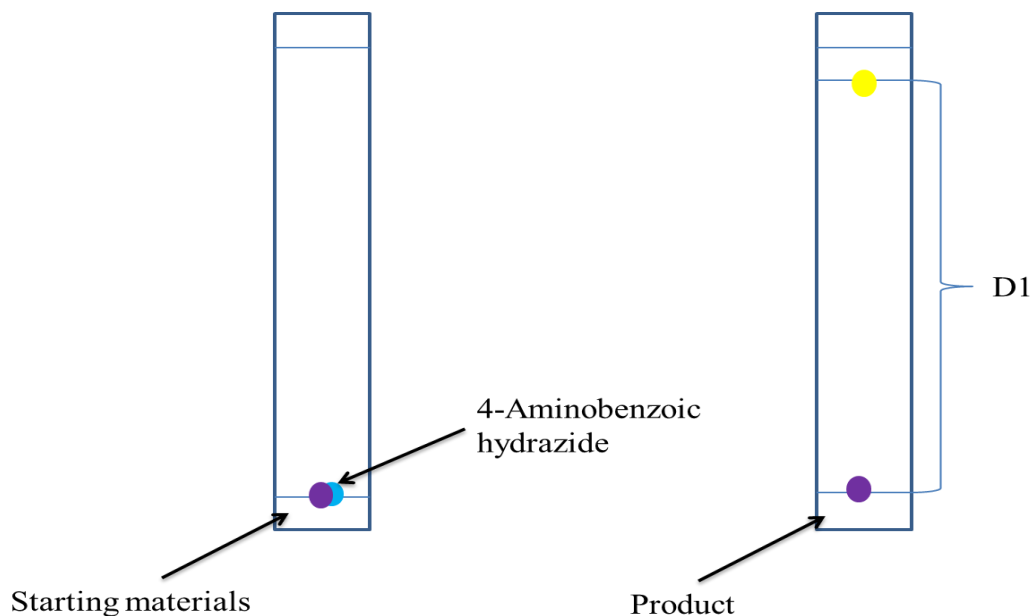


Figure 40- Chromatogram of TLC plate D1.

The FTIR spectrum of D1 is shown in Figure 41.

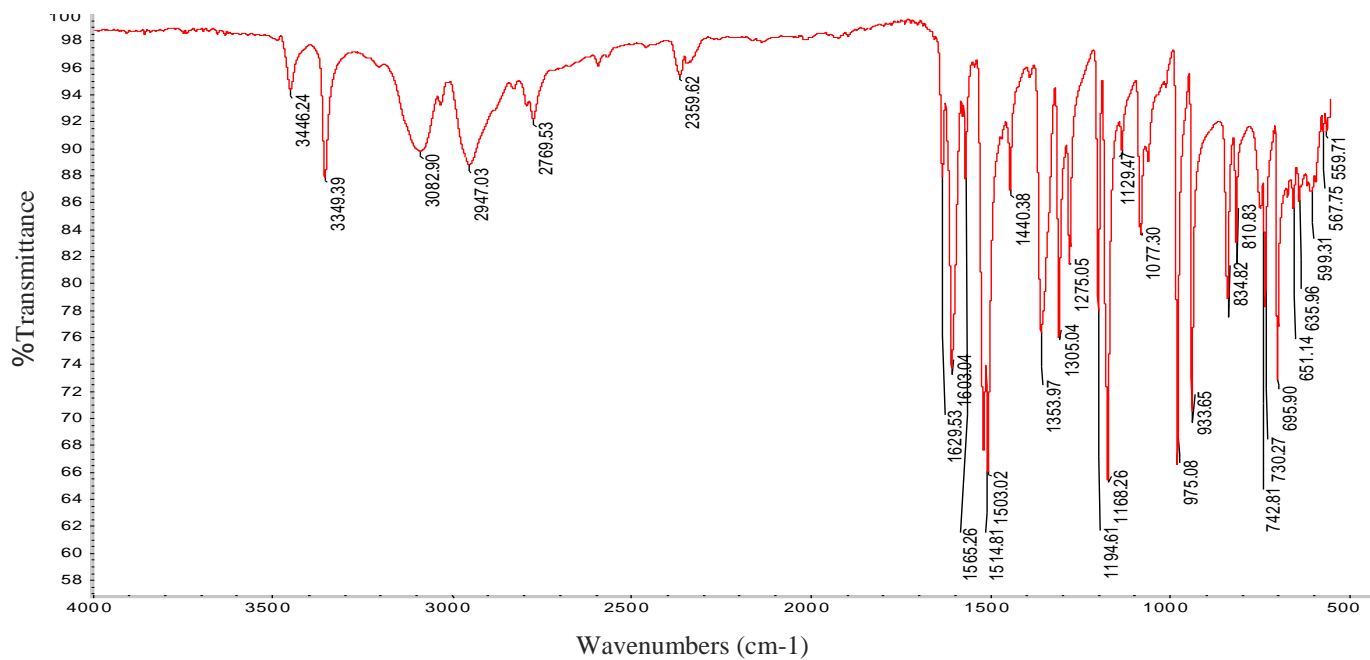


Figure 41- FTIR spectrum of D1.

The compound show characteristic band for primary amine group at 3446 cm^{-1} and 3349 cm^{-1} . The band observed at 1440 cm^{-1} to 1514 cm^{-1} is due to -C=C- starch (aromatic).

Table 9- Summary of functional D1.

Compound code	Frequency, cm^{-1}	Bond	Functional group
D1	3446, 3349	N-H Stretch	Primary amines
	3082	C=C	Aromatics
	2947, 2769	C-H Stretch	Alkane
	2359	S-H	Thiol
	1629	C=N	Imines
	1603	N-H bend	Primary amines
	1514	=C-H bend	Alkenes
	1440	-C-O-C-	Ether
	1353	-C=C-	Aromatics
	1201	-C-H bend	Alkanes
	1077	C-N stretch	Aromatic amines

The $^1\text{H-NMR}$ spectrum of compound D1 is shown in Figure 42. The following peaks appear in the compound spectrum: at 6.65 ppm (d, aromatic protons in position 2 and 6, 2H) and 7.5 ppm (d, aromatic protons in position 3 and 5, 2H).

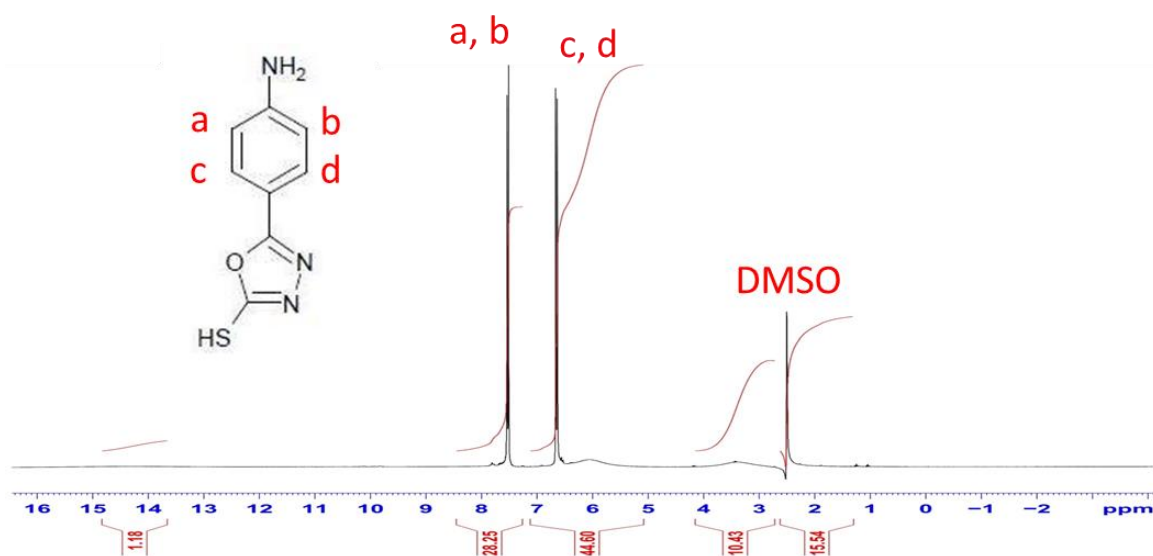


Figure 42- $^1\text{H-NMR}$ spectra of D1 in DMSO carried out using 300MHz NMR at $25\text{ }^\circ\text{C}$.

The peak assignments for D1 were as follows (Figure 43): the peaks of aromatic group at positions *meta* and *ortho* 113.5 ppm, 127.4 ppm respectively, while *para* at 108.2 ppm and 152.5 ppm. The spectrum also indicates signals at 161.5 ppm and 176.4 ppm which belong to oxadiazole carbons ring.

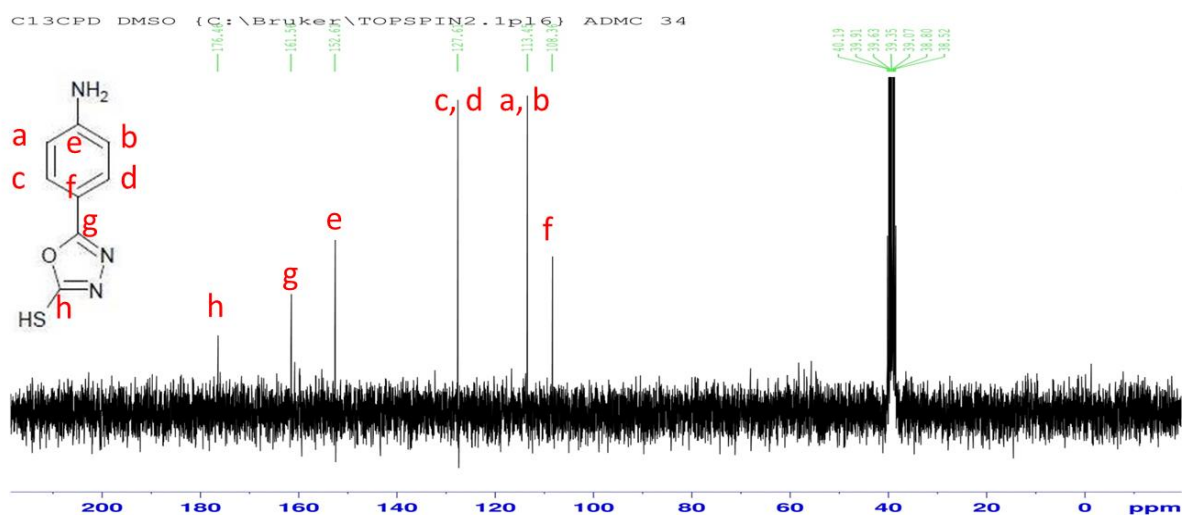


Figure 43- ^{13}C NMR spectra of D1 in DMSO carried out using 300MHz NMR at 25 °C.

2.4.2.5- Characterization of 4-oxo-4-([4-(5-sulfanyl-1,3,4-oxadiazol-2-yl)phenyl] amino)butanoic acid (D2)

TLC analysis (Figure 44) (ethyl acetate: petroleum ether 1:1) indicated formation of D2 ($R_f = 0.43$). D2 is high-purity as established by analytical TLC.

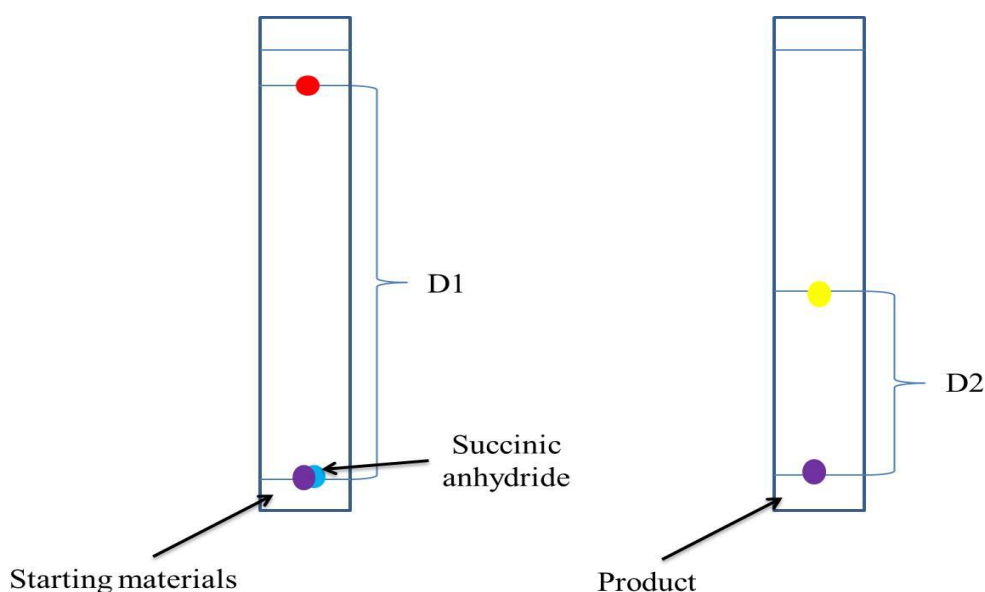


Figure 44- Chromatogram of TLC plate D2.

The FTIR spectrum of D2 is shown in Figure 45.

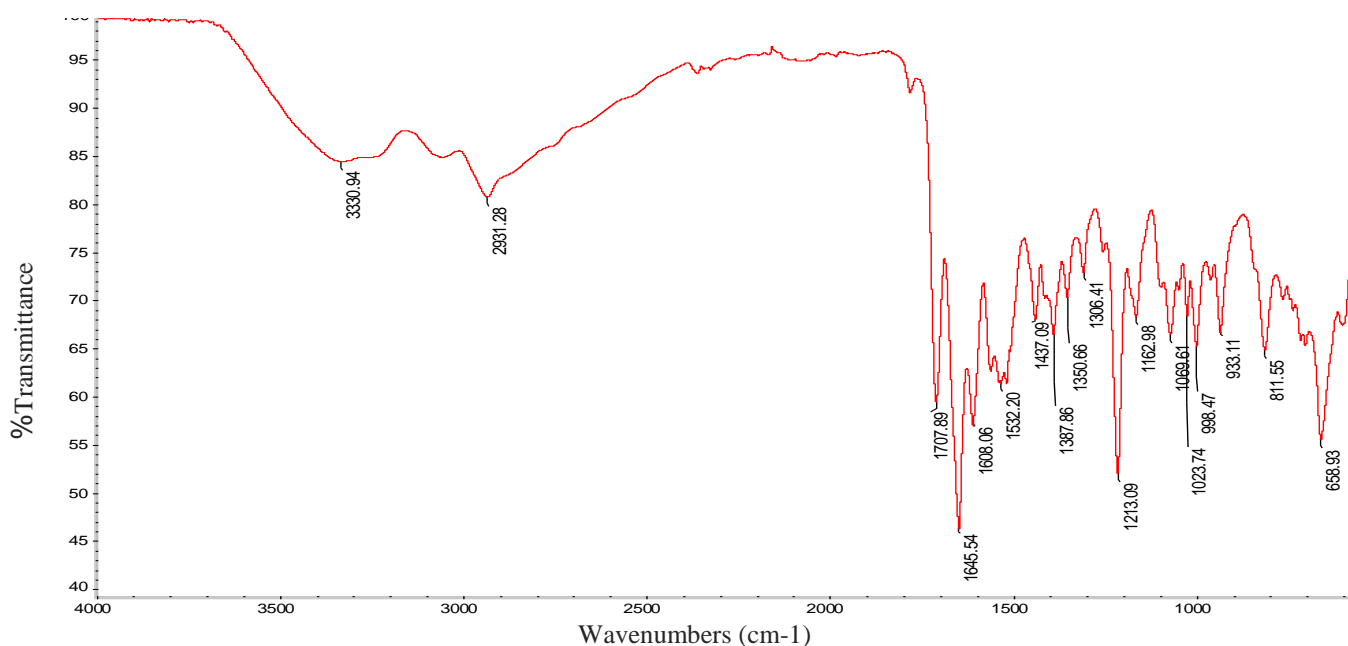


Figure 45- FTIR spectrum of D2.

The FTIR spectrum of D2 (Figure 45) shows broad band at 3330 cm^{-1} was assigned to the O-H Stretch this absorption overlaps the N-H stretching peaks, in addition of two strong absorption of carbonyl band at 1707 cm^{-1} and 1645 cm^{-1} were observed, which confirmed the creation of D2.

Table 10- Summary of functional D2.

Compound code	Frequency, cm^{-1}	Bond	Functional group
D2	3330	O-H	Carboxylic acid
		N-H Stretch	Secondary amines
	2931	C-H Stretch	Alkane
	2359	S-H	Thiol
	1707	C=O Stretch	Carboxylic acid
			carbonyl
	1645		Amide carbonyl
	1608	N-H bend	Secondary amines
	1532	C=N	Imines
	1437	-C-O-C-	Ether
	1306	=C-H bend	Alkenes
1213	C-N stretch	Aromatic amines	

	1162	C-H bend	Alkanes
	933	O-H bend	Carboxylic acid

The ^1H chemical shift data (Figure 46) for D2 compound are presented a peak at 2.5 ppm (t, the aliphatic protons, 4H), and 6.6 ppm, 6.8 ppm, 7.45 ppm and 8.18 ppm (d, the aromatic protons, 4H).

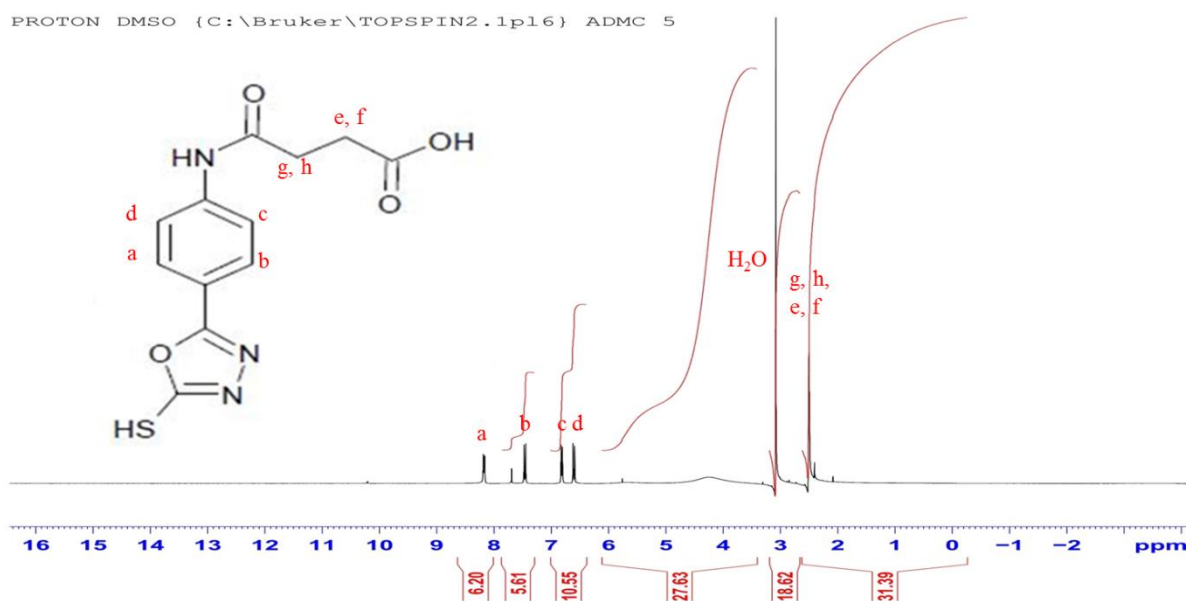
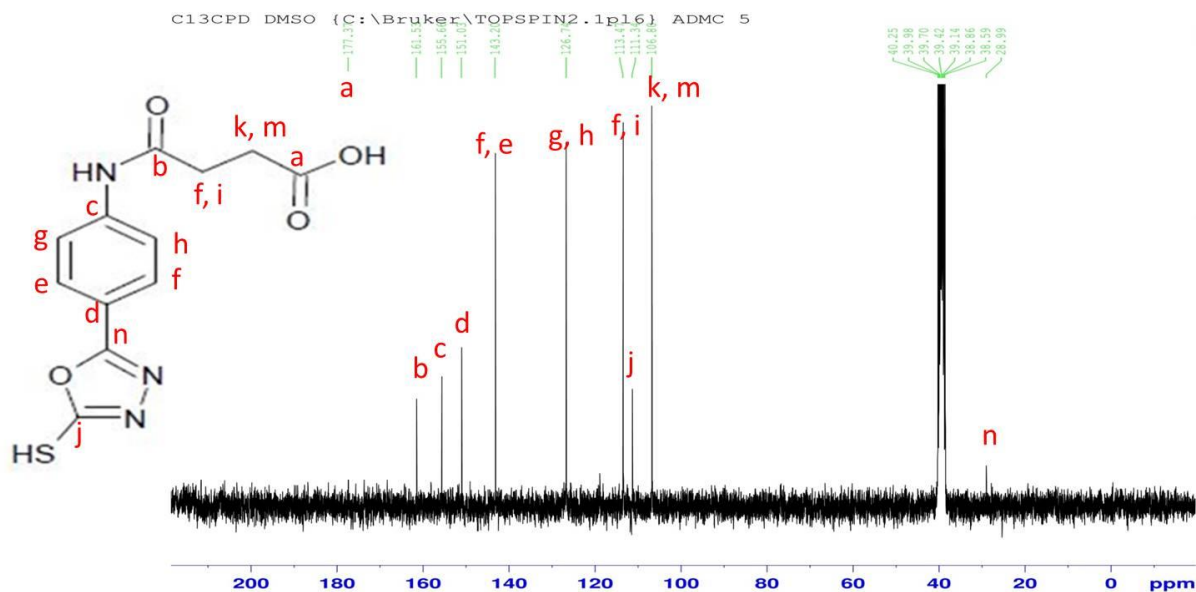


Figure 46- ^1H NMR spectra of D2 in DMSO carried out using 300MHz NMR at 25 °C.

The results obtained from ^{13}C NMR spectrum (Figure 47) show the peaks of carbonyl group at 161.5 ppm and 177.3 ppm, peaks at 28.99 ppm and 111.3 ppm, which are characteristics of the oxadiazole ring. The spectrum displays two peaks at 106.8 ppm and 113.4 ppm, corresponding to aliphatic carbons. The spectrum also indicates signals at 126.7 ppm, 143.2 ppm, 155.6 ppm and 151 ppm which belong to aromatic carbons.



2.4.2.6- Characterization of 4-[(2,5-dioxopyrrolidin-1-yl)oxy]-4-oxo-N-[4-(5-sulfanyl-1,3,4-oxadiazol-2-yl)phenyl]butanamide (D3)

TLC analysis (Figure 48) indicated the formation of D3 ($R_f = 0.89$) with around 100% purity.

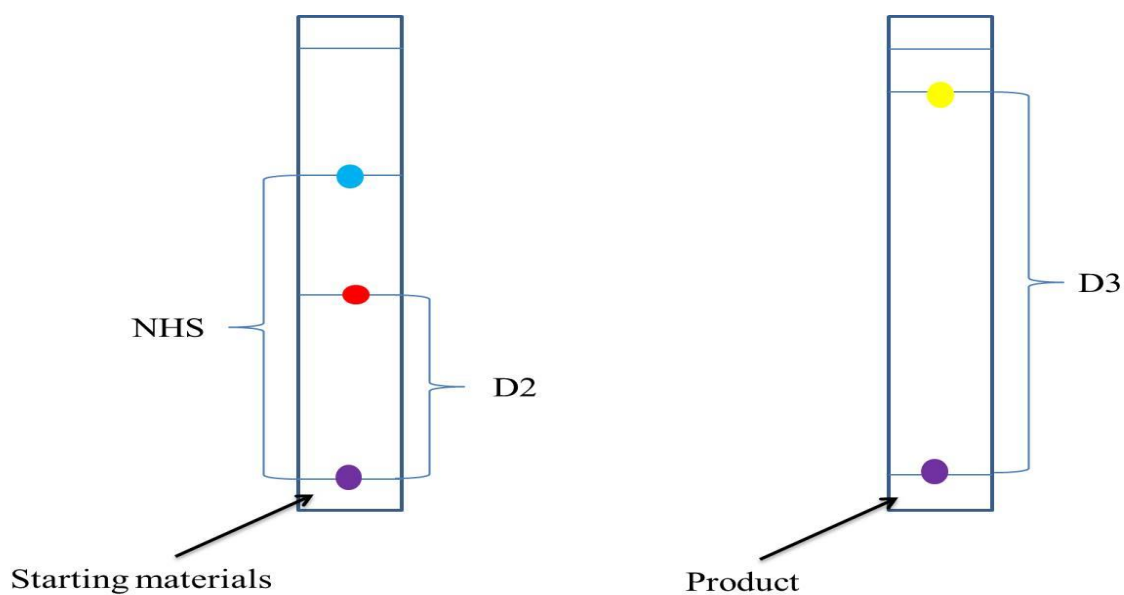


Figure 48- Chromatogram of TLC plate D3.

The FTIR spectrum of D3 is shown in Figure 49.

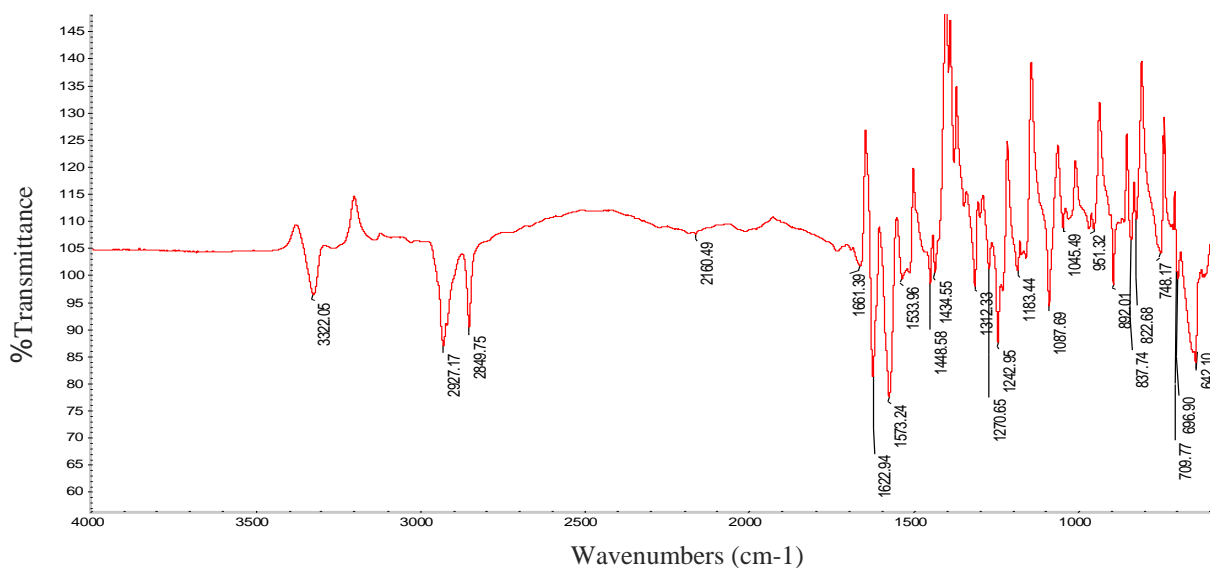


Figure 49- FTIR spectrum of D3.

The disappearance of hydroxyl groups peaks at around 3300 cm^{-1} suggest the substitution reaction between D2 and NHS occurred.

Table 11- Summary of functional D3.

Compound code	Frequency, cm^{-1}	Bond	Functional group
D3	3322	N-H Stretch	Secondary amines
	2929	C-H Stretch	Alkane
	2849		
	2160	S-H	Thiol
	1622	C=O Stretch	Succinimide and amide Carbonyl
	1573		
	1611	N-H bend	Secondary amines
	1533	C=N	Imines
	1448, 1434	C-C stretch (in-ring)	Aromatics
	1312	=C-H bend	Alkenes
	1240	-C-O-C-	Ether
	1242	C-N stretch	Aromatic amines
	1201	C-H bend	Alkanes
	1087	C-N stretch	Aliphatic amines

Figure 50 illustrates ^1H NMR spectrum for D3. In ^1H NMR signals at: 2.47 ppm and 2.76 ppm (t, succinimide protons, 4H), 2.8 ppm and 3.07 ppm (t, $\text{CO}-\text{CH}_2-\text{CH}_2-\text{CO}$, 4H), 6.9, 7.4, 7.9 and 8.2 ppm (d, aromatic protons, 4H).

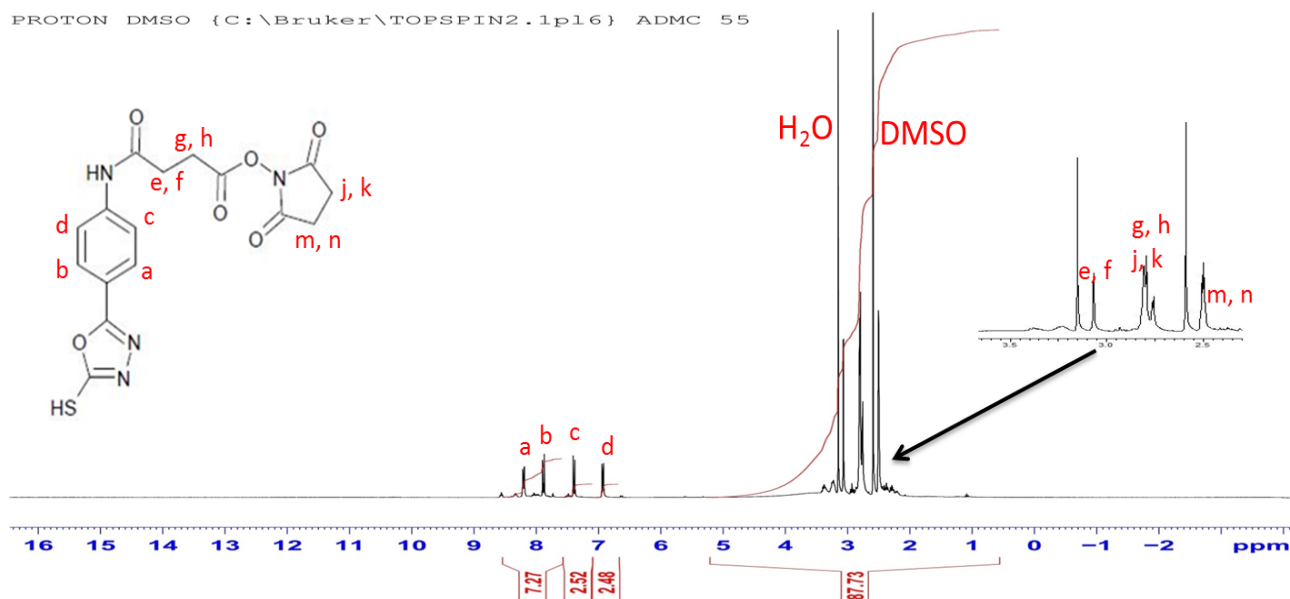


Figure 50- ^1H NMR spectra of D3 in DMSO carried out using 300MHz NMR at 25 °C.

The peak assignments for D3 were as follows (Figure 51): the peaks of carbonyl group at 172.8 ppm, 170.89 ppm, 161.57 ppm and 155.99 ppm, while the aromatic carbons 126.8 ppm, 125.8 ppm, 113 ppm, 111 ppm and 106.8 ppm. The spectrum also indicates signals at 151.2 ppm, 142 ppm which belong to oxadiazole carbons ring. The rest of peaks are corresponding to aliphatic carbons along the compound skeleton.

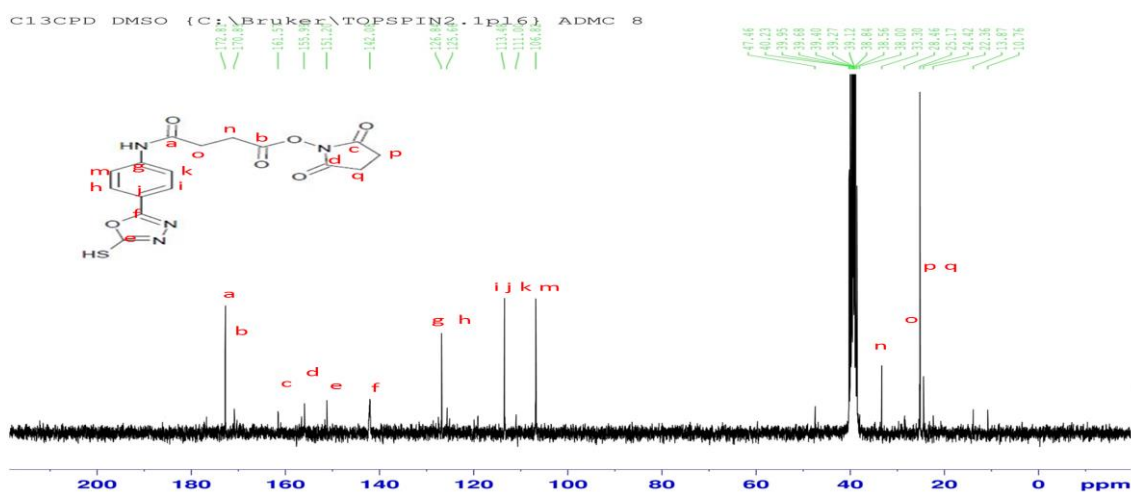


Figure 51- ^{13}C NMR spectra of D3 in DMSO carried out using 300MHz NMR at 25 °C.

2.4.2.7- Characterization of (O-APMA)

TLC analysis (Figure 52) indicated the formation of O-APMA ($R_f = 0.8$) with around 100% purity.

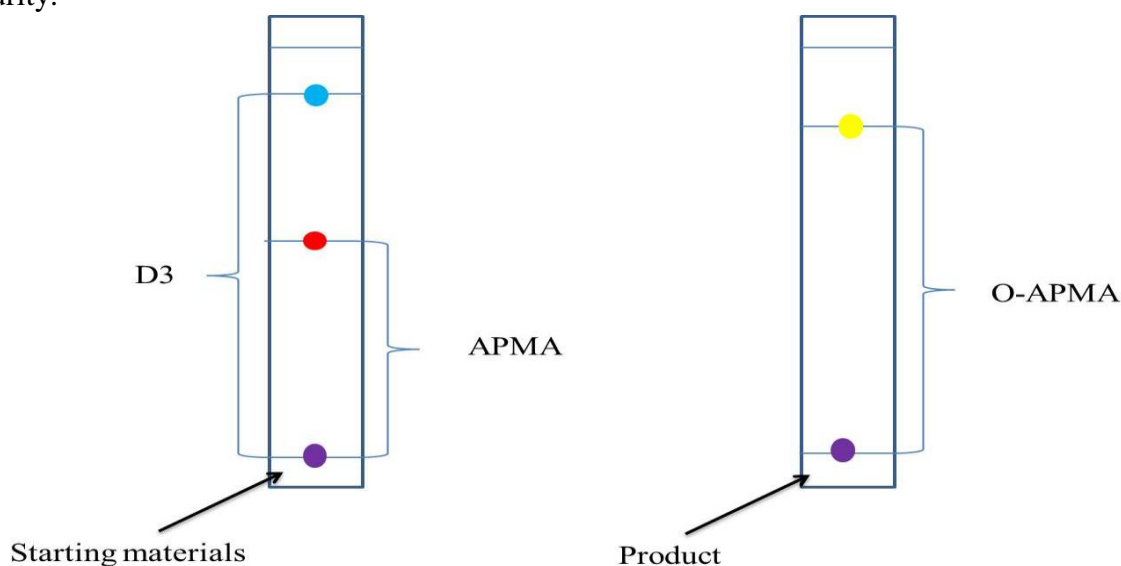


Figure 52- Chromatogram of TLC plate (O-APMA).

The FTIR spectrum of O-APMA is shown in Figure 53.

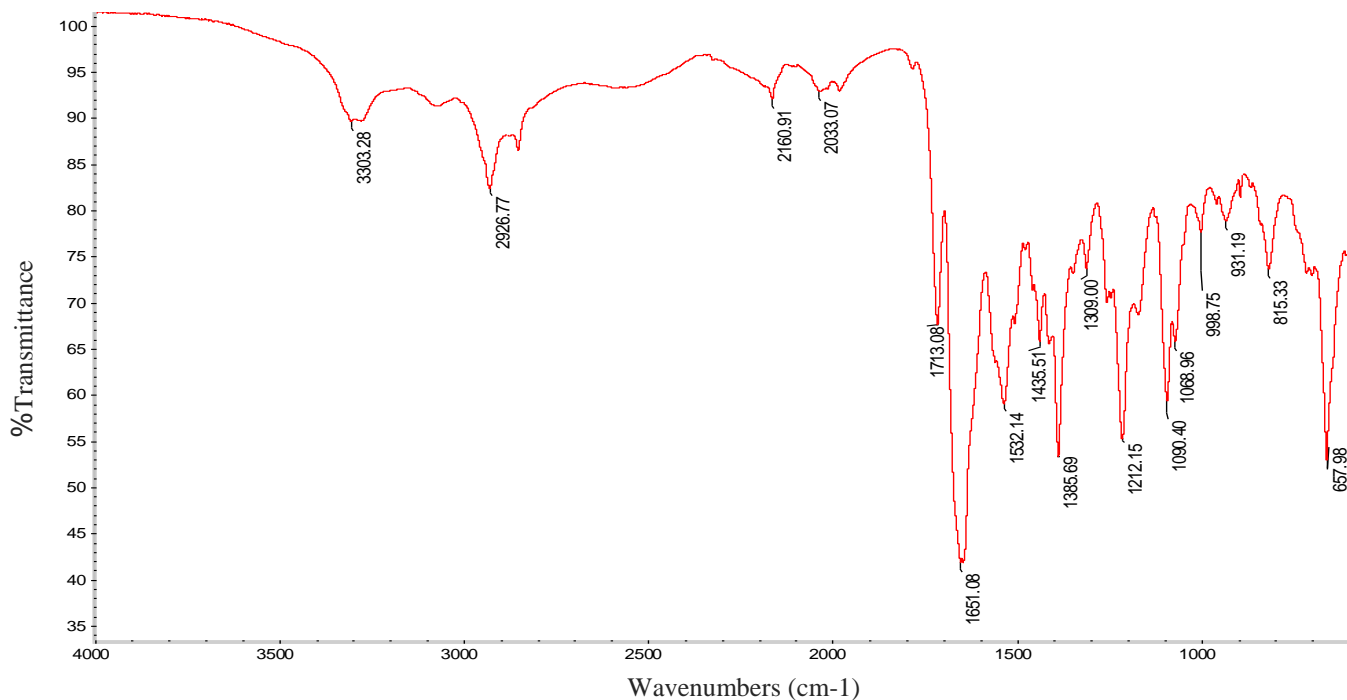


Figure 53- FTIR spectrum of O-APMA.

The FTIR spectrum of O-APMA (Figure 53) showed the presence of N-H, S-H and C=O peaks due to absorbance at 3303 cm^{-1} , 2033 cm^{-1} and 1661 cm^{-1} respectively indicating the presence of the main groups of the backbone and the oxadiazole moiety.

Table 12- Summary of functional O-APMA.

Compound code	Frequency, cm^{-1}	Bond	Functional group
O-APMA	3303	N-H Stretch	Secondary amines
	2926	C-H Stretch	Alkane
	2830		
	2160	S-H	Thiol
	2033	C-N Stretch	Imine
	1713	C=O Stretch	Carbonyl
	1661		
	1532	N-H bend	Secondary amines
	1435	=C-H bend	Alkenes
	1386	-C-O-C-	Ether
	1309	-C=C-	Aromatic
	1212	C-H bend	Alkenes
	1094	C-N stretch	Aromatic and Aliphatic amine
	998		
	931, 667	=C-H bend	Alkenes

The ^1H NMR spectrum (Figure 54) of compound O-APMA shows the oxadiazole group and the linker at the following position: 2.5 ppm (t, $\text{CO}-\underline{\text{CH}}_2-\underline{\text{CH}}_2-\text{CO}$, 4H), 6.63 ppm, 6.93 ppm, 7.49 ppm and 8.21 ppm (m, aromatic protons, 4H) and APMA at: 1.74 ppm (m, $\text{NH}-\underline{\text{CH}}_2-\underline{\text{CH}}_2-\text{NH}$, 2H), 1.86 ppm (s, $\underline{\text{CH}}_3-\text{C}(\underline{\text{CH}}_2)-\text{CO}$, 3H), 3.16 ppm (t, $\text{NH}-\underline{\text{CH}}_2-\underline{\text{CH}}_2-\underline{\text{CH}}_2-\text{NH}$, 4H), 5.34 ppm, 5.69 ppm (s, $\text{CO}-\text{C}(\underline{\text{CH}}_3)-\underline{\text{CH}}_2$, 2H), 7.93 ppm (s, $\text{CO}-\underline{\text{N}}\text{H}(\underline{\text{CH}}_2)_3-\underline{\text{N}}\text{H}-\text{CO}$, 2H).

PROTON DMSO {C:\Bruker\TOPSPIN2.1p16} ADMC 13

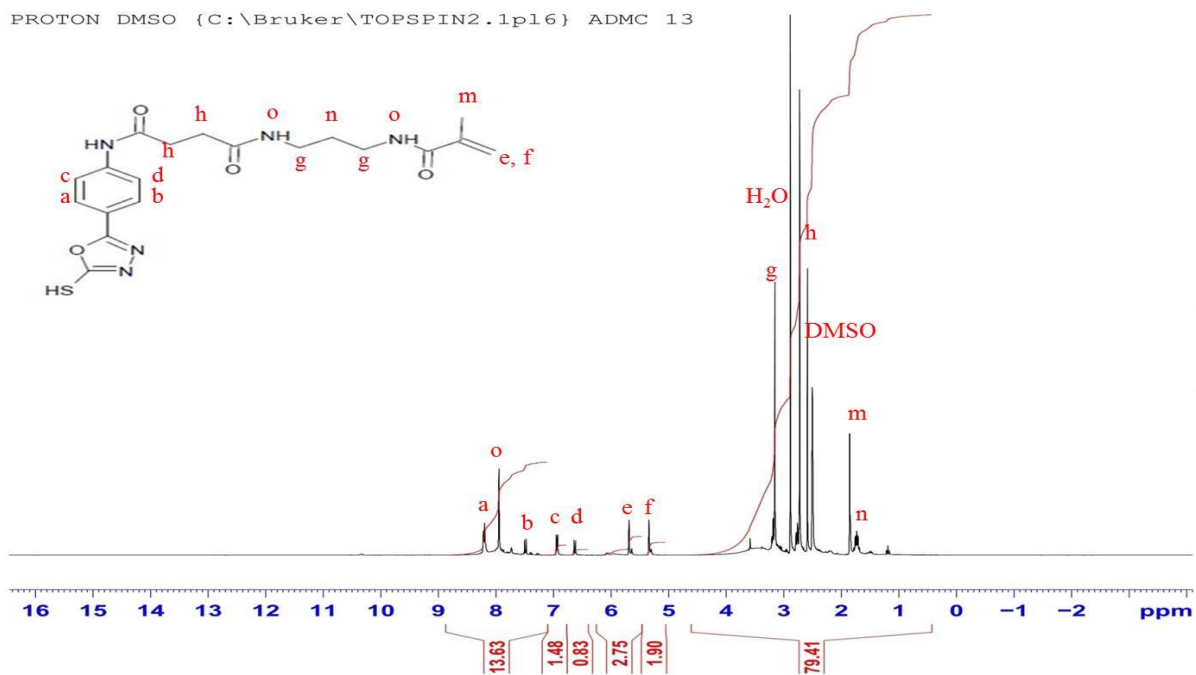


Figure 54- ^1H NMR spectra of O-APMA in DMSO carried out using 300MHz NMR at 25 °C.

The ^{13}C -NMR spectrum (Figure 55) of O-APMA in DMSO shows the peaks of carbonyl groups at 162.28 ppm, 167.67 ppm and 172.78 ppm, peaks at 106.87 ppm, 113.45 ppm, 119.29 ppm, 127.21 ppm, 139.66 ppm and 151.96 ppm are characteristic for aromatic carbons. The signals at 36.56 ppm and 156.58 ppm were attributed to carbons in oxadiazole ring. The rest of peaks are corresponding to aliphatic carbons along the compound skeleton.

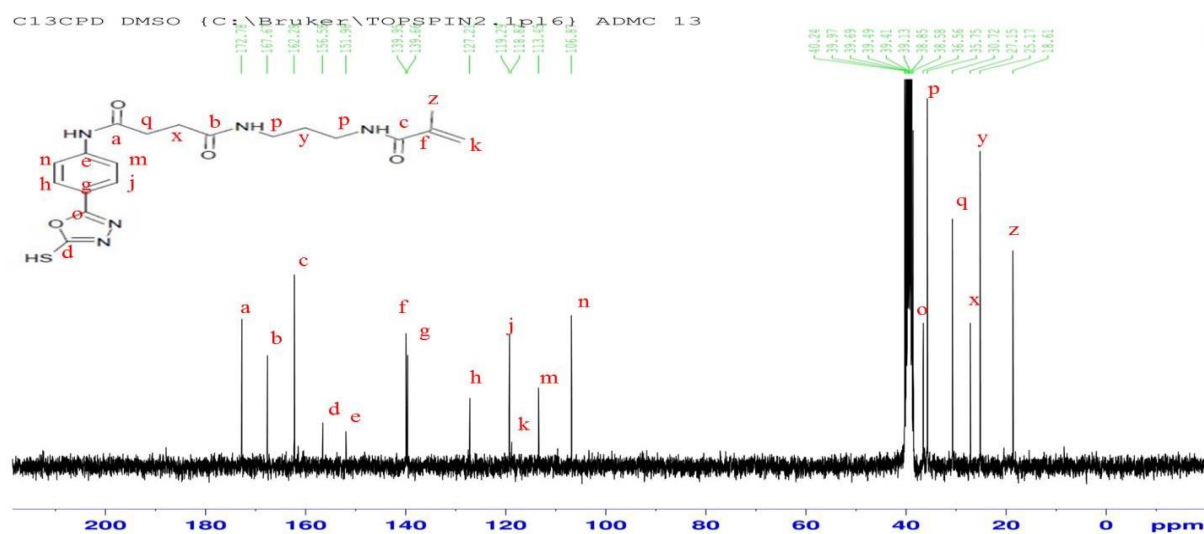


Figure 55- ^{13}C NMR spectra of O-APMA in DMSO carried out using 300MHz NMR at 25 °C.

2.4.2.8- Characterization of RAFT polymerization of HPMA with modified APMA

The FTIR spectrum of poly(HPMA-co-HPMA-P) is shown in Figure 56.

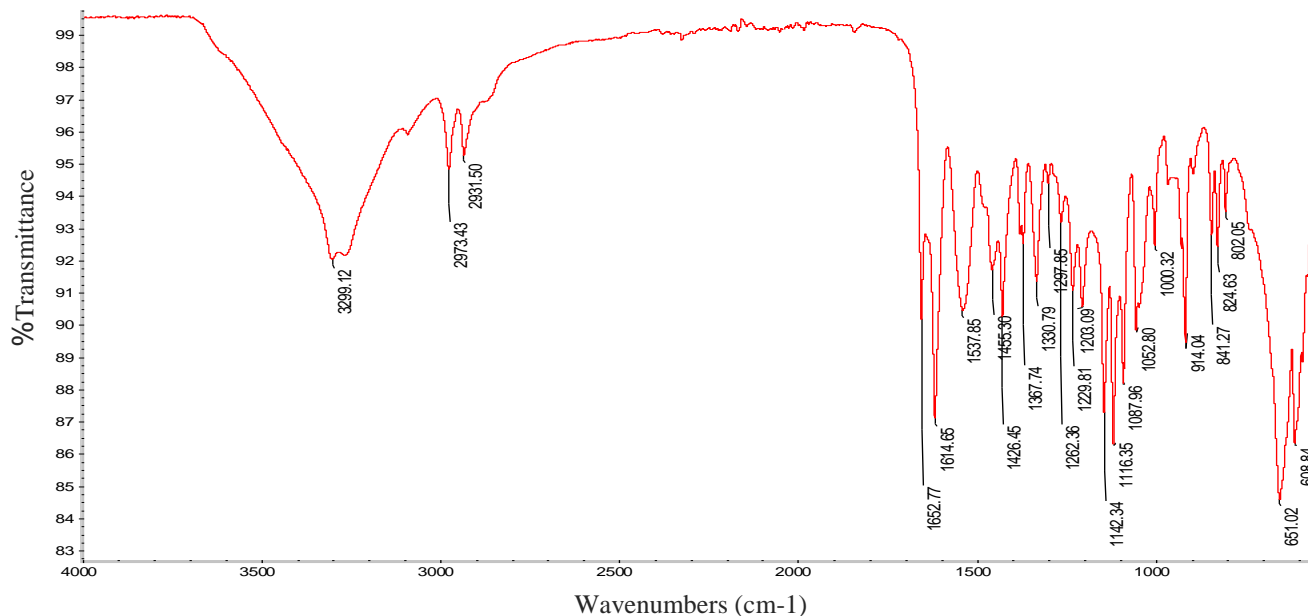


Figure 56- FTIR spectrum of poly(HPMA-co-HPMA-P).

The peak assignment for the FTIR spectra of poly(HPMA-co-HPMA-P) (Figure 56) showed the presence of the broad big band with two peaks band at 3351 cm^{-1} which indicated presence of hydroxyl group from HPMA O-H overlap with the N-H band, peak at 1639 cm^{-1} due to C=O group. Other peaks bandwidth of the principle bands are shown in Table 13.

Table 13- Summary of functional poly(HPMA-co-HPMA-P).

Compound code	Frequency, cm^{-1}	Bond	Functional group
poly(HPMA-co-HPMA-P)	3351	O-H Stretch N-H Stretch	Alcohol Secondary amines
	2968	C-H Stretch	Alkane
	2926		
	1639	C=O Stretch	Carbonyls (general)
	1615	-C=C- stretch	Alkenes
	1528	N-H bend	Secondary amines
	1134	C-N stretch	Aliphatic amines
	1113, 581	C-H bend	Alkenes

The $^1\text{H-NMR}$ spectra of poly(HPMA-co-HPMA-P) (Figure 57) shows the following Peaks palmitoyl group at: 1.00 ppm (t, $\text{CH}_2\text{-CH}_2\text{-CH}_3$, 3H), 1.27 ppm (m, $\text{CH}_3(\text{CH}_2)_{12}$, 24H), 1.4 ppm (m, $\text{CO-CH}_2\text{-CH}_2\text{-CH}_2$, 2H), 1.9 ppm (t, $\text{CO-CH}_2\text{-CH}_2$, 2H) APMA at: 1.65 ppm (m, $\text{NH-CH}_2\text{-CH}_2\text{-CH}_2\text{-NH}$, 2H), 2 ppm (s, $\text{CH}_3\text{-C}(\text{CH}_2)\text{-CO}$, 3H), 3.1 ppm (t, $\text{NH-CH}_2\text{-CH}_2\text{-CH}_2\text{-NH}$, 4H), HPMA at: 1.8 ppm (d, $\text{NH-CH}_2\text{-CH}(\text{CH}_3)\text{OH}$, 1H), 1.13 ppm (d, $\text{CH}_3\text{-CH}(\text{OH})\text{-CH}_2$, 3H), 3.85 ppm (h, $\text{CH}_3\text{-CH}(\text{OH})\text{-CH}_2$, 1H), OH group at 4.9 ppm, amine protons at 7.5 ppm and the end group 5.4 ppm -5.7 ppm, (s, 2H).

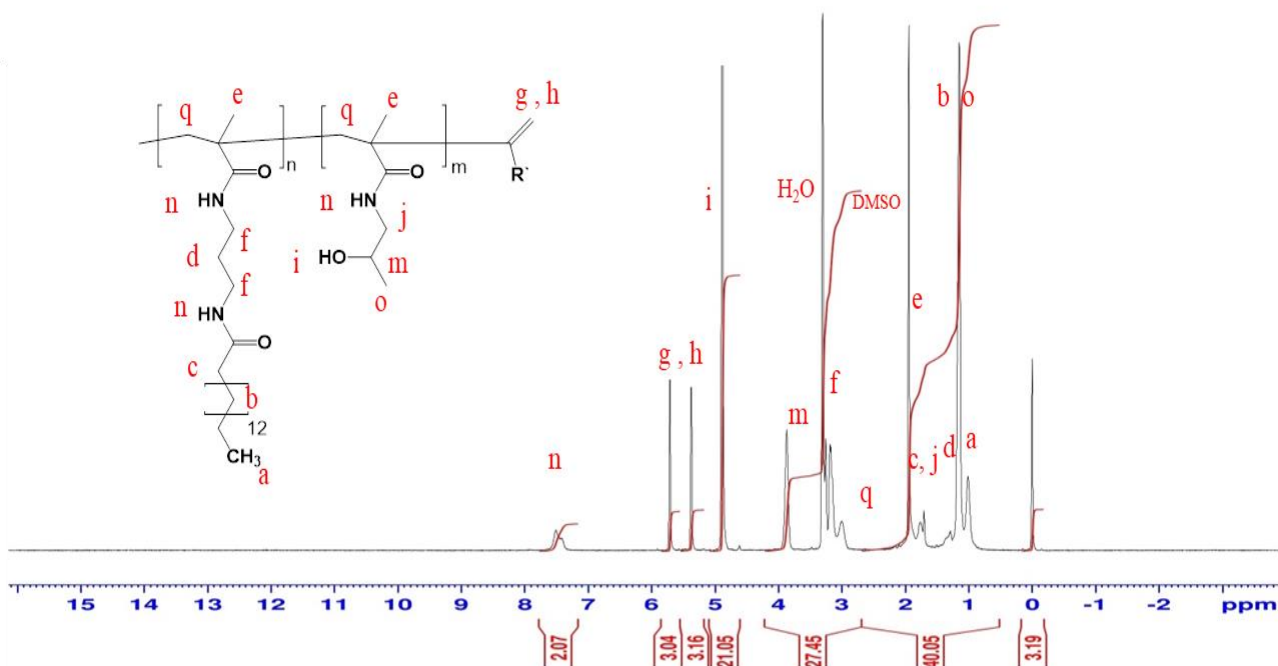


Figure 57- ^1H NMR spectra of poly(HPMA-co-HPMA-P) in DMSO carried out using 300MHz NMR at 25 °C.

The FTIR spectrum of poly(HPMA-co-HPMA-D) is shown in Figure 58.

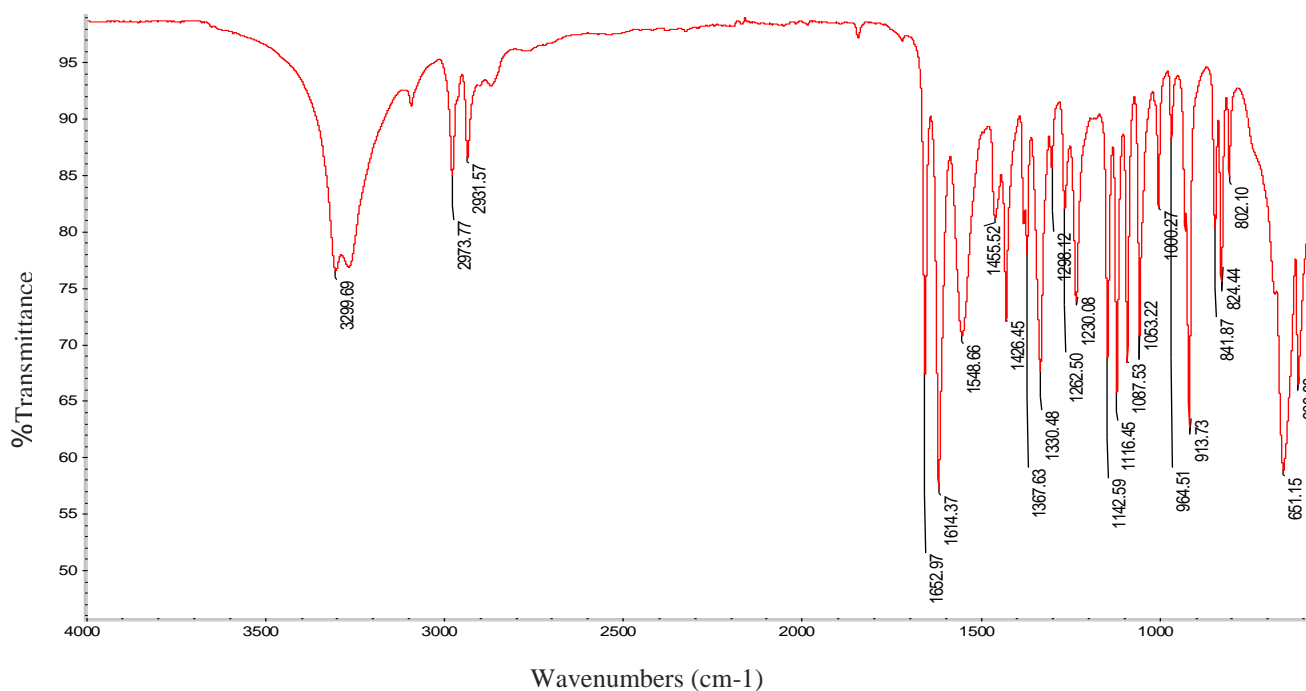


Figure 58- FTIR spectrum of poly(HPMA-co-HPMA-D).

The FT-IR spectrum (Figure 58) indicates the presence of a broad band of O-H overlap with the N-H band and present as a big band with two peaks at 3299 cm⁻¹, sulphonyl group 1652 cm⁻¹, C=O group at 1614 cm⁻¹, and C-C aromatic 1426 cm⁻¹ -1367 cm⁻¹ peaks.

Table 14- Summary of functional poly(HPMA-co-HPMA-D).

Compound code	Frequency, cm ⁻¹	Bond	Functional group
poly(HPMA-co-HPMA-D)	3299	O-H Stretch N-H Stretch	Alcohol Secondary amines
	2973	C-H Stretch	Alkane
	2931		
	1652	S=O Stretch	Sulphonyl
	1614	C=O Stretch	Carbonyl
	1548	-C=C- stretch	Alkenes
	1456	N-H bend	Secondary amines
	1426	C-C stretch (in-ring)	Aromatics
	1367		
	1330	=C-H bend	Alkenes
	1298	S=O	Sulphonyl

	1230	C–N stretch	Aromatic amines
	1142	C–H bend	Alkanes
	1116, 1087	C–N stretch	Aliphatic amines
	1000, 609	=C–H bend	Alkenes

The ^1H NMR spectrum (Figure 59) of poly(HPMA-co-HPMA-D) shows the dansyl group at the following position: 3 ppm (s, N-CH₃, 6H), 7.25 ppm (d, naphthalene proton in position 6, 1H), 7.65 ppm (q, naphthalene protons in position 3 and 8, 2H), 8.13 ppm (d, naphthalene protons in position 4, 1H), 8.3 ppm (d, naphthalene protons in position 7, 1H), 8.48 ppm (d, naphthalene proton in position 2, 1H) and APMA at: 1.6 ppm (m, NH-CH₂-CH₂-CH₂-NH, 2H), 1.9 ppm (s, CH₃-C(CH₂)-CO, 3H), 3.38 ppm (t, NH-CH₂-CH₂-CH₂-NH, 4H), HPMA at: 1.8 ppm (d, NH-CH₂-CH(CH₃)-OH, 1H), 1.13 ppm (d, CH₃-CH(OH)-CH₂, 3H), 3.85 ppm (h, CH₃-CH(OH)-CH₂, 1H), OH group at 4.9 ppm, amine protons at 7.85 ppm and the end group 5.4-5.7 ppm, (s, 2H).

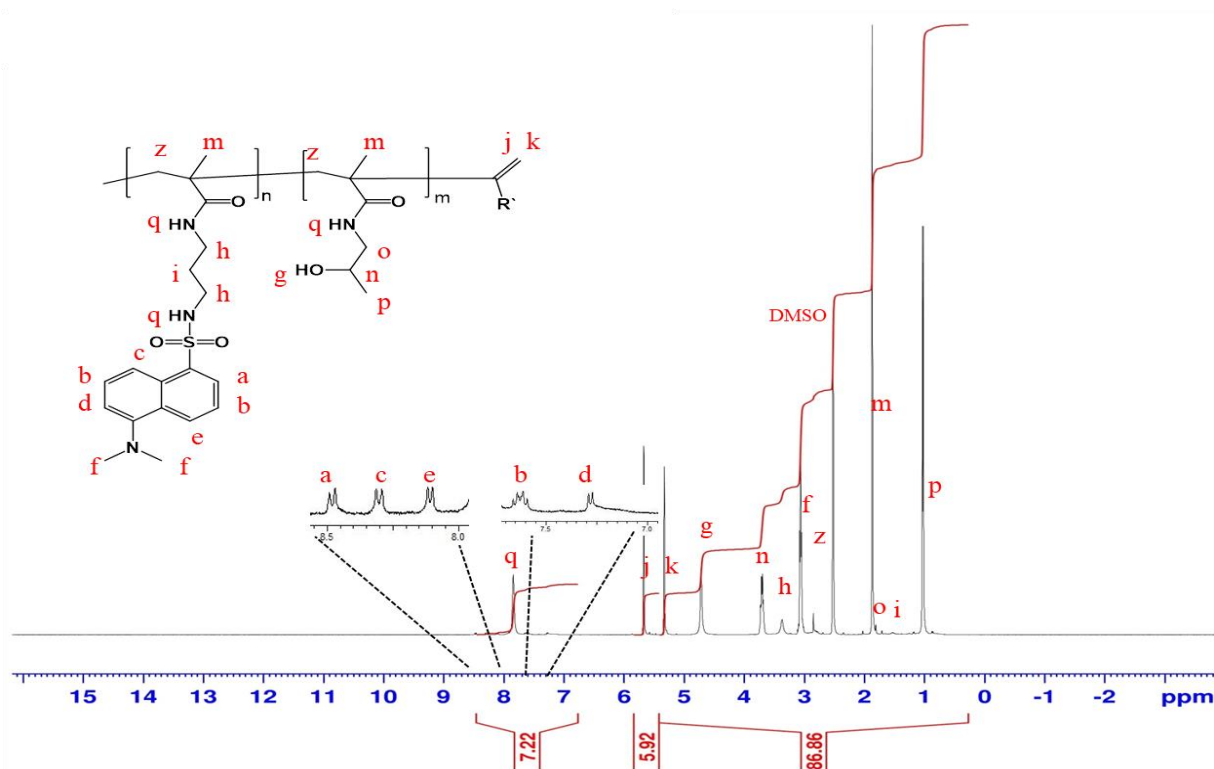


Figure 59- ^1H NMR spectra of poly(HPMA-co-HPMA-D) in DMSO carried out using 300MHz NMR at 25 °C.

The FTIR spectrum of poly(HPMA-co-HPMA-C) is shown in Figure 60.

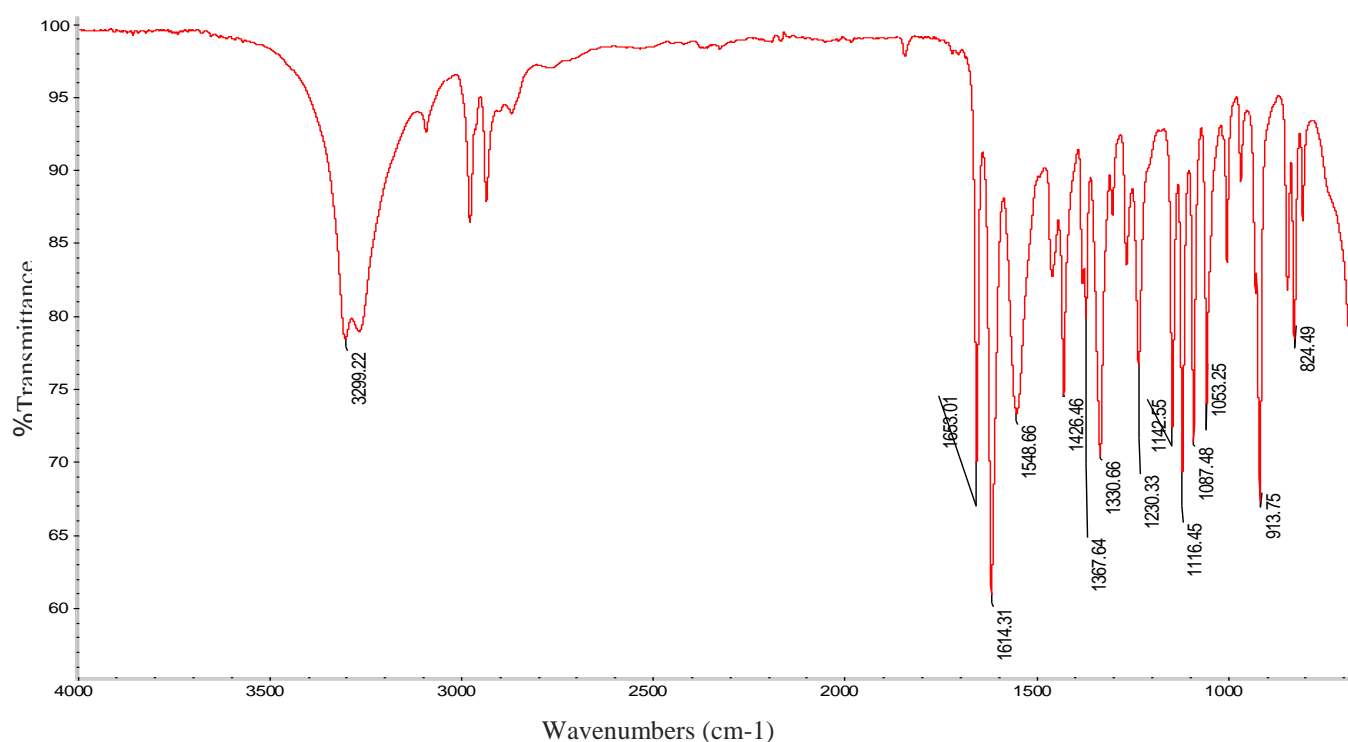


Figure 60- FTIR spectrum of poly(HPMA-co-HPMA-C).

The FTIR spectrum indicate presence of a broad band of O-H overlap with the N-H band and present as a big band with two peaks at 3299 cm^{-1} . The peak at 1614 cm^{-1} is assigned to C=C stretching while the peak at 1655 cm^{-1} due to C=O stretching. Other peaks bandwidth of the principle bands are shown in Table 15.

Table 15- Summary of functional poly(HPMA-co-HPMA-C).

Compound code	Frequency, cm^{-1}	Bond	Functional group
Poly(HPMA-co-HPMA-C)	3299	O-H Stretch N-H Stretch	Alcohol Secondary amines
	2973	C-H Stretch	Alkane
	2931		
	1655	C=O Stretch	Carbonyls (general)
	1614	-C=C- stretch	Alkenes
	1548	N-H bend	Secondary amines
	1426,1330	C-C bend	Alkanes
	1314	C-O stretch	Esters

	1230	C–N stretch	Aliphatic amines
	1142, 1116	C–O Bend	Carbonyl
	1087, 1053	C–O stretch	Esters
	1015	C–N stretch	Aliphatic amines
	913	C–O Bend	Carbonyl
	824, 610	=C–H bend	Alkenes

The ^1H NMR spectrum (Figure 61) poly(HPMA-co-HPMA-C) shows the cholesteryl group at the following position: 1 ppm ($(\text{CH}_3)_2\text{-CH-CH}_2$, 6H), 0.67 ppm-2 ppm (m, cholesteryl protons, 38H), 2.37 ppm (m, CH_2 , 2H), 4.45 ppm (b, oxycyclohexyl, 1H), 6.2 ppm (b, alkenyl, 1H), and APMA at: 0.88 ppm (m, $\text{NH-CH}_2\text{-CH}_2\text{-CH}_2\text{-NH}$, 2H), 1.98 ppm (s, $\text{CH}_3\text{-C(CH}_2\text{)-CO}$, 3H), 3.24 ppm (t, $\text{NH-CH}_2\text{-CH}_2\text{-CH}_2\text{-NH}$, 2H), HPMA at: 1.7 ppm (d, $\text{NH-CH}_2\text{-CH(CH}_3\text{)OH}$, 1H), 1 ppm (d, $\text{CH}_3\text{-CH(OH)-CH}_2$, 3H), 3.85 ppm (h, $\text{CH}_3\text{-CH(OH)-CH}_2$, 1H), OH group at 4.1 ppm, amine protons at 7.35 ppm and the end group 5.4 ppm-5.7 ppm, (s, 2H).

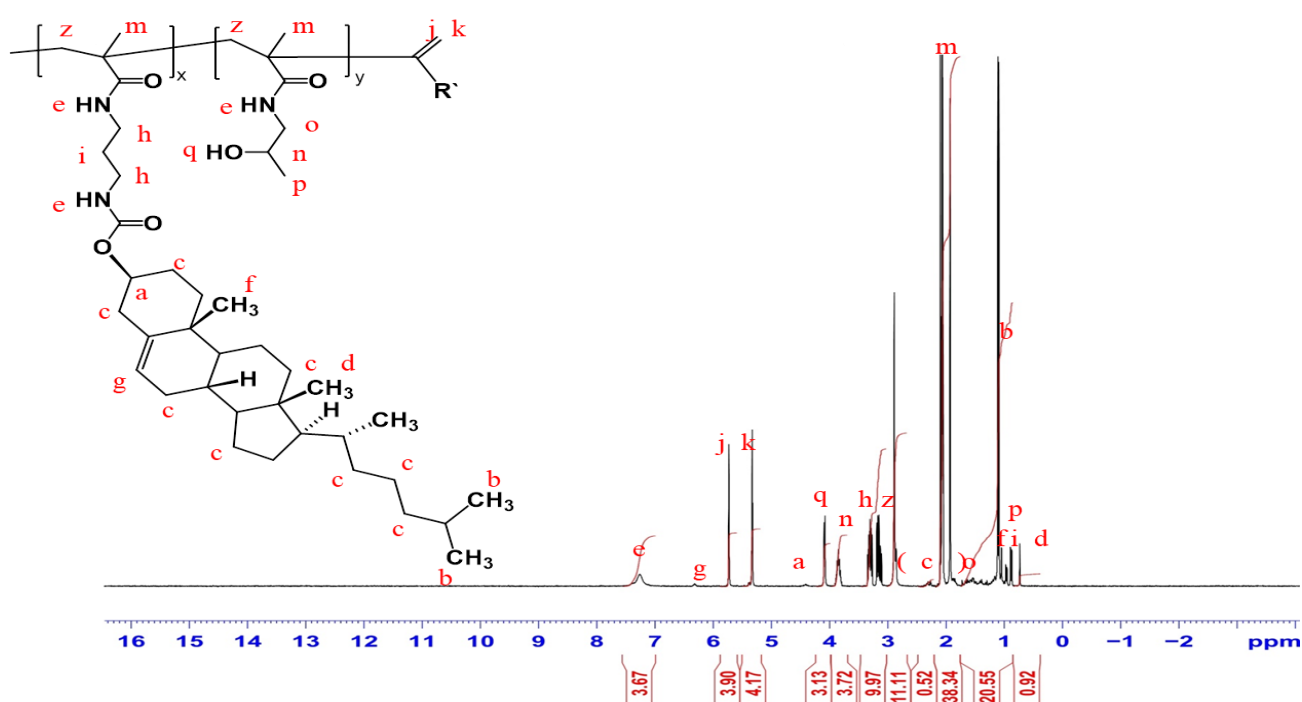


Figure 61- ^1H NMR spectra of poly(HPMA-co-HPMA-C) in DMSO carried out using 300MHz NMR at 25 °C.

The FTIR spectrum of poly(HPMA-co-HPMA-O) is shown in Figure 62.

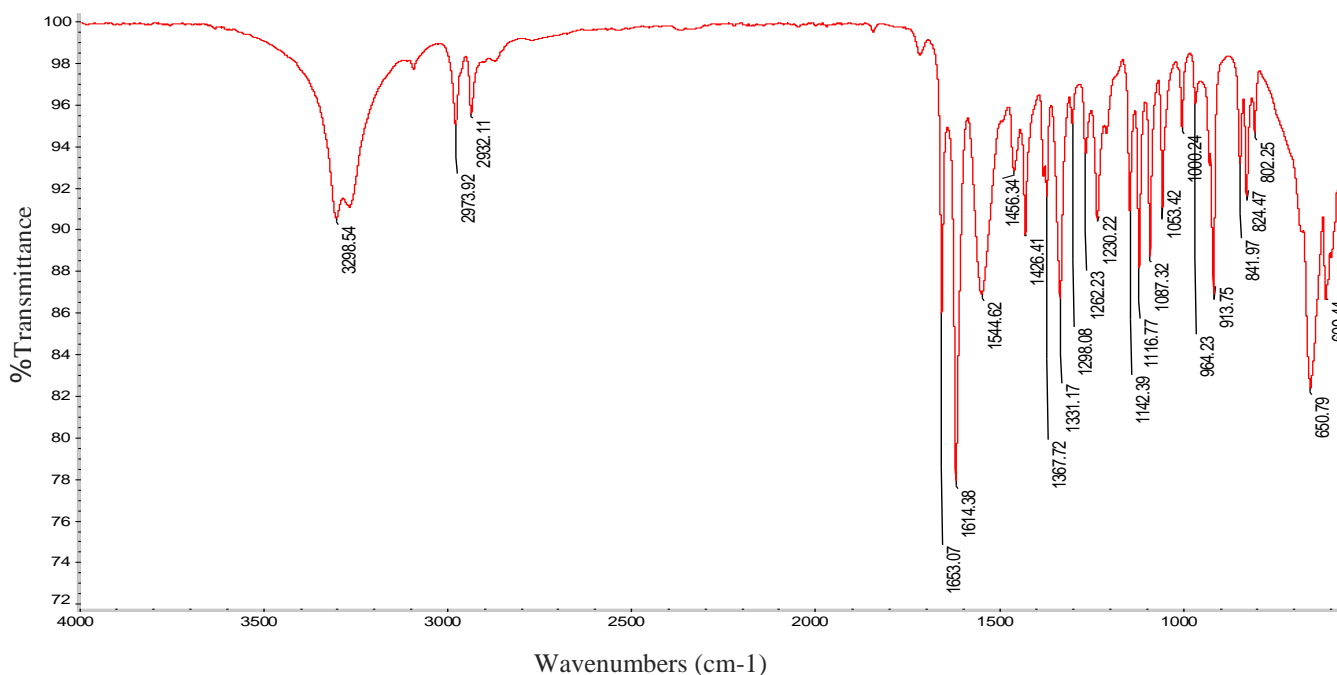


Figure 62- FTIR spectrum of poly(HPMA-co-HPMA-O).

The FT-IR spectrum (Figure 62) showed the presence of hydroxyl and amine group as on broad peak at 3298 cm^{-1} , couple peaks at 1653 cm^{-1} and 1614 cm^{-1} and due to presence two types of C=O group.

Table 16- Summary of functional poly(HPMA-co-HPMA-O).

Compound code	Frequency, cm^{-1}	Bond	Functional group
Poly(HPMA-co-HPMA-O)	3298	O-H Stretch N-H Stretch	Alcohol Secondary amines
	2973	C-H Stretch	Alkane
	2932		
	1839	S-H	Thiol
	1715	C=N Stretch	imine
	1653	C=O Stretch	Carbonyl
	1614		
	1544	N-H bend	Secondary amines
	1456	=C-H	Alkene

	1331	-C=C-	Alkene
	1230	C-H bend	Alkane
	1087, 1000	C-N Stretch	Amine
	913-650	=C-H bend	Alkene

The ^1H NMR spectrum (Figure 63) of poly(HPMA-co-HPMA-O) shows the oxadiazole group and the linker at the following position: 2.65 ppm (t, $\text{CO-CH}_2\text{-CH}_2\text{-CO}$, 4H), 6.7, 6.93, 7.9 and 8.1 ppm (m, aromatic protons, 4H) and APMA at: 1.02 ppm (m, $\text{NH-CH}_2\text{-CH}_2\text{-CH}_2\text{-NH}$, 2H), 1.86 ppm (s, $\text{CH}_3\text{-C}(\text{CH}_2)\text{-CO}$, 3H), 3.16 ppm (t, $\text{NH-CH}_2\text{-CH}_2\text{-CH}_2\text{-NH}$, 4H), HPMA at: 1.8 ppm (d, $\text{NH-CH}_2\text{-CH}(\text{CH}_3)\text{OH}$, 1H), 1.13 ppm (d, $\text{CH}_3\text{-CH}(\text{OH})\text{-CH}_2$, 3H), 3.85 ppm (h, $\text{CH}_3\text{-CH}(\text{OH})\text{-CH}_2$, 1H), OH group at 4.9 ppm, amine protons at 7.5 ppm and the end group 5.4 ppm-5.7 ppm, (s, 2H).

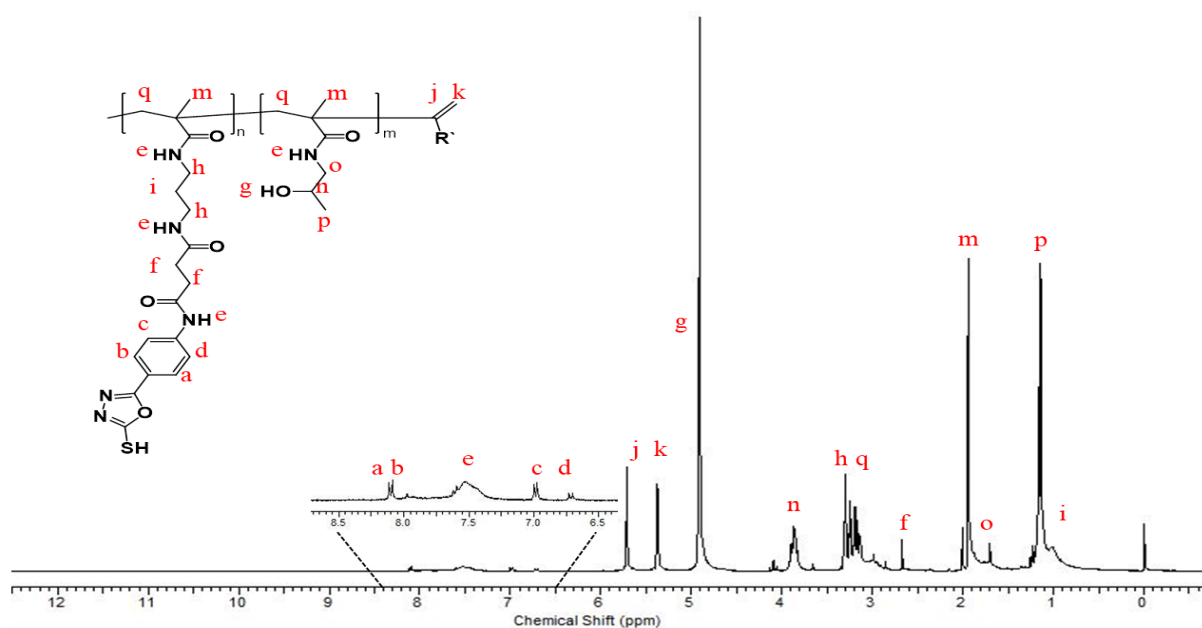


Figure 63- ^1H NMR spectra of poly(HPMA-co-HPMA-O) in DMSO carried out using 300MHz NMR at 25 °C.

2.4.2.9- Characterization of block copolymerization

The FTIR spectrum of poly(HPMA-co-HPMA-O)-*b*-PEG is shown in Figure 64.

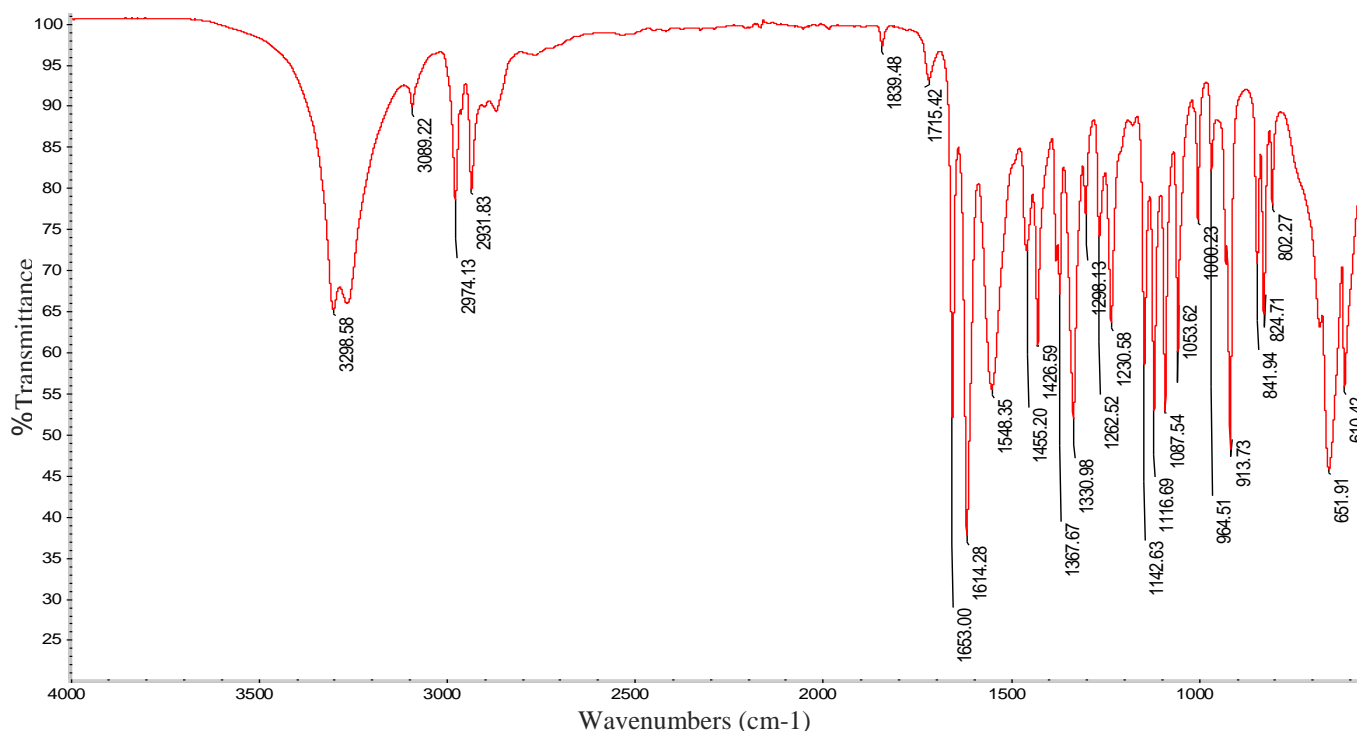


Figure 64- FTIR spectrum of poly(HPMA-co-HPMA-O)-*b*-PEG.

The poly(HPMA-co-HPMA-O)-*b*-PEG exhibits absorptions those of hydroxyl and amine group at 3298 cm^{-1} . The increase of the transmission peak of hydroxyl and amine groups confirm the PEG incorporation into the (HPMA-co-HPMA-O) polymer.

Table 17- Summary of functional poly(HPMA-co-HPMA-O)-*b*-PEG.

Compound code	Frequency, cm^{-1}	Bond	Functional group
Poly(HPMA-co-HPMA-O)-<i>b</i>-PEG	3298	O-H Stretch N-H Stretch	Alcohol Secondary amines
	3089	=C-H Stretch	Alkene
	2974, 2931	C-H Stretch	Alkane
	1839	S-H	Thiol
	1715	C=N Stretch	imine
	1653, 1614	C=O Stretch	Carbonyl
	1548	N-H bend	Secondary amine
	1455	=C-H	Alkene

	1330	-C=C-	Alkene
	1230	C-H bend	Alkane
	1087, 1000	C-N Stretch	Amine
	913-610	=C-H bend	Alkene

The ^1H NMR spectrum (Figure 65) of poly(HPMA-co-HPMA-O)-*b*-PEG shows the oxadiazole group and the linker at the following position: 2.65 ppm (t, CO-CH₂-CH₂-CO, 4H), 6.7 ppm, 6.93 ppm, 7.9 ppm and 8.1 ppm (m, aromatic protons, 4H) and APMA at: 1.02 ppm (m, NH-CH₂-CH₂-CH₂-NH, 2H), 1.86 ppm (s, CH₃-C(CH₂)-CO, 3H), 3.16 ppm (t, NH-CH₂-CH₂-CH₂-NH, 4H), HPMA at: 1.8 ppm (d, NH-CH₂-CH(CH₃)-OH, 1H), 1.13 ppm (d, CH₃-CH(OH)-CH₂, 3H), 3.85 ppm (h, CH₃-CH(OH)-CH₂, 1H), OH group at 4.9 ppm, amine protons at 7.5 ppm and the end group 5.4-5.7 ppm, (s, 2H), PEG peaks at: 3.5 ppm (t, O-CH₂-CH₂, 2H) and 4.19 ppm (t, O-CH₂-CH₂, 2H), joint group 6 ppm (s, 2H).

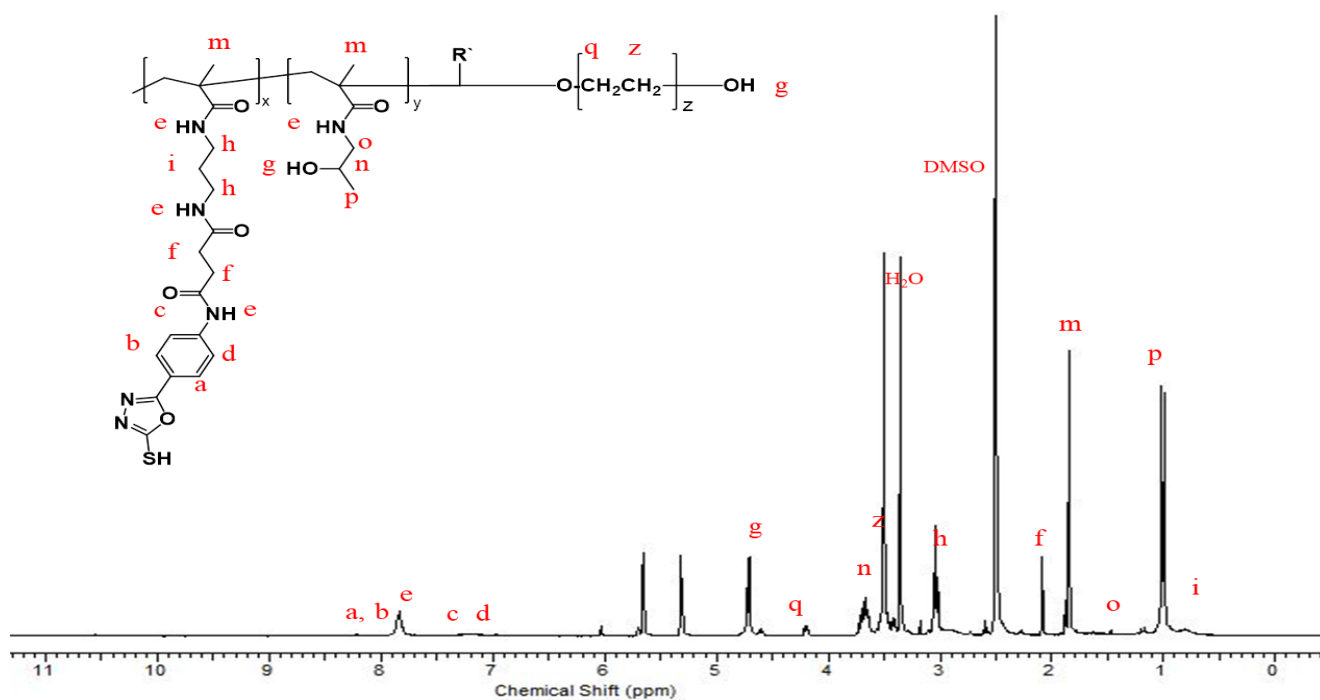


Figure 65 - ^1H NMR spectra of poly(HPMA-co-HPMA-O)-*b*-PEG in DMSO carried out using 300MHz NMR at 25 °C.

The FTIR spectrum of poly(HPMA-co-HPMA-D)-*b*-PEG is shown in Figure 66.

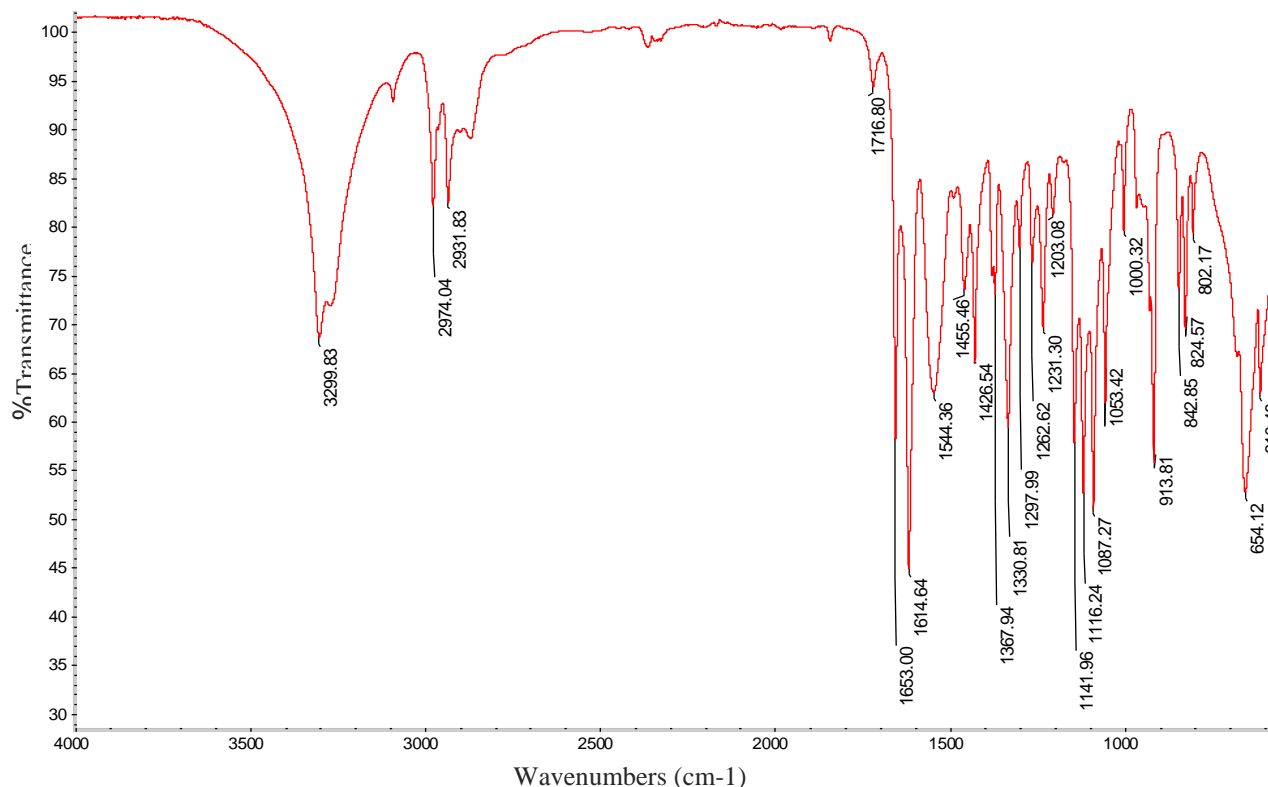


Figure 66- FTIR spectrum of poly(HPMA-co-HPMA-D)-*b*-PEG.

The peak assignment for the FTIR spectra of poly(HPMA-co-HPMA-D)-*b*-PEG showed the presence of the broad band with two peaks 3299 cm^{-1} . These peaks indicated OH and NH groups had occurred, block copolymerization with PEG was confirmed by the increase in the transmission of this peak.

Table 18 - Summary of functional poly(HPMA-co-HPMA-D)-*b*-PEG.

Compound code	Frequency, cm^{-1}	Bond	Functional group
Poly(HPMA-co-HPMA-D)-<i>b</i>-PEG	3299	O-H Stretch N-H Stretch	Alcohol Secondary amines
	2974	C-H Stretch	Alkanes
	2931		
	1653	S=O Stretch	Sulphonyl
	1614	C=O Stretch	Carbonyl
	1544	-C=C- stretch	Alkenes
	1456	N-H bend	Secondary amines

	1426	C–C stretch (in–ring)	Aromatics
	1367		
	1330	=C–H bend	Alkenes
	1298	S=O	Sulphonyl
	1230	C–N stretch	Aromatic amines
	1142	C–H bend	Alkanes
	1116-1087	C–N stretch	Aliphatic amines
	1000-609	=C–H bend	Alkenes

The ^1H NMR spectrum (Figure 67) of poly(HPMA-co-HPMA-D)-co-PEG shows the dansyl group at the following position: 3 ppm (s, N-CH₃, 6H), 7.25 ppm (d, naphthalene proton in position 6, 1H), 7.65 ppm (q, naphthalene protons in position 3 and 8, 2H), 8.13 ppm (d, naphthalene protons in position 4, 1H), 8.3 ppm (d, naphthalene protons in position 7, 1H), 8.48 ppm (d, naphthalene proton in position 2, 1H) and APMA at: 1.6 ppm (m, NH-CH₂-CH₂-NH, 2H), 1.9 ppm (s, CH₃-C(CH₂)-CO, 3H), 3.38 ppm (t, NH-CH₂-CH₂-CH₂-NH, 4H), HPMA at: 1.8 ppm (d, NH-CH₂-CH(CH₃)OH, 1H), 1.13 ppm (d, CH₃-CH(OH)-CH₂, 3H), 3.85 ppm (h, CH₃-CH(OH)-CH₂, 1H), OH group at 4.9 ppm, amine protons at 7.85 ppm and the end group 5.4-5.7 ppm, (s, 2H), PEG peaks at: 3.15 ppm (t, O-CH₂-CH₂, 2H) and 4.19 ppm (t, O-CH₂-CH₂, 2H), joint group 5.7 ppm (s, 2H).

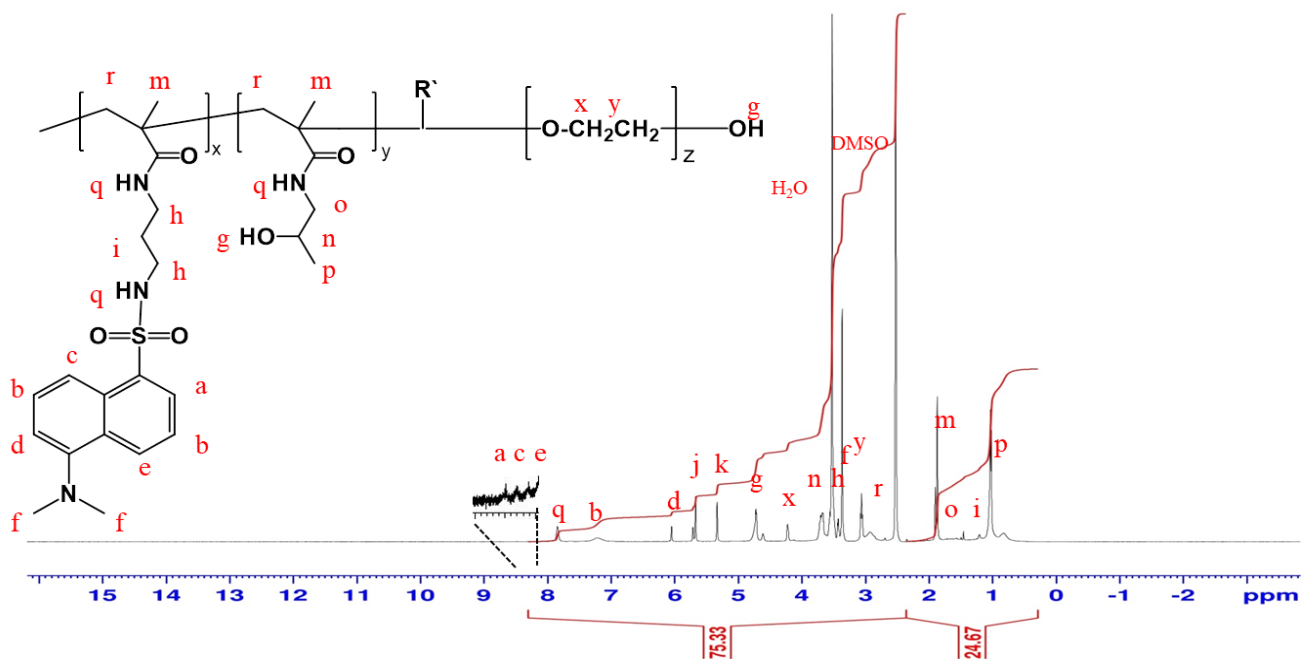


Figure 67- ^1H NMR spectra of poly(HPMA-co-HPMA-D)-b-PEG in DMSO carried out using 300MHz NMR at 25 °C.

2.5- Discussion

Our TLC, FTIR and NMR analysis of the products show that we successfully grafted APMA amino groups with palmitoyl, dansyl, cholesteryl and oxadiazole moieties.

Our choice of pendant group to add onto the APMA monomer was based on the literature. Our first pendant group was addition of a palmitoyl moiety. *Yogesh et al.*, acylated low molecular weight chitosan (LMWC) at the amine group with palmitoyl chloride. Acylation of LMWC showed a dramatic increase in the drug loading from $13.8 \pm 0.95\%$ to $30.2 \pm 1.9\%$ in addition to $80 \pm 2.08\%$ as maximum drug released in 10 h while only $52.3 \pm 2.14\%$ was released in 24 h for low molecular weight palmitoyl chitosan (LMWPC) (*Yogesh et al.*, 2012).

Acylation is one of the chemical modification methods that is used to increase the hydrophobic character of polymers that is used in gene and drug delivery systems, benefiting from the amphiphilic structure, hydrophilic core and many hydrophobic tails to: (A) improve the organic solubility of some natural polymers like chitosan (*Radrigues, 2005*), (B) increase drug loading capacity of polymer and sustained drug release (*Yogesh et al.*, 2012), and (C) can effectively decrease the dendrimer cytotoxicity (*Wang et al.*, 2012).

In this respect, Thompson and colleges reported the use of amphiphilic poly(allylamine) (PAA) consisting of randomly grafted palmitoyl moieties followed by quaternising with methyl iodide to study the capability of these self-assembled polymers to form nano-complexes with insulin in pH 7.4 Tris buffer (*Thompson et al.*, 2009). They reported that all the polymers had less cytotoxicity than PAA and showed high insulin complexation efficiency between 78% and 93% (*Thompson et al.*, 2009). Further carried out research done by Katugampola and Winstead studied the substitution degree 42%, 44% and 81% of palmitoyl chloride chitosan on the rheological behaviour and thermal stability, they found increasing thermal stability and crystallinity of palmitoyl chitosan with increase in the substitution degree (*Katugampola and Winstead, 2014*).

The FTIR spectra for P-APMA (Figure 29) shows the presence of three sharp intense peaks at 3294 cm^{-1} , 2916 cm^{-1} and 1637 cm^{-1} and were assigned to the -NH, C-H and carbonyl groups respectively, which occurred in both APMA and palmitoyl moiety. The ^1H and ^{13}C NMR spectra confirm the chemical structure for P-APMA; the ^1H NMR spectrum (Figure 30) indicates two significant peaks at 0.75 ppm and 1.27 ppm which belong to palmitoyl units

and three important bands at 5.36 ppm, 5.8 ppm and 6.12 ppm, 6.75 ppm which are characteristics of the APMA unit. The ^{13}C NMR spectrum (Figure 31) displays the peaks at 14.15 ppm and 18.67 ppm, corresponding to the methyl groups of palmitoyl and APMA respectively. Especially, the spectrum shows two peaks at 139.7 ppm and 119.9 ppm due to vinyl group. The spectrum also indicates two signals at 174 ppm and 168 ppm which belongs to carbonyl groups, all these peaks suggested the formation of the P-APMA.

The second and third hydrophobic pendant groups we used were dansyl and cholesteryl respectively. Dansyl and cholesteryl moieties work as universal hydrophobic drug solubilizers when it's substituted as a grafted group on polymers (Hoskins *et al.*, 2012a).

Fluorescent nanoparticles have been attracting much attention because of their: (a) high brightness, (b) improved photostability, and (c) tunable emission properties. Additionally, fluorescent nanoparticles are a powerful alternative tool for traditional molecular fluorophores in a wide range of applications such as labelling or sensing tools (Ouadahi *et al.*, 2012). Dansyl moiety, which is used in the current work, has been commonly used as a fluorescent label in later biological characterisation due to the occurrence of the conjugated aromatic ring systems. More precise representation of nanoparticles *in vivo* fate can be obtained by using fluorescent labels. On the other hand, polymer cytotoxicity and physical properties can be changed due to occurrence of its (Hoskins *et al.*, 2012a).

In the FTIR spectrum of the D-APMA (Figure 33), showed the occurrence of broad band of N-H at around 3289 cm^{-1} . Also peaks of sulphonyl group at 1712 cm^{-1} , C=O group at 1655 cm^{-1} , and C-C aromatic 1530 cm^{-1} - 1406 cm^{-1} were seen confirming the combination of the APMA with the dansyl group. The ^1H NMR spectrum (Figure 34) shows peaks observed between 7.2 ppm and 8.38 ppm, these were due to the hydrogen atoms on the aromatic rings of naphthalene structures. Besides, the spectrum displays a single peak at 5.67 ppm which is indicative of the vinyl group and two peaks at 6.14 ppm and 7.27 ppm which arise from the hydrogen atoms of amine groups. The ^{13}C NMR data (Figure 35) are consistent with the ^1H NMR data confirming the combination of the APMA with dansyl group.

Cholesterol and its derivatives are soluble-fat-molecules that occur in nature and are defined as amphiphilic or hydrophobic groups based on the chemical structure of the subunits that are present in the molecule (Zhou *et al.*, 2009). Cholesterol has the ability to cross cellular

membranes making it an effective component to use in therapeutic delivery systems (Sevimli *et al.*, 2012). Ashlynn *et al.*, achieved high paclitaxel loading 14% and an encapsulation efficiency around 92% by using cationic micelles self-assembled from an amphiphilic copolymer poly{(N-methyldietheneamine sebacate)-co-[(cholesteryl oxocarbonylamido ethyl) methyl bis(ethylene)ammonium (PMDS)} (Ashlynn *et al.*, 2011). This type of micelles self-assembled had been conjugated to poly (ethylene glycol) (PEG) with different cholesterol grafting degrees to improve the stability of micelle/DNA complexes in the blood for systemic *in vivo* gene delivery. Wanga *et al.*, found that PMDS and PEG-PMDS without cholesterol could not form stable micelles but formed large particles (Wanga *et al.*, 2007).

The FTIR spectrum of C-APMA (Figure 37) indicates two peaks appeared at 3386 cm^{-1} and 3272 cm^{-1} due to NH group. Further peaks at 1659 cm^{-1} and 1702 cm^{-1} are assigned to C=C stretching and C=O stretching respectively. The ^1H NMR spectrum (Figure 38) shows the peaks at 0.67-2 ppm which are characteristics of the cholesteryl protons in the C-APMA. The spectrum also displays two singlet peaks at 5.3, 5.76 ppm, corresponding to the vinyl group, in addition to two singlet peaks at 6.67 ppm and 7.26 ppm due to the amine group in the APMA. The ^{13}C -NMR spectrum (Figure 39) shows two significant peaks of carbonyl groups at 157 ppm and 168 ppm for cholesteryl and APMA respectively, peaks at 11.86, 18.70 and 22.85 ppm due to the methyl groups in the cholesteryl and APMA, and the peaks at 22.54 and 139.85 ppm corresponding to vinyl groups in the cholesteryl and APMA.

Lastly, we tried to conjugate an oxadiazole moiety onto the APMA monomer. 1,3,4-oxadiazole moiety is a hydrophobic heterocyclic compound due to its aromatic structure and also contains two nitrogen atoms and an oxygen atom in a five-membered ring attached to a thiol (SH) group. This group has the ability to make strong dative covalent attachment with colloidal gold surfaces for the HNPs (Barnett *et al.*, 2013). Compounds containing 1,3,4-oxadiazole cores have been used in wide rang as anticancer, antifungal, antibacterial and anti-inflammatory (Oliveira *et al.*, 2012).

The reaction between APMA with 5-(4-chlorophenyl)-1,3,4-oxadiazole-2-thiol was not successful when we used the direct substitution reaction. This can be interpreted that the chlorine atom is attached to a benzene ring, overlapping of the p-orbital of the chlorine atom with the π orbitals of the benzene ring, thus making the carbon-chlorine bond stronger, and it

is far less reactive than when in a haloalkane. So we created a new way to prepare this compound by building up this molecule throughout 4 steps.

For the reaction of the aminobenzoylhydrazine with carbon disulphide the FTIR spectrum (Figure 41) indicates that the desired product 5-(4-Aminophenyl)-1,3,4-oxadiazole-2-thiol was formed, showing the characteristic primary amine group peak at 3446 cm^{-1} and 3349 cm^{-1} and aromatic C=C at 1440 cm^{-1} , 1503 cm^{-1} and 1514 cm^{-1} . The ^1H NMR spectrum (Figure 42) indicates two significant peaks at 6.65 ppm and 7.5 ppm due to the aromatic protons. The ^{13}C -NMR spectra (Figure 43) of D1 showed the presence of the aromatic group peaks and oxadiazole aliphatic carbons peaks.

D2 was synthesized by using the most common activation method of carboxylic group, (Veronese and Morpurgo, 1999) by reacting D2 with NHS in the present of DCC as a catalyst to produce active form (D3) which is suitable for the next step which involves coupling with the primary amines of the APMA.

The FTIR spectra for D2 (Figure 45) shows broad peaks of hydroxyl at 3330 cm^{-1} as carboxylic acids exist mainly as dimers due to the intermolecular hydrogen bonding, this led OH peak to be broad and medium intensity compared with non-dimeric form, (Lin-Vien *et al*, 1991) in addition to two peaks exhibited at 1707 cm^{-1} and 1645 cm^{-1} due to the absorbance of carboxylic acid and amide carbonyl groups respectively (Stuart, 2004).

The result obtained from (Figure 46) for D1 showed two sets of peaks were observed, the addition of succinic anhydride to the 5-(4-Aminophenyl)-1,3,4-oxadiazole-2-thiol (D1) produced extra peaks at 2.5 ppm (Figure 47), due to the aliphatic hydrogen's of succinic moiety attached to the amine group. Four sets of doublets are observed between 6.6 ppm - 8.18 ppm these were due to aromatic protons with one neighbouring proton therefore forming a doublets peak. The presence of aliphatic carbons in addition to aromatic carbons at ^{13}C NMR spectrum (Figure 48) strongly suggests the attachment of the succinic moiety to D1.

FTIR spectra of D3 (Figure 49) exhibited characteristic peaks attributed to NH group and carbonyl groups respectively, as well as the absence of hydroxyl group of carboxylic acid (D2) which confirms the formation of amide bond. In the ^1H NMR spectrum (Figure 50), the peaks 2.47 ppm and 2.76 ppm which are characteristics of the succinimide group. The

spectrum also displays four doublet peaks corresponding to the benzene group, in addition to two triplet peaks due to linker group in the D3.

The presence of thiol group at 2033 cm^{-1} , N-H and 3303 cm^{-1} as well as C=N at 1713 cm^{-1} on the FTIR of O-APMA (Figure 53) suggested the attachment of the APMA moiety had been successful. Furthermore, peaks were also evident due to the C=C bonds within the APMA moiety. The evidence for the D3 and APMA conjugation was also obtained by ^1H and ^{13}C NMR.

The free radical polymerization reaction mechanism consists of three steps: initiation, propagation and termination, the termination step could take either route A or B as shown in Figure 68. The ^1H NMR spectrum (Figure 57, 69, 61, 73, 65 and 67) of HPMa copolymers show the presence of a couple of peaks in the region of olefinic protons at 5.4 ppm-5.7 ppm. These peaks arise from the hydrogen atoms of the olefin groups which give us evidence that the disproportionation reaction taken route A (Hatada *et al.*, 1986).

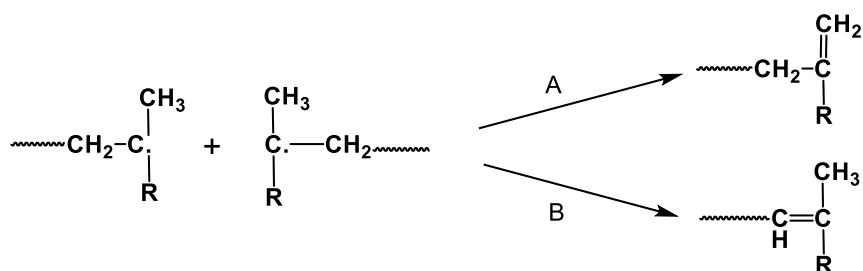


Figure 68- Disproportionation termination routes.

Fourier transform infrared spectroscopy was used to characterize all the copolymer derivatives in order to identify the functional groups attributed to the feeder monomers. FTIR spectra show the copolymerization reaction between HPMa and APMA-R has been successful. PEG block copolymerization reaction caused increase in the intensity peak of hydroxyl and amine groups in FTIR spectra, in addition to the presence of a new single band at 5.7-6 ppm in NMR spectra which related to the CH_2 joint group. All that confirms the PEG incorporation into the (HPMa-co-HPMa-O) and (HPMa-co-HPMa-D) polymers was successful.

2.6- Conclusion

In summary, APMA modified monomers and HEMA-co-APMA-R-b-PEG copolymers were successfully prepared. The successful synthesis of the copolymers and modified monomers (structure and properties) was confirmed by ^1H NMR, ^{13}C NMR, FTIR, melting point and thin layer chromatography.

Chapter Three

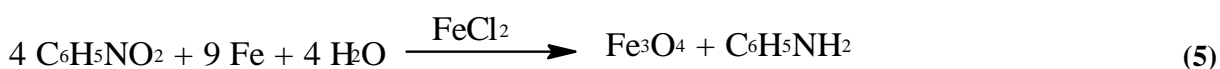
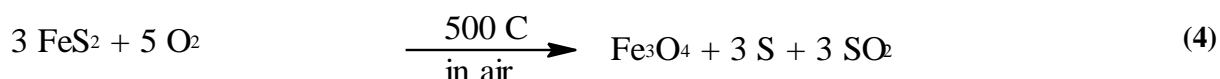
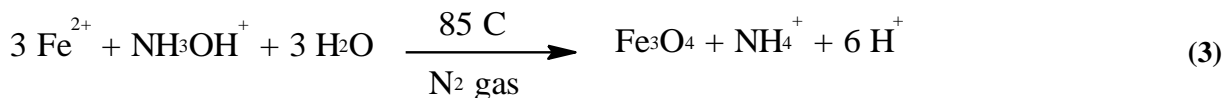
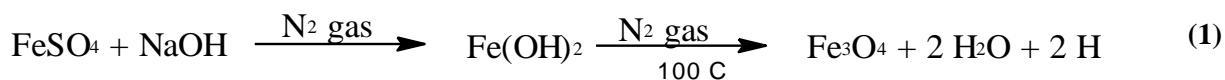
Synthesis and characterisation of hybrid nanoparticles

3.1- Introduction

Over the last two decades, magnetic nanoparticles (MNPs) have emerged as new front runners in the race for the treatment of cancer. Extensive studies have been carried out in order to incorporate diagnostic and therapeutic functions for this matter forming theranostic agents. Many magnetic nanoparticle systems in combination with gold, iron oxide, quantum dots, silver nanoparticles and carbon nanotubes have been investigated (Nekolla *et al.*, 2016, Modugno *et al.*, 2015, Boncel *et al.*, 2017). Gold coated magnetic iron oxide nanoparticles (hybrid nanoparticles, HNPs) have been reported for their potential for image guided cancer therapy (Barnett *et al.*, 2012, Hoskins *et al.*, 2012b). The unique properties of these nanoparticles arise from their architecture. The iron oxide core displays extraordinary magnetic properties, while the gold surface offers enhanced biocompatibility, facilitates attachment with thiolated (-SH) molecules and has potential to act as a triggered heat source after laser irradiation. Changing the size, charge, shape and gold shell thickness have been used to tune and tailored the optical and magnetic properties of this particles (Barnett *et al.*, 2012, Saimon *et al.*, 2016, Sailor and Park, 2012).

A limitation associated with MNPs in sensing applications arises from the problems of low surface charge at neutral pH and large surface area to volume ratio, which leads the MNP aggregation whilst dispersed in solvents; in addition to low electrical conductivity and limited optical properties. However, these entire problems can be tackled by coating MNPs with a gold shell (Saimon *et al.*, 2016). HNP synthesis involves two steps, iron oxide core synthesis and subsequent gold coating. Various chemical methods such as co-precipitation, micro-emulsion and thermal decomposition have been used for the synthesis of the iron oxide core. Co-precipitation is the common method used in the fabrication of these nano particles. Several synthetic recipes have been reported by Cornwell and Schwertmann (Equation 1-5) (Teja and Koh, 2009, Mutasim, 2015).

Gold deposited onto MNPs can be formed either directly or indirectly. The differences in the surface nature of MNPs and gold make directly coating more difficult. Many new techniques have been investigated to address this problem.



In a study by Zhang and colleagues, a novel method combining wet chemistry and laser irradiation. The gold layer was formed onto the MNPs cores (which were fabricated by wet chemistry) by laser irradiation of Au powder in liquid medium. Ban and colleagues, reported successful coating of 11 nm iron cores by 2.5 nm gold shell via partial replacement reaction in a polar aprotic solvent (Verma *et al.*, 2014, Zhang *et al.*, 2006, Ban *et al.*, 2005).

Another technique consists of using polymer layers or glue layers between the magnetic core and the outer golden shell. This technique is known as indirect gold coating. Polymer coating of MNPs has been successfully employed by using poly (N-vinylpyrrolidone) (PVP), poly (4-vinylpyridine), poly (vinyl alcohol) (PVA), poly (ethylene glycol) (PEG), chitosan and poly(ethyleneimine) (PEI) (Saha *et al.*, 2012).

Jin and co-workers reported developing a new class of HNP by coating the iron oxide nanoparticles within phospholipid-polyethylene glycol terminated with carboxylic acid (PL-PEG-COOH) followed by a layer of poly-L-histidine. The outer gold shell formed through the reduction of gold chloride onto the chelating agent with hydroxylamine (Figure 69). In comparison with the direct method, HNP particles tend to be more uniform and compact in size (Jin *et al.*, 2010).

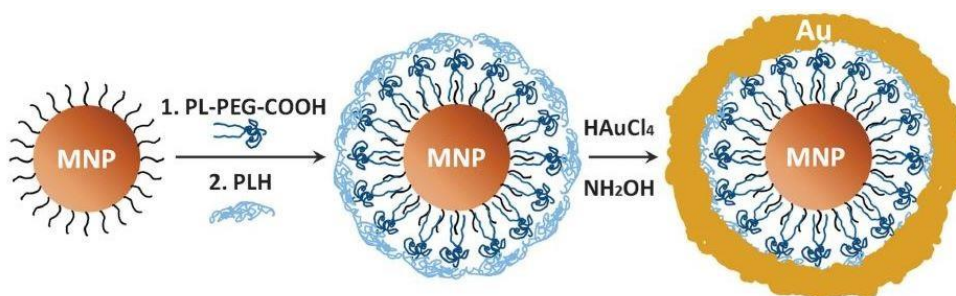


Figure 69- Schematic of MNP-gold core-shell NPs

In 2009 Goon and colleagues reported that coating of magnetite core with PEI before saturation of the surface with 2 nm gold seeds enhances the chemical resistance of the magnetite core in addition to enhancement in the HNPs stability against aggregation.

Synthesis of HNPs must be fully characterised in terms of metal content, surface charge and particle size. In order to do this, a number of techniques are used. The principles of which are documented below.

3.1.1- Inductively Coupled Plasma – Optical Emission Spectroscopy (ICP-OES)

Inductively Coupled Plasma Optical Emission Spectroscopy (ICP-OES) is a useful analytical technique used for quantitative measurement of metal elements within a sample. ICP-OES technique has been used commercially available since 1983 in a huge range of applications (Warra and Jimoh, 2011). Basically, ICP-OES consists of two parts: Inductively coupled plasma ICP which is used to create plasma to convert the sample atoms to ions, then the ions will be separated and detected by the optical emission spectrometer OES part. A schematic diagram of ICP-OES can be seen in Figure 70 (Boss and Fredeen, 1997).

ICP-OES has several advantages over other techniques, including low sample consumption, low detection limit, high sensitivity and multi-element analysis technique (Warra and Jimoh, 2011). Generally speaking, samples are introduced as fine aerosols into the ICP plasma by using argon as sample carrier gas. Once the sample and argon are mixed an applied spark causes formation of argon ions which will lead to create argon discharge or plasma. (Boss and Fredeen, 1997)

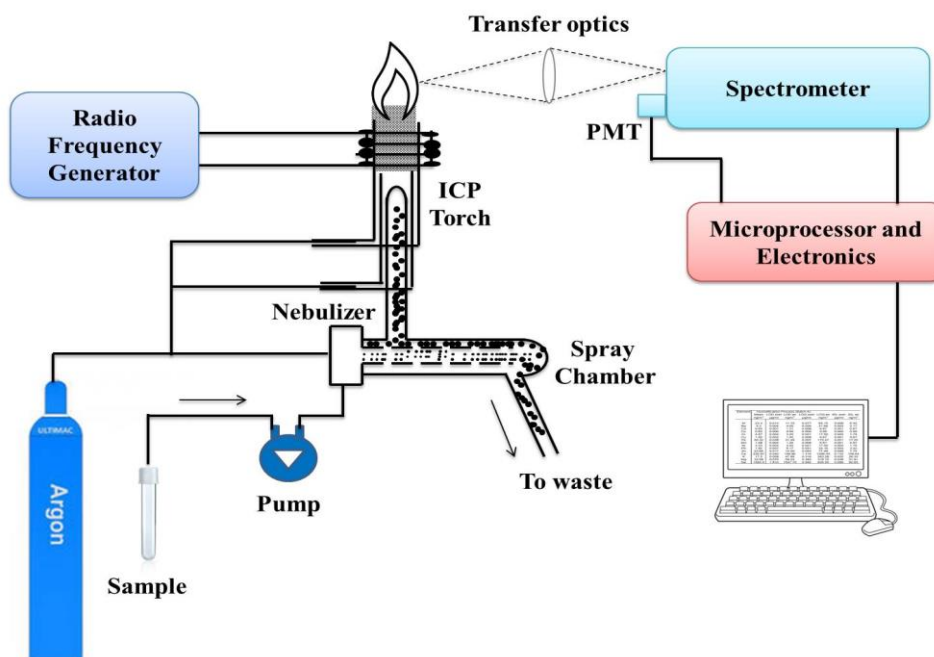


Figure 70- Schematic diagram illustrate the essential features of ICP-OES.

3.1.2- Transmission electron microscopy TEM

Transmission electron microscopy (TEM) is a powerful technique used to study samples in nanoscale size. TEM is an ideal method can be used to study a wide range of materials such as metals and biological materials, also it can be utilised to characterize biophysical and morphological properties of antibody aggregates formation. In this technique, a beam of electrons with high energy is allowed to pass through a very thin layer of specimen which causing scattered by the internal structures (Hongbao *et al.*, 2006, Joyce *et al.*, 2015).

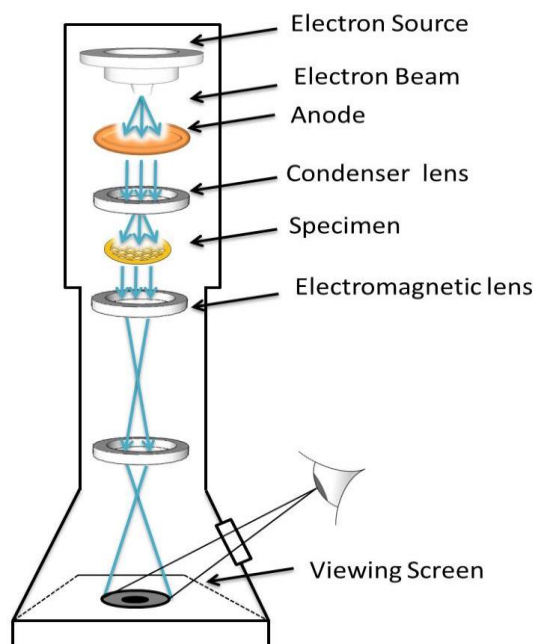


Figure 71- Schematic diagram illustrate the essential features of TEM.

3.1.3- Photon correlation spectroscopy

One of the most important techniques used to determined macromolecules and nanoparticles size and shape in solution is photon correlation spectroscopy (PCS) (Figure 72) and it is also known as Dynamic light scattering (DLS); this technique was developed by Robert Pecora in 1964 (Pecora, 1985). When a monochromatic light beam passes through a sample solution, Brownian motion of the solution particles causes fluctuations in scattered intensity, this occurs in a very short time (Novich and Ring, 1984). Particles in solutions have a random movement and speed level affected directly by their size, as large particles move more slowly in a liquid than smaller particles, speed of motion is used to measure the particle size (Figure 73).

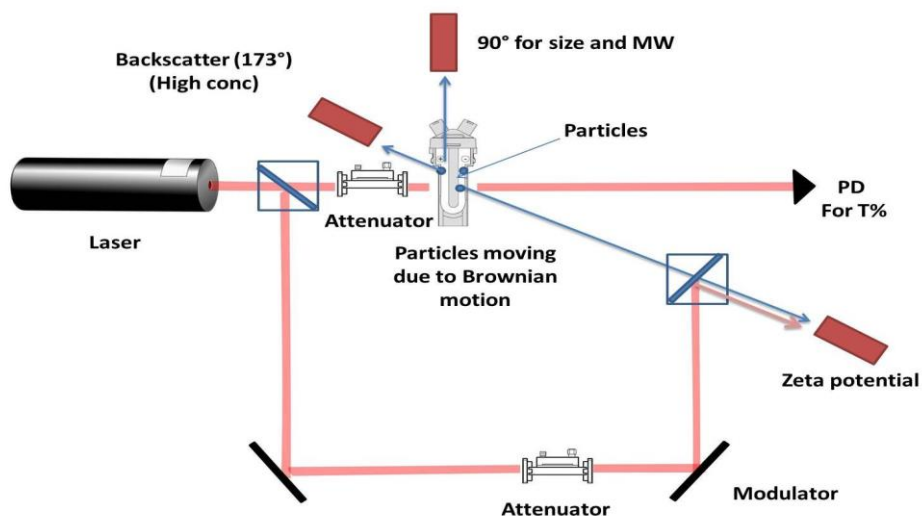
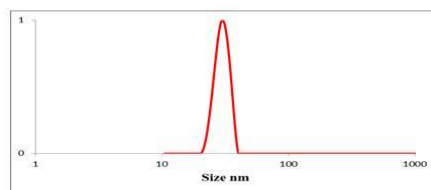
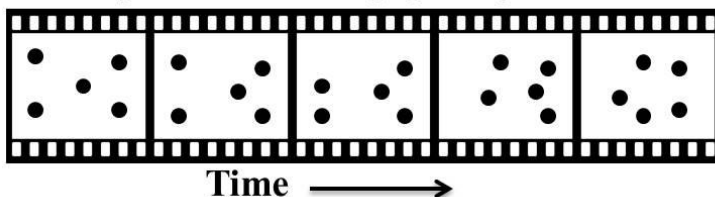


Figure 72- Schematic diagram illustrate the essential features of PCS.

Small particles moving quickly



Large particles moving slowly

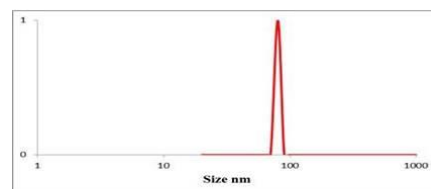
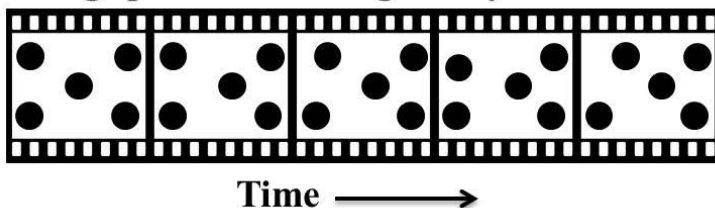


Figure 73- Particles size effect on their movement.

3.1.4- Ultraviolet- visible spectroscopy

UV-Vis Spectroscopy is the most common method used in qualitative and quantitative analysis as well as in characterisation of nanoparticles optical properties and electronic structure. It has become a useful tool to most scientists to study, metal or ligand binding, the stability of compounds and reaction kinetics (Mohamed *et al.*, 2012, Alison and Bruce, 2010). An ultraviolet and visible (UV-Vis) spectrophotometer is a device designed to

measure the transmittance or absorbance of a beam of light when it passes through an unknown sample. The spectral range is between 190 nm and 800 nm. (Brian, 2002) The instrument is made up of the components shown in Figure 74.

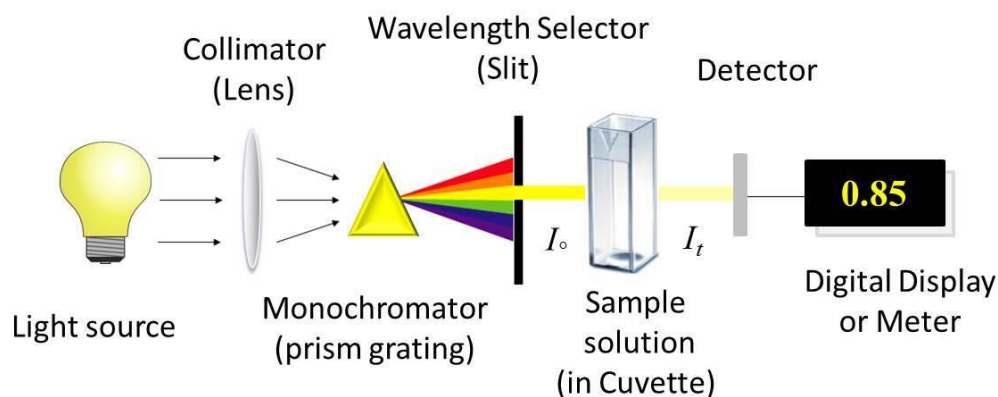


Figure 74- Schematic diagram illustrate the essential features of UV-Vis spectrophotometer.

Ultraviolet-visible spectroscopy absorption occurs due to π -electrons or non-bonding electrons (n-electrons) transitions resulting in a transition to an excited state.

3.1.5- Aims and Objectives

The aim of this chapter was fabrication of HNPs for incorporation into the intrinsic HPMA based polymer backbone (Chapter 4) which will act as laser initiated nano-heaters resulting in drug release as well as allowing for real time imaging using MRI. The particles will be fabricated and characterised using zeta potential measurement, photon correlation spectroscopy, inductively coupled plasma -optical emission spectroscopy (ICP-OES), transmission electron microscopy and ultraviolet- visible spectroscopy.

3.2- Materials and Methods

3.2.1- Materials

Item No	Material	Supplier
1	Sodium borohydride, 99%	Acros organics
2	Hydroxyl amine, 50 wt. % in H ₂ O	Sigma-Aldrich Co.
3	Potassium carbonate, \geq 99%	Fisher Scientific, UK
4	Poly(ethylenimine) Mn 750,000 & 2000	Sigma-Aldrich Co.
5	Sodium hydroxide, 99%	Fisher Scientific, UK
6	Potassium nitrate, 99%	Sigma-Aldrich Co.
7	Iron III sulfate heptahydrate, 99.5%	Acros organics
8	Sulfuric acid, 99%	Sigma-Aldrich Co.
9	Gold III chloride hydrate, 99.99%	Sigma-Aldrich Co.
10	Nitric acid, 70%	Fisher Scientific, UK
11	Hydrochloric acid, 37%	Fisher Scientific, UK
12	Gold standard for ICP	Fluka analytical
13	Iron standard for ICP	Fluka analytical

3.2.2- Methods

The synthesis of HNPs involves four key processes, iron oxide core synthesis, polymer coating of iron core, gold seeding and the subsequent gold coating. Synthesis of HNPs in this work was carried out as Goon and colleagues described (Goon *et al.*, 2009). This method involves using a “glue layer” of PEI between the magnetic iron core and the outer gold shell which is called indirect gold coating.

3.2.2.1- Synthesis of iron oxide nanoparticles

Co-precipitation of iron in a basic aqueous solution, which was performed by Sugimoto *et al.*, is one of the common methods used in the synthesis of iron oxide nanoparticles (Sugimoto *et al.*, 1980). Briefly, 1.03 g of sodium hydroxide and 1.82 g of potassium nitrate were dissolved in 180 mL deionised water. Nitrogen gas was bubbled into the reaction solution, and then it was stirred magnetically at 90 °C for 1 h, while 3.89 g of Iron III sulfate

heptahydrate was dissolved in 20 mL sulfuric acid with sonication. The resultant solutions were mixed together. A magnetic stirrer and bar was used to stir the suspension. After 24 h stirring at 90 °C under nitrogen, the resultant Fe₃O₄ were collected magnetically and then washed with deionised water several time. Afterwards, the resultant product was suspended in 25 mL water.

3.2.2.2- Polymer coating of iron oxide nanoparticles

Based on the electrostatic interaction method, negatively charged iron oxide was coated by the cationic PEI in this stage (Figure 75). In addition to prevent the magnetic core aggregate and maintain nanoparticle stability, PEI provides an active surface to attached gold nano-seeds onto iron core. Poly(ethylenimine) MW 750,000 (100 mL, 5 mgmL⁻¹) was probe sonicated with 5 mL of the previous suspension for 2 h using Soniprep 150 plus, MSE Co, MSS150.CX4.5. The coated iron core was separated magnetically from the solution and washed with water for several times before being suspended in 5 mL of water.

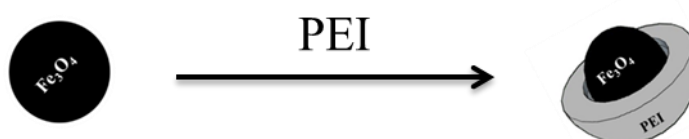


Figure 75- Schematic diagram of iron oxide nanoparticles coating by PEI.

3.2.2.3- Gold seeding

Gold seeds \approx 2 nm diameters were synthesized by adding 375 μ L of 4 % HAuCl₄ and 500 μ L of 0.2 M K₂CO₃ to 100 mL icy cold water. The reaction was stirred at room temperature for 10 min, followed by adding 5 x 1mL portions of 0.5 mgmL⁻¹ of sodium borohydride solution slowly. The pale yellow solution instantly turned deep red upon mixing with the borohydride solution. After that, solution left to stir on ice bath for further 10 mins.

Following this step, nanoparticles gold seeds attached to the Fe₃O₄-PEI (Figure 76), 90 mL of gold seeds suspension and 2 mL of Fe₃O₄-PEI solution were added to the flask under constant stirring at room temperature for 2 h, the HNPs were magnetically separated from the solution

and the active product was washed several times with water and then suspended in 5 mL of water.



Figure 76- Schematic diagram of gold seeding process.

During the final stage, gold chloride is reduced onto the NPs to form the external gold shell (Figure 77). Firstly, NPs particles were added to 20 mL PEI₂₀₀₀ (1 mgmL⁻¹) and stirred for 10 min to stabilize gold seeds. Particles were washed with water and freshly prepared 110 mL of 0.01 M sodium hydroxide was added, stirring the mixture at 60 °C. Followed by, adding 750 μL of 0.2 M NH_2OH solution and 500 μL of 1 % HAuCl_4 . After 10 min, 250 μL of NH_2OH and 500 μL of 1 % HAuCl_4 were added four times. The resultant were magnetically separated from the solution and washed several times with water and then diluted in 5 mL of water.

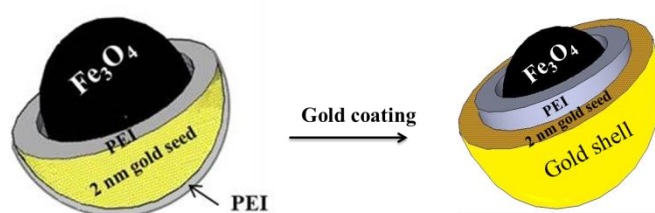


Figure 77- Schematic diagram of gold coating process.

3.3- Hybrid nanoparticles Characterisation

3.3.1- Inductively Coupled Plasma - Optical Emission Spectroscopy (ICP-OES)

A PerkinElmer (ICP-OES, Optima 7000V DV, PerkinElmer, Wokingham, UK) was used to determine iron and gold content of the HNPs. Prior to analysis; samples were digested using an acid digestion procedure (1:10 sample: acid). This digestion is carried out using a concentrated solution of hydrochloric acid: nitric acid (1:1) at 100 °C. Samples then diluted with deionised water (1:10) to be ready for analysis (Barentt *et al.*, 2013a).

The amount of iron and gold present in the samples were quantified by comparing to a standard calibration carried out previously with iron and gold standard solutions (0.05 -10 µg mL⁻¹), R² = 0.999.

3.3.2- Transmission electron microscopy TEM

Gold nanoparticles were visualised using JEOL JEM-12 microscope (Jeol, Japan) using analysis software. Sample aliquots of 2 µL were drop-cast onto formvar-coated mesh copper grids (200 mesh, Agar Scientific Co, UK). The grid then was allowed to air dry face up.

3.3.3- Photon correlation spectroscopy

Particle size, polydispersity index and zeta potential of each step were measured via photon correlation spectrometry (PCS, Zetasizer Nano-ZS, Malvern Instruments, UK). All measurements were performed in triplicate at 25 °C and the mean of three readings was determined.

3.3.4- Ultraviolet- visible spectroscopy

UV-visible spectra were acquired using UV-2600 UV-Vis (NIR) with an ISR-2600 Plus Integrated sphere, Shimadzu, Germany spectrophotometer. HNPs suspensions were placed in 1 cm sample cells and their maximum absorbance was recorded at room temperature between 350 nm-600 nm.

3.4- Results

3.4.1- Inductively Coupled Plasma-Optical Emission Spectrometry (ICP-OES)

Gold and iron content analysis of the NPs was carried out using ICP-OES. A standard solution with a mixture of the iron and gold (Fe and Au respectively) metals analysed was made up. Calculation from the standard curves showed Fe: Au ratio in the HNPs was 5:1 approximately.

The following Figure 78 shows the comparison of the leaching results from HNPs sample detected by ICP-OES.

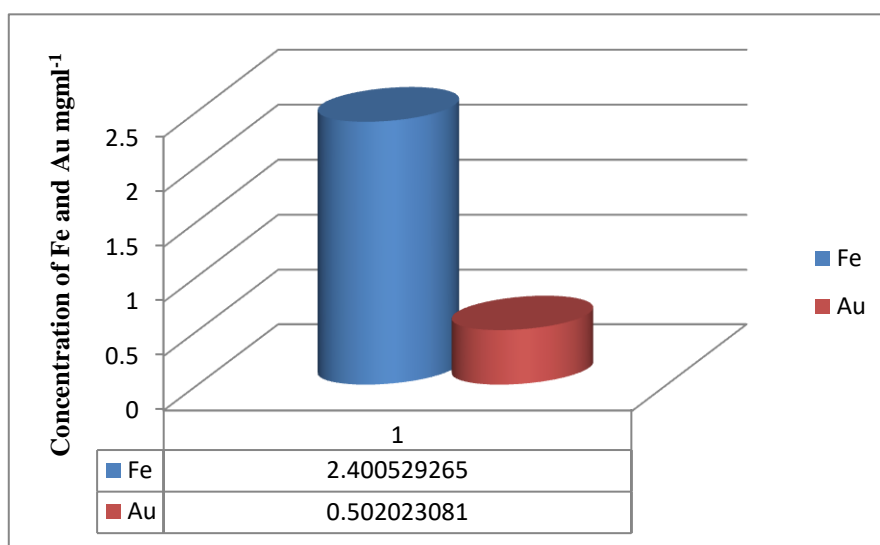


Figure 78- A graph showing the concentrations of Fe and Au in HNPs detected by ICP-OES.

3.4.2- Transmission electron microscopy imaging

TEM is the one of the most powerful and popular techniques to characterize nanoparticles (Wang *et al.*, 1999). In this technique, real images of NPs were taken. A typical TEM micrograph for Fe₃O₄ is shown in Figure 79A. Fe₃O₄ nanoparticles images detailed out the shape and size, with a diameter of 0.1 μm approximately. Figure 79C represented Fe₃O₄-PEI nanoparticles, which were seeded with gold particles (2 nm), have a unique ‘bobbly’ surface. It was observed from the TEM images of the fully coated HNP nanoparticles (Figure 79D); particles seemed to have a star shape with around 0.05 μm diameter.

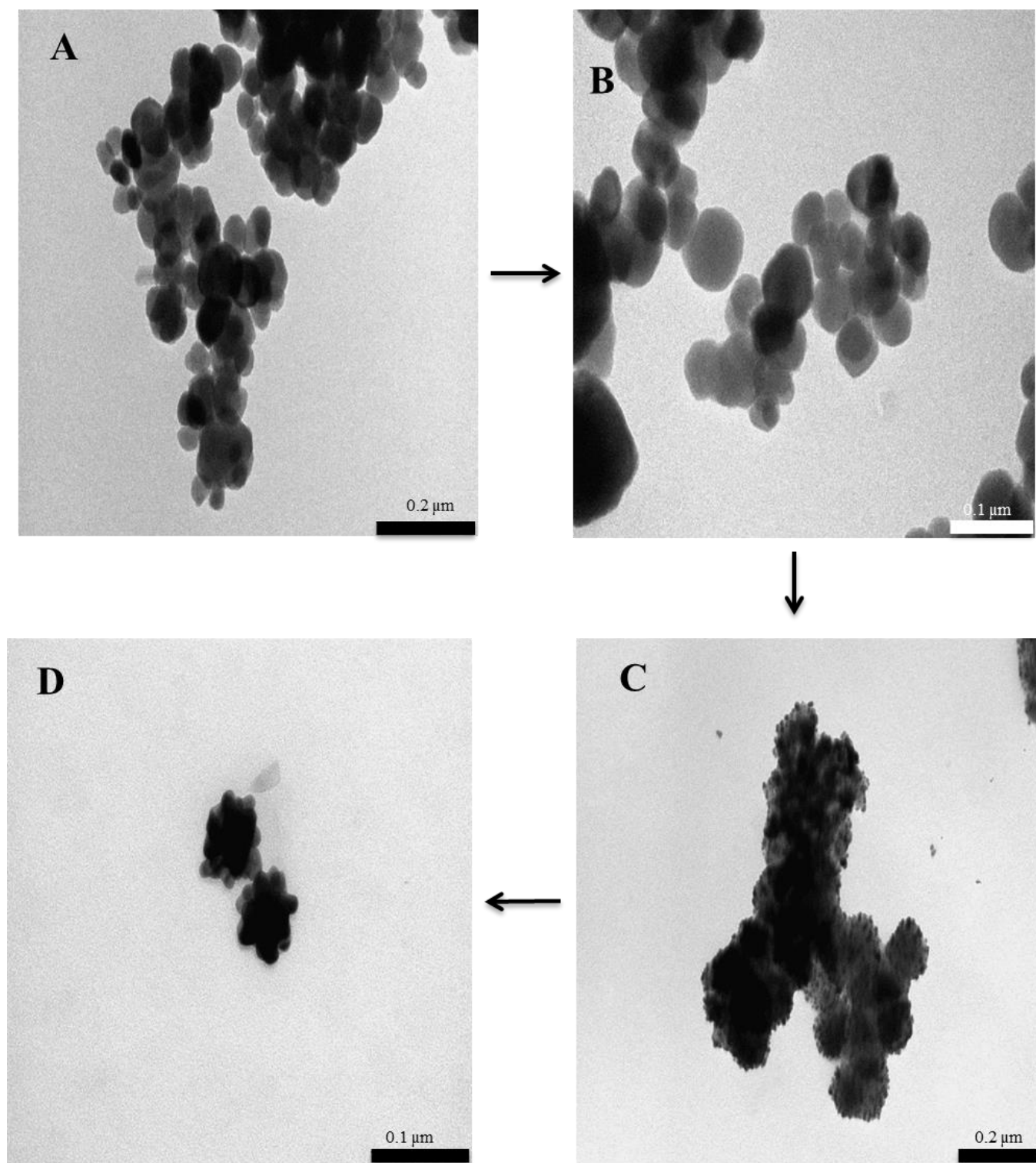


Figure 79-TEM images of (A) Fe_3O_4 nanoparticles, (B) Fe_3O_4 -PEI nanoparticles, (C) Fe_3O_4 -PEI-Au seed-PEI and (D) HNPs.

3.4.3- Photon correlation spectroscopy

As shown in Table 19, the zeta potential value of the Fe₃O₄ particles that are shielded with cationic PEI changed significantly comparing with the naked Fe₃O₄. The overall charge of Fe₃O₄-PEI was +33.7 mV due to the presence of charged primary amine groups in the PEI backbone while Fe₃O₄ was - 25.9 mV, this is attributed to the presence of sulphate moieties on the surface as previously reported (Mailänder and Landfester, 2009). The observed effect of gold atoms (negative charge) on Fe₃O₄-PEI NPs charge was quite clear in gold seeded and coated steps. The addition of gold showed a decrease in zeta potential of the optimized Fe₃O₄-PEI-Au_{seed}-PEI and Fe₃O₄-PEI-Au_{coat} NPs which found to be + 31.7 mV and + 19.7 mV respectively.

Particle size of the iron core particles (Table 19) was found to be 1.32 μm ± 0.02 μm. This suggests that strong magnetic properties of the iron oxide cores resulted in stronger interactions between the Fe₃O₄ particles forming larger aggregate clusters. Table 19 also shows a significant decrease in size when the Fe₃O₄ coated with PEI due to decreases the aggregation of the particles, while the Fe₃O₄-PEI-Au_{seed}-PEI NPs, 0.67 μm ± 0.04 μm, are slightly bigger. Such an increase in size maybe caused by the addition of gold seeds on the surface of the Fe₃O₄-PEI. Because of the negative charge of the gold shell, it produces repulsion between the HNPs and prevents the aggregation, which leads these NPs to separate in small particles.

In general, all the nanoparticles prepared herein experienced to a high polydispersity index (PDI), which is an indication size distribution (Table 19). Due to the particle aggregation in solution this is understandable.

Table 19- Size, polydispersity index and zeta potential analysis for 1 mgmL⁻¹ aqueous polymer solutions n=3, ave (SD).

Particle	Hydrodynamic Radius $\mu\text{m} \pm \text{SD}$	Polydispersity Index $\pm \text{SD}$	Zeta Potential mV $\pm \text{SD}$
Fe₃O₄	1.32 \pm 0.02	0.42 \pm 0.06	- 25.9 \pm 1
Fe₃O₄-PEI	0.57 \pm 0.05	0.38 \pm 0.09	+ 33.7 \pm 5
Fe₃O₄-PEI-Au_{seeds}-PEI	0.67 \pm 0.04	0.38 \pm 0.03	+ 31.7 \pm 2
Fe₃O₄-PEI-Au_{coat}	0.34 \pm 0.04	0.41 \pm 0.06	+ 19.7 \pm 3

3.4.4- UV/Visible spectroscopy

UV-Vis measurements were carried out to provide further characterization of the nanoparticle properties based on the surface plasmon resonance (SPR). SPR is one of the most exciting and emerging surface-sensitive techniques for detecting noble metal, especially Au and Ag. In general when light is applied to the NPs, polarization of free electrons occurs induced by the exposed light. This results in a charge separation. The SPR persuades a strong absorption of the applied light, thus can be measured by using a UV–Vis spectrometer (Xiaohua and Mostafa, 2010).

Based on the literature, Au-NPs show an absorption band between 500 nm and 550 nm. The NPs light absorption range is affected directly by their size and shape (John *et al.*, 2013). Figure 80 shows a UV-visible spectrum of NPs in aqueous solution with and without gold functionalization. Fe₃O₄ and Fe₃O₄-PEI NPs showed a spectrum that is featureless, which indicates that no plasmon resonance occurs. The reason for this observation is due to these particles not consisting of any gold. Such a red-shift is characteristic for the gold seeded magnetic nanoparticles as a result of the addition of gold. The UV-Vis spectrum shows an absorption spectrum at 480 nm for the Fe₃O₄-PEI-Au_{seed}-PEI NPs. It can be seen clearly that the maximum absorption wavelength of Fe₃O₄-PEI-Au_{coated} was shifted to be 610 nm. This indicates that the full gold coating of the surface of particles was successfully achieved.

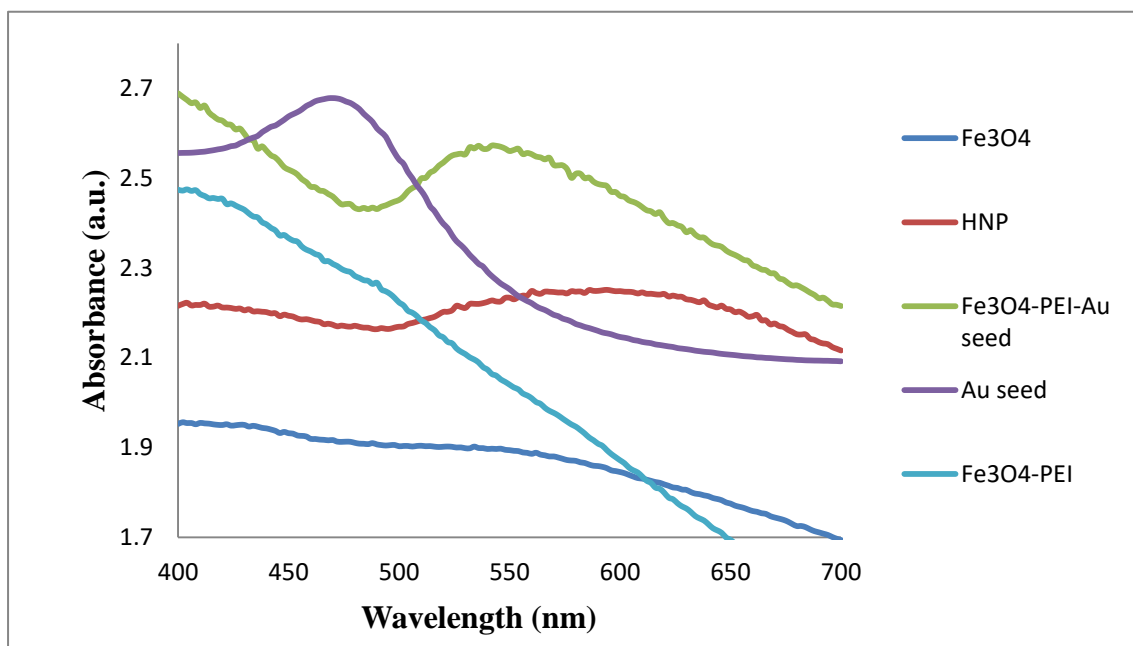


Figure 80- Shows the absorbance spectra of HNP particles.

3.5- Discussion

The characterisation results suggested that the hybrid iron oxide-gold nanoparticles were successfully synthesised. HNPs were prepared in this chapter using Goon *et al* synthesis method as fully described in section 3.2.2 and its subsections. For the characterisation of the hybrid iron oxide-gold nanoparticles, four different techniques approach were applied.

Fe₃O₄ core nanoparticles were synthesized by a sequential reduction procedure described by Sugimoto *et al.*, 1980. Particle size, zeta potential and morphology of the NPs were investigated by photon correlation spectrometer (Table 19) and transmission electron microscopy (Figure 79). For the NPs samples, the hydrodynamic z-average values measured with PCS was 1.32 $\mu\text{m} \pm 0.02 \mu\text{m}$. Zeta potentials of the Fe₃O₄ before and after coating with PEI were -25.9 mV ± 1 mV and +33.7 mV ± 5 mV, respectively. Surface charge inversion observation is a suitable indication that layer-by-layer surface coating of iron core surfaces with PEI (cationic polymers) was successful. The sizes of the Fe₃O₄-PEI NPs showed different range as the naked Fe₃O₄ size. Fe₃O₄-PEI has PCS z-average size of 0.57 $\mu\text{m} \pm 0.05 \mu\text{m}$. TEM images of the synthesised Fe₃O₄ NPs with and without PEI have clearly manifested the semi spherical shapes (Figure 79).

As shown in Table 19, the zeta potential of the Fe₃O₄-PEI NPs that are seeded with 2 nm gold nanoparticles shows the decrease in positive zeta-potential whereas that of the full coated

gold shell shows further decrease in positive zeta-potential as a result of the presence of gold, which possess negative charge .

The presence of gold NPs in the outer shell was confirmed by UV-Vis absorbance measurement which exhibits the NPs localised surface plasmon resonance (LSPR) behaviours. The absorption bands around 480 nm and 610 nm for the Fe₃O₄-PEI-Au_{seed}-PEI and Fe₃O₄-PEI-Au_{coated} NPs respectively, are the plasmon resonance band which is a characteristic of gold. All the NPs prepared herein are uniform with a narrow polydispersity index (PDI). The formation of uniform NPs was further characterized using transmission electron microscopy. The TEM image (Figure 79) exhibits that the HNPs have heptagon morphology.

A significant variation of the particle size by PCS and TEM methods is noted for the nanoparticles prepared here. The NPs size estimated by TEM analysis is smaller than PCS in each synthesis step. This phenomenon is possible due to the very small fraction of the sample represented in TEM image. Moreover, a number of factors have a great influence on the hydrodynamic diameter of the particles measured by dynamic light scattering such as polymer shells, hydration layer or other stabilisers, which lead the particles size to be seen larger in general (Heinz *et al.*, 2014).

In comparison with naked iron oxide, polymer coated iron oxide NPs tend to be smaller and more uniform; this result correlates well with the aim of using the polymer layer as stabiliser. Increase of the solution stability leads to decrease of particle agglomeration and size. Iron oxide NPs agglomerates and form large clusters due to the hydrophobic interactions between the NPs because of its large surface area-to-volume ratio and hydrophobic surfaces properties (Wei *et al.*, 2008). A small increase in size was found in the gold seeding stage, and furthermore, zeta potential became less. This indicated that the gold seeds successfully bound to the coated NPs. Gold coating of the NPs reduced the hydrodynamic radius to $0.34 \mu\text{m} \pm 0.04 \mu\text{m}$, this exhibited an increase in solution stability, and the significant decrease in zeta potential from $+ 31.7 \text{ mV} \pm 2 \text{ mV}$ to $+ 19.7 \text{ mV} \pm 3 \text{ mV}$ confirmed this assumption (Table 19).

In general, previous studies have shown that the ratio of iron oxide in HNPs formulations was 4-fold of gold (Malekigorji *et al.*, 2017, Curtis *et al.*, 2015). Our finding is consistent with previous studies in that the ratio of Au:Fe in formulation was approximately 1:5. The

electron micrograph (Figure 79) exhibited that the final HNPs particles have star shape. It has been reported that the surface-enhanced Raman scattering (SERS) activity of star-shaped structure nanoparticles was stronger than that of the spherical Au NPs which have similar size (Esenturk and Walker, 2009). Surface enhanced Raman of nano-stars molecules make them extremely useful for potential applications in the field of biosensors and molecular cancer imaging (Harmsen *et al.*, 2015, Wang *et al.*, 2010).

These findings suggest that the morphological and physical properties of the HNPs after gold coating process showed good agreement with the biological and clinical standards.

3.6- Conclusion

The aim of this chapter is to produce gold-NPs and characterise them in order to incorporate into the intrinsic HPMA based polymer backbone to act as laser initiated nano-heaters. NPs were successfully prepared and investigated. The combination of TEM and PCS provided detailed information on the size of the NPs. Polymer layer between iron core and outer gold shell has been found to increase the solution stability by decreasing the particle agglomeration and size.

Chapter Four

Drug loading and release kinetics from polymeric aggregates

4.1- Introduction

Triggered release of contents from polymeric nanoparticles has been extensively studied to date. Sudden shrinking of thermo-responsive polymers above the critical temperature makes this type of polymeric micelle ideal carrier vehicles to deliver anticancer agents to tumour sites (Aaron *et al.*, 2011, Priya *et al.*, 2009).

By grafting (palmitoyl, dansyl, cholesteryl and oxadiazole) hydrophobic pendant groups onto the primary amine in the APMA monomer and then polymerised with water soluble thermo-responsive HPMA spontaneous self-assemblies can be formed in aqueous environment where hydrophobic drugs are encapsulated inside the hydrophobic core.

There are plenty of methods that have been used to enhance the pharmacokinetic and pharmacodynamics properties for a wide range of drug molecules. Most of these applications have been focused on using solvent evaporation, nanoprecipitation, emulsification/solvent diffusion, dialysis and supercritical fluid technology (SCF) to prepare biodegradable nanoparticles (Nagavarma *et al.*, 2012). Tobias *et al.*, have compared three different methods Oil/Water emulsion, direct dialysis and co-solvent evaporation to loaded dexamethasone into poly(ethylene glycol)-block-poly-4-(vinylpyridine) micelles, they reported that co-solvent evaporation was a more effective loading method than others (Tobias *et al.*, 2013).

Although, some of these techniques have shown promising results, using organic solvents to dissolve hydrophobic drugs has major disadvantages such as residual solvent toxicity. So to avoid this limitation, ultrasonic promoted drug encapsulation inside micelles was developed and is one of the most effective techniques to create nanoparticles in aqueous environments (Chih *et al.*, 2012, Dutta and Sahu, 2012).

Studies showed the advantage of the structural change of thermo-sensitive polymers at the LCST (Lower Critical Solution Temperature) to release encapsulated drug compounds into the surrounding environment (Stephanie *et al.*, 2012). Incorporation of hybrid nanoparticles (HNPs) into the intrinsic structure of the thermo-sensitive polymer provides a localised trigger point for heating after laser irradiation which can lead to accelerated drug release (Roach *et al.*, 2013).

4.1.1- Model Drugs

In this study four types of hydrophobic drugs were used in order to study the efficiency of the HPMA-APMA copolymers derivatives to enhance drug solubility.

Propofol or 2,6-diisopropylphenol ($C_{12}H_{18}O$, MW = 178.271) (Figure 81) is one of the most popular general intravenous anaesthetic agents, the chemical structure belongs to the alkylphenol family. Propofol has been used in a wide range of clinical situations since its introduction in 1985's (Trapani *et al.*, 2000 and Wang *et al.*, 2015). Propofol is a powerful antioxidant (Murphy *et al.*, 1992), and has anticancer activities (Azmat *et al.*, 2013 and Rafat *et al.*, 2015). The hydrophobic structure of propofol led to restrict the aqueous solubility to $100 \mu\text{g mL}^{-1}$ at 25°C (Hoskins *et al.*, 2016). Therefore, an emulsion of oil-in-water (10mg mL^{-1}) is formulated for intravenous administration (Morgan *et al.*, 2002).

Such formulations should be very stable and have a very small droplet size, otherwise, the pulmonary capillaries it may embolism (Jihong *et al.*, 2001). Some additives including antimicrobial agents should be added to this system to prevent sepsis (Baker and Naguib, 2005). Furthermore, emulsion intravenous administration often association with pain on injection (Adam *et al.*, 2004).

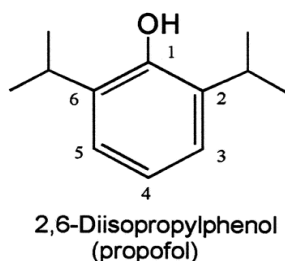


Figure 81- Chemical structure of propofol.

Griseofulvin ($C_{17}H_{17}ClO_6$, MW = 353) (Figure 82) is an orally administered antibacterial and antifungal drug used in treatment of ringworm and dermatophyte infections. Singh and colleagues reported the combination of griseofulvin with other anticancer drugs have a significant use in cancer chemotherapy (Singh *et al.*, 2008). Griseofulvin is a white to creamy powder and has a hydrophobic structure. This results in poor solubility in aqueous solutions with around ($200 \mu\text{g mL}^{-1}$ at 25°C) (Townley, 1979, Royal Pharmaceutical Society of Great Britain, 2000). However, its poor solubility in aqueous solutions led to the absorption at gastrointestinal tract to be variable and patient dependant. There are many techniques which

are used to enhance griseofulvin solubility and bioavailability including reduction in particle size, polymeric formulation and co-administration with fatty meals (Sandy *et al.*, 2016).

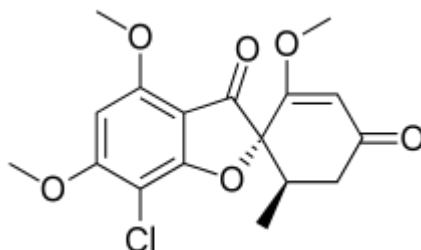


Figure 82- Chemical structure of griseofulvin.

Prednisolone (C₂₁H₂₈O₅ MW = 360) (Figure 83) is man-made corticosteroid used in the treatment of inflammatory diseases such as, asthma, hepatitis, congenital adrenal hyperplasia and arthritis (Vogt *et al.*, 2007). Prednisolone belongs to class II drugs according to the Biopharmaceutics Classification System (BCS), which indicated that it has high permeability and low solubility (215 µgmL⁻¹ at 25 °C) (Alkazzaz *et al.*, 2015). Over the years, several attempts (Win *et al.*, 1976, Parvin *et al.*, 2011, Neelam and Purshotam, 2007) have been made to improve prednisolone dissolution rate with different degrees of success. Prednisolone is administered as a suspension, (Katrina and Leisa, 2000) injection, (Roberto *et al.*, 2013) ointment, (Lobenhoffer and Meyer, 2001) and as eye drops (André *et al.*, 2014).

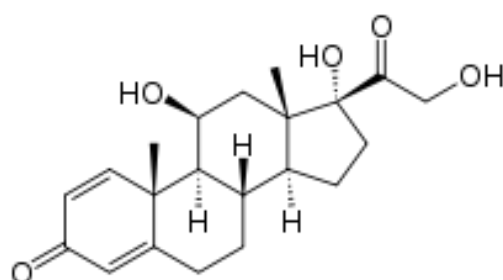


Figure 83- Chemical structure of prednisolone.

Paclitaxel (PTX) (C₄₇H₅₁NO₁₄ MW = 853) (Figure 84), is a microtubule-stabilizing drug against depolymerisation used in wide application for the treatment of certain cancers including ovarian, breast, lung and pancreatic cancer (Beth, 2014, Wen and Manuel, 2013).

However, its potential application for cancer treatment has been hindered due to extremely low aqueous solubility of $0.3 \mu\text{g mL}^{-1} \pm 0.02 \mu\text{g mL}^{-1}$. Several different approaches have been performed to overcome this problem such as using ethanol or poly(oxyethylated) castor oil (Cremaphor) to solubilize paclitaxel for intravenous administration. However, intravenous administration of (Crepaclitaxel; Taxol) emulsion caused many side effects such as infusion hypersensitivity reaction and often has to be pre-medication with steroids and antihistamines. Another pharmacological effect which has been observed with this formulation is the alteration in the toxicity profile and anticancer efficacy (Lee *et al.*, 2003, Wen and Manuel, 2013). These side effects of formulation of paclitaxel efficacy suggest the need for new formulation to enhance aqueous solubility. This work will examine the ability of our novel copolymer formulation to address this problem.

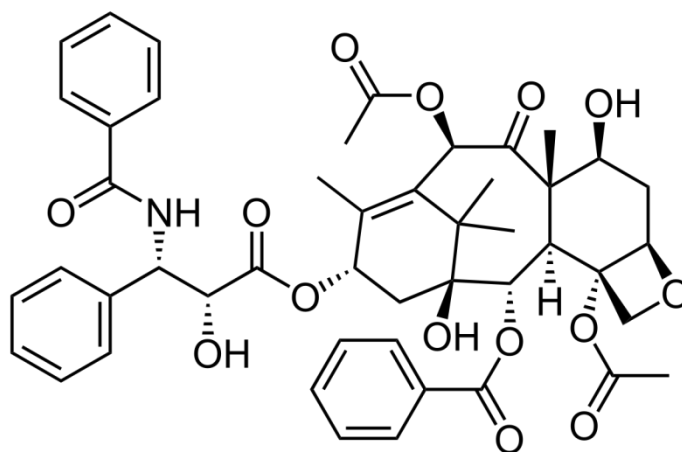


Figure 84- Chemical structure of paclitaxel.

Drug formulation into polymeric micelles is a common form of technology used to improve solubility and hence efficacy. After formulation it is very important to characterise excipient efficiency based on drug loading and release. This characterisation is usually carried out using high performance liquid chromatography described below.

4.1.2- High performance liquid chromatography (HPLC)

Chromatography as discussed in Chapter 2, is a great separation technique which can be utilised to analyse complex mixtures of molecules based on distribution between stationary and mobile phases (Jared *et al.*, 2015).

One of the most important types of chromatography is HPLC; become commonly used nowadays for separations and purifications in a wide range of areas including food industries, biotechnology, polymer, environment and pharmaceuticals (Hema *et al.*, 2009).

In a typically HPLC system (Figure 85) the eluent (mobile phase) is pumped by the solvent reservoirs at adjust flow rate, then the auto-sampler will inject a fixed amount of the sample into the flow, the eluent and the sample will pass through the column, which is packed with the stationary phase (usually silica), where the separation occurs under high pressure followed by the detector. The whole system is connected to a built-in computer interface control.

Based on the molecule properties like size, polarity and charge, chromatographic separation can be subdivided into number modes include: reversed-phase (RP), size exclusion (SE), ion exchange (IE) (Chi-San, 1995, Haddad and Jackson, 1990).

Reversed-phase (RP) is the most common over other HPLC modes, and nearly all substances can be separated by RP technique (Snyder *et al.*, 2010). Separation mechanism based on the hydrophobic binding of the solute molecule in the mobile phase (polar) to the immobilised hydrophobic stationary phase such as inorganic polymers with large surface areas, silica gel and carbon (Rubinson and Rubinson, 2000).

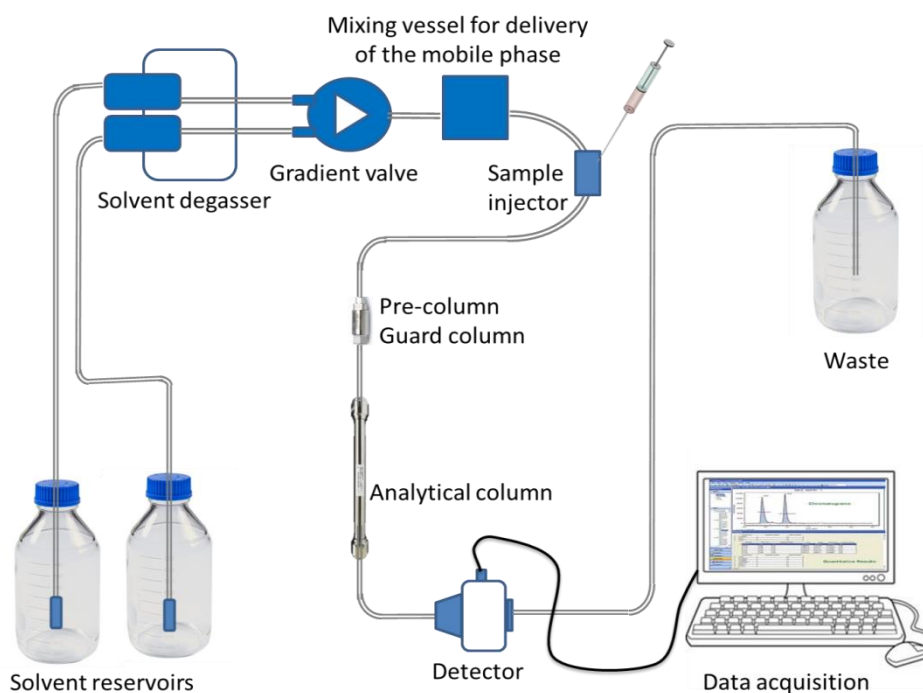


Figure 85- Schematic diagram illustrate the essential features of HPLC.

4.1.3- Aims and Objectives

Polymeric nanoparticles have been shown high efficiency in drug delivery applications. The aim of this chapter is to study drug loading and release properties of different copolymer derivatives using propofol, griseofulvin, prednisolone and paclitaxel as hydrophobic drug model molecules. Drug loading capacity and release was determined using HPLC instrument. Micelles average diameter and size distribution were determined using photon correlation spectroscopy.

4.2- Materials and Methods

4.2.1- Materials

Item No	Material	Supplier
1	Propofol, $\geq 97\%$	Sigma-Aldrich Co.
2	Griseofulvin, 97 %	Alfa Aesar
3	Prednisolone, $\geq 99\%$	Sigma-Aldrich Co.
4	Paclitaxel, 99.64 %	Medchem express
5	HPMA-APMA-R and (HPMA-APMA-R)- <i>b</i> -PEG copolymers	Synthesised in Chapter Two
6	HNPs	Synthesised in Chapter Three
7	0.45 μ m GDX PVDF filters	Fisher Scientific, UK
8	HPLC Grade methanol	Fisher Scientific, UK
9	HPLC Grade acetonitrile	Fisher Scientific, UK
10	Potassium dihydrogen phosphate, HPLC grade	Sigma-Aldrich Co.
11	Orthophosphoric acid, 85 %	Sigma-Aldrich Co.

4.2.2- Methods

4.2.2.1- Copolymer Solubility Study

Structural modifications of Poly (HPMA) included copolymerization ratio and type have different effects on the poly(HPMA) dissolution in water. The effects of hydrophobic grafted groups (APMA-P, APMA-D, APMA-C and APMA-O) on the solubility of thermo-responsive water-soluble poly(HPMA) were investigated.

4.2.2.2- (HPMA-co-AMPA-O)-b-PEG-HNP Conjugation

A 6 mg/mL 90% (HPMA 99%-co-AMPA-O 1%)-b-PEG 10% (10 mL) solution was prepared in deionised water followed by ultrasonication using a probe sonicator for 10 min before adding HNPs (60 μ L). All the mixture was sonicated for a further 10 min.

4.2.2.3- Drug Loading

Serial concentrations (1 mgmL^{-1} , 3 mgmL^{-1} , and 6 mgmL^{-1}) of polymer in deionised water were probe sonicated by (Soniprep 150 plus, MSN, UK) for 10 min. Followed by, adding hydrophobic drugs at 1:1, 1:5 and 1:10 initial polymer: drug weight ratio, 10 min further probe sonication was run for the polymer-drug solutions to get the maximum drug encapsulation. Samples were left to reach room temperature, then 0.45 μm syringe filters (with pre-filters) were used to remove the unencapsulated drugs. Exception: Paclitaxel solution was filtered by filter paper because the non-soluble drug particles blocked filter pores.

For all the formulations, the loading capacity (LC) and encapsulation efficiency (EE) was calculated using equations 6 and 7 respectively.

$$\% \text{ LC} = (\text{drug determined by HPLC} / \text{polymer concentration}) \times 100\% \dots\dots\dots(6)$$

$$\% \text{ EE} = (\text{drug determined by HPLC} / \text{original drug concentration}) \times 100\% \dots\dots\dots(7)$$

4.2.2.4- Solubility Study

4.2.2.4.1- Determination of Propofol

The quantity of propofol in the samples was determined by an isocratic reverse-phase HPLC (Perkin Elmer Flexar LC, Netherlands) using a Symmetry column (Pinnacle DB C18 5 μm x 150 mm x 3.2 mm) at 25°C. The mobile phase consisted of methanol : water (80:20 v/v) with a flow rate of 1.0 mLmin⁻¹. An UV-Vis detector was set at 229 nm. Propofol concentrations in the self-assemblies samples were obtained by comparing the resultant peak at 2.2 min with propofol standard calibration curve ($R^2 = 0.998$).

4.2.2.4.2- Determination of Griseofulvin

Griseofulvin levels contained in the polymeric micelles formulation were measured using (Perkin Elmer Flexar, US) HPLC. A reverse-phase Pinnacle DB C18 5 μm x 150 mm x 3.2 mm HPLC column was used with flow rate of 1 mLmin⁻¹ (45:55 v/v of acetonitrile: 45 mM potassium dihydrogen phosphate in water and adjusted to pH 3 with orthophosphoric acid) in an isocratic mode. Griseofulvin detection was achieved using an ultraviolet detector set at 293 nm. The resultant peak at 2.8 min was analysed and compared to a standard calibration of griseofulvin dissolved in the same mobile phase $R^2 = 0.999$ to quantify the drug contents in the samples.

4.2.2.4.3- Determination of Prednisolone

Prednisolone concentration in the self-assemblies was determined by comparing the resultant peak at 1.65 min with standard calibration containing the prednisolone dissolved in the mobile phase $R^2 = 0.999$. A reverse-phase pinnacle DB C18 5 μm x 150 mm x 3.2 mm HPLC column from Restek Co. UK was used as stationary phase. The mobile phase consisted of 64:36 (v/v) water:acetonitrile, which flowed at a rate of 1 mLmin⁻¹. UV detection was performed at 243 nm.

4.2.2.4.4- Determination of Paclitaxel

Quantification of paclitaxel was performed by reverse phase HPLC (pinnacle DB C18 5 μm x 150 mm x 3.2 mm HPLC column from Restek Co. UK) with flow rate of 1 mLmin⁻¹ of the mobile phase (55:45 v/v) water : acetonitrile. Paclitaxel peak was obtained at 6.2 min by

using UV/Vis detector at 227 nm. Paclitaxel quantification was achieved by reference to a calibration curve produced from dissolving paclitaxel in water : acetonitrile (55:45 v/v) $R^2 = 0.999$.

4.2.2.5-Particle size and size distribution measurements

Particle size and polydispersity index measurements were carried out for all the polymer-drug formulations which were prepared in section 4.2.2.2 and polymer alone in water with photon correlation spectrometry (Zetasizer Nano-ZS, Malvern Instruments, UK). All measurements were performed in triplicate at 25 °C and the mean of three readings was used determined.

4.2.2.6- Transmission electron microscopy

TEM imaging of the (HPMA-co-APMA-O)-*b*-PEG in the presence or absences of HNPs were viewed under the TEM. This was carried out as previously reported in section 3.3.2

4.2.2.7- In vitro drug release

Dynamic dialysis procedure has been used to determine the rates of drug release from polymers. Briefly, 2 mL of each sample was transferred into a dialysis tube (MW cut off = 12000-14000 Da). Subsequently, the polymer containing dialysis tube was dialyzed against 200 mL deionised water for 24 h with stirring at different temperatures. 1 mL of the external deionised water was periodically sucked up and replaced with 1 mL of fresh deionised water. The amount of the released drug was determined by using HPLC. Equation 8 describes the rate of release of the drug from optimum formula

$$\% \text{ Drug release} = \frac{\text{Amount of drug released}}{\text{The initial amount of drug in optimum}} \times 100 \quad (8)$$

4.3- Results

4.3.1- Copolymer Solubility Study

The results obtained illustrate the association behaviour of the hydrophobic groups attached to the polymer. As shown in Table 20, poly(HPMA) derivatives solubility tend to decrease as the extent of hydrophobic pendants increase. The individual copolymers solubility considers, for the cholesteryl copolymer we found that even a relatively low copolymerization ratio of APMA-C (1 %) is sufficient to make the polymer insoluble.

Table 20- Effect of grafted hydrophobic groups onto copolymer solubility.

Copolymerization Ratio %	HPMA-co-APMA-P /Copolymer Code	HPMA-co-APMA-D / Copolymer Code	HPMA-co-APMA-C / Copolymer Code	HPMA-co-APMA-O / Copolymer Code
0.25	✓ P-0.25	✓ D-0.25	✓ C-0.25	✓ O-0.25
1	✓ P-1	✓ D-1	✗	✓ O-1
2	✗	✓ D-2	✗	✓ O-2
5	✗	✗	✗	✓ O-5
10	✗	✗	✗	✓ O-10

4.3.2- Solubility Study

To consider the applicability of copolymer derivatives which were prepared in chapter three to be used as solubilising agents the loading capacity of the formulations was considered.

4.3.2.1- Determination of Propofol Solubility in HPMA-co-APMA-R

Figure 86 shows the maximum concentration of propofol solubilised by each copolymer formula. Comparing the solubilisation values is observed that O-1 presented relatively high solubilisation in comparison with the other formulations, the solubility of propofol in P-0.25, C-0.25 and D-2 ranged from 313-fold, 317-fold and 346-fold respectively, to being up to 411-fold higher (O-1) as compared to the aqueous solubility.

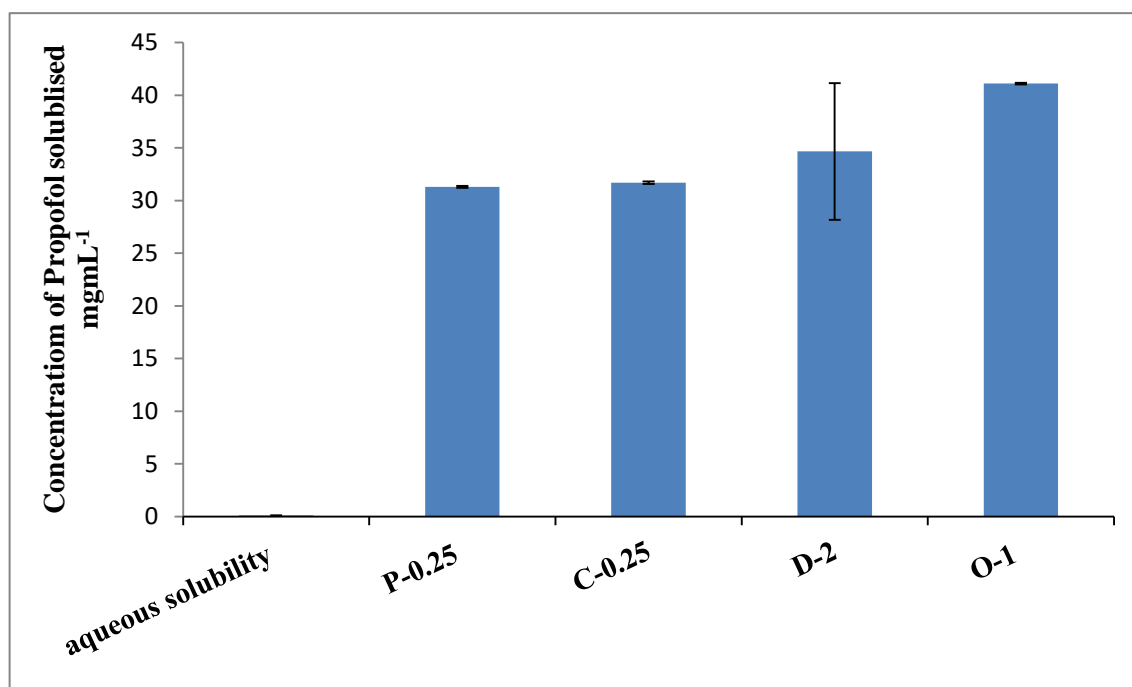


Figure 86- Maximum concentration of propofol solubilised by each copolymer formula (6 mgmL⁻¹) at 1:1, 1:5 or 1:10 initial polymer:drug loading ratios (n=3, ave ± SD).

Results of propofol loading on different APMA-R grafting ratio are presented in Figures 87 and 88. Figure 87a compares drug loading of various APMA-P grafting ratio. The comparative loading study showed, the highest propofol loading was found for the 0.25 % palmitoyl formulation, where a high polymer concentration (6 mgmL⁻¹) was used. At 3 mgmL⁻¹, the data obtained indicated the amount of solubilised propofol 1:5 polymer:drug initial feed ratio was quite similar for both grafting ratios. The observed slight reduction at higher polymer concentration in the 1 % grafting ratio (10.6 mgmL⁻¹) compared to 12.5 mgmL⁻¹ at 0.25% formula. Additionally, the data obtained at higher polymer concentration for the 0.25% grafting ratio at 1:5 polymer:drug initial feed ratio formulations was higher than their corresponding at 1 %. In fact, the here presented method allows to achieve a propofol amount of 31.3 mgmL⁻¹, demonstrating a 313-fold increase to the reported aqueous solubility of propofol, 0.1 mgmL⁻¹ (Hoskins *et al.*, 2012).

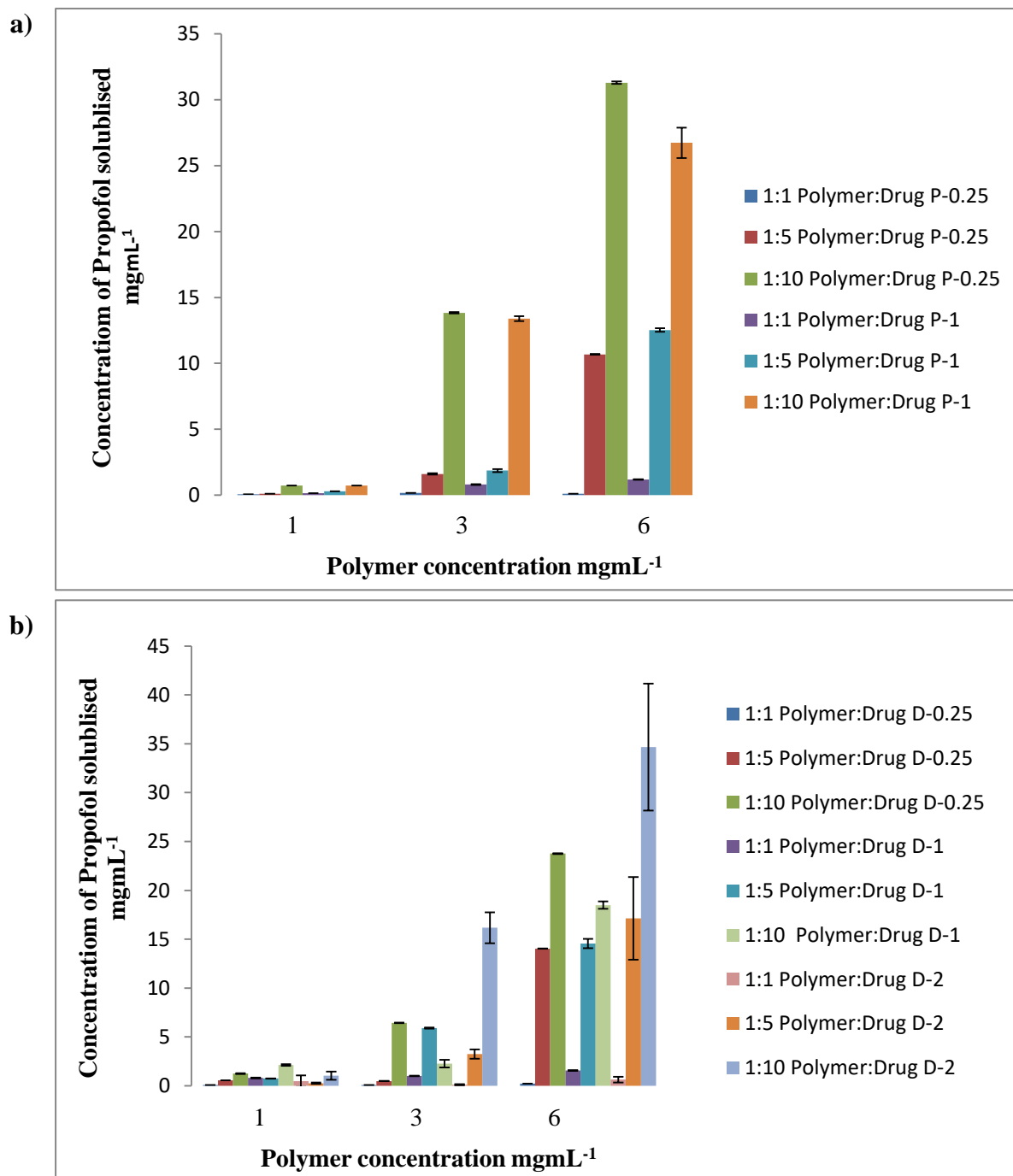


Figure 87- Drug loading of propofol onto a) HPMA-co-APMA-P and b) HPMA-co-APMA-D at varied grafting ratio and different initial drug:polymer loading ratios (n=3, ave \pm SD).

Interestingly, increasing the APMA-D ratio in HPMA-co-APMA-D showed significant improvement in the propofol solubility. Results of propofol solubilised at each concentration (1 mgmL⁻¹, 3 mgmL⁻¹ and 6 mgmL⁻¹) and drug:polymer ratio are presented in Figure 87b. Of the three polymer concentrations, 6 mg/ml showed equal or higher solubility of propofol as compared to other concentrations. At 2 % molar grafting was found to display the highest

propofol concentration at 1:10 polymer:drug ratio (34.66 mgmL^{-1}). For 0.25 % and 1 % molar grafting, 1:10 polymer:drug initial feed ratio seem to have a sufficient drug-loading values, whereas other initial feed ratio have less drug entrapped into the copolymer structure. Similarly, 2 % molar grafting formula accepts almost double of the drug as compared with the 1:5 polymer:drug initial feed ratio.

Solubilisation effect of C-0.25 at higher copolymer concentrations on propofol is stronger than that of at lower polymer concentration. This behaviour is a consequence of the increasing the scaffold micelles. Figure 88a shows the concentration of propofol solubilised at each concentration (1 mgmL^{-1} , 3 mgmL^{-1} and 6 mgmL^{-1}) and drug:polymer ratio. The surfacing effect of C-0.25 at 6 mgmL^{-1} and 1:10 polymer:drug initial feed ratio resulted in 317-fold.

The HPMa-co-APMA-O ratio optimization data are shown in figure 88b. These results showed that the solubility is significantly improved in the case of the copolymer with propofol ratio of 1:10. Changing the ratio to 1:1 and 1:5 produced less significant enhancement in solubility. Furthermore, with increasing the copolymerization ratio of APMA-O the solubility of propofol was also increase. However with further increase of the grafting ratio more than 1 % the efficiency of the system goes down. The loaded amounts onto O-1 at 6 mgmL^{-1} and 1:10 polymer:drug initial feed ratio exceeded the reported aqueous solubility values as 41.1 and 0.1 mg/ml respectively, which mean propofol solubility increased 411-fold.

To examine whether increased propofol solubility with the HPMa-co-APMA-R copolymer translated into an increase in other drugs solubility. The extent of griseofulvin and prednisolone solubility was measured for this purpose.

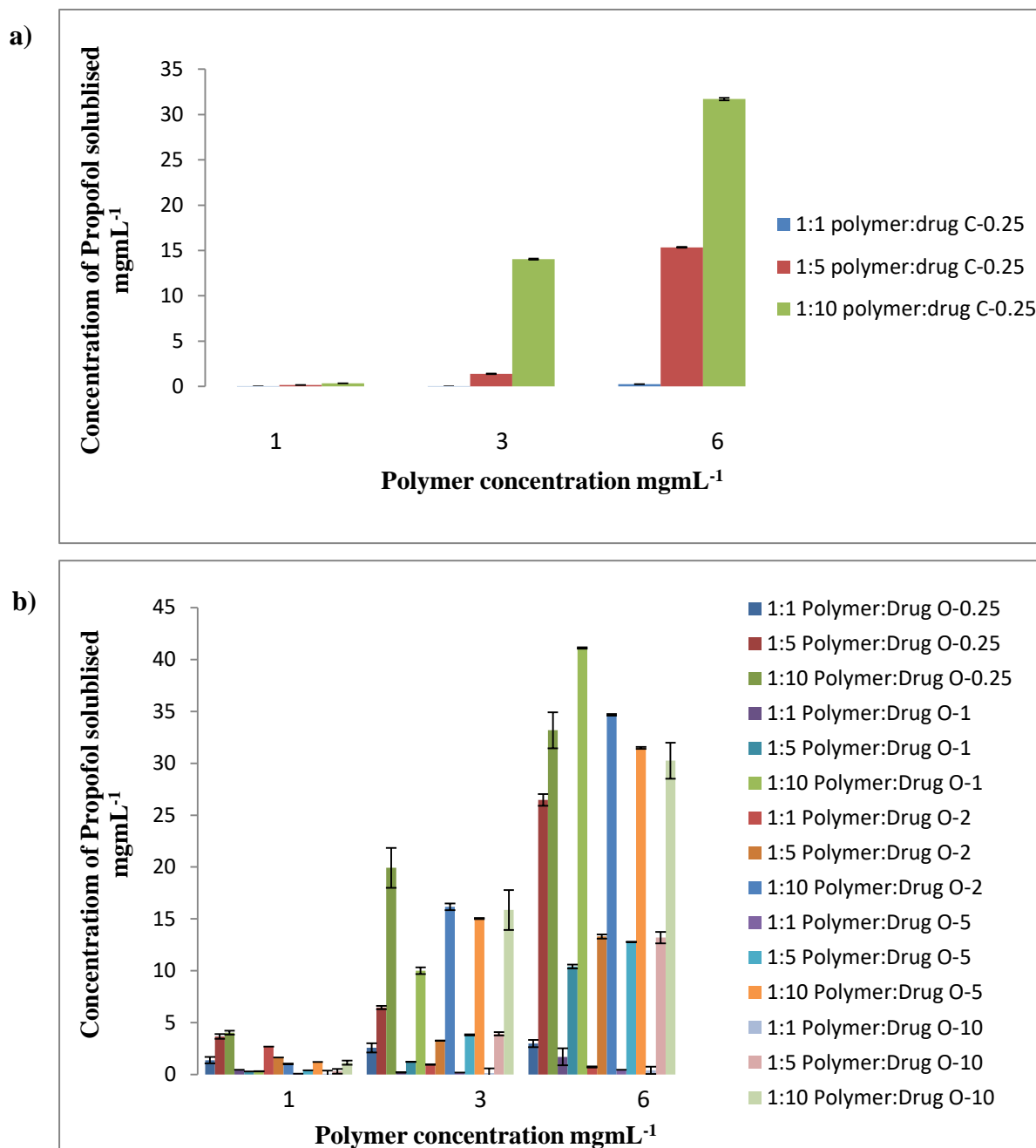


Figure 88- Drug loading of propofol onto a) HPMA-co-APMA-C and b) HPMA-co-APMA-O at varied grafting ratio and different initial drug:polymer loading ratios (n=3, ave ± SD).

4.3.2.2- Determination of Griseofulvin Solubility in HPMA-co-APMA-R

The maximum enhancement in the dissolution data for griseofulvin is provided in (Figure 89). These data show that copolymer formulas significantly enhanced the solubility of griseofulvin compared with the aqueous solubility. From the dissolution profiles it is seen

that palmitoyl pendant groups were the most high effective in solubilizing the griseofulvin compared to dansyl, cholesteryl and oxadiazole which exhibited the lowest drug encapsulation, representing a 103-fold, 51-fold, 60-fold and 54-fold improvement in efficiency over the reported aqueous solubility 0.2 mg/ml respectively, (Townley., 1979, Royal Pharmaceutical Society of Great Britain., 2000).

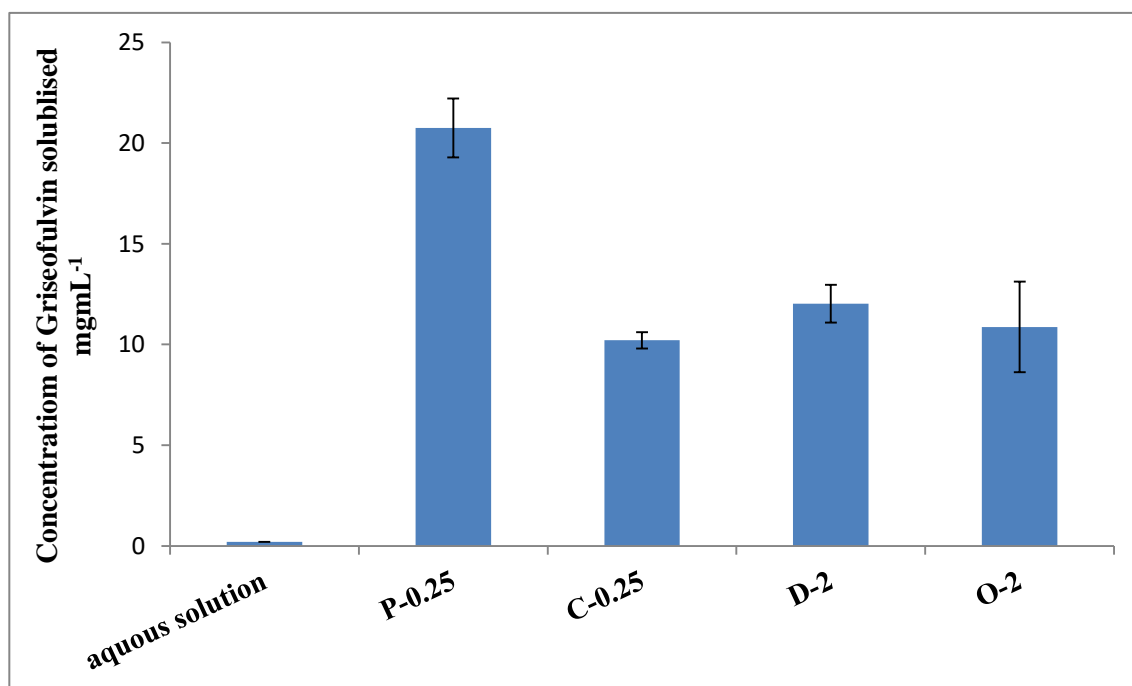


Figure 89- Maximum concentration of griseofulvin solubilised by each copolymer formula (6 mgmL⁻¹) at 1:1, 1:5 or 1:10 initial polymer:drug loading ratios (n=3, ave ± SD).

Figure 90a shows the concentration of griseofulvin solubilised in HPMA-co-APMA-P at each concentration (1 mgmL⁻¹, 3 mgmL⁻¹ and 6 mgmL⁻¹) and polymer:drug ratio. Higher griseofulvin loading was obtained for the 1:10 polymer:drug initial feed ratio at 6 mg/ml (20.75 mgmL⁻¹) of P-0.25, than for the P-1 (9.2 mgmL⁻¹). Current trends revealed well correlation between griseofulvin and propofol solubilisation. Furthermore, the amount of griseofulvin solubilized was significantly increased with increasing polymer concentration for both copolymers. P-0.25 exhibited more than 103-fold (20.75 mgmL⁻¹) increase in dissolution in at high polymer concentration compared to 46-fold (9.2 mgmL⁻¹) for P-1. It is obvious that sometimes increasing initial polymer:drug mass loading ratio, resulted in lower drug solubilisation. This could be due to remove highly griseofulvin accommodated self-assembly during the filtration process.

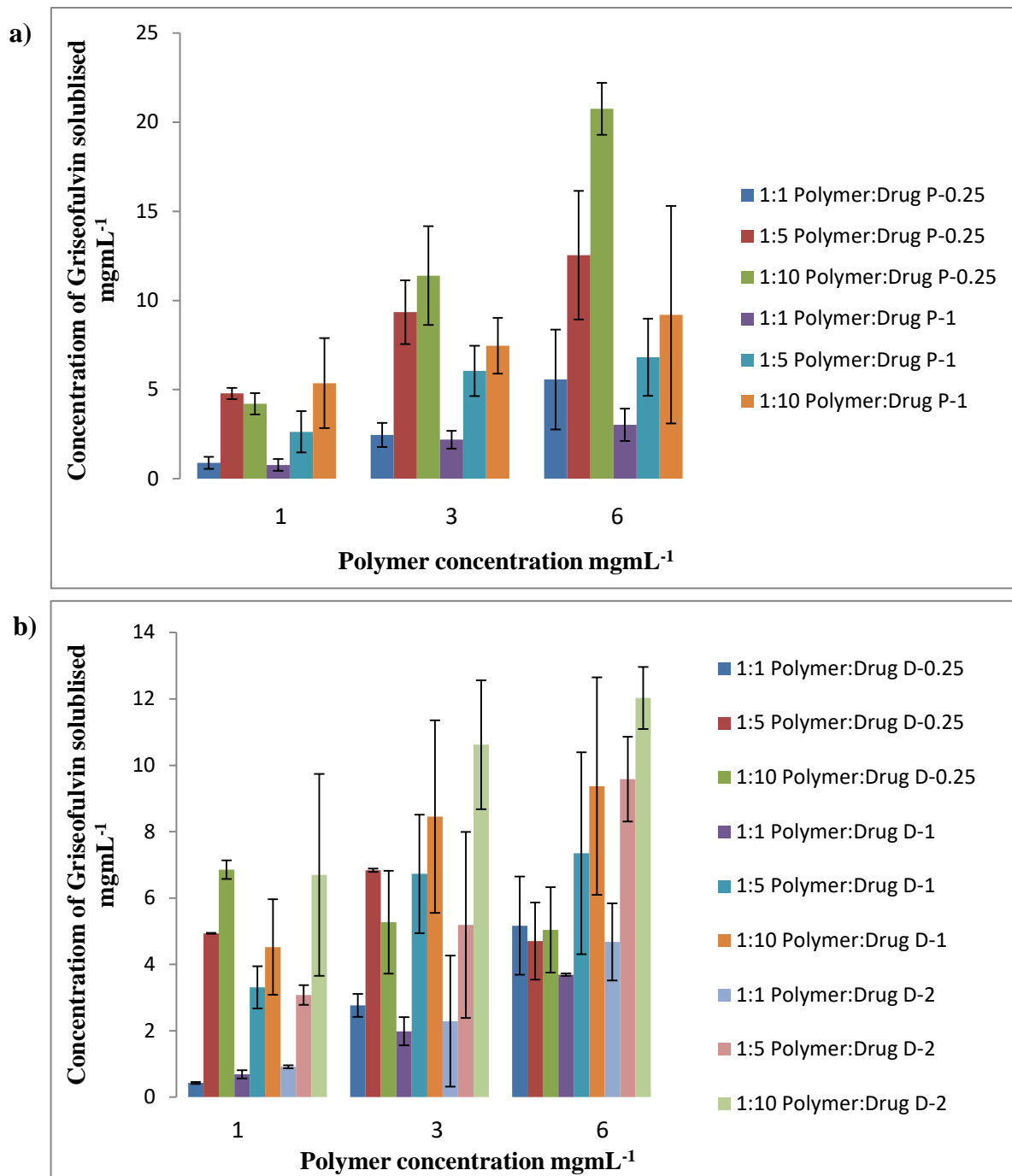


Figure 90- Drug loading of griseofulvin onto a) HPMA-co-APMA-P and b) HPMA-co-APMA-D at varied grafting ratio and different initial drug:polymer loading ratios ($n=3$, $\text{ave} \pm \text{SD}$).

Results of drug loading on different grafting molar ratio of APMA-D are presented in Figures 90b. HPMA-co-APMA-D exhibited griseofulvin solubility increase profiles due to the amphiphilic properties. However, HPMA-co-APMA-D self-assemblies showed a much different trend to the cholesteryl copolymers. D-2 with more grafting ratio, more than D-0.25 and D-1, improved solubility by greater extent, this was expected since it has higher hydrophobic portion. Rank order of solubility improvement is as follows, D-0.25 (50 fold), D-1 (93 fold) and then D-2 (120 fold).

Griseofulvin was loaded at various polymer:drug ratios, and the loading efficiencies are shown in Figure 91a . Both 1:5 and 1:10 initial feed ratio at 1 mgmL^{-1} demonstrated similar loading efficiencies. A sharp increase in drug loading was observed at 1:10 initial feed ratio with increasing copolymer concentration to 3 mgmL^{-1} , and further but moderate increase was found at 6 mgmL^{-1} , while the level of drug loading drop down to more than 2 mgmL^{-1} at 1:5 initial feed ratio for both copolymer concentrations. With 1:10 initial feed ratio, there is some loading that is gradual for the 1 mgmL^{-1} whereas for higher copolymer concentrations, loading is almost double.

Griseofulvin solubility study, using HPMA-co-APMA-O, showed that APMA-O demonstrated extended drug solubility in water at different grafting ratio. The O-1 showed increase in the aqueous solubility up to 54-fold compared to 42-fold, 46-fold and 41-fold of O-2, O-5 and O-10 respectively. Higher solubility increment can be noticed with increase in copolymer concentration. This result suggests that drug molecules preferably tend to solubilize in hydrophobic portion of the copolymer.

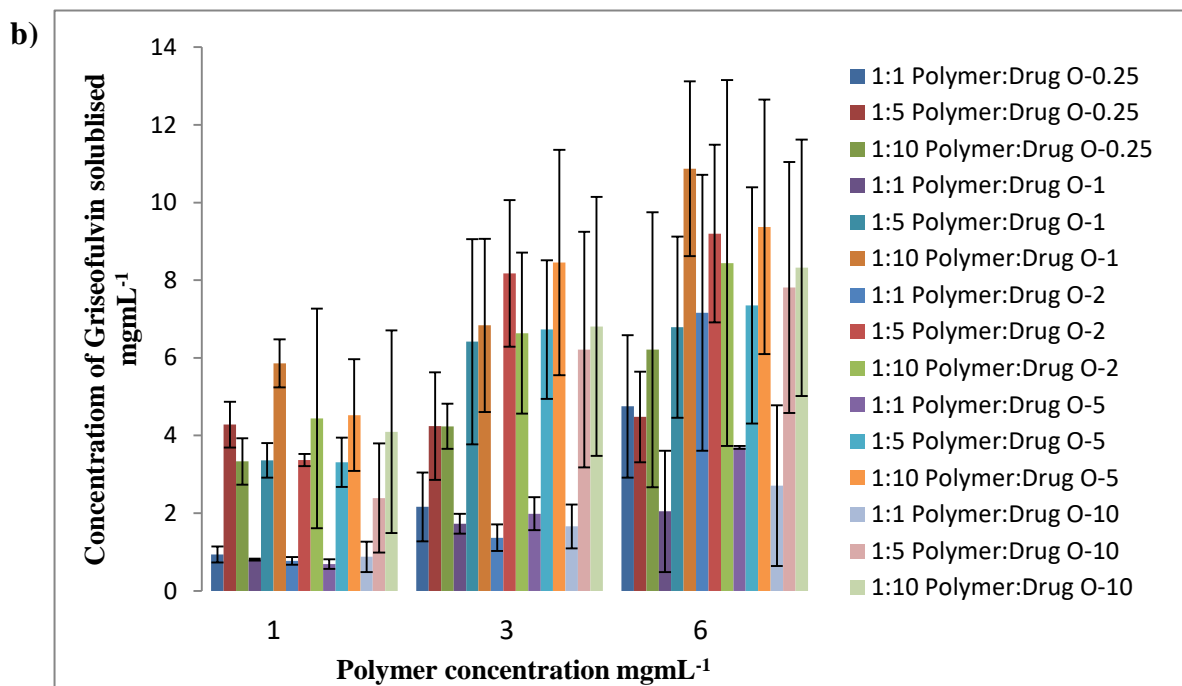
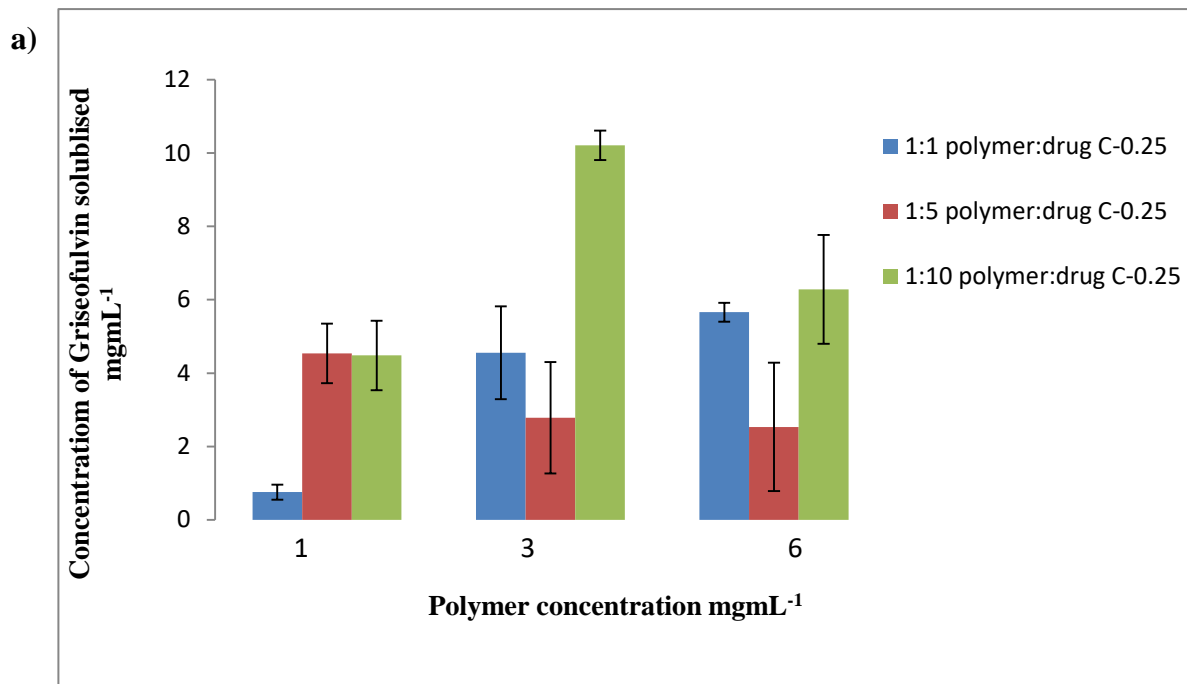


Figure 91- Drug loading of griseofulvin onto a) HPMA-co-APMA-C and b) HPMA-co-APMA-O at varied grafting ratio and different initial drug:polymer loading ratios (n=3, ave \pm SD).

4.3.2.3- Determination of Prednisolone Solubility in HPMA-co-APMA-R

Figure 92 presents comparative maximum drug loading for HPMA-co-APMA-R. All formulas present herein had higher drug solubility compared to that in aqueous medium. In contrast to griseofulvin, prednisolone demonstrates more solubility in D-2 and O-1. In fact, D-2 induces more than 60-fold increase in the solubility of prednisolone while O-1 56-fold. Similar trends were observed to P-0.25 and C-0.25 with around 51-fold and 46-fold higher solubility.

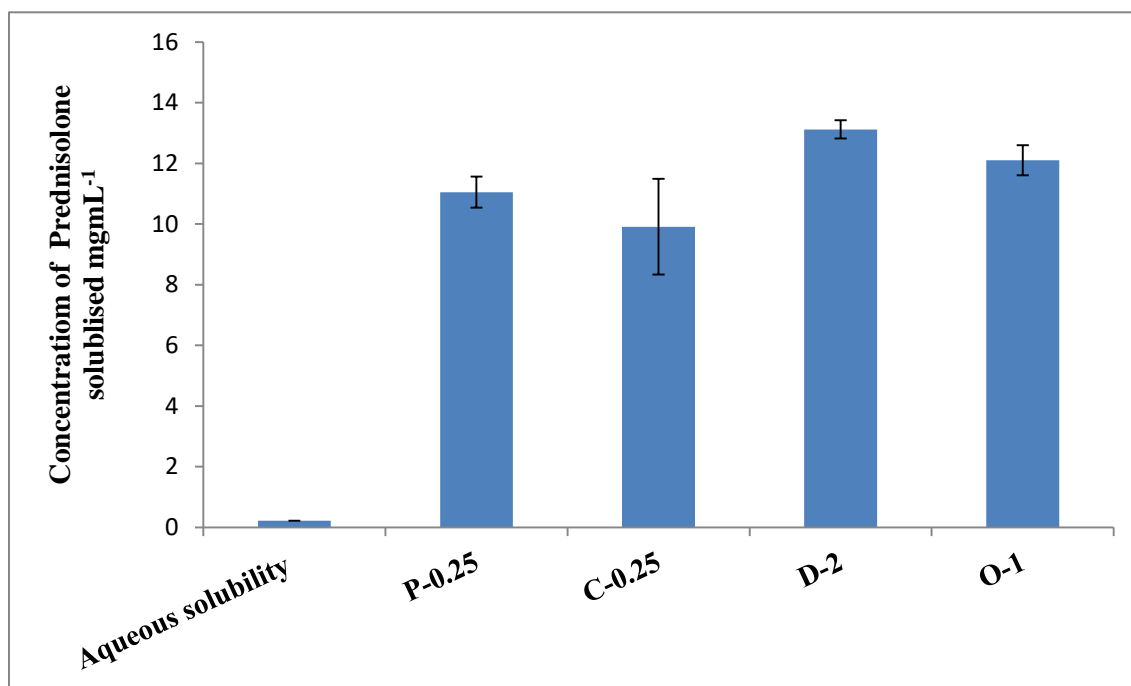


Figure 92- Maximum concentration of prednisolone solubilised by each copolymer formula (6 mgmL⁻¹) at 1:1, 1:5 or 1:10 initial polymer:drug loading ratios (n=3, ave ± SD).

The solubility of prednisolone dramatically increased, with 1:1 polymer:drug initial feed ratio in the 3 mg or 6 mg of P-1 solution, which is 46 times higher than that found for aqueous medium. However, increasing the initial feed ratio effect was not regular as it fluctuated. The rate of prednisolone loading onto P-1 was higher than P-0.25 at all initial feed ratio, but just lower than P-0.25 at 6 mgmL⁻¹ (1:10 polymer:drug) (Figure 93a).

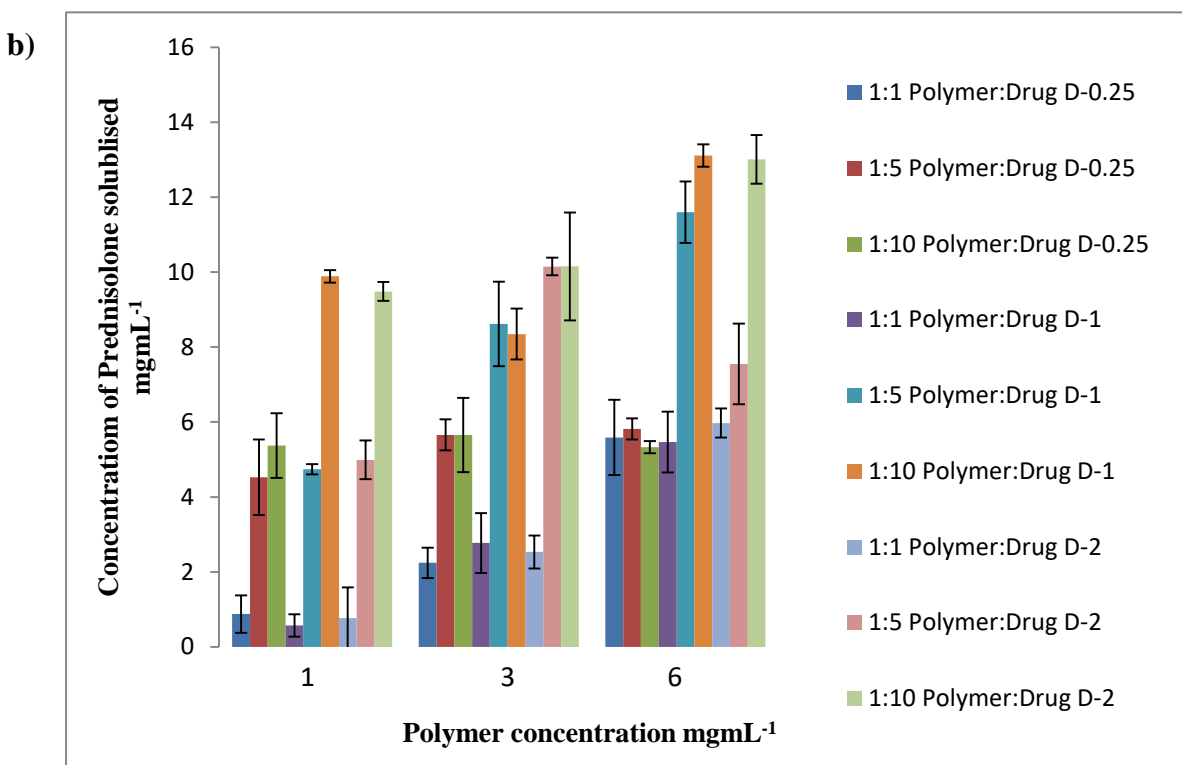
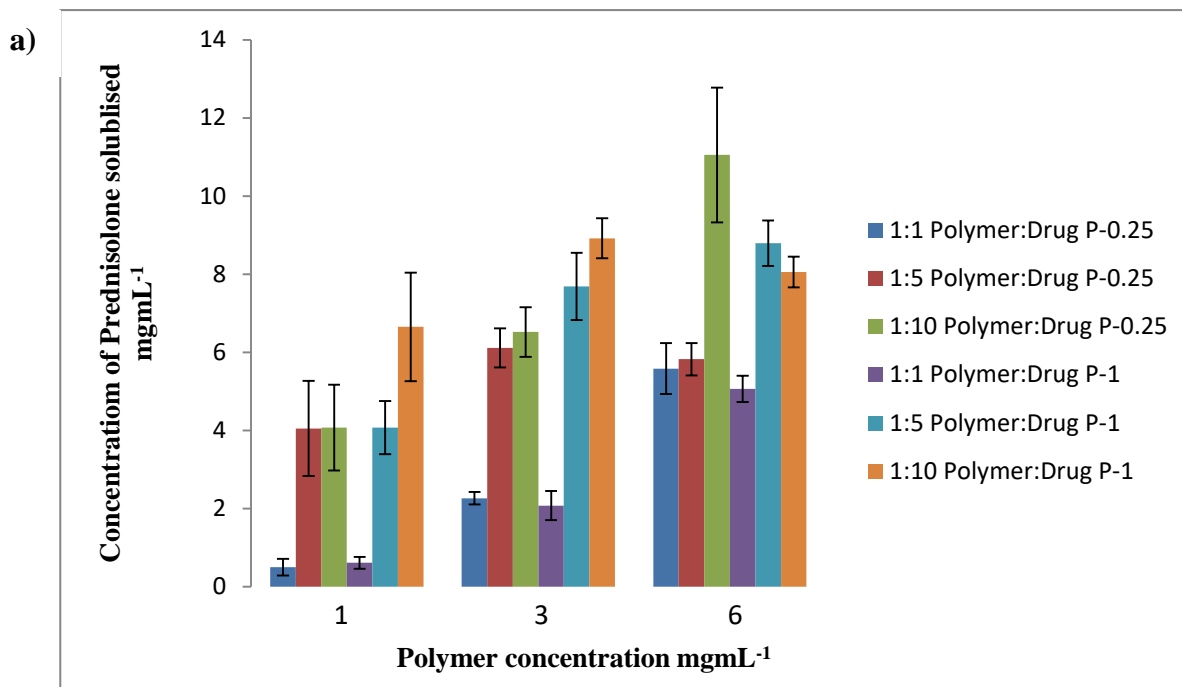


Figure 93- Drug loading of prednisolone onto a) HPMA-co-APMA-P and b) HPMA-co-APMA-D at varied grafting ratio and different initial drug:polymer loading ratios (n=3, ave \pm SD).

The highest drug loading was found for the both D-1 and D-2 formulations, where a high polymer concentration was used, and the initial polymer:drug feed was at a high ratio. However, changing polymer concentration of D-0.25 and polymer:drug feeding ratio did not exhibit significant change in prednisolone solubility (Figure 93b).

Three of the copolymer concentrations with basic APMA-C moieties, 1 mgmL⁻¹, 3 mgmL⁻¹ and 6 mgmL⁻¹, were unaffected significantly by increasing the polymer:drug initial feed ratio (Figure 94a). However, at 1:5 polymer:drug initial feed ratio, the solubility of prednisolone was increased slightly with a relative copolymer increase. This perhaps was due to loaded the maximum drug concentration on copolymer causes expansion of the micelles size bigger than the filter pores, which lead to passed small particles that have the same amount of drug.

At higher polymer concentrations both the O-1 and O-5 appeared to load the maximum concentration of prednisolone at 1:10 polymer:drug initial feed ratio. However at higher grafting ratio O-2 and O-10 respectively this was less. Results also showed that amount of drug solubilised by the O-0.25 invariable as copolymer concentration was increased. This could be to low hydrophobic moieties percentage in copolymer backbone (Figure 94b).

Based on the previous drug loading results, C-0.25, P-0.25, D-2 and O-1 exhibited the highest improvement in drug aqueous solubility for the three hydrophobic drugs. In this respect, it is generally accepted that high improvement in drug aqueous solubility achieved with D-2 and O-1. This finding helps to reduce the range of polymers used in next step.

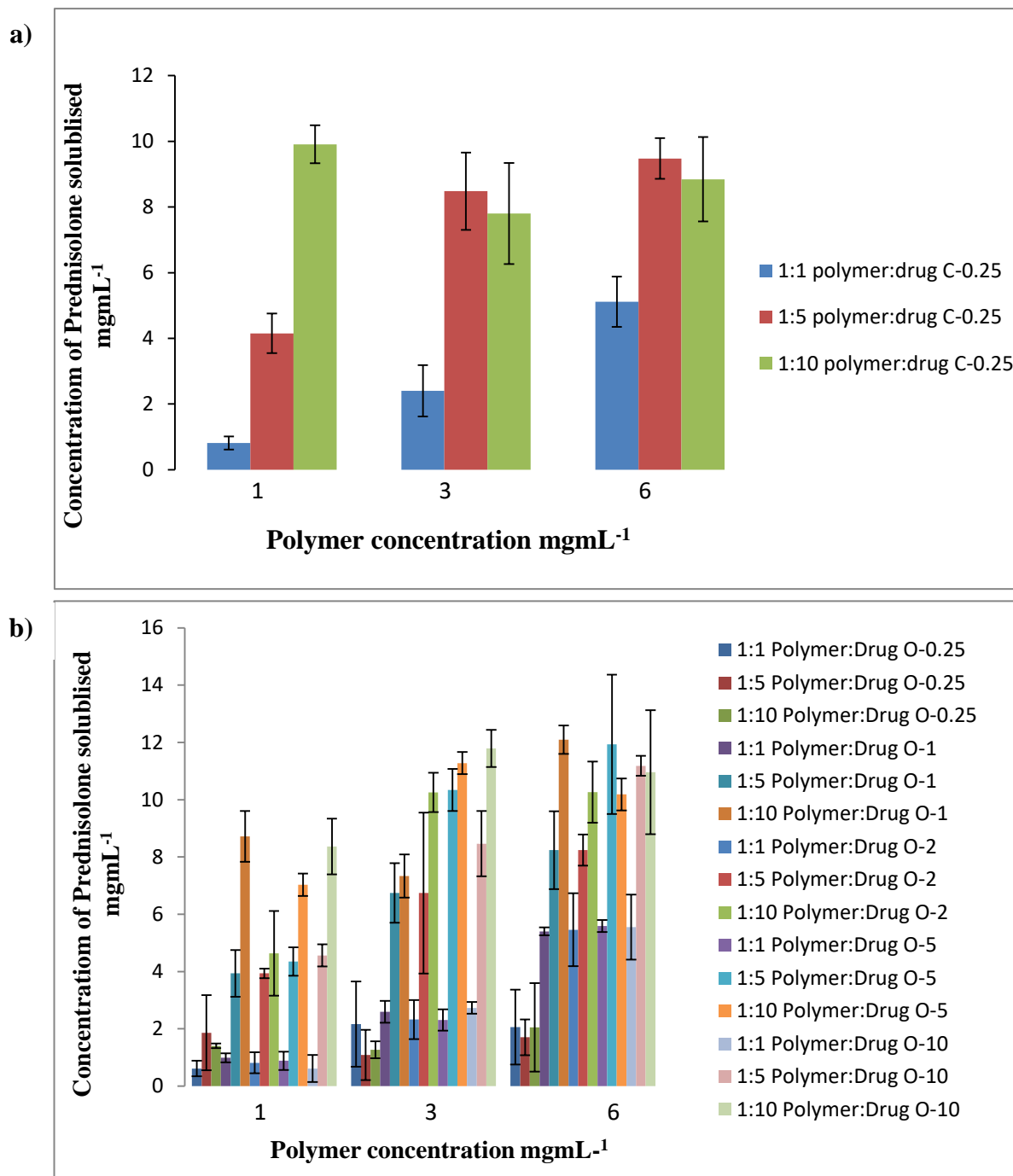


Figure 94- Drug loading of prednisolone onto a) HPMA-co-APMA-C and b) HPMA-co-APMA-O at varied grafting ratio and different initial drug:polymer loading ratios (n=3, ave \pm SD).

4.3.2.4- Determination of Propofol, Griseofulvin and Prednisolone Solubility in (O-1)-b-(PEG) and (D-2)-b-(PEG)

In this step block copolymers have been prepared individually from D-2 or O-1 with PEG (as described in chapter 2) in two different ratios 90%:10% and 80%:20% respectively. The results of 80% : 20% copolymers formulas showed no remarkable differences in drug solubility and release from 90%:10% copolymers formulas (appendix, Figure 1-4). In this sense, the rest of this study was performed with ratio of D-2 or O-1: PEG 90%:10%.

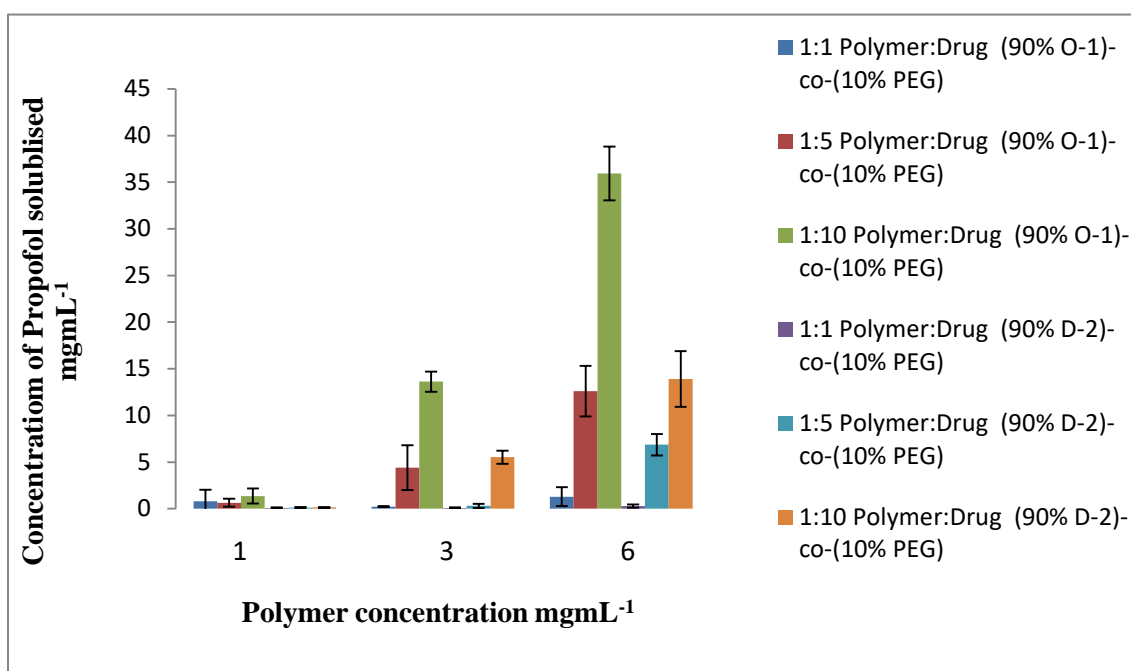


Figure 95- Drug loading of propofol onto (O-1)-b-(PEG) and (D-2)-b-(PEG) at different initial drug:polymer loading ratios (n=3, ave ± SD).

The second part of the drug loading study was performed to determine the effect of PEG addition on solubilising efficiency of D-2 and O-1. Solubilisation effect of (D-2)-b-(PEG) on propofol and prednisolone was less strong than that of D-2. This behaviour is a consequence of the hydrophilic properties of PEG which lead to reduce the ability of the amphiphilic copolymer. However, griseofulvin solubility did not effect. (D-2)-b-(PEG) exhibited improvement in drug aqueous solubility demonstrating 138-fold for propofol, 69-fold for griseofulvin and 37-fold for prednisolone respectively (Figures 95, 96 and 97). Block copolymer comprised of O-1 has been found to be less affected by PEG addition than those containing relative D-2 amounts, indicating greater stability. Figure 95 presents drug loading onto (O-1)-b-(PEG). These profiles suggest that we get 359-fold for propofol, 53-fold for

griseofulvin and 48-fold for prednisolone respectively. As indicated above, the addition of PEG caused a decrease in the solubilising efficiency of D-2 and O-1, but they still have excellent effect on the solubility of hydrophobic drug models.

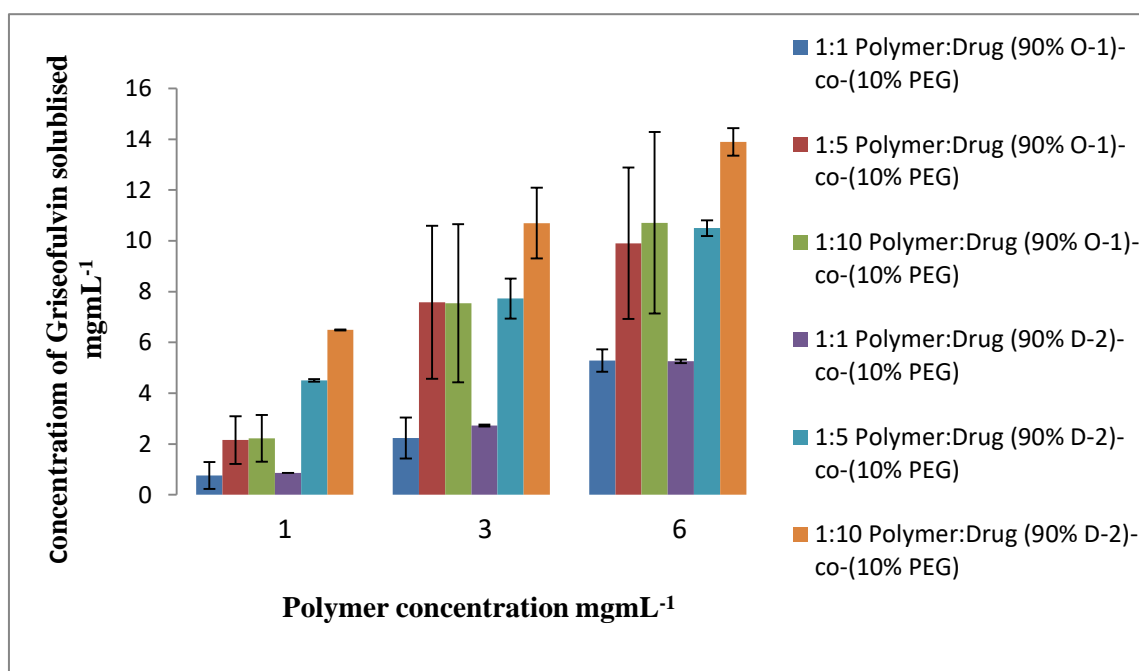


Figure 96- Drug loading of griseofulvin onto (O-1)-*b*-(PEG) and (D-2)-*b*-(PEG) at different initial drug:polymer loading ratios (n=3, ave ± SD).

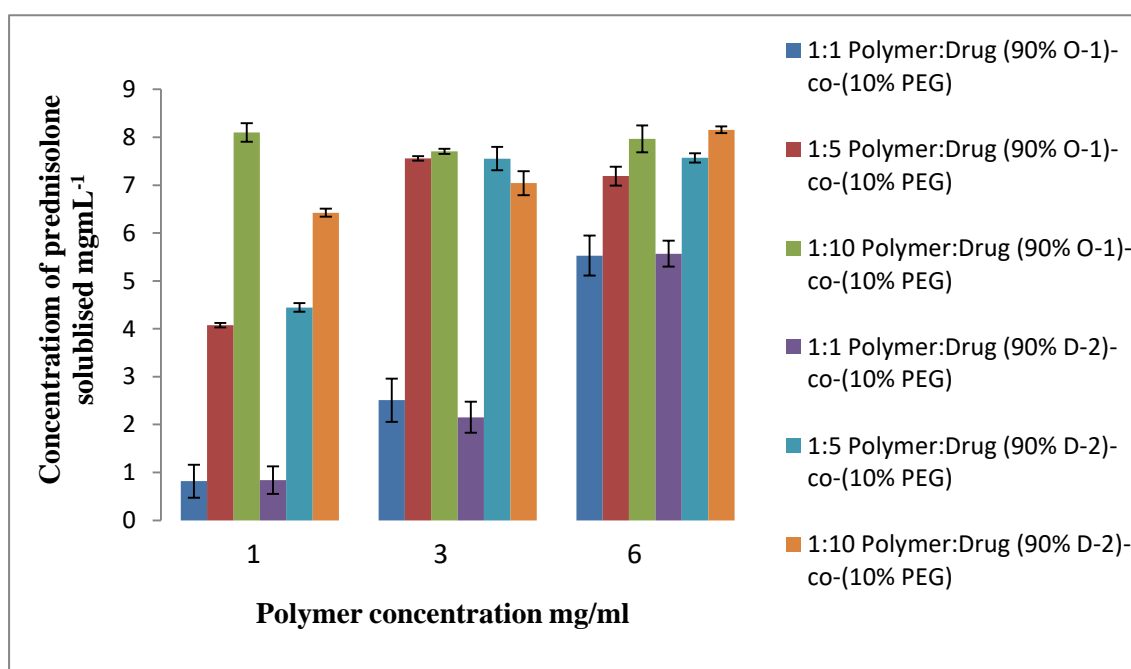


Figure 97- Drug loading of prednisolone onto (O-1)-*b*-(PEG) and (D-2)-*b*-(PEG) at different initial drug:polymer loading ratios (n=3, ave ± SD).

4.3.2.4- Determination of Propofol, Griseofulvin and Prednisolone Solubility in (O-1)-b-(PEG)-HNPs

HNPs were used in this study as laser initiated nano-heaters resulting in drug release as well as allowing for real time imaging using MRI. For this purpose, HNPs were being incorporated into the intrinsic (O-1)-b-(PEG) copolymer backbone. The effect of the HNPs addition on hydrophobic drugs solubility efficacy was determined. At 6 mgmL⁻¹, (O-1)-b-(PEG)-HNPs seem to have sufficient drug-loading values. Figure 98 illustrates that copolymer formula was capable of solubilising up to 28.9 mgmL⁻¹, 13.5 mgmL⁻¹ and 10.5 mgmL⁻¹ of propofol, griseofulvin and prednisolone respectively using 1:10 initial polymer:drug feed ratio. For these drug candidates, propofol loading showed as much as 289-fold increase in the solubility profile from the aqueous solubility of the drug, flowed by griseofulvin 68-fold then prednisolone 49-fold. However, propofol solubility was relatively lower compared to (O-1)-b-(PEG) while griseofulvin and prednisolone showed increased in solubility.

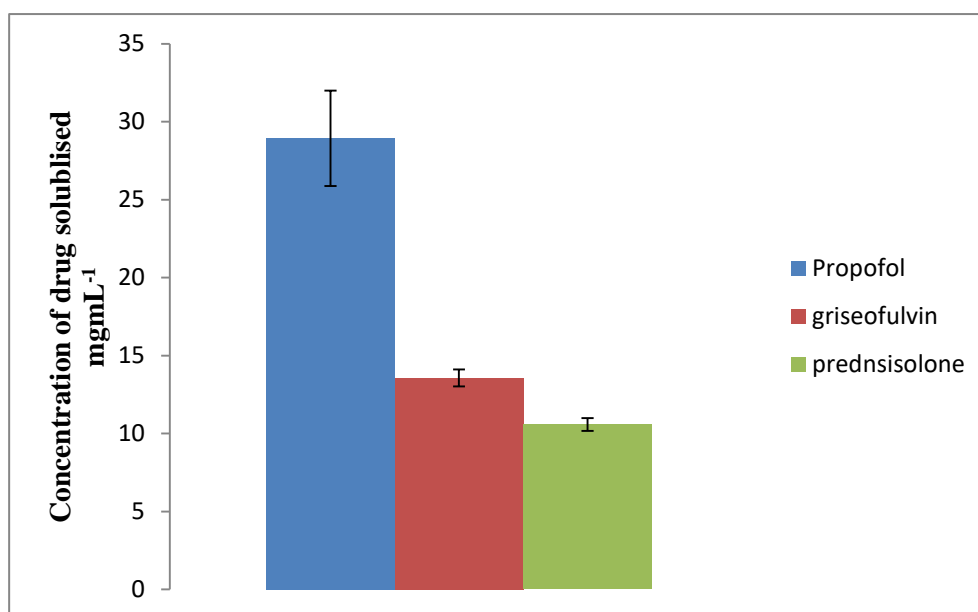


Figure 98- Maximum concentration of propofol, griseofulvin and prednisolone solubilised by (O-1)-b-(PEG)-HNPs copolymer formula (6 mgmL⁻¹) at 1:10 initial polymer:drug loading ratios (n=3, ave ± SD).

4.3.2.5- Determination of Paclitaxel Solubility in (O-1)-b-(PEG) and (O-1)-b-(PEG)-HNPs

Based on the previous results, a strategy of using (O-1)-b-(PEG) and (O-1)-b-(PEG)-HNPs to improve PTX solubility was adopted. The solubility tests of PTX with 6 mgmL^{-1} of both copolymers formulations, using 1:1 initial polymer:drug mass ratio were carried out. The results indicated that the (O-1)-b-(PEG) and (O-1)-b-(PEG)-HNPs were capable of solubilising $0.936 \text{ mgmL}^{-1} \pm 0.2 \text{ mgmL}^{-1}$ and $0.841 \text{ mgmL}^{-1} \pm 0.2 \text{ mgmL}^{-1}$ of PTX respectively (Figure 99). This was an incredible increase in the aqueous solubility ($0.3 \text{ } \mu\text{gmL}^{-1}$) by 3,120-fold and 2,803-fold respectively.

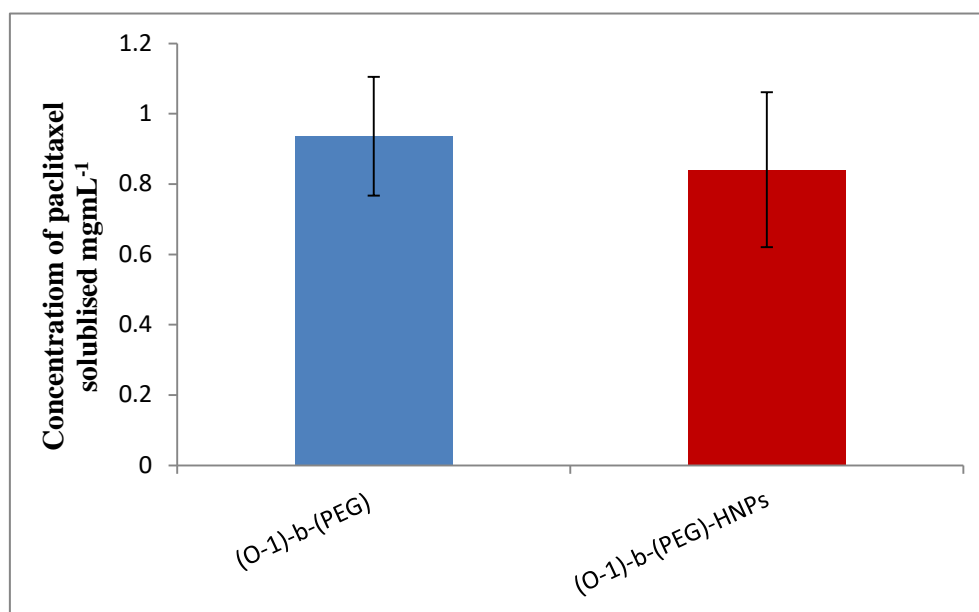


Figure 99- Maximum concentration of paclitaxel solubilised by (O-1)-b-(PEG)-HNPs copolymer formula (6 mgmL^{-1}) at 1:1 initial polymer:drug loading ratios ($n=3$, ave \pm SD).

Table 21- Summary of polymer-drug formulation conditions and encapsulation properties (encapsulation efficiency (EE) and loading capacity (LC)), results shown as average, n=3.

Copolymer	% LC				% EE			
	Pro	Gris	Pred	PTX	Pro	Gris	Pred	PTX
P-0.25	521	345	217	---	52	35	22	---
C-0.25	528	340	990	---	53	34	99	---
D-2	577	200	433	---	58	20	43	---
O-1	685	181	201	---	69	18	12	---
(D-2)-b-(PEG)	231	231	135	---	23	23	14	---
(O-1)-b-(PEG)	598	178	350	15	60	18	35	15
(O-1)-b-(PEG)-HNPS	482	226	176	14	48	23	18	14

Pro= propofol, **Gris**= griseofulvin, **Pred**= prednisolone, **PTX**= paclitaxel.

4.3.3-Particle size and size distribution

Particle size distributions of optimal copolymer formulations are shown in Table 22. The data clearly show that size of self-assemblies of copolymers loaded with different model drugs can be varied. Change in particle size distribution was dependent on the drug molecule size and the amount of drug loaded. As expected for copolymer alone samples, particle size was in the range of nanometres and smaller than loaded samples. Particle size of P-0.25, C-0.25, D-2 and O-1 without drug was found to be $0.14 \mu\text{m} \pm 0.02 \mu\text{m}$, $0.1 \mu\text{m} \pm 0.01 \mu\text{m}$, $0.2 \mu\text{m} \pm 0.01 \mu\text{m}$ & $0.1 \mu\text{m} \pm 0.005 \mu\text{m}$, with the poly dispersity index (PDI) of 0.7 ± 0.2 , 0.7 ± 0.2 , 0.5 ± 0.06 and 0.6 ± 0.2 respectively (Table 22).

The effect of drug loading on the resulting self-assemblies size distribution was quite clear with propofol and griseofulvin formulations. Increasing the drug loading caused increase in the mean diameter of the copolymer self- assemblies. The expansion of the O-1 self-assembly to accommodate larger quantities of propofol (41.1 mgmL^{-1}) resulted in an increase in the copolymer size to $2.3 \mu\text{m} \pm 0.05 \mu\text{m}$ compared to griseofulvin formulation with solubilisation of 10.87 mgmL^{-1} and a size of $0.2 \pm 0.04 \mu\text{m}$. In agreement with this hypothesis is the fact that even the molecule size for griseofulvin is doubled that of the propofol molecule, but the solubilizing amount of propofol 4-times bigger than griseofulvin. This illustrates the high drug solubilizing resulting in large particles size.

The synergistic effect of prednisolone molecule size and loaded amount resulted in huge increasing D-2 self-assembly formula size to ($5 \mu\text{m} \pm 0.04 \mu\text{m}$) compared to ($0.2 \mu\text{m} \pm 0.01 \mu\text{m}$) of griseofulvin formulation which have almost the same amount of solubilised drug, 13.11 mgmL^{-1} and 12.02 mgmL^{-1} respectively. Similar behaviour was observed for the P-0.25, C-0.25 and O-1 samples. Another cause of the synergistic effect was observed in the solubilisation of griseofulvin and prednisolone by (D-2)-*b*-(PEG) and (O-1)-*b*-(PEG). The (O-1)-*b*-(PEG) size was increased from $0.22 \mu\text{m} \pm 0.04 \mu\text{m}$ to $0.31 \mu\text{m} \pm 0.006 \mu\text{m}$ upon encapsulation of the paclitaxel while there was significant increased from $0.12 \mu\text{m} \pm 0.005 \mu\text{m}$ to $0.7 \mu\text{m} \pm 0.08 \mu\text{m}$ in (O-1)-*b*-(PEG)-HNPs size.

Table 22- Photon correlation spectrometry size analysis of optimal Copolymers formulations at 6 mg/ml with initial polymer:drug feed ratio of 10:1, (n=3, ave).

Copolymer	Formulation Size (μm)					Formulation PDI				
	Alone	Pro	Gris	Pred	PTX	Alone	Pro	Gris	Pred	PTX
P-0.25	0.14 ± 0.02	0.9 ± 0.09	0.2 ± 0.007	1.1 ± 0.2	---	0.7 ± 0.2	0.3 ± 0.02	0.4 ± 0.04	0.8 ± 0.03	---
C-0.25	0.1 ± 0.01	0.5 ± 0.02	0.3 ± 0.01	0.6 ± 0.008	---	0.7 ± 0.2	0.4 ± 0.008	0.2 ± 0.009	0.3 ± 0.04	---
D-2	0.2 ± 0.01	3.3 ± 0.09	0.2 ± 0.01	5 ± 0.4	---	0.5 ± 0.06	0.3 ± 0.1	0.8 ± 0.3	0.7 ± 0.1	---
O-1	0.1 ± 0.005	2.3 ± 0.05	0.2 ± 0.04	0.9 ± 0.1	---	0.6 ± 0.2	0.1 ± 0.06	0.6 ± 0.2	0.8 ± 0.1	---
(D-2)-b-(PEG)	0.2 ± 0.003	1.5 ± 0.1	0.2 ± 0.04	0.9 ± 0.1	---	0.4 ± 0.01	0.4 ± 0.04	0.7 ± 0.1	0.8 ± 0.05	---
(O-1)-b-(PEG)	0.22 ± 0.04	1.8 ± 0.02	0.5 ± 0.03	2 ± 0.1	0.3 ± 0.006	0.5 ± 0.09	0.3 ± 0.05	0.4 ± 0.03	0.3 ± 0.1	0.3 ± 0.03
(O-1)-b-(PEG)-HNPS	0.12 ± 0.005	1.3 ± 0.04	1.2 ± 0.1	1.2 ± 0.1	0.7 ± 0.08	0.4 ± 0.09	0.3 ± 0.05	0.5 ± 0.01	0.8 ± 0.2	0.3 ± 0.1

Pro= propofol, **Gris**= griseofulvin, **Pred**= prednisolone, **PTX**= pachtaxel

4.3.4- Characterisation of (O-1)-b-(PEG) in the absence and in the presence of HNPs Nanoaggregates

Transmission electron micrograph is particularly useful to evaluate the morphology and the size of the aggregate copolymer micelles. Figure 100 displays transmission electron micrographs of aggregates obtained from (O-1)-b-(PEG) in the absence and in the presence of HNPs. None of the TEM images in this study required stain for visualization. In samples corresponding to copolymer alone the micrograph (Figure 100a) shows nearly spherical aggregates at 6 mg/ml, approximately 0.25 μm in size, that were visualized by TEM on a copper grid, size observed on the micrograph correlated well with the dynamic light scattering experiment value (Table 22).

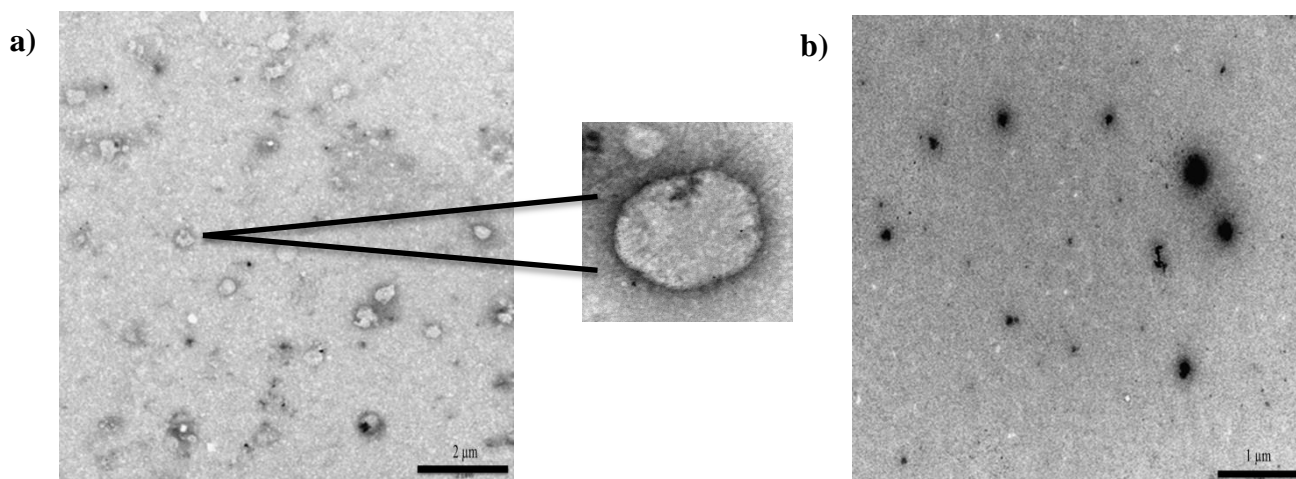


Figure 100-TEM micrographs of optimal formulations nano-aggregates of (O-1)-b-(PEG) 6 mgmL^{-1} sample a) in the absence of HNPs, b) in the presence of HNPs.

In the synthesis of (O-1)-b-(PEG)-HNPs nanoaggregates, (O-1)-b-(PEG) were conjugated directly onto the HNP via dative covalent linkage between gold surface and the thiol (-SH) moiety in the oxadiazole pendant group (Figure 21). The low concentration and steric hindrance effects of HNPs suggest that only one -SH group was capable to attach to one HNP (Christopher *et al.*, 2013). (O-1)-b-(PEG)-HNPs copolymer forms $\approx 0.12 \mu\text{m} \pm 0.005 \mu\text{m}$ aggregates in aqueous suspension, as detected by PCS (Table 22). These nano-aggregates could be captured in electron micrographic images on copper grids and these sizes correlated well with the previous value. TEM image for 6 mg/ml solution of copolymer concentration

(Figure 100b) show that the (O-1)-*b*-(PEG)-HNPs are formed spherical micelles with a micelle radius $\approx 0.13 \mu\text{m}$ in agreement with light scattering results. Moreover, some large aggregates of different sizes were detected.

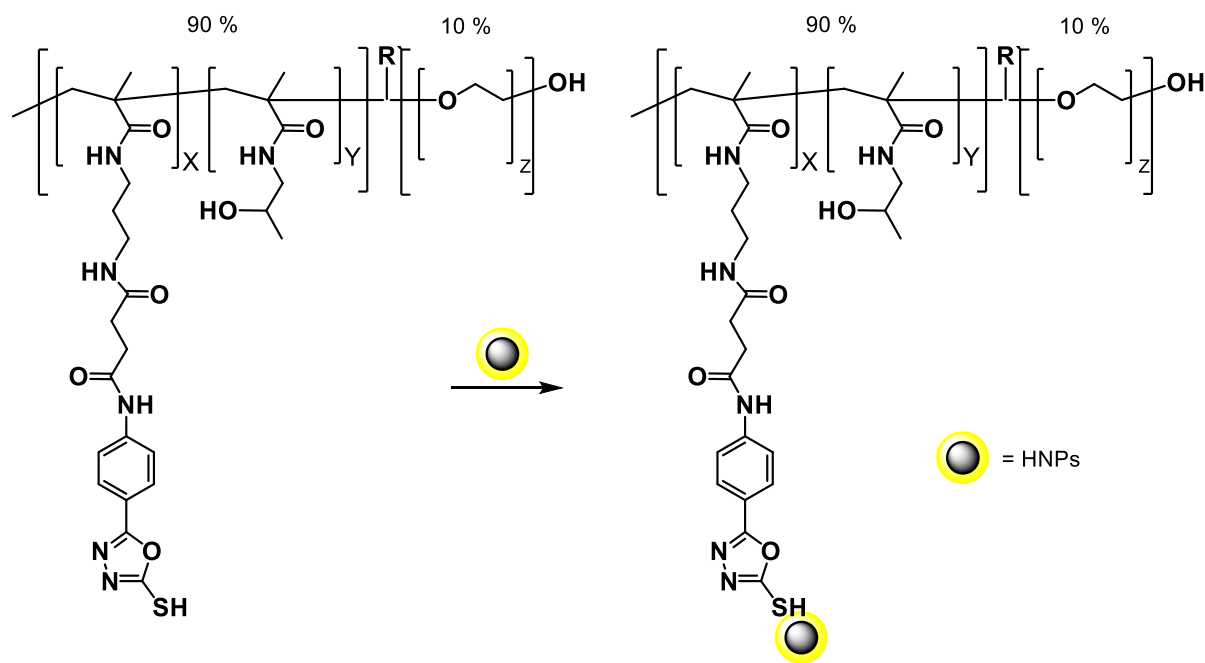


Figure 101- Representation of the (O-1)-*b*-(PEG) conjugation to gold surface of HNPs via oxadiazole pendant group.

Zeta potential was experimentally identified for the amphiphilic (O-1)-*b*-(PEG) self-aggregated nanoparticles in water and found to be 9.9 ± 1 , suggesting that the positively charged amine and carbonyl groups in the O-1 molecules were mainly distributed on the outer surface of the nanoparticles contributing to the hydrophilic potential. Subsequently the zeta potential shifted to $0.25 \text{ mV} \pm 0.2 \text{ mV}$ after the HNPs were added (Figure 102b). The reduced surface charge is possibly due to the attachment of HNPs with thiol (-SH) group that presence in the oxadiazole structure which force APMA amine and carbonyl groups to be driven to an interior micellar structure away from the water.

A decrease in hydrodynamic radius $121 \text{ nm} \pm 5 \text{ nm}$ (Figure 102a) and TEM particle diameter $\approx 130 \text{ nm}$ was observed, hence indicating that attachment was successful.

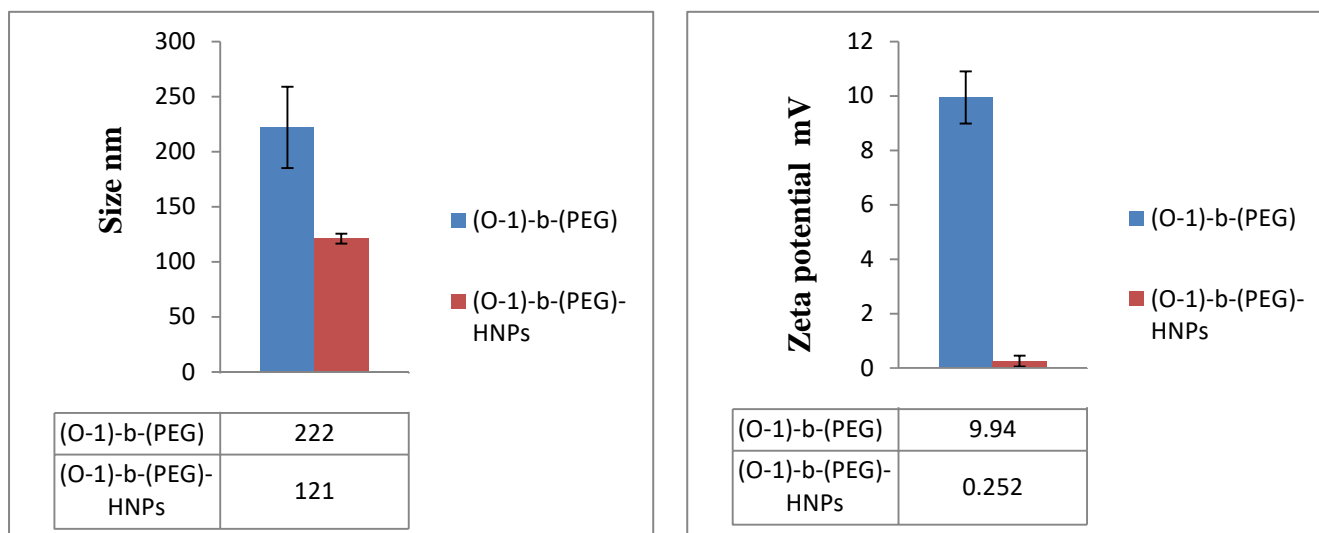


Figure 102- Representation a) size and zeta potential of optimal formulations nano-aggregates of (O-1)-b-(PEG) 6 mgmL⁻¹ sample in the absence and in the presence of HNPs.

4.3.5- In vitro drug release

The temperature effects on the drug release behaviours of the optimal formulations of copolymers were investigated at four different temperatures 5 °C, 30 °C, 40 °C and 50 °C. This investigation is carried out in sink conditions over 24 h in triplicate with a magnetic stirrer. Measurements of propofol release from highest drug loading formulations (Figures 103-106) show that HPMA-co-APMA-R copolymers did not respond to change in surrounded temperature. Furthermore, altering the pH of the outer solution also failed to achieve any enhancement in the dissolution profiles of the propofol from HPMA-co-APMA-R at different temperature.

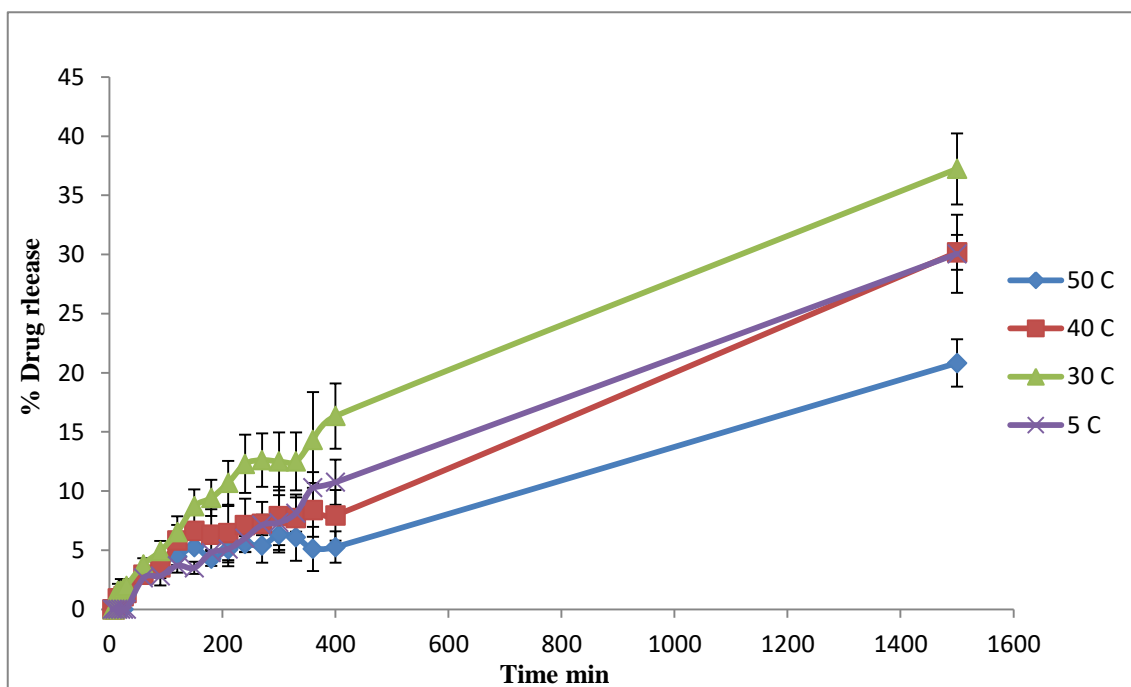


Figure 103- *In vitro* release of propofol from P-0.25 formulation at different temperatures.

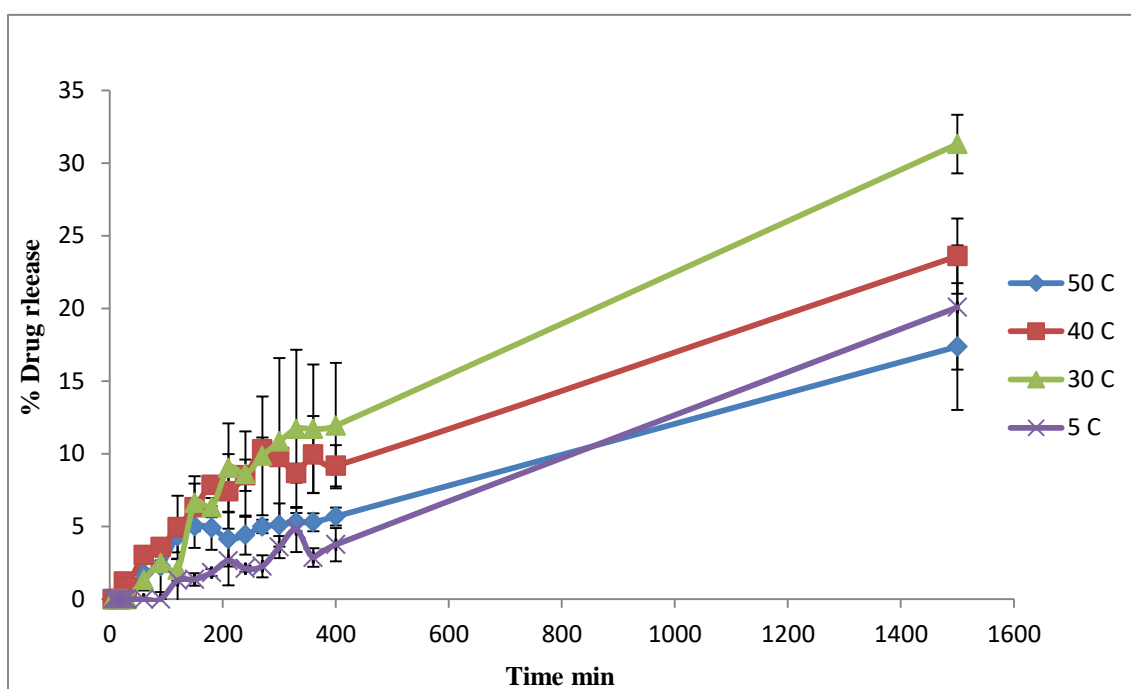


Figure 104- *In vitro* release of propofol from D-2 formulation at different temperatures.

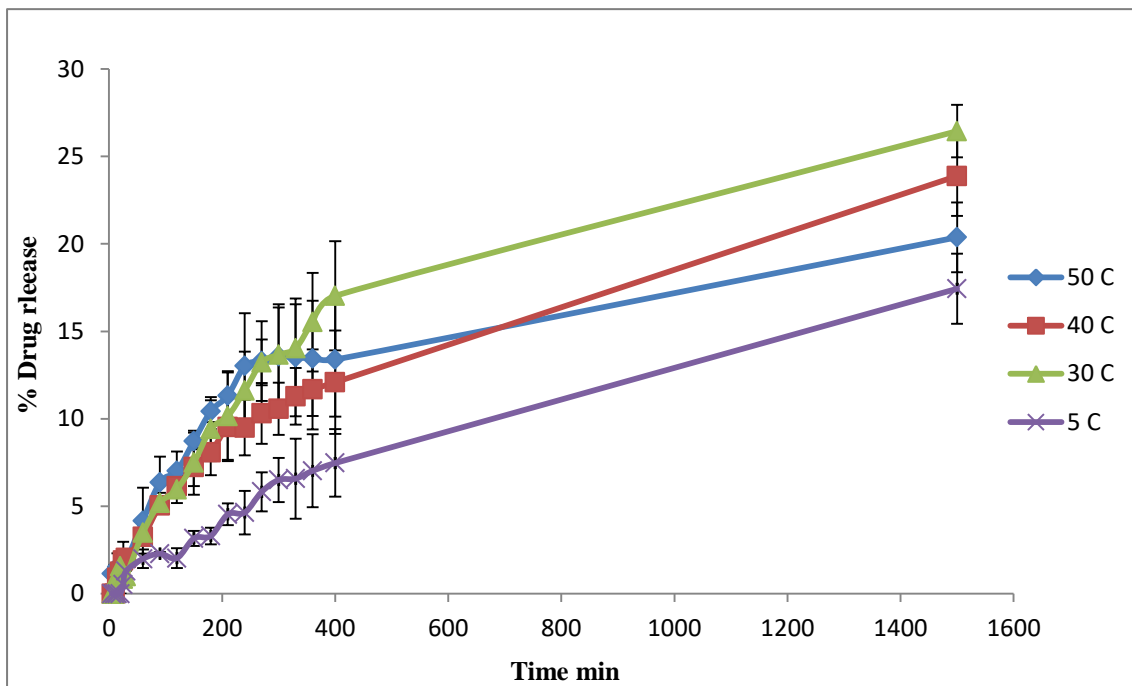


Figure 105- *In vitro* release of propofol from C-0.25 formulation at different temperatures.

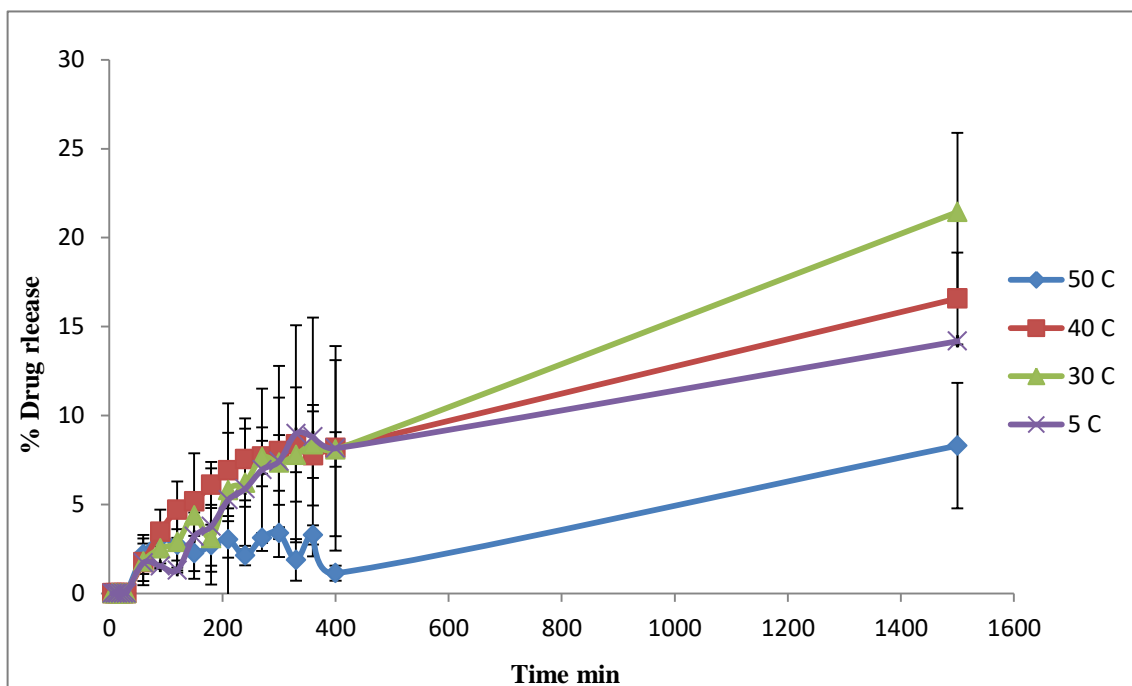


Figure 106- *In vitro* release of propofol from O-1 formulation at different temperatures.

To set-up thermos-responsive copolymer for controlled drug release, approaches based on introducing an appropriate amount of poly ethylene glycol (PEG) block as a part of O-1 and D-2 amphiphilic copolymers. A significant enhancement in response to the change in temperature as the drug was released across the membrane was improved when the PEG was present for the three hydrophobic drugs models (Figure 107 and 108).

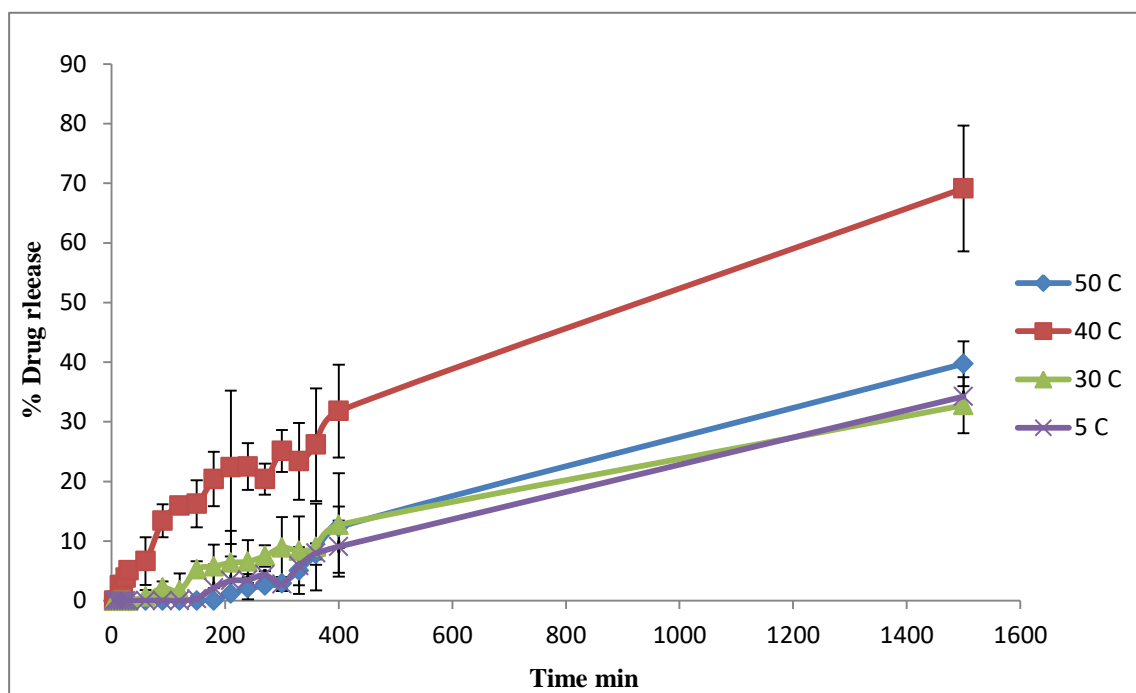


Figure 107- *In vitro* release of propofol from (D-2)-*b*-(PEG) formulation at different temperatures.

Propofol release profile from the (O-1)-*b*-(PEG) was slightly higher in response than that from the (D-2)-*b*-(PEG) especially at 50 °C. The drug release from (D-2)-*b*-(PEG) at 40 °C was greater than 2/5 of the amount released at 50 °C, 30 °C and 5 °C. However, no significant difference in drug release between these temperatures (Figure 107) was seen.

The release profile of propofol from (O-1)-*b*-(PEG) at 40 °C and 50 °C was quite similar at the first 150 min. However, the pattern at 50 °C tends to display much slower release than that at 40 °C, over the followed period (Figure 108).

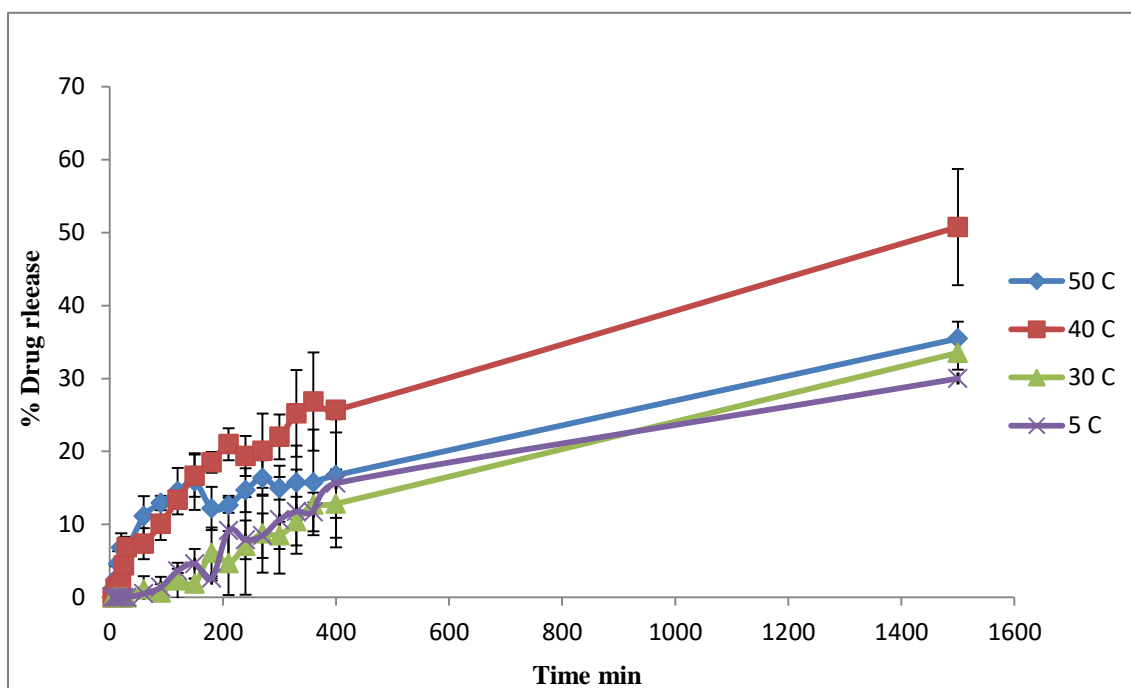


Figure 108- *In vitro* release of propofol from (O-1)-*b*-(PEG) formulation at different temperatures.

When griseofulvin was incorporated in (D-2)-*b*-(PEG) copolymer, the effect of temperature was even more pronounced and the hydrophobic griseofulvin drug, which still released more efficiently than from (O-1)-*b*-(PEG).

At 50 °C and 40 °C, the amount of the released griseofulvin was around 2-fold and 1-fold respectively, compared to the released at 5 °C, whereas the increase was less, compared to the released at 30 °C (Figure 109).

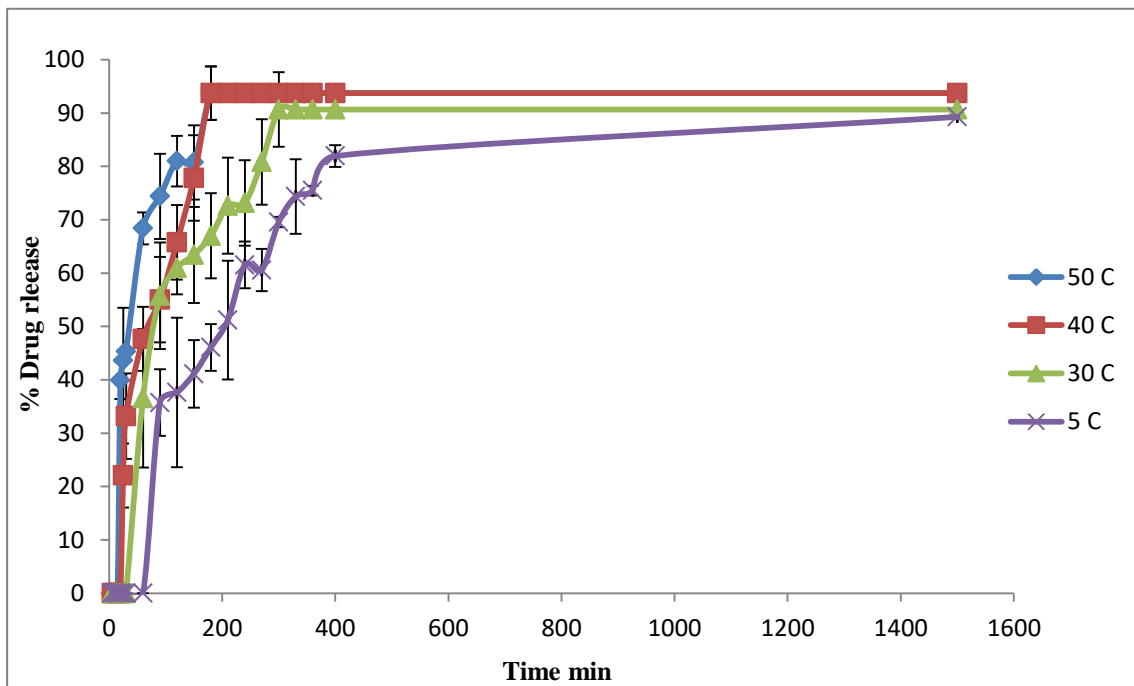


Figure 109- *In vitro* release of griseofulvin from (D-2)-b-(PEG) formulation at different temperatures.

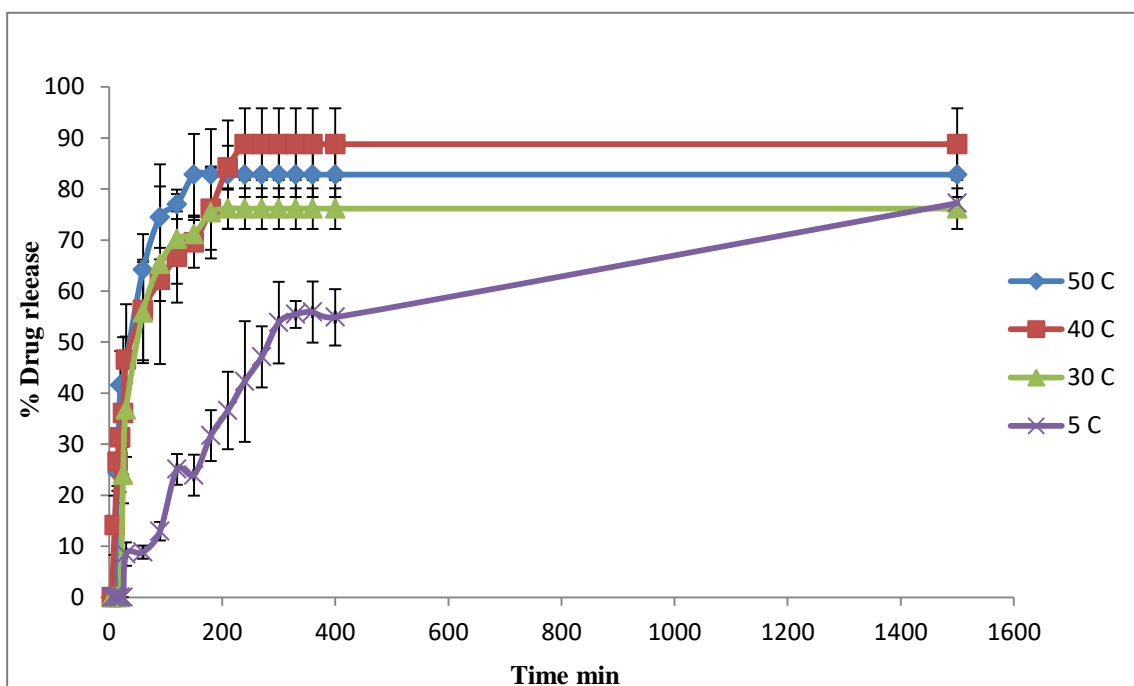


Figure 110- *In vitro* release of griseofulvin from (O-1)-b-(PEG) formulation at different temperatures.

In 50 °C, around 50 % of prednisolone released from (D-2)-b-(PEG), after 15 min, while these amount of drug released after 30 min , 45 min and 330 min at 40 °C, 30 °C and 5 °C

respectively, it appeared that no more prednisolone was released after around 90 min at both 40 °C and 50 °C while the drug was consistently released at 30 °C and 5 °C until after 120m and 330 min respectively (Figure 111). The same pattern was observed in (O-1)-*b*-(PEG), and again the higher release occurred in higher temperature (Figure 112). The release from (O-1)-*b*-(PEG) formulations was significantly faster than (D-2)-*b*-(PEG).

The results demonstrated that increasing temperature significantly enhanced the release rate of hydrophobic drugs from both formulations. In general, griseofulvin and prednisolone release from (D-2)-*b*-(PEG) and (O-1)-*b*-(PEG) were faster than those containing propofol, which showed similar release profiles. The results also confirmed that PEGylated copolymer formulations possessed respond to change in environmental temperature compared to the unPEGylated formulations.

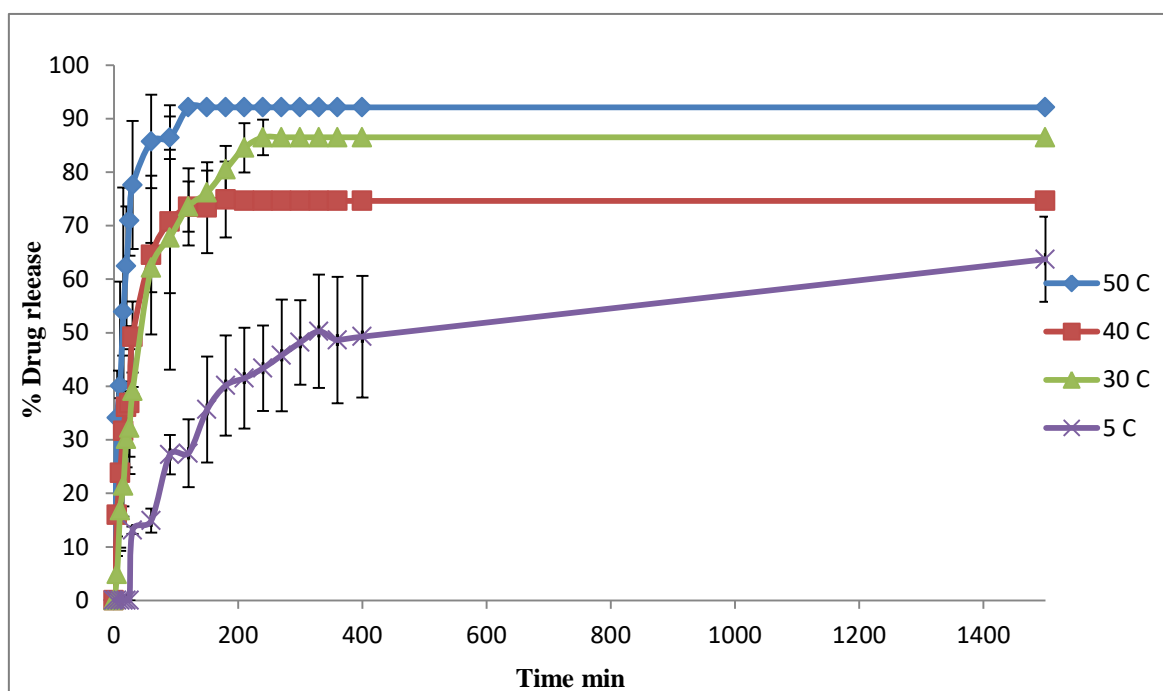


Figure 111- *In vitro* release of prednisolone from (D-2)-*b*-(PEG) formulation at different temperatures.

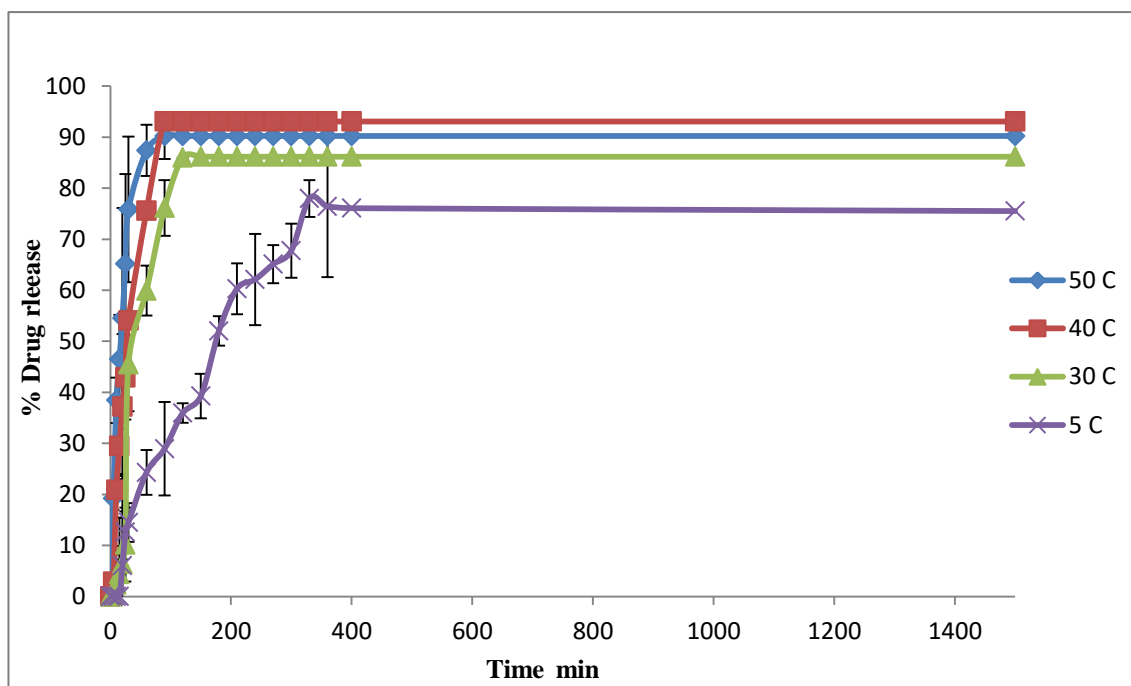


Figure 112- *In vitro* release of Prednisolone from (O-1)-*b*-(PEG) formulation at different temperatures.

Propofol release from the (O-1)-*b*-(PEG)-HNPs during the 24 h experiments was clearly attenuated when compared to the (O-1)-*b*-(PEG) with every different temperature studied. Figure 113 illustrates that propofol was released from the polymer structure but it was still entrapped in the interior layers of the membrane, this is possibly because of the phenol tending to ionize in water and having a negative charge which causes a type of weak ionic bonding with the copolymer formula. Also, the release of propofol from (O-1)-*b*-(PEG)-HNPs was found to be more efficient at 40 C than other temperatures (Figure 114).

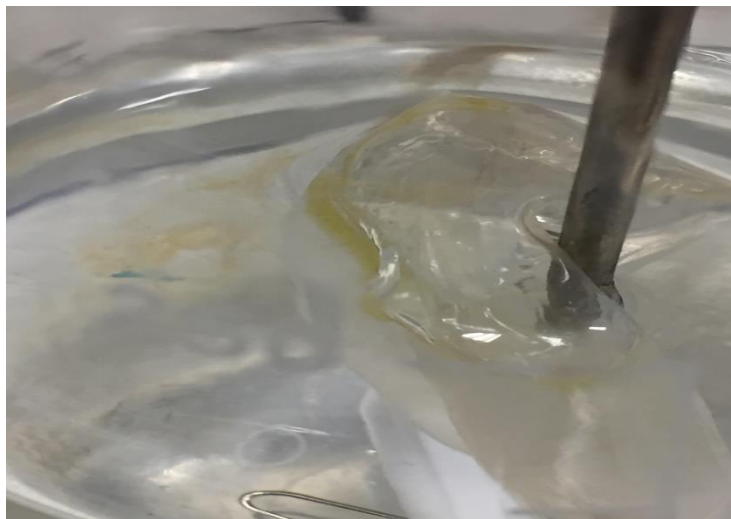


Figure 113- Propofol entrapped in the interior layers of the membrane.

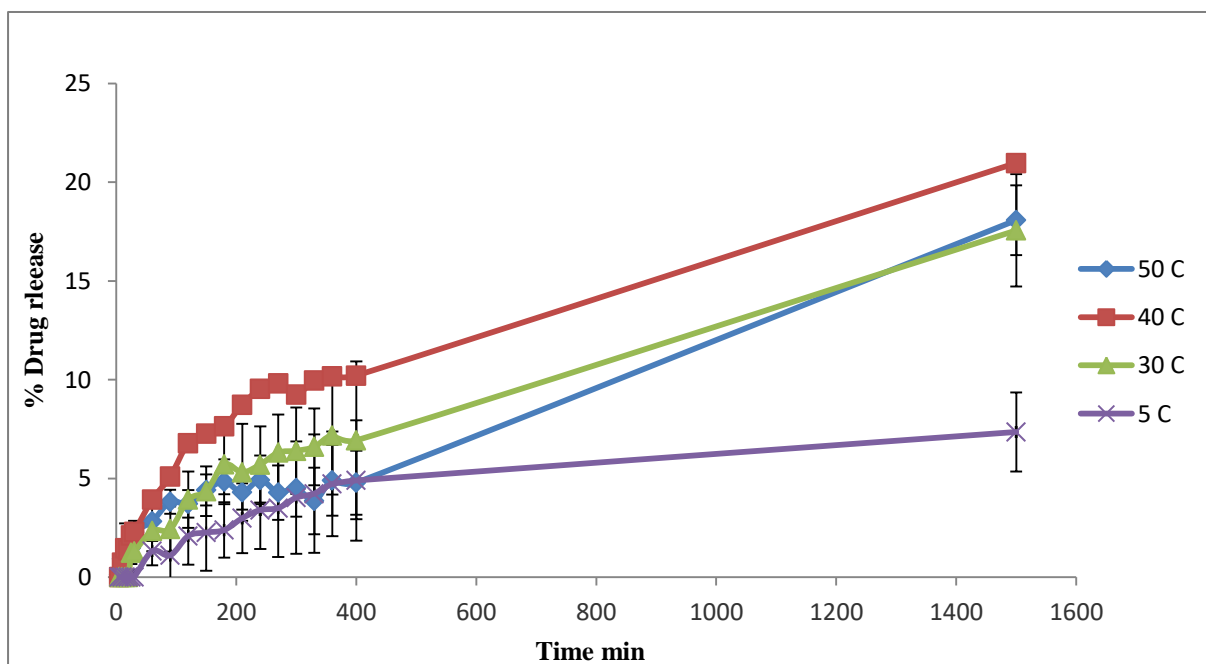


Figure 114- *In vitro* release of propofol from (O-1)-b-(PEG)-HNPs formulation at different temperatures.

The *in vitro* release rate of griseofulvin from (O-1)-*b*-(PEG)-HNPs was evaluated, a fast drug release rate was observed in response to temperature increase. The higher release rate was observed at 50 °C while the release rate of griseofulvin at lower temperatures was found to be much lower. In contrast, (O-1)-*b*-(PEG)-HNPs exhibited a release of griseofulvin of about 86% for 120 min at 50 °C and 40 °C. Whereas the griseofulvin release at 30 °C and 5 °C show up to 74% and 62% cumulative release in 210 min and 300 min respectively. It is necessary to mention here, that the release rate of griseofulvin after HNPs added is a bit higher than that before it (Figure 115).

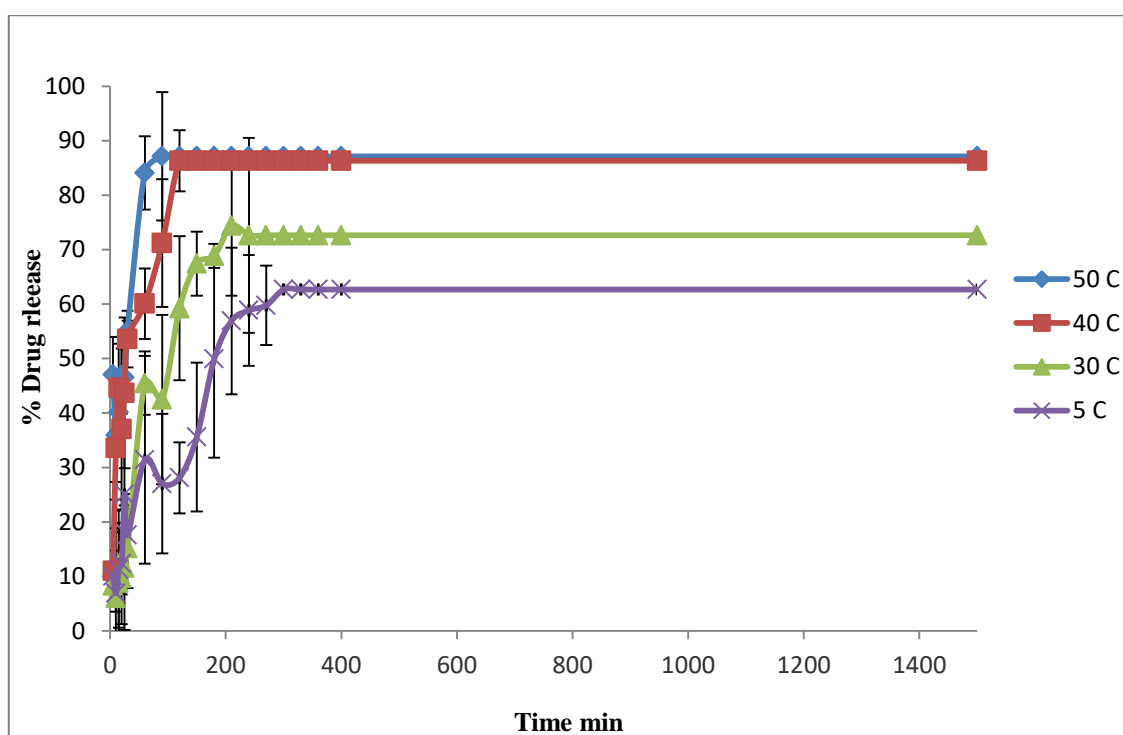


Figure 115- *In vitro* release of griseofulvin from (O-1)-*b*-(PEG)-HNPs formulation at different temperatures.

Prednisolone release profiles from (O-1)-*b*-(PEG)-HNPs, processed at different temperatures are presented in Figure 116. When the processing temperature increased, a significant increase in the prednisolone release rate was observed; around 94 % and 93 % of the drug was released at 50 °C and 40 °C after 120 min respectively from (O-1)-*b*-(PEG)-HNPs. Furthermore, prednisolone release rate was further accelerated with increasing temperature as a result of adding HNPs.

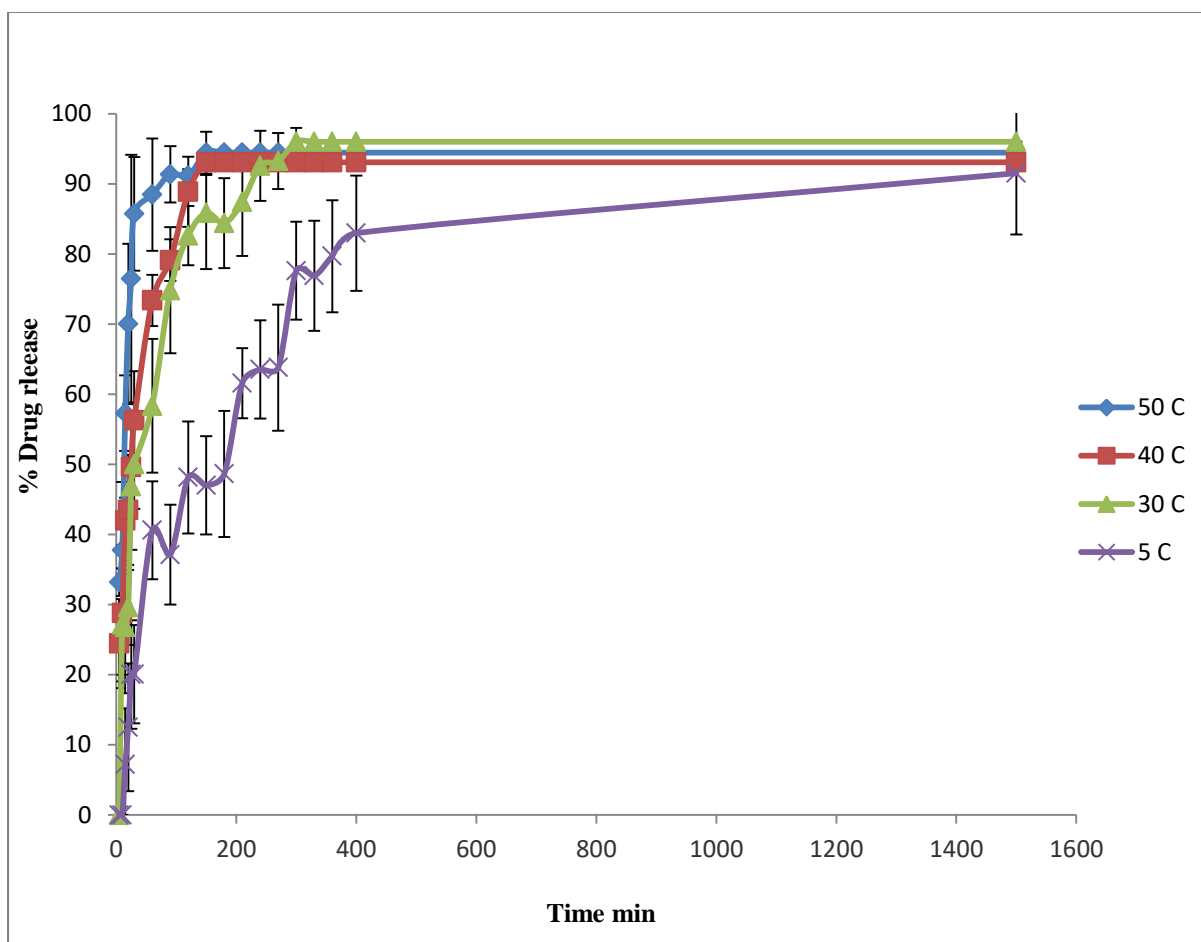


Figure 116- *In vitro* release of prednisolone from (O-1)-b-(PEG)-HNPs formulation at different temperatures.

4.4- Discussion

Thermo-responsive polymers are a class of smart polymers that respond to change in temperature. This property makes this type of polymers useful materials in a wide range of applications especially, in the field of drug delivery systems. However, stimuli-responsive polymers such as pHPMA have been limited to carrying hydrophobic drugs due to their hydrophilic nature. To improve drug loading capacity, it can be modified or grafted with hydrophobic moieties to serve as a micellar core and enables incorporation of poorly water-soluble drugs. The two most important factors for determining the stability, drug loading capacity and drug release profile of polymeric micelles are chemical nature and molecular weight of the hydrophobic moieties (Talelli *et al.*, 2010).

To enable a comparative study of HPMA stimuli-responsive copolymers in terms of improving hydrophobic drugs solubility in aqueous medium and regulate the release of drugs in response to an internal or external temperature change. Four different hydrophobic groups, including palmitoyl, dansyl, cholesteryl and oxadiazole groups grafted onto APMA monomers were ultimately be polymerised with water-soluble thermo-responsive HPMA. Modification ratios were altered in order to achieve the most relevant properties for our purpose. These hydrophobic groups were already reported as solubilisers for hydrophobic drugs (Trivedi *et al.*, 2010, Mourya *et al.*, 2011). In this context, poly(allylamine) (PAA) modified with different types of aromatic pendant groups have been reported to possess great solubilizing capacity for different hydrophobic drugs (Hoskins *et al.*, 2012).

In this investigation, HPMA copolymer derivatives were used as the hydrophobic solubilisers. It was observed that all the copolymer formulas have the ability to enhance drug solubility. The chemical structure of the candidate hydrophobic pendant group played an important role in determining the solubility of copolymer as the hydrophobic properties increased with increasing the copolymerisation ratio and hence lead to limited the grafting ratio for some formulations especially those that contain cholesteryl and palmitoyl moieties. On the other hand, it is also an essential property that plays an important character in the solubility of the model drugs. Dansyl and oxadiazole formulations had showed great increase in propofol solubility compared with palmitoyl and cholesteryl formulations. The aromaticity of these moieties can explain this behaviour as propofol is a small aromatic molecule and tends to make strong π - π stacking interactions, which facilitates the drug solubility (Figure 86). The same trend was apparent for prednisolone samples but

this time the difference was less than propofol. Although similar to cholesteryl group and prednisolone, prednisolone has even less solubility in cholesteryl copolymer formulations; this can be attributed to steric hindrance that occurs between these two large size groups (Figure 89). By contrast, palmitoyl proved to be the best solubilising moiety for griseofulvin (Figure 92). The relative steric hindrance experienced by other pendant groups whilst drug incorporation is occurring when a core expansion occurring with palmitoyl formulation.

Typically, with increasing copolymerisation ratio, the grafted copolymers showed an increased ability to solubilise hydrophobic drugs. However, a further increase of hydrophobicity due to increased copolymerisation ratio and high drug loading leads to make them more easily aggregate to form large clusters. Particles that are larger than the filter pores cannot pass through the filter and that will reflect on drug loading efficacy.

In general, drug loading shifted to higher values with increased initial polymer:drug mass loading ratios. However this was not true in some cases. As the amount of incorporated drug has been increased this could lead to high lipophilic character which makes the hydrophobic interaction between drug-drug molecules much higher than that between drug-copolymers (Mingming *et al.*, 2010).

Based on the observations, O-1 and D-2 seemed to be the best alternative formulations to enhance model hydrophobic drugs solubility. These two formulas have been utilized to prepare block copolymers with PEG to boost copolymer responsivity to temperature change. It has been reported that PEGylation can results in an increase in controlled drug diffusion. Maeda and colleagues administered four-fold increase in IVM release velocity from silicone -rod formulation as a result of addition of poly (ethylene glycol) (PEG4000) in the matrix (Maeda *et al.*, 2003). Block copolymers of poly (ethylene glycol) with poly (trimethylene carbonate) (PEG-PTMC) undergo controlled reverse thermal gelation at temperatures between 20 to 75 °C by changing polymer concentration, molecular weight and composition of the polymer (So *et al.*, 2007).

Data from HPLC analysis showed that (O-1)-*b*-(PEG) and (D-2)-*b*-(PEG) was capable of solubilising model drugs with the same efficiency of the non-PEGylated or sometime less (Figures 95-97). This was expected since the PEG block has hydrophilic properties which lead to reduce the ability of the amphiphilic copolymer to solubilised hydrophobic drugs.

HNPs have been used by our research group to formulate various types of drug delivery systems. Herein, we used HNPs as localised nano-heaters to accelerated drug release from our system in response to temperature change. The influence of HNPs on the drug loading efficiency of (O-1)-b-(PEG) formulation was characterized.

(O-1)-b-(PEG)-HNPs amphiphiles appeared to increase the maximum concentration of griseofulvin and prednisolone solubilised. This might be due to (O-1)-b-(PEG)-HNPs adopting different conformations, which are less compact, that lead to accommodate larger amounts of drug molecules (Christopher *et al.*, 2012). The loading concentrations for each drug were 13.57 mgmL^{-1} and 10.57 mgmL^{-1} (Figure 98). By contrast, the addition of HNPs appeared to decrease propofol loading slightly comparing with (O-1)-b-(PEG) (Figure 98). This was unexpected given the HNPs were in competition with the drug molecules for area on the copolymer structure. Loading capacities were 482 %, 226 % and 176 % and drug encapsulation efficiencies were 48 %, 23 % and 18 % for propofol, griseofulvin and prednisolone respectively (Table 21).

The results of the solubility studies indicated that such models possessed high drug loading capacity and encapsulation efficiency (Table 21). Furthermore, these copolymer systems showed high capability to solubilise four different poorly soluble drugs that have different chemical structures, formula mass, water solubility and states. Accordingly, it is generally accepted that HPMA-co-APMA copolymer formulations can be used as a universal solubiliser for pharmaceutical applications.

Propofol, griseofulvin and prednisolone were chosen by many researchers as module hydrophobic drugs in solubility improving methods because they are relatively inexpensive, poorly-soluble in water and have different problems associated with these formulations. Recently, Hoskins *et al.*, reported that the use of sulfonated calix[4]resorcinarenes as drug solubilising agents improved propofol and griseofulvin solubility in aqueous medium. The data showed that the increasing carbon-alkyl chains on the lower rim of calix[4]resorcinarenes compounds from 4 to 7 enhance solubility of both drugs up to 3 mgmL^{-1} and 8 mgmL^{-1} , respectively (Hoskins *et al.*, 2017). Amphiphilic chitosan-based polymers ($M_w < 20 \text{ kDa}$) that self-assemble in aqueous media were used by Xioazhong *et al.*, to enhance solubilisation and bioavailability of propofol and prednisolone. They reported the carbohydrate amphiphiles formed micellar clusters in aqueous environments, the optimal amphiphiles polymer formulations with propofol and prednisolone were at 5 mgmL^{-1}

with 4.43 mgmL⁻¹ and 1 mgmL⁻¹ of drug being solubilised respectively (Xioazhong *et al.*, 2006). The results obtained in this work are exceeding the previous works; our formulations were capable of increasing the aqueous solubility of propofol up to 41.1 mgmL⁻¹ (O-1), griseofulvin 20.75 mgmL⁻¹ (P-0.25) and prednisolone 13.11 mgmL⁻¹ (D-2).

Paclitaxel (PTX) has been reported to be an effective anticancer agent used to treat a variety of tumours. However, its low solubility and permeability hampered PTX's pharmacological advantage (Zhijun *et al.*, 2015). Several techniques have been proposed to solve these problems, including polymer nanoparticles, solid lipid nano-spheres and nano-emulsions (Fu-Heng *et al.*, 2015). Tomohiro and colleagues loaded water-soluble and biocompatible 2-methacryloyloxyethyl phosphorylcholine polymers with PTX. The maximum concentration of PTX reported in the polymer aqueous solution reached 5.0 mgmL⁻¹ (Tomohiro *et al.*, 2003). Herein, the data showed (O-1)-*b*-(PEG) and (O-1)-*b*-(PEG)-HNPs formulations were capable of improving the PTX solubility in aqueous medium. Optimum solubilisation was achieved at 6 mgmL⁻¹ concentration and 1:1 polymer:drug feed ratio (Figure 99). (O-1)-*b*-(PEG) improved drug aqueous solubility to 0.936 mgmL⁻¹ compared to 0.841 mgmL⁻¹ by (O-1)-*b*-(PEG)-HNPs.

Elevated temperature has been extensively utilised to accelerate drug release rate from different drug delivery systems (Shen and Burgess, 2012, Zolnik *et al.*, 2006, Jie *et al.*, 2016). Thermo-responsive polymers show a sharp change in properties in response to internal or external temperature changes; this feature makes them an ideal candidate for the loading and delivery of anticancer agents. Aniket and colleagues developed new magnetic-based core-shell particles (MBCSP) consisting of a thermo-responsive shell of poly (*N*-isopropylacrylamide-acrylamide-allylamine) and a core of poly (lactic-co-glycolic acid) (PLGA) to target skin cancer cells. Aniket reported that (MBCSP) rapidly released loaded drugs in response to changes in temperature (Aniket *et al.*, 2012). In this study, the *in vitro* release measurements of propofol from the highest drug loading formulations indicate that change in surrounding temperature had no effect on the release profile of the HPMA-co-APMA-R copolymers (Figures 103-106). The addition of APMA-R moieties to HPMA in copolymerisation reaction can shift alteration of the transition temperature to a large extent or it can even disappear. This is due to alter the hydrophilic/hydrophobic balance (Arijit *et al.*, 2015)

Typically, by adding a hydrophilic block such as PEG to HPMA-co-APMA-R the problem can be tackled. (D-2)-*b*-(PEG) and (O-1)-*b*-(PEG) results strengthen this concept by obtaining controlled release in response to temperature changes, as drug release was significantly accelerated at elevated temperatures. In general, the drug release from the (D-2)-*b*-(PEG) was attenuated when compared to the (O-1)-*b*-(PEG). Also, the release rates of the griseofulvin and prednisolone were faster than propofol on the same conditions of release, as can be seen in Figures 107-112. During the release experiments, the hydrophobic drug models were released more efficiently from the copolymer formulations at high temperature.

Magnetic nanoparticles (MNPs) are getting very important and attraction in biomedical applications due to their ability to act as localised nano-heaters which offers combined therapies involves killing cancer cells by hyperthermia and drug that release from a thermo-responsive polymer in response to temperature changes (Aniket *et al.*, 2012). In this respect, the potential of HNP to act as thermal triggers for drug release is evaluated *in vitro* and the rate of drug release in response to thermal increase investigated as well. The results showed that HNP addition had accelerated griseofulvin and prednisolone released. By contrast, propofol release attenuated as compared to (O-1)-*b*-(PEG), this could be due to propofol behaviour in aqueous medium as propofol belong to phenolic drugs family and has $pK_a = 11$ (weak acid) (Eriksson *et al.*, 1997). Phenols can lose a hydrogen ion to give the phenoxide anion (Figure 117). Since the HNP are positively charged, force of attraction between these oppositely charged ions will lead to delay propofol release.

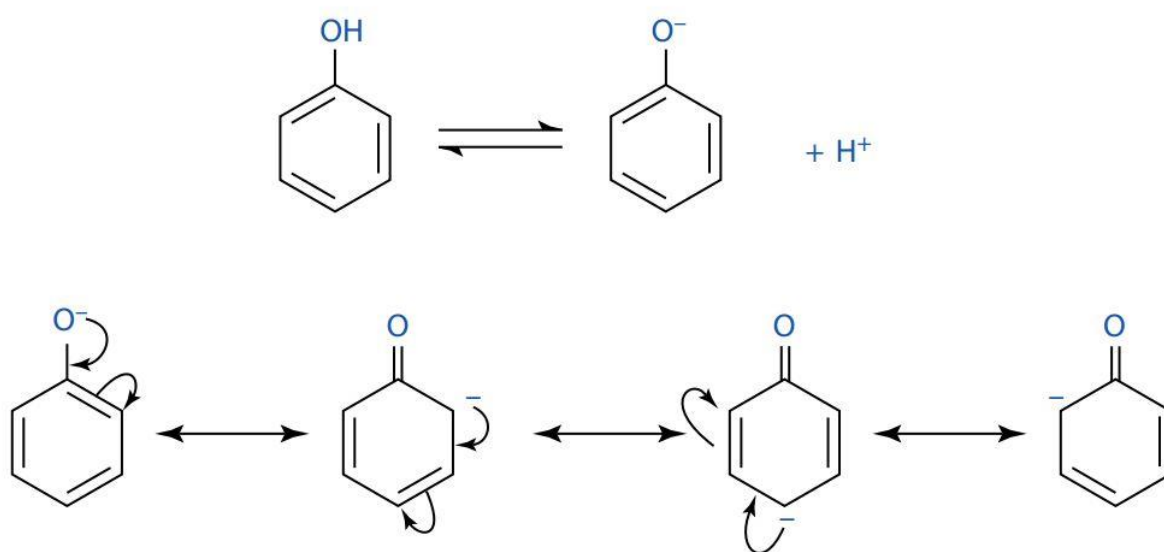


Figure 117- The ionisation of phenols.

4.5- Conclusion

The purpose of this work was to investigate the potential of HPMA-co-APMA-R copolymers derivatives for effective delivery of model hydrophobic drugs. The prepared systems were characterized for particle size, PDI, zeta potential, drug loading capacities and drug release. The loaded amounts of the hydrophobic drugs used herein were considerably high upon using the HPMA copolymers. The drug release of HPMA-co-APMA-R copolymers in aqueous solution showed no response to change in surrounding temperature, but the addition of PEG enhanced the thermo-responsive behaviour. Furthermore, drug release was further accelerated with increasing temperature as a result of adding HNPs. The resulting block copolymer (O-1)-*b*-(PEG) with/without HNPs formed micellar structures in water.

Chapter Five

Biological Characterisation of the Novel Thermo-responsive Amphiphilic Copolymer Formulations

5.1- Introduction

Any drug development process must proceed through some steps including drug discovery, preclinical development and clinical studies. The fundamental element of preclinical and clinical studies is investigation of the effects of the molecularly targeted agents on the specific molecular targets. In order to reveal potential hazards and recommended starting dose for the use in humans, several of toxicological and pharmacological studies have to be performed before a clinical trial begins (Anthöfer, 2015). Typically, there are two types of testing which should be performed in the preclinical stage including *in vitro* and *in vivo* studies. It is desirable to use *in vitro* studies instead of *in vivo* studies due to these being more cost effective both in monetary terms and in ethical terms (James, 2008). *In vitro* studies which are based on using cell and tissue cultures that grow outside the body in a laboratory environment are regularly utilized to check the toxicity and efficacy of potential drug or chemical molecules (Sonali *et al.*, 2015). However, *in vivo* testing is required to adequately characterise the *in vitro* data (James, 2008).

In the present study, pancreatic cancer cells (BxPC-3) were used as a modal cancer in order to investigate the ability of our copolymer formulations to improve cancer chemotherapy.

Based on literature, pancreatic cancer is classified as one of the aggressive human malignancies with an increase in incident worldwide. An analysis predicts pancreatic cancer to be the second leading causes of cancer-related death in the United States by 2030 (Rahib *et al.*, 2014). Therefore, more effort should be made to face this disease actively.

5.1.1- Bioavailability Investigation

Although the *in vivo* studies are vital in determination of biomaterial-tissue biocompatibility, many *in vitro* assays including cytotoxicity assays and drug uptake analysis should be used first.

5.1.1.1- Cytotoxicity evaluation

The assessment of cell viability *in vitro* is an important factor in verifying the cytotoxic effect of the therapy. Both the MTT and Trypan blue assays have been used previously to assess the viability of cells.

5.1.1.1.1- MTT Assay

The MTT (3-(4,5-dimethylthiazol-2-yl)-2,5-diphenyltetrazolium bromide) tetrazolium reduction assay has been a popular research method. The MTT assay has been widely used by researchers in thousands of published articles as evidence (Terry *et al.*, 2013). It is a quantitative colorimetric assay proposed by Mosmann to quantitate cell survival and proliferation for mammalian cells. The MTT assay has been shown to be inexpensive, simple and a reliable test to screen the cytotoxicity of a drug. The assay is used to assess cytotoxicity, proliferation or activation via measuring the signal generated from living cells, which is dependent on the degree of activation of the cells (Mosmann, 1983, Kumaravel and Begum, 2015). The MTT assay methodology is based on the reduction of the tetrazolium salt through the mitochondrial dehydrogenase of viable cells to form a purple formazan crystal. The quantity of formazan is measured by dissolving the formazan crystal in dimethyl sulfoxide (DMSO), following recording the absorbance at 570 nm by using a microplate reading spectrophotometer. The number of living cells extant in culture is proportionate to the amount of formazan produced. The exact reduction mechanism of MTT is still not well-understood. It has been proposed that MTT involves reaction with NADH or accepted electrons from other reducing molecules (Figure 118) (Terry *et al.*, 2013).

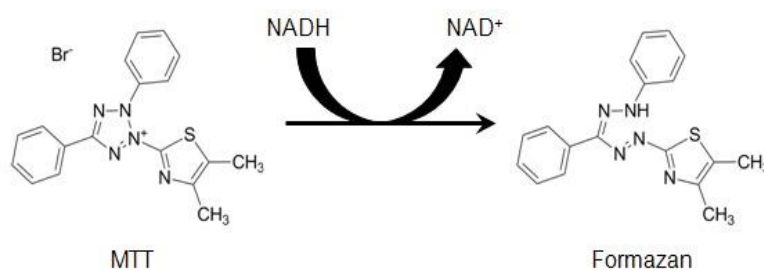


Figure 118- Mechanism of MTT reduction into formazan.

5.1.1.1.2- Trypan blue exclusion assay

The trypan blue (TB) assay is a widespread method for assessing cytotoxicity in experimental examination; it also provides cell number and viability information. The idea behind this method is based on uptake of TB by dead cells cytoplasm (stain dead cells blue) due to loss of membrane selectivity while it cannot produce colour in live cells which have an intact cell membrane. As a result, dead cells will appear darker than the viable cells. Therefore, the

fraction of unstained (live) and stained (dead) cells can be measured and calculated either by a haemocytometer, microscope or cell counting instruments (Freitas *et al.*, 2014). In this work, TB assay is carried out by treating cells in the exponential growth phase to a formulation for a period of time. Cell death can be visualized by staining with trypan blue in 50/50 ratio and the number of viable cells is counted.

5.1.1.2- Intracellular drug uptake

Understanding the interactions of drug formulations with cells and how these interactions impact their cellular uptake is vital to discovering the biomedical applications of these formulations, especially for drug delivery.

In medicine, abundant drugs are facing problems to cross a strong barrier called the cell membrane. Typically the cell membrane is described as phospholipid bi-layers, regulating the exchange of materials between the cell and outside environment. Moreover, cell surface charge plays an important role on drug penetration. Molecules that have negative charge do not enter the cell wall at all as both sides of the bilayer phospholipid membrane surface are also negatively charged. By contrast, positively charged materials can penetrate deep into cell membranes (Sabina *et al.*, 2013).

Various techniques have been reported to enhance the ability of drug molecules to penetrate cell membranes such as encapsulating them in a polymeric material (chemical technique), use of biological carriers commonly viruses to deliver drugs to targeted tissues (biological technique), a physical force (physical technique), microinjection, ultrasound etc. (Judith *et al.*, 1995, Robert *et al.*, 2013, Flanagan *et al.*, 1999, Mikhail *et al.*, 2015).

In this work, intracellular drug uptake experiment was used for determination of intracellular drug concentrations through the combination of chemical and physical techniques *via* using polymer, HNPs and heat to improve drug uptake and release.

5.1.2- Aims and Objectives

The aims of this chapter were to determine the cytotoxic activity of the following: paclitaxel alone; (O-1)-*b*-(PEG); (O-1)-*b*-(PEG)-HNPs; (O-1)-*b*-(PEG)-PTX and (O-1)-*b*-(PEG)-HNPs-PTX on BxPC-3. Cytotoxic activity was determined using the MTT assay. Intracellular drug uptake will be determined. The effect of heat on cell viability will also be undertaken to determine the temperature change effect.

5.2.1- Materials

Item No	Material	Supplier
1	Paclitaxel	Medchem express
2	Hybrid nanoparticles (HNPs)	Synthesised in Chapter Three
3	(O-1)- <i>b</i> -(PEG)	Synthesised in Chapter Two
4	(O-1)- <i>b</i> -(PEG)-HNPs	Synthesised in Chapter Four
5	BxPC-3 cell line	LGC Standards Co., UK
6	PRMI culture medium	Life technologies Co., UK
7	Trypsin-EDTA 0.05 %	Life technologies Co., UK
8	Foetal bovine serum	Fisher Scientific, UK
9	Phosphate buffered saline	Fisher Scientific, UK
10	Penicillin streptomycin	Life technologies Co., UK
11	3-[4,5-dimethylthiazol-2-yl]-2,5-diphenyltetrazolium bromide (MTT)	Sigma-Aldrich Co.
12	Highly purified water	Millex Q system (UK)
13	HPLC Grade acetonitrile	Fisher Scientific, UK
14	DMSO Fisher Scientific, UK	DMSO Fisher Scientific, UK

5.2.2- Methods

5.2.2.1- Cell culture preparation

In this study, a BxPC-3 cell line was used as the pancreatic cancer cell model to study the toxicity of (O-1)-*b*-(PEG) with/without HNPs. The BxPC-3 cell line was cultured in RPMI-1640 media containing 1 % penicillin streptomycin and 10 % foetal bovine serum (FBS), at 37 °C in a 5% CO₂ atmosphere.

To determine the effect of paclitaxel, (O-1)-*b*-(PEG), (O-1)-*b*-(PEG)-HNPs, (O-1)-*b*-(PEG)-paclitaxel and (O-1)-*b*-(PEG)-HNPs-paclitaxel on BxPC-3 cell, eleven different concentrations of these substances were prepared. Briefly, a 20 mgmL⁻¹ stock solution was prepared by dissolving 200 mg of each substance in 10 mL sterile water (except paclitaxel

was dissolved in 50:50 of sterile water:DMSO). Serial dilution solutions were made from these stock solutions (1×10^{-1} - 1×10^{-9} mgmL⁻¹) using media as the diluent (Table 23).

Table 23- Preparation of Excipient Solutions for MTT assay.

Drug concentration (mgmL⁻¹)	Volume of 20 mgmL⁻¹ drug stock solution (μL)	Total volume of media (ml)
0.1	22.5	4.5
0.05	11.5	4.5
0.025	5.6	4.5
0.01	2.25	4.5
0.005	1.125	4.5
* 0.001	90	4.5
* 0.0001	9	4.5
* 0.00001	1	4.5
** 0.000001	450	4.5
** 0.0000001	45	4.5
** 0.00000001	4.5	4.5

* Sample was made from 0.05 mgmL⁻¹ concentration as a stock solution.

** Sample was made from 0.00001 mgmL⁻¹ concentration as a stock solution.

5.2.2.2- Cytotoxicity evaluation

Cytotoxicity of the copolymer formulations was investigated by using the MTT assay; the tests were carried out in BxPC-3 cells line.

5.2.2.2.1- MTT assay procedure

Firstly, 100 μLwell⁻¹ of BxPC₃ cells suspension in RPMI-1640 medium was seeded at densities of around 15,000 cells per well in 96-well plate and allowed to adhere for 24 h inside an ESCO CO₂ Incubator at 5% CO₂ at 37 °C. After this time, the media was replaced with 100 μL of freshly prepared culture medium containing various treatment samples as prepared above in a format shown in Figure 119.

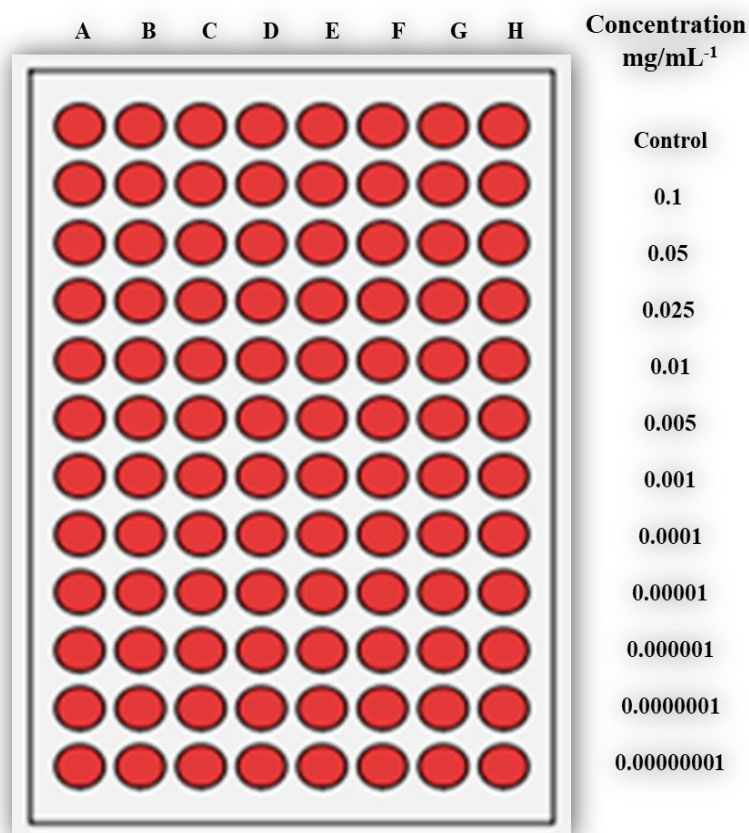


Figure 119- Illustration the 96-well plate assembly for the MTT assay.

The 96-well plates were further incubated for 24 h before the media was removed and replaced with a 175 μL solution of 10 % MTT in media and then incubated for 4 h in the cell incubator. After removing the MTT solution from the wells, 100 μL of DMSO was added to dissolve the purple formazan crystals trapped in cells. The light absorbance of the resultant purple colour was determined at 570 nm by using a microplate reader (Tecan, infinite 200 pro, GmbH 5082, Australia). All assays were performed in triplicate. Cell viabilities were averaged and normalized to the untreated cells, which worked as negative controls cultured in the cell medium without sample added. Percentage cell viability and IC_{50} was calculated according to Equation 8.

$$\% \text{ Cell viability} = \frac{\text{Absorbance of drug} - \text{Absorbance of PBS}}{\text{Absorbance of control} - \text{Absorbance of PBS}} \times 100 \quad (8)$$

5.2.2.3- Determine intracellular drug concentrations in cellular uptake

For cell uptake experiments, BxPC-3 pancreatic cancer cells were seeded at a density of (50,000 cells/well) in 6-well plates and cultured in RPMI-1640 media containing 1 % penicillin streptomycin and 10 % foetal bovine serum (FBS). Next, the media was replaced with 3 mL of a 0.05 mgmL⁻¹ solution of PTX, polymer alone, polymer-HNPs, polymer-PTX or polymer-HNPs-PTX in RPMI-1640 media and incubated for 1 h, 4 h and 24 h at 37 °C in a humidified atmosphere of 95% air and 5% CO₂ (Figure 120). At each time point, the culture media was removed; cells were washed three times with PBS to remove the trace amounts of the substances, followed by the addition of 185 µL trypsin. Plates were then placed in an incubator until the cells began to detach before 0.815 mL of the media was added. Trypan blue assay was then used to determine the density of viable cells per mL. To count viable cells, A mixture of 75 µL of cell suspension and 75 µL of trypan blue solution was prepared in an Eppendorf tube, a prorated amount of this mixture was pipetted into an automated cell counter (Invitrogen Countess®, UK). Percentage cell viability was calculated according to the Equation 9.

$$\% \text{ Cell viability} = \frac{\text{Number of viable cells in sample}}{\text{Number of control cell}} \times 100 \quad (9)$$

The appropriate volume containing 100,000 cells was transferred to Eppendorf tubes and completed to 1 mL with deionised water, and then centrifuged at 500 rpm for 5 min in a Hermule Z-323 centrifuge. The supernatant was removed and cells were re-suspended in acetonitrile : water (45:55).

The concentration of PTX was quantified using reverse phase high performance liquid chromatography (HPLC) (pinnacle DB C18 5 µm x 150 mm x 3.2 mm HPLC column from Restek Co. UK) with flow rate of 1 mLmin⁻¹ of the mobile phase (55:45 v/v) water: acetonitrile, which was discussed in Chapter Four (Section 4.2.2.4.4). The drug accumulated in each cell was calculated by dividing each resulted calculated concentration by 100,000 (cells number). All assays were performed in triplicate.

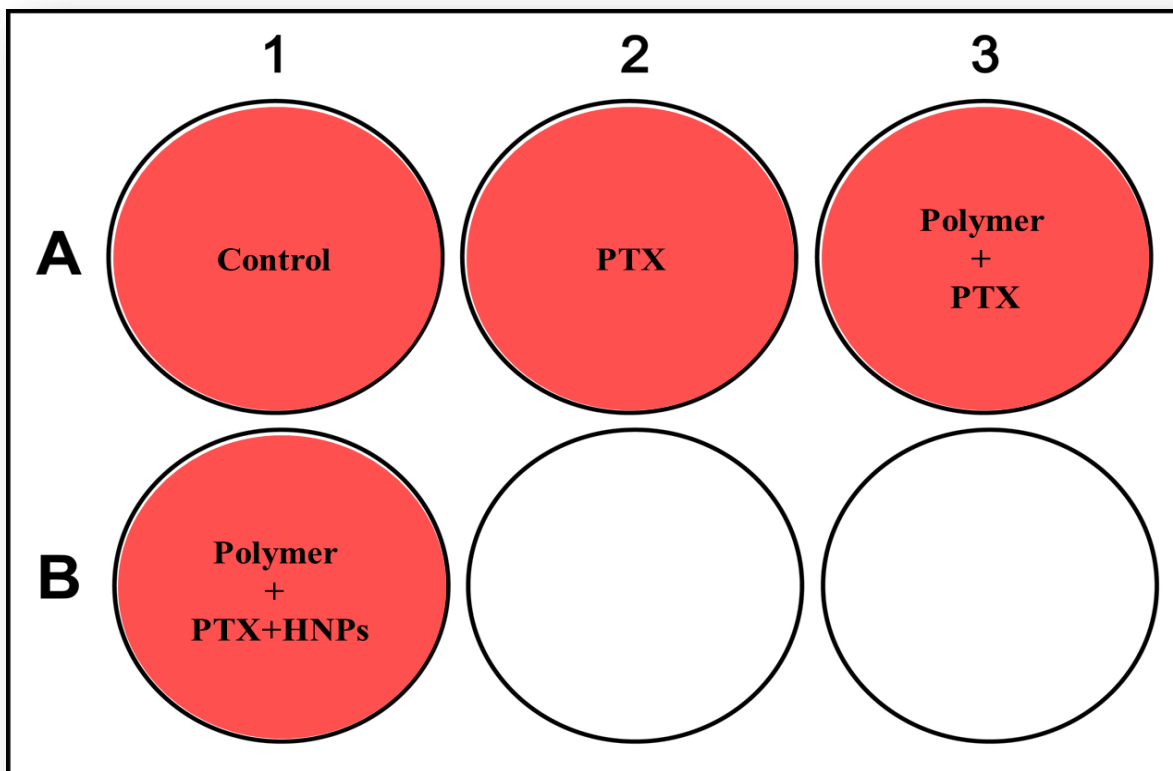


Figure 120- Illustration the 6-well plate assembly for the drug uptake study.

5.2.2.4- In vitro thermo-responsive cytotoxicity assay

Heating by exposure to laser irradiation in terms of accelerating the release of PTX from the thermo-responsive polymer-HNPs formulations is the suggested method in a clinical application. The heat-triggered release behaviours by external heating were studied herein via repeating the MTT procedure which was mentioned above, a small change was made in the previous assay including the following: after the 96-well plates were treated with samples as prepared above in a format shown in Figure 119 they were pre-incubated for 4 h at 37°C in a humidified atmosphere of 95% air and 5% CO₂. After this time, 96-well plates were removed and placed into a pre-warmed incubator type Memmert IN-30 and heated at 44 °C for half an hour, the 44 °C incubator, has a thermal variant that can mimic the heat generated by the SPR of laser irradiated HNP gold coatings, after an incubation time 96-well plates were returned back into the 37 °C, 50 % CO₂ incubator. The IC₅₀ was determined for all the plates and the heat activated IC₅₀ results were compared to the non-activated plates in order to investigate the effect of temperature on cell cytotoxicity.

5.3- Results

5.3.1- MTT Assay

In order to know whether (O-1)-*b*-(PEG) with/without HNPs were capable of increasing the cytotoxic effect of paclitaxel on pancreatic cancer cell lines, the MTT cytotoxicity test was carried out to determine their effect on the cell viability of BxPC-3 at eleven different concentrations (Figures 121 and 122). In general, results showed that all five substances have antiproliferative potential against the tested cell lines. When compared to paclitaxel alone, (O-1)-*b*-(PEG)-HNPs-PTX and (O-1)-*b*-(PEG)-PTX, they were highly efficient in reducing the cell viability of cancer cell lines.

For polymer alone and polymer-HNPs formulations, no significant effects in viability were observed after 24 h up to $0.1 \mu\text{g mL}^{-1}$ but the cell viability reduced significantly between the concentration of $1 \mu\text{g mL}^{-1}$ and $100 \mu\text{g mL}^{-1}$. The half-inhibitory concentration IC_{50} was obtained around $47 \mu\text{g mL}^{-1}$ for the polymer alone formulation and $50 \mu\text{g mL}^{-1}$ for polymer-HNP formulation (Figure 121 and 122).

The cytotoxic effect of PTX on BxPC-3 cell line in the eleven different concentrations was examined. When the BxPC-3 cell line was exposed to PTX, a steady increase in cytotoxicity was experienced with increasing PTX concentration at the same incubation time. It appeared that the PTX had a much lower IC_{50} values than the polymer alone and polymer-HNPs formulations. The observed IC_{50} for pure PTX was found out to be ($1 \mu\text{g mL}^{-1}$). However, the same drug when loaded into (O-1)-*b*-PEG demonstrated a significant decreased in IC_{50} value from $1 \mu\text{g mL}^{-1}$ to around $0.55 \mu\text{g mL}^{-1}$. Data indicated that polymer formulation can improve the therapeutic effect of the PTX compared with the free PTX. Furthermore, it showed that the cytotoxicity of polymer-PTX on BxPC-3 is roughly 2 times higher than free PTX; this can be attributed to the higher uptake rate of the drug on BxPC-3 cells.

Moreover, the (O-1)-*b*-(PEG)-HNPs-PTX exhibited significant cytotoxicity *in vitro* against a model pancreatic cell line. The half-maximal inhibitory concentration (IC_{50}) of the (O-1)-*b*-(PEG)-HNPs-PTX was higher than (O-1)-*b*-(PEG)-PTX and free PTX. The IC_{50} of hybrid formulation conjugated with polymer and loaded with PTX was around 10-fold and 20-fold less than that of the (O-1)-*b*-(PEG)-PTX and free drugs, respectively.

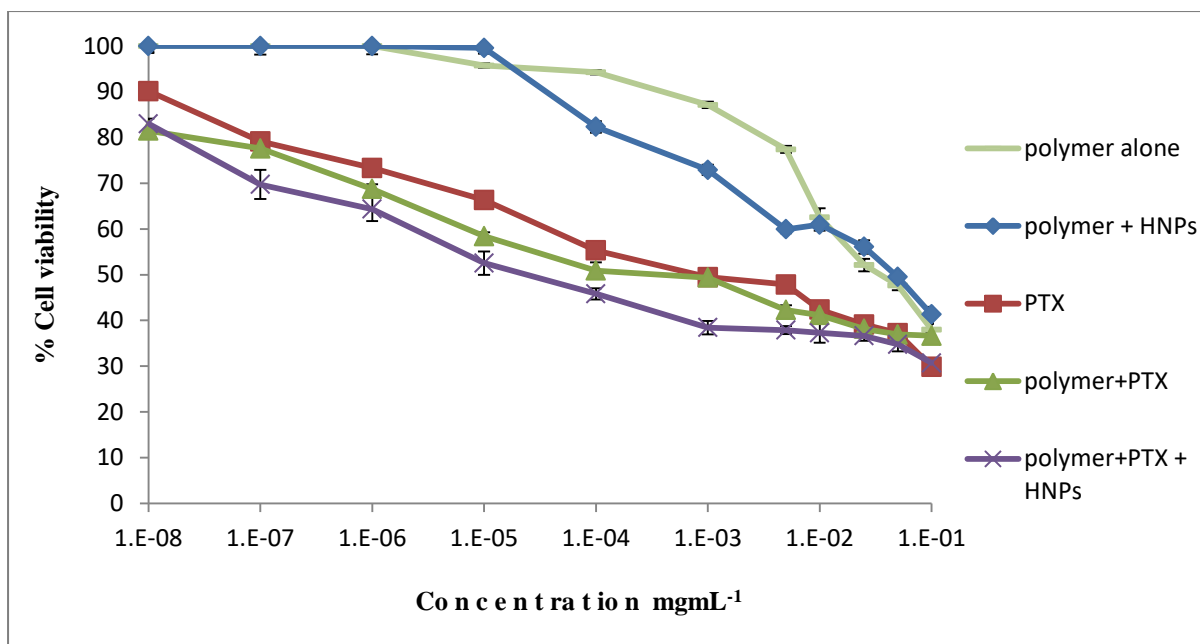


Figure 121- BxPC-3 cell viability (%) as determined by MTT assay after 24 h exposure to varied concentrations of PTX and polymer formulations (n=3, ave ± SD).

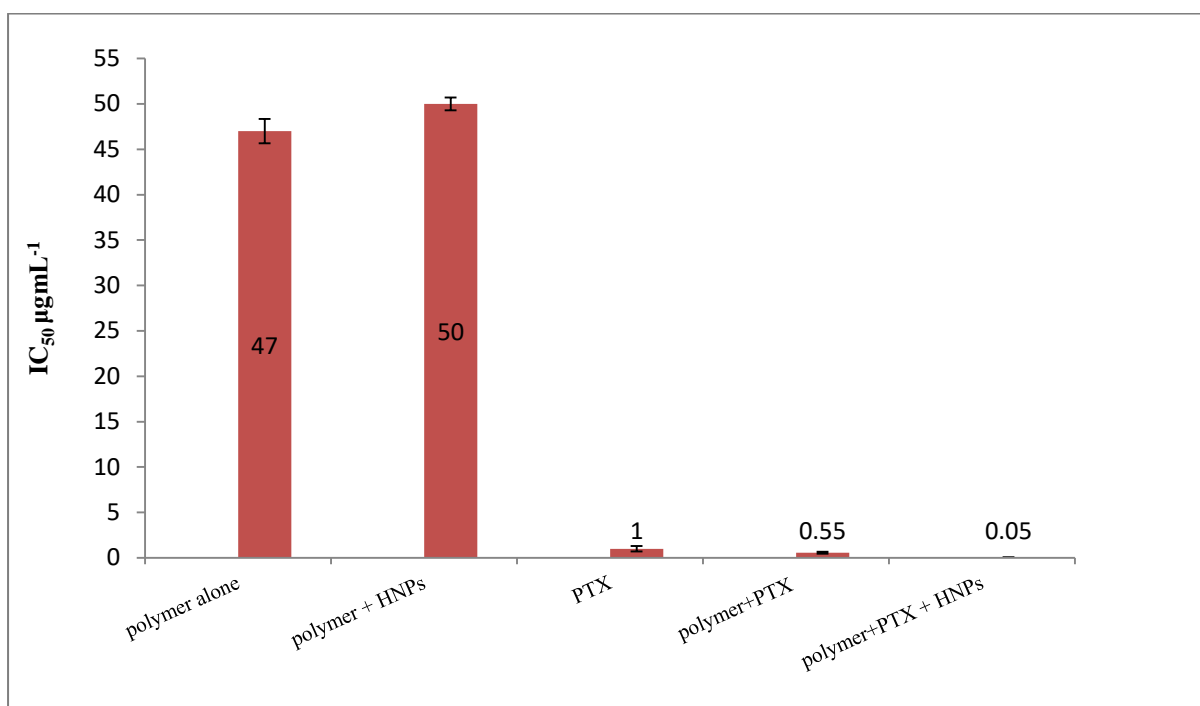


Figure 122- IC₅₀ (µg/ml) of PTX and polymer formulas as determined by MTT assay, after 24 h (n=3, ave ± SD).

5.3.2-Determine intracellular drug concentrations in cellular uptake

In order to get a more complete picture of the effect of polymer formula and HNPs it was crucial to determine the absorption rate and the amount of drug taken up. In Figure 123 the results of the drug uptake experiment are shown in which the course of PTX alone, (O-1)-*b*-(PEG)-PTX and (O-1)-*b*-(PEG)-HNPs-PTX formulations was followed over a period of 1 h, 4 h and 24 h.

(O-1)-*b*-(PEG)-HNPs-PTX formula showed a highest increasing initial uptake into BxPC-3 cells at each time point, followed by (O-1)-*b*-(PEG)-PTX formula then PTX alone. For naked PTX, drug uptake on BxPC-3 cells was non-detectable by HPLC after 1 h of incubation, this amount increased to 3458 pg and 5240 pg after 4 h and 24 h incubation with the same incubation concentrations of PTX respectively. By contrast, both (O-1)-*b*-(PEG)-PTX and (O-1)-*b*-(PEG)-HNPs-PTX formulas showed increased of drug accumulated from the first incubation hour to reach 3458 pg and 3564 pg in each cell, respectively. At 4 h of incubation, the uptake of both (O-1)-*b*-(PEG)-PTX and (O-1)-*b*-(PEG)-HNPs-PTX formulas has been expressed as almost double that for free drug. The readings for the 24 h showed increased PTX uptake to reach 5969 pg for (O-1)-*b*-(PEG)-PTX, while there are more increased with (O-1)-*b*-(PEG)-PTX to hit 7008 pg per cell. Overall, it seems that PTX uptake pattern on BxPC-3 cells is more time dependant (Figure 123).

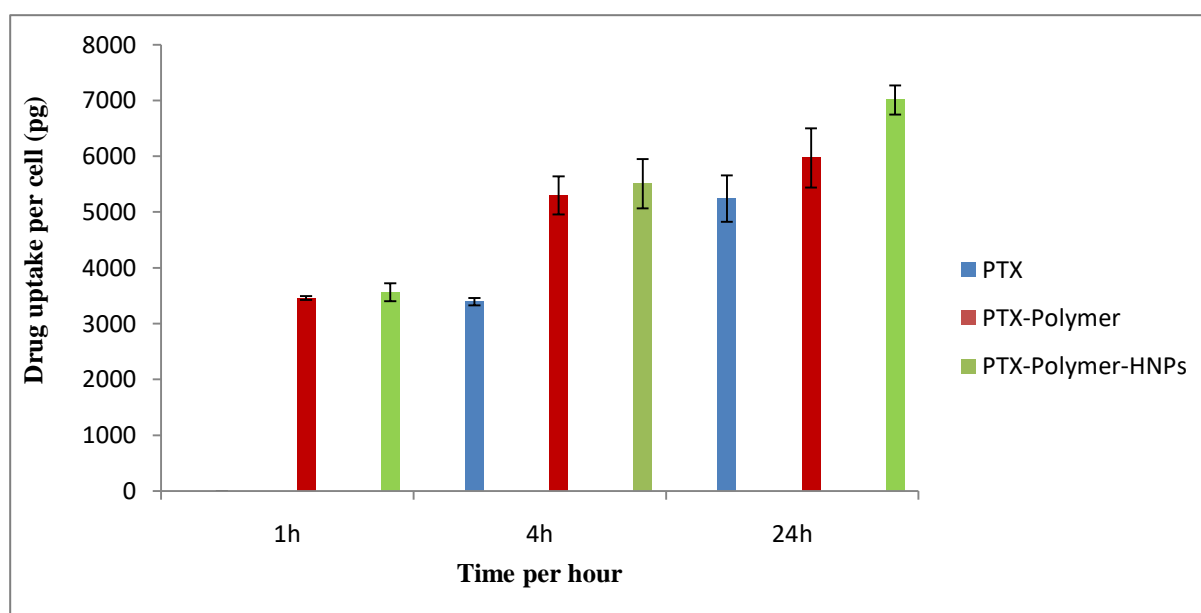


Figure 123- Cellular uptake study on BxPC-3 cell line after 1 h, 4 h and 24 h exposure with PTX, (O-1)-*b*-(PEG)-PTX and (O-1)-*b*-(PEG)-HNPs-PTX (n=3, ave \pm SD).

5.3.3-In vitro thermos-responsive cytotoxicity assay

In order to investigate the effect of temperature on cell cytotoxicity, the IC₅₀ was determined for the heat activated plates and compared to the non-activated plates.

In general, heat treatment did not result in a significant impact on cytotoxicity of polymer alone. The viability of BxPC-3 cells treated with polymer alone formulations at 37 °C and 44 °C showed the same cytotoxicity pattern (Figure 124). By contrast, increasing the temperature from 37 °C to 44 °C decreased the viability of the BxPC-3 cells treated with (O-1)-*b*-PEG-HNPs significantly, which suggests that introduction of HNPs onto the polymer backbone increased the cytotoxicity effect of the (O-1)-*b*-PEG at 44 °C (Figure 124). The half-maximal inhibitory concentration IC₅₀ of heat treatment formulation was around 2 times less than that of the non-heat treatment formulation (Figure 125).

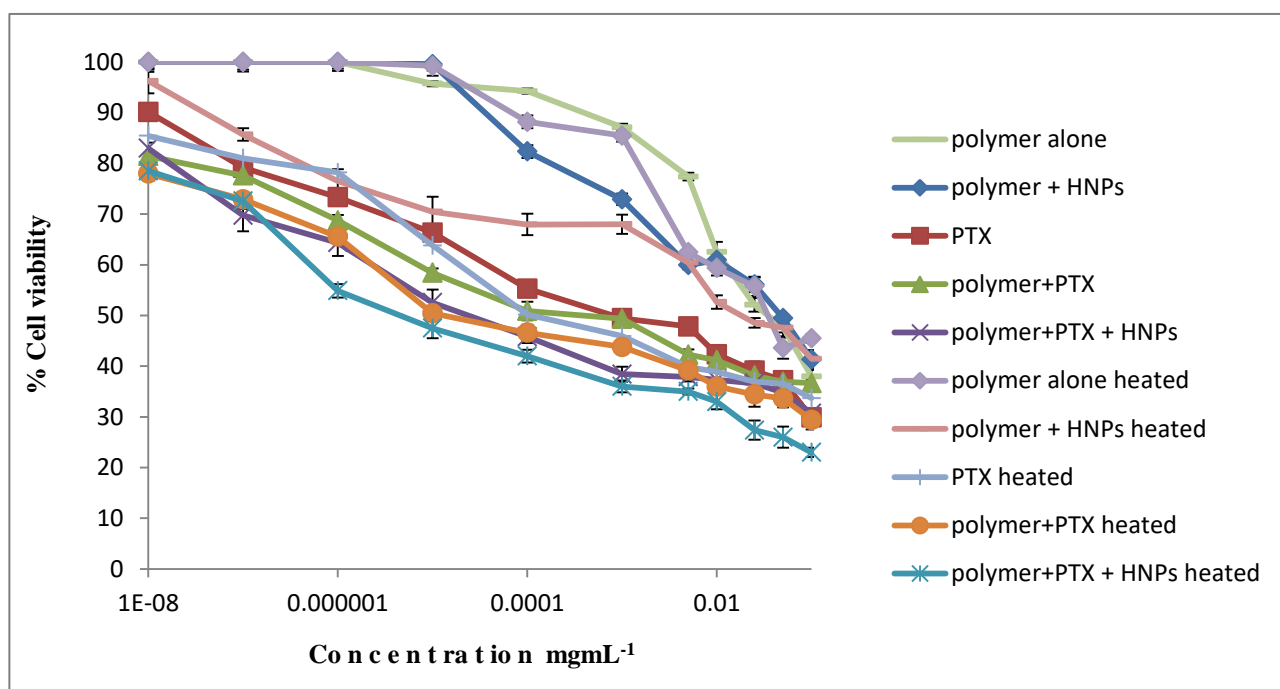


Figure 124- *In vitro* thermos-responsive cytotoxicity test on BxPC-3 cell line as determined by MTT assay after exposure to varied concentrations of PTX and polymer formulations (n=3, ave ± SD).

(O-1)-*b*-PEG-PTX was then tested after incubation at 44 °C for 30 min followed by 24 h incubation. This resulted in a significant decrease in the viability of the BxPC-3 cells (Figure 124) and IC₅₀. These results indicate that our thermo-responsive polymer responded to heat treatment and released PTX faster. Incubation of BxPC-3 with (O-1)-*b*-PEG-PTX for half an

hour at 44 °C reduced the IC₅₀ to 0.1 μgmL⁻¹ compared to 0.55 μgmL⁻¹ for non-heat treatment formulation. In other words, the IC₅₀ of (O-1)-*b*-PEG-PTX formulation decreased more than five times when exposed to high temperate.

Further reduction in cell viability and IC₅₀ was achieved upon treatment of BxPC-3 with (O-1)-*b*-PEG-HNPs-PTX in comparison with (O-1)-*b*-PEG-PTX. Cell viability of BxPC-3 treated with (O-1)-*b*-PEG-HNPs-PTX decreased significantly upon incubating at 40 °C (30 min), which might be due to the higher amount of PTX being released from the particles at this temperature as a result of introducing HNPs which act as localised nano-heaters (Figure 124). The IC₅₀ value of (O-1)-*b*-PEG-HNPs-PTX on BxPC-3 at heat treatment trial was 0.04μg/ml (Figure 125).

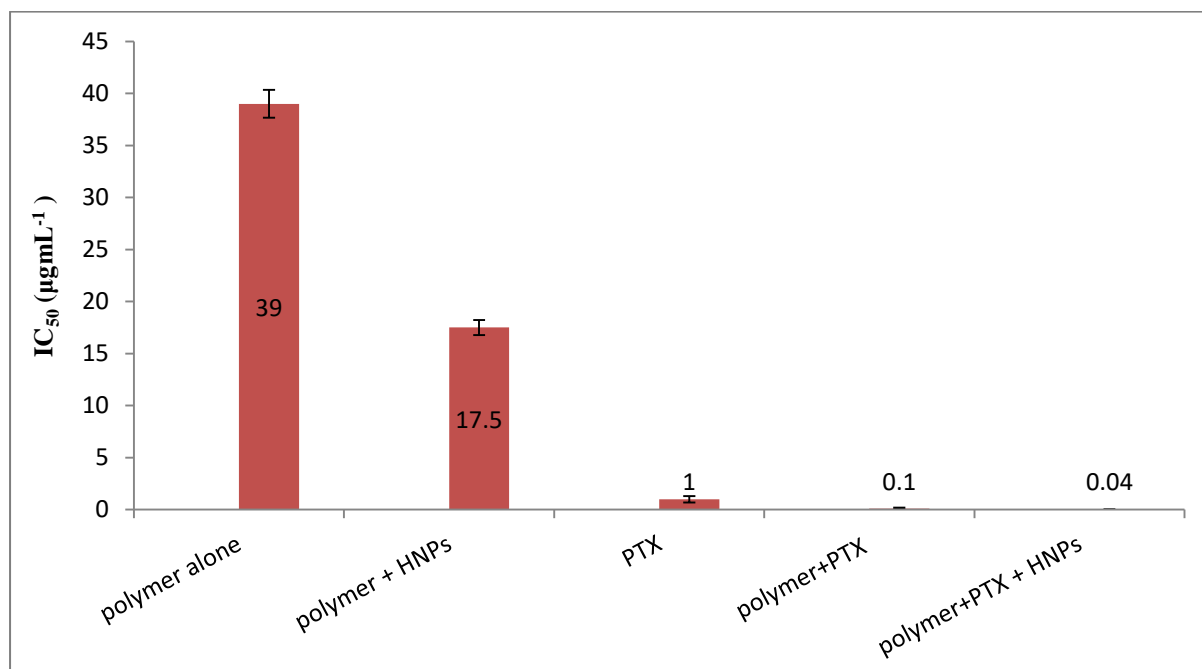


Figure 125- IC₅₀ (μgmL⁻¹) of heat-treated PTX and polymer formulations as determined by MTT assay, after 24 h (n=3, ave ± SD).

5.4-Discussion

In other studies PTX was loaded to different carriers such as carbon nano-shell (Hui *et al.*, 2017), polymeric NPs (Lipeng *et al.*, 2017), liposomes (Yunjie *et al.*, 2015), cyclic oligomers such as Calix[4]arene (Mo *et al.*, 2016), however, few attempts focused on formulating a combination treatment based on using PTX and thermos-responsive polymers conjugated to Au-NPs.

In this study, Chapter two and Chapter three have developed a thermo-responsive targeted drug delivery system able to improve drug solubility and control the release of drugs in response to change in temperature. In chapter four, PTX was loaded to (O-1)-*b*-PEG with/without HNPs. PTX loading was confirmed by HPLC. The results indicated that the (O-1)-*b*-(PEG) and (O-1)-*b*-(PEG)-HNPs were capable of solubilising $0.936 \text{ mgmL}^{-1} \pm 0.1 \text{ mgmL}^{-1}$ and $0.841 \text{ mgmL}^{-1} \pm 0.2 \text{ mgmL}^{-1}$ of PTX respectively.

Since promising drug loading and *in vitro* release, the thermo-responsive polymers conjugated to Au-NPs system has been translated to *in vitro* study to evaluate biological activities, focusing on cytotoxicity properties, cellular uptake and evaluating the effect of temperature on polymer-drug formulations cytotoxicity.

Possessing high cytotoxicity and specific delivery are the most important characteristics of any anti-cancer drug or formulation. The cytotoxicity of PTX and polymer formulations was examined on BxPC-3 cells by the MTT assay.

In this study the fabricated copolymer had little cytotoxic impact on the BxPC-3 cell line, over the concentration range tested ($100 \text{ }\mu\text{gmL}^{-1} - 1.0 \times 10^{-5} \text{ }\mu\text{gmL}^{-1}$). Addition of HNPs to the polymer backbone exhibits an improved cell cytotoxicity profile compared to polymer alone especially, between the concentration $0.01 \text{ }\mu\text{gmL}^{-1}$ and $10 \text{ }\mu\text{gmL}^{-1}$. IC_{50} values for copolymer alone and copolymer-HNPs achieved by the MTT assay after 24 h, were around $47 \text{ }\mu\text{gmL}^{-1}$ and $50 \text{ }\mu\text{gmL}^{-1}$ respectively (Figure 121). That implies HNPs addition to copolymer does not appear to have any impact on IC_{50} values comparing to copolymer alone (Figure 122).

The cytotoxicity results of the PTX formulation on the BxPC-3 cell line revealed significant reduction of cell viability after 24 h (compared with the free drug copolymer formulations),

where the cytotoxic effect of PTX formulation was about 47-fold and 50-fold greater than the cytotoxicity of copolymer alone and copolymer-HNPs, respectively (Figure 121 and 122).

(O-1)-*b*-PEG-PTX formulation showed higher cytotoxicity on cancer BxPC-3 cells compared to naked drug (Figure 121 and 122). These results confirm the high efficacy of the copolymer formulation which could be associated with the higher uptake rate, leading to enhanced accumulation of the drug in cancer cells.

The effect of (O-1)-*b*-PEG-HNPs-PTX displayed similar trend to that of (O-1)-*b*-PEG-PTX but the IC₅₀ value on BxPC-3 cells was 0.05 µg mL⁻¹, and its inhibitory effect on normal cells (BxPC-3) was extremely stronger.

Based on previous study, PEG-*b*-PHPMA derivatives demonstrated some combined pros, such as high drug loading efficiency, extracellular stability and biocompatibility, in addition to triggered intracellular drug release, which are considered to be a promising system for anticancer drug development (Rongran *et al.*, 2012). The cytotoxic effects of these DOX-loaded core-cross-linked PEG-*b*-PHPMA-lipoic acid micelles on HeLa and HepG2 cells were characterised. IC₅₀ values achieved by the MTT assays after 48 h, were around 6.7 and 12.8 DOX equiv/mL, respectively. For blank micelles, no significant reduction in viability was observed after 48 h up to 1.0 mg mL⁻¹.

In another study, Christopher and colleagues conjugated HNPs to poly(allylamine) (PAA) polymer grafted with hydrophobic oxadiazole (Ox) pendant group. They also reported that the treatment of BxPC-3 cell lines with the novel polymer formulations results in increased drug uptake and decreased IC₅₀ values compared with free drug. The IC₅₀ value for PAA-OX5 and PAA-OX5-HNPs were 60 µg mL⁻¹ and 55 µg mL⁻¹ respectively, while for PAA-OX5-6TG and PAA-OX5-HNPs-6TG were 15 µg mL⁻¹ and 0.95 µg mL⁻¹ respectively (Christopher *et al.*, 2013).

Our findings indicate that the IC₅₀ of (O-1)-*b*-PEG alone and (O-1)-*b*-PEG-HNPs were 47 µg mL⁻¹ and 50 µg mL⁻¹ respectively, which is consistent with the previous report. By contrast, the (O-1)-*b*-PEG-PTX and (O-1)-*b*-PEG-HNPs-PTX appeared to be the more effective formulations when compared with previous studies. IC₅₀ of (O-1)-*b*-PEG-PTX was 0.55 µg mL⁻¹, (O-1)-*b*-PEG-HNPs-PTX was 0.05 µg mL⁻¹, this was around 3-fold and 19-fold decrease compared to the PAA-OX5-6TG and PAA-OX5-HNPs-6TG respectively.

Enhanced cellular uptake and boosting the penetration efficacy of anti-cancer agents inside tumours is vitally important to successful anti-cancer therapy. Various courier formulations have been attempted for this purpose including polymers, dendrimers and gold nanoparticles etc. (Liu *et al.*, 2015, Akiya *et al.*, 2016, Jianfeng *et al.*, 2016). It has been found, that the polymeric micelles can enhance aqueous formulations of hydrophobic drugs, improve the cellular uptake and prolong *in vivo* circulation time and passive tumor targeting by the enhanced permeability and retention (EPR) effect (Yang *et al.*, 2015). Jin and colleagues loaded N-octyl-O-sulfate chitosan micelles with anticancer PTX for treating multidrug-resistant (MDR) cancer. They reported that the polymer micelles loaded PTX had demonstrated high cellular uptake around 2-fold more than PTX, and the lowest efflux rate of PTX, thus leading to optimal cytotoxicity on both the human hepatocellular liver carcinoma (HepG2) and the MDR HepG2 (HepG2-P) cells (Jin *et al.*, 2014).

On the other hand, there have been several studies evaluating gold-nanoparticle (AuNPs) uptake in *in vitro* systems. Heo and colleague have designed and prepared a theranostic agent based on AuNPs surface-functionalized with anti-cancer paclitaxel drug and biotin receptors. They examined the intracellular uptakes of the functionalized AuNPs by three cancer cell lines, HeLa human breast, A549 human lung carcinoma and MG63 human osteosarcoma, it was found that biotin conjugated AuNPs surface-functionalized PEG, biotin and rhodamine B linked b-CD effectively induce intracellular uptake into the cancer cells (Heo *et al.*, 2012). Results of other gold-nanoparticles functionalized with a thiolated poly(ethylene glycol) (PEG) monolayer capped with a carboxylate group conjugated to oxaliplatin have shown unusual ability to penetrate the nucleus in the lung cancer cells (Brown *et al.*, 2010).

In the quantitative analysis of the cellular uptake of the PTX, (O-1)-b-PEG-HNPs-PTX showed the highest cellular uptake into the BxPC-3 cells; non- HNPs conjugated formulations, (O-1)-b-PEG-PTX, showed a bit lower cellular uptake at 1h and 4h and much lower at 24 h; while the naked PTX formula showed the lowest cellular uptake at all the time points (Figure 123). These results confirmed (O-1)-b-PEG formulations with/without HNPs significantly facilitated the uptake of PTX in the BxPC-3 cells. This enhancement could be due to improved bioavailability via increase in the drug solubility and protecting them from inactivation in the biological milieu which leads to extend circulation time, hence micelles could accumulate in the tumours to a greater extent, with higher uptake via the enhanced permeability and retention (EPR) effect provides a basis for the selective

accumulation. Furthermore, the positive charged of the (O-1)-*b*-PEG-PTX and (O-1)-*b*-PEG-HNPs-PTX formulations makes these molecules readily cross cell membranes since the cell membrane is lipophilic and negatively charged (Jhaveri and Torchilin, 2014, Nori and Kopecek, 2015). The results of cellular uptake were in agreement with cytotoxic effect results, which confirmed the higher cytotoxic effect of hybrid formulations comparing with free drug, especially.

Controlling the drug release from thermo-responsive polymers using temperature as a stimulus makes it a more attractive strategy, by exploiting exogenous variation in the local temperature, typical for tumour tissues. Drug release can be induced by tumour tissues as it has been shown to have slightly higher temperatures comparing to healthier tissues. Also, an additional temperature can be used to accelerate drug release by external source (Shirakura *et al.*, 2014, Coelho *et al.*, 2010). Poly(*N*-isopropylacrylamide-*co*-*N*, *N*-dimethylacrylamide)-*b*-poly(*d*,*l*-lactide-*co*-glycolide) [P(NIPAAm-*co*-DMAAm)-*b*-poly(*d*,*l*-lactide-*co*-glycolide) (PLGA)] with different compositions and lengths of PLGA block was synthesised by Liu and colleagues. This thermo-responsive polymer used to synthesis micelles containing doxorubicin (DOX). They reported that the DOX-loaded micelles possessed high stability in PBS containing serum at 37 °C, increasing the temperature above the normal body temperature (39.5 °C) caused deform the micelles, thus triggering DOX release (Liu *et al.*, 2005).

In another interesting piece of research, Thermo-responsive core-shell magnetic nanoparticles consisting of γ -Fe₂O₃ iron oxide magnetic nanoparticles (MNP) coated with the thermo-responsive polymer poly(*n*-isopropylacrylamide) (PNIPAM) have been formulated to encapsulate doxorubicin (DOX) anticancer agent. *In vitro* release experiments revealed that DOX release at temperatures above and below the LCST of PNIPAM (34 °C) had a weak dependence on swelling behaviour. Moreover, the *in vitro* simultaneous hyperthermia and drug release of therapeutically relevant quantities of DOX was achieved, 14.7% of loaded DOX was released over the period of 47 min at hyperthermia temperatures. The particles showed Fickian diffusion release kinetics, 41% was the maximum drug release observed at 42 °C after 101 h. *In vitro* experiments also showed that 14.7% of the total drug content was released after 47 min at hyperthermia temperatures (Purushotham *et al.*, 2009).

In this work, the polymeric micelles, which released their drug content at 44 °C displayed a much higher cytotoxicity compared to micelles at 37 °C. This result establishes that temperature is, in fact, an effective tool for controlled release of drug and hence, the efficacy of micelles. Moreover, *in vitro* thermo-responsive cytotoxicity results from BxPC-3 cell lines showed that the viability of treated cells with (O-1)-*b*-PEG-PTX and hybrid formulations mostly decreased by increasing the temperature to 44 °C while the naked PTX showed temperature independent responses.

Heat treatment of the samples increased (O-1)-*b*-PEG-PTX and (O-1)-*b*-PEG-HNPs-PTX inhibitory activities 5-fold and 1-fold respectively comparing with untreated samples. Increase in the temperature induced dehydration and increased hydrophobicity of the (O-1)-*b*-PEG and (O-1)-*b*-PEG-HNPs, which led to release of PTX for subsequent diffusion to tumour cells.

5.5-Conclusion

PTX, (O-1)-*b*-(PEG), (O-1)-*b*-(PEG)-HNPs, (O-1)-*b*-(PEG)-PTX and (O-1)-*b*-(PEG)-HNPs-PTX were tested for *in-vitro* cytotoxicity on BxPC-3 cells. *In-vitro* MTT assay results established the ability of (O-1)-*b*-(PEG)-PTX and (O-1)-*b*-(PEG)-HNPs-PTX novel formulations to accumulate and kill pancreatic cancer cells more effectively, compared to the free PTX. *In vitro* drug uptake study also indicated that the copolymer and its hybrid formulations internalise and accumulate inside pancreatic cancer cells significantly higher than that observed for the free drug administration. The effect of higher temperature has been studied and the results showed that the toxicity of PTX-copolymer formulations was increased by few folding after heating to 44 °C.

Finally, this study confirmed that combining PTX and HNPs/copolymeric NPs at very low doses possess a synergic cytotoxic effect on BxPC-3 cells. Although this result was observed in triplicate, further investigation is required in order to fully understand if this finding is reliable.

Chapter Six

General Conclusions and Future Work

6.1- General conclusion

In this study, a novel thermo-responsive copolymer system has been prepared, which has the potential to act both as a drug delivery system and to enhance the solubility of some poor water-soluble drug via grafted hydrophobic groups onto the primary amine group of APMA monomers using palmitoyl, dansyl, cholesteryl and 5-(4-aminophenyl)-1,3,4-oxadiazole to incorporate into the HPMA copolymer at varied molar ratio. Block copolymer was prepared from these derivatives via copolymerize with poly ethylene glycol (PEG) to improve the thermo-responsive behaviour of the polymer.

The hydrophobic groups of palmitoyl, dansyl, cholesteryl and 5-(4-aminophenyl)-1,3,4-oxadiazole were successfully grafted onto the primary amine group of APMA monomers. Three grafted groups, palmitoyl, dansyl and cholesteryl, are substituted onto the primary amine group of APMA in one step. However, due to the strong bonding of chlorine-carbon in oxadiazole structure, this forced as to create a new way to prepare this compound by building up this molecule throughout 4 steps. These monomers were polymerised with water soluble thermo-responsive HPMA. Optimal substitution onto the backbone of both hydrophobic and hydrophilic groups onto the primary amines of the polymer was determined. The chemical structures of new amphiphilic copolymers based on PHPMA as hydrophilic thermo-responsive part and palmitoyl, dansyl cholesteryl and oxadiazole as hydrophobic grafted groups was investigated using various techniques including NMR, FTIR and melting point.

The hydrophobic effect of grafted moieties played a significant role in determining the solubility of copolymers as shown in Table 20. The introduction of hydrophobic pendent moieties into the poly(HPMA) structure caused reduction in the aqueous solubility based on grafting ratio and grafted group structure. When the feeding ratio of APMA-P, APMA-D or APMA-C were increased from 0.25 % to 10 % the solubility of poly(HPMA) derivatives decreased dramatically, thereby indicating that the modified APMA moieties significantly improved the hydrophobic properties of the final amphiphilic copolymers. However, even at high APMA-O grafting ratios, those copolymers still possessed high aqueous solubility due to the amphiphilic nature of APMA-O.

Hybrid nanoparticles (HNPs) were successfully synthesised. The prepared hybrid nanoparticles were characterised by different techniques. The inductively coupled plasma-optical emission spectroscopy (ICP-OES) analysis showed that the ratio of iron: gold within

the formulation was around 5: 1. The transmission electron microscopy (TEM) grids of HNPs were analysed to observe the particle morphology and size parameters. HNPs particles seemed to have a star shape with around 50 nm diameter. Photon correlation spectroscopy, zeta potential and UV/Visible spectroscopy measurement results taken together suggest that the coating process of particles with poly(ethylenimine) (PEI), subsequently gold seeding then gold coating were successes.

Four types of hydrophobic drugs, propofol, griseofulvin, prednisolone and paclitaxel, were used in order to study the efficiency of the HPMA-APMA copolymer derivatives to enhance drug solubility. The results of the solubility studies indicated that such models possessed high drug loading capacity and encapsulation efficiency. Furthermore, these copolymer systems exhibited high capability to solubilise insoluble drug candidates that having different chemical structures, formula mass, water solubility and states. Hence, it is generally accepted that HPMA-co-APMA copolymer formulations can be used as a universal solubiliser for pharmaceutical applications. The maximum amount of solubilised propofol ranged from 31.3 to 41.1 mgmL⁻¹, griseofulvin from 10.21 to 20.75 mgmL⁻¹ and prednisolone from 8.91 to 13.11 mgmL⁻¹. Drug release from HPMA-co-APMA-R copolymers in aqueous solution revealed no response to change in temperature. This could be attributed to change in the LCST of pHPMA as a result of grafted with the APMA-R groups.

To tackle this problem, an approach based on introducing an appropriate amount of poly ethylene glycol (PEG) block as a part of O-1 and D-2 amphiphilic copolymers was taken. O-1 and D-2 appeared to be the best alternative formulations to enhance candidate hydrophobic drug solubility. These two formulas have been utilized to prepare block copolymers with PEG to boost copolymer responsivity to temperature change. HPLC results revealed that (O-1)-*b*-(PEG) and (D-2)-*b*-(PEG) have the same drug loading efficiency as the non-PEGylated or sometime less. This could be attributed to the hydrophilic properties of PEG, which eventually lead to reduce the ability of the amphiphilic copolymer to solubilise hydrophobic drugs. On the other hand, it was shown that the O-1 and D-2 block copolymerisation with a PEG block enhances release of the contents remarkably at a higher temperature. As it is explained in results and discussion of chapter 4, this point attributed to maintenance of the hydrophilic/hydrophobic balance. Addition of the HNPs showed further acceleration in drug release with increasing temperature.

Paclitaxel (PTX) anticancer drug was encapsulated onto the (O-1)-*b*-(PEG) with/without HNPs. Drug loading, stability and drug release studies were carried out. Paclitaxel-polymer formulations have shown excellent drug solubilisation capacities. At 6 mg/ml the (O-1)-*b*-(PEG) polymer achieved paclitaxel solubility more than 2000-fold greater than its aqueous solubility.

In vitro cytotoxicity assays using (O-1)-*b*-(PEG)-PTX and (O-1)-*b*-(PEG)-HNPs-PTX novel formulations revealed that when BxPC-3 cells were exposed to the formulations, enhanced therapeutic efficacy was observed compared to the free PTX.

Quantitative comparison of the uptake of PTX indicated that the copolymer and its hybrid formulations internalise and accumulate inside pancreatic cancer cells considerably greater than that observed for the free drug administration. These results were in agreement with the cytotoxicity assay results, confirming a higher cytotoxic effect of the copolymer formulations comparing with free PTX, especially the copolymer-HNPs formulation. Furthermore, the effect of increased temperature exhibits a larger impact on the toxicity of copolymer formulations than on free drug because of the increased PTX release. These effects are evident in a decrease in the IC₅₀ of BxPC-3 cells.

To sum up, this work has produced novel thermo-responsive copolymers based on amphiphilic poly(HPMA)-*co*-APMA derivatives. The results suggest that these derivatives are capable of solubilising poorly soluble hydrophobic drugs such as propofol, griseofulvin, prednisolone and paclitaxel efficiently. Successful control release of loaded drugs has been achieved by incorporation of appropriate amount of PEG block as a part of O-1 and D-2 amphiphilic copolymers. Our *in vitro* data suggested that copolymer-PTX micelles had stronger cytotoxicity than free drug. Furthermore, the introduction of HNPs into the polymer backbone increased PTX cytotoxicity at 37 °C and 44 °C. These results taken together suggest that we are successful to reach the main goals of this research.

6.2- Future work

The aim of the thesis was preparation of an amphiphilic graft polymer composed of a poly(N-(2-hydroxypropyl) methacrylamide) pHPMA backbone in order to produce thermo-responsive drug carriers for pancreatic cancer therapy. The results look promising, but more experiments are required to prove the utility of this system, such as studying the formulation stability in order to determine their potential as pharmaceutical excipients, study the ability of this system to solubilise another poor-soluble drug and carry out further *in vitro* release via laser irradiation instead of hot plate or oven.

Further experiments should investigate the effect of pH on the copolymer structure and drug release profile. Many studies have confirmed the pH-responsivity behaviour of pHPMA derivatives (Choi *et al.*, 1999, Jäger *et al.*, 2015, Holley *et al.*, 2013). It would be beneficial also to investigate the ability of these copolymers to be glucose-responsive insulin release systems as HPMA copolymers had showed this feature before (Ishihara *et al.*, 1984). Outstanding opportunities exist in combining temperature, pH and bio-responsive control strategies to create systems with multi-state transitions.

The thermo-responsive copolymer system used in the research was well optimised for the BxPC-3 cells. It is still unknown if the new thermo-responsive system is working on other cells/cell lines or not. Therefore, further investigations using a wider variety of cells/cell lines and assays are required. Also we investigated the biological effect of one copolymer derivative in conjugation with HNPs. In further investigation it's necessary to the study the biological effect of the rest of the copolymer derivatives

References

- 1- Aaron P. Esser-Kahn, Susan A. Odom, Nancy R. Sottos, Scott R. White, Jeffrey S. Moore, (2011), **Triggered Release release from Polymer polymer Capsulescapsules**, *Macromolecules*, Volume 44, 5539-5553.
- 2- Abd Ellah Noura, Leeanne Taylor, Weston Troja, Kathryn Owens, Neil Ayres, Giovanni Pauletti, Helen Jones, (2015), **Development of non-viral, trophoblast specific gene delivery for placental therapy**, *PLoS ONE*, Volume 10, Issue 10, 1-13.
- 3- Achilias S. Dimitris, Siafaka I. Panoraia, (2017), **Polymerization kinetics of poly(2-hydroxyethyl methacrylate) hydrogels and nanocomposite materials**, *Processes*, Volume 5, Issue 21.
- 4- Adam S, van Bommel J, Pelka M, Dirckx M, Jonsson D, Klein J, (2004), **Propofol-induced injection pain: comparison of a modified propofol emulsion to standard propofol with premixed lidocaine**, *Anaesthesia Analgesia*, Volume 99, Issue 4, 1076-1079.
- 5- Akiya Akahoshi, Eiji Matsuura, Eiichi Ozeki, Hayato Matsui, Kazunori Watanabe, Takashi Ohtsuki, (2016), **Enhanced cellular uptake of lactosomes using cell-penetrating peptides**, *Science and Technology of Advanced Materials*, Volume 17, Issue 1, 245-252.
- 6- Alfurhood A. Jawaher, Sun Hao, Bachler R. Patricia, Sumerlin S. Brent, (2016), **Hyperbranched poly(N-(2-hydroxypropyl) methacrylamide) via RAFT self-condensing vinyl polymerization**, *Polymer Chemistry*, Volume 7, 2099-2104.
- 7- Alison A Edwards and Bruce D Alexander, (2010), **Organic applications of UV-visible absorption spectroscopy**, Elsevier Ltd.
- 8- Alkazzaz S Zuhair, Wedad Kamal Ali, (2015), **Design and in-vitro evaluation of colon targeted prednisolone solid dispersion tablets**, *UK Journal of Pharmaceutical and Biosciences*, Volume 3, Issue 6, 30-41.
- 9- André Sá Couto, Joana Vieira, Helena F. Florindo, Mafalda A. Videira, Helena M. Cabral-Marques (2014), **Characterisation of DM- β -cyclodextrin:prednisolone complexes and their formulation as eye drops**, *J Inclusion Phenomena and Macrocyclic Chemistry*, Volume 80, 155-164.
- 10- Aniket S. Wadajkar, Zarna Bhavsar, Cheng-Yu Ko, Bhanuprasanth Koppolu, Weina Cui, Liping Tang, Kytai T. Nguyen, (2012), **Multifunctional**

- particles for melanoma-targeted drug delivery**, Acta Biomaterialia, Volume 8, Issue 8, 2996-3004.
- 11**-Anthöfer J, (2015), **Drug development and critical analysis of the reliability of preclinical studies**, Master thesis, Universität Bonn.
 - 12**-Arijit Gandhi, Abhijit Paul, Suma Oommen Sen, Kalyan Kumar Sen, (2015), **Studies on thermoresponsive polymers: phase phase behaviour, drug delivery and biomedical applications**, Asian journal of pharmaceutical sciences, Volume 10, Issue 2, 99-107.
 - 13**-Ashbrook E Sharon, McKay David, (2016), **Combining solid-state NMR spectroscopy with first-principles calculations - a guide to NMR crystallography**, Chemical Communications, Volume 52, 7186-7204.
 - 14**-Ashlynn L, Yong Wang, Shazib Pervaiz, Weimin Fan, Yi Yan Yang, (2011), **Synergistic anticancer effects achieved by co-delivery of TRAIL and paclitaxel using cationic polymeric micelles**, Macromolecular Bioscience, Volume 11, 296-307.
 - 15**-Assche G Van, Van Mele B, Li T and Nies E, (2011), **Adjacent UCST Phase behavior in aqueous solutions of poly(vinyl methyl ether): detection of a narrow low temperature UCST in the lower concentration range**, Macromolecules, Volume 44, Issue 4, 993-998.
 - 16**-Azmat Ali Khani, Amerm Aalnazi, Mumtaz Jabeen, Arun Chauhan, Ali Sabir Abdelhameed, (2013), **Design, synthesis and in vitro anticancer evaluation of a stearic acid-based ester conjugate**, Anticancer Research, Volume 33, 2517-2524.
 - 17**-Bae C, Lambert M, Sonae S, Prausnitz M, (1991), **Cloud-Point curves of polymer solutions from thermo-optical measurements**, Macromolecules, Volume 24, Issue 15, 4403-4407.
 - 18**-Baker M T, Naguib M, (2005), **Propofol: the challenges of formulation**, Anaesthesiology, Volume 103, Issue 4, 860-76.
 - 19**-Balmayor E. R, Azevedo H. S, Reis R. L, (2011), **Controlled delivery systems: from pharmaceuticals to cells and genes**, Pharmaceutical Research, Volume 28, Issue 6, 1241-1258.

- 20-**Ban Z, Barnakov YA, Li F, Golub VO, O'Connor CJ, (2005), **The synthesis of core-shell iron@gold nanoparticles and their characterization**, Journal Materials Chemistry, Volume 15, 4662-4660.
- 21-**Barnett C M, Martin R. Lees, Curtis D.M Anthony, Kong T. L Pual, Cheng W. Ping, Hoskins Clare, (2013), **Poly(allylamine) magnetomicelles for image guided drug delivery**, Pharmaceutical Nanotechnology, Volume 1, Issue 3, 224-238.
- 22-**Barnett C, Gueorguieva M, Lees M, McGarvey D, Hoskins C, (2013a), **Physical stability, biocompatibility and potential use of hybrid iron oxide-gold nanoparticles as drug carriers**, Journal of nano research, Volume 15, Issue 6, 1076.
- 23-**Beth A. Weaver, (2014), **How Taxol/paclitaxel kills cancer cells**, Molecular of Biology of the Cell, Volume 25, Issue 18, 2677-2681.
- 24-**Boncel Sławomir, Pluta Anna, Skonieczna Magdalena, Gondela Andrzej, Maciejewska Barbara, HermanP. Artur, Jędrzyiak G. Rafal, Sebastian Budniok, Kamila Komędera, Artur Błachowski, Krzysztof Z. Walczak, (2017), **Hybrids of Iron-Filled Multiwall Carbon Nanotubes and Anticancer Agents as Potential Magnetic Drug Delivery Systems: In Vitro Studies against Human Melanoma, Colon Carcinoma, and Colon Adenocarcinoma**, Journal of Nanomaterials, Volume 2017 , Article ID 1262309.
- 25-**Boss B. Charles, Fredeen J. Kenneth, (1997), **Concepts, instrumentation and techniques in inductively coupled plasma optical emission spectrometry**, 2nd Edition, The Perkin-Elmer Corporation
- 26-**Brian M. Tissue, (2002), **Ultraviolet and visible absorption spectroscopy**, Characterization of Materials, Second edition, John Wiley & Sons, Inc.
- 27-**Brown D. Sarah, Nativo Paola, Smith Jo-Ann, Stirling David, Edwards R. Paul, Venugopal Balaji, Flint J. David, Plumb A. Jane, Graham Duncan, Wheate J. Nial, (2010), **Gold nanoparticles for the improved anticancer drug delivery of the active component of oxaliplatin**, Journal of American Chemistry Society, Volume 132, Issue13, 4678-4684.
- 28-**Burke S. Rob, Pun H. Suzie, (2010), **Synthesis and characterization of biodegradable HPMA-Oligolysine copolymers for improved gene delivery**, Bioconjugate Chemistry, Volume 21, Issue 1, 140-150.

- 29-**Cabral Horacio, Kataoka Kazunori, (2010), **Multifunctional nanoassemblies of block copolymers for future cancer therapy**, Science and Technology of Advance Material, Volume 11, Issue 1.
- 30-**Censi Roberta, Tina Vermonden, Hendrik Deschout, Kevin Braeckmans, Piera di Martino, Stefaan C. De Smedt, Cornelus F. van Nostrum, Wim E. Hennink, (2010), **Photopolymerized thermosensitive poly(HPMA lactate)-PEG-based hydrogels: effect of network design on mechanical properties, degradation, and release behavior**, Biomacromolecules, Volume 11, 2143-2151.
- 31-**Chakraborty Tanushree, Chakraborty Indranil, Ghosh Soumen, (2011), **The methods of determination of critical micellar concentrations of the amphiphilic systems in aqueous medium**, Arabian Journal of Chemistry, Volume 4, 265-270.
- 32-**Chanon Sansuk, Sopitcha Phetrong, Peerasak Paoprasert, (2017), **Preparation of pH-responsive crosslinked materials from natural rubber and poly(4-vinylpyridine)**, Polymer International, Volume 66, Issue 6, 787-794.
- 33-**Chih-ping Tso, Cheng-min Zhung, Yang-hsin Shih, Young-Ming Tseng, Shian-chee Wu and Ruey-an Doong, (2010), **Stability of metal oxide nanoparticles in aqueous solutions**, Water Science & Technology, Volume 61, Issue 1, 127-133.
- 34-**Chi-San Wu, (1995), **Handbook of Size Exclusion Chromatography**, Volume 6, Marcel Dekker, New York.
- 35-**Choi W. M, Kopečková P, Minko T, Kopeček J, (1999), **Synthesis of HPMA copolymer containing adriamycin bound via an acid-labile spacer and its activity toward human ovarian carcinoma cells**, Journal of Bioactive and Compatible Polymer, Volume 14, 447-456.
- 36-**Christopher M. Barnett, Martin R. Lees, Anthony D.M. Curtis, Paul K.T. Lin, Woei P. Cheng, Clare Hoskins, (2013), **Poly(allylamine) magnetomicelles for image guided drug delivery**, Pharmaceutical Nanotechnology, Volume 1, 224-238.
- 37-**Chu D. S, Sellers D. L, Bocek M. J, Fishedick A. E, Horner P. J, Pun S. H, (2015), **MMP9-sensitive polymers mediate environmentally-responsive bivalirudin release and thrombin inhibition**, Biomaterial Science, Volume 3, 41-45.

- 38-**Coelho J F, Paula C. Ferreira, Patricia Alves, Rosemeyre Cordeiro Ana C. Fonseca, Joana R. Góis, Maria H. Gi, (2010), **Drug delivery systems: advanced technologies potentially applicable in personalized treatments**, EPMA Journal, Volume 1, 164-209.
- 39-**Contreras-García Angel, Carmen Alvarez-Lorenzo, Angel Concheiro, Emilio Bucio, (2010), **PP films grafted with N-isopropylacrylamide and N-(3-aminopropyl) methacrylamide by γ radiation: synthesis and characterization**, Radiation Physics and Chemistry, Volume 79, Issue 5, 615–621.
- 40-**Cor Koning, Martin Van Duin, Pagnouille Christophe, Jérôme Robert, (1998), **Strategies for compatibilization of polymer blends**, Progress in Polymer Science, Volume 23, Issue 4, 707-757.
- 41-**Cornwel P. A, (2018), **a review of shampoo surfactant technology: consumer benefits, raw materials and recent developments**, International Journal of Cosmetic Science, 2018, Volume 40, 16-30.
- 42-**Coskun Ozlem, (2016), **Separation techniques: chromatography**, Northern Clinics of Istanbul, Volume 3, Issue 2, 156-160.
- 43-**Cowie J, McEwen I, Garay M, (1986), **Polymer cosolvent systems – synergism and antisnergism of solvent mixtures for poly(methyl methacrylate)**, Polymer Communications, Volume 27, 122-124.
- 44-**Cunningham V. J, Liam P. D. Ratcliffe, Adam Blanz, Nicholas J. Warren, Andrew J. Smith, Oleksandr O. Mykhaylyk, Steven P. Armes, (2014), **Tuning the critical gelation temperature of thermo-responsive diblock copolymer worm gels**, Polymer Chemistry, Volume 5, Issue 21, 6307-6317.
- 45-**Curtis Anthony, Malekigorji Maryam, Holman Joseph, Skidmore Mark, Hoskins Clare, (2015), **Heat dissipation of hybrid Iron oxide-gold nanoparticles in an agar phantom**, Journal of Nanomedicine and Nanotechnology, Volume 6, Issue 6.
- 46-**Dehbari Nazila , Tavakoli Javad , Khatrao Singh Simranjeet , Tang Youhong , (2017), **In situ polymerized hyperbranched polymer reinforced poly(acrylic acid) hydrogels**, Materials Chemistry Frontiers, Volume 1, Issue 10, 1995-2004.
- 47-**Dhembre G.N, Moon R.S, Kshirsagar R.V, (2009), **A review on polymeric micellar nanocarriers**, International Journal of Pharma and Bio Sciences, Volume 2, Issue 2, 109-116.

- 48-**Dong Yizhou , Wang Weiheng, Veisheh Omid, Appel A. Eric, Xue Kun, Webber J. Matthew, Tang C. Benjamin, Yang Xi-Wen, Weir C. Gordon, Langer Robert, Anderson G. Daniel, (2016), **Injectable and glucose-responsive hydrogels based on boronic acid--glucose complexation**, *Langmuir*, Volume 32 , Issue 34, 8743–8747.
- 49-**Dutta RK, Sahu S, (2012), **Development of a novel probe sonication assisted enhanced loading of 5-FU in SPION encapsulated pectin nanocarriers for magnetic targeted drug delivery system**, *European Journal of Pharmaceutics and Biopharmaceutics*, Volume 82, Issue 1, 58-65.
- 50-**Elena V. Batrakova, Alexander V. Kabanov, (2008), **Pluronic block copolymers evolution of drug delivery concept from inert nanocarriers to biological response modifiers**, *Journal of Control Release*, Volume 130, Issue 2, 98-106.
- 51-**Equbal Asif, Morten Bjerring, P. K. Madhu and Niels Chr. Nielsen, (2015), **A unified heteronuclear decoupling strategy for magic-angle-spinning solid-state NMR spectroscopy**, *The Journal of Chemical Physics*, Volume 142, 184-201.
- 52-**Eriksson M, Englesson S, Niklasson F, Hartvig P, (1997), **Effect of lignocaine and pH on propofol-induced pain**, *British Journal of Anaesthesia*, Volume 78, Issue 5, 502-506.
- 53-**Esenturk E. Nalbant, Walker A. R. Hight, (2009), **Surface-enhanced Raman scattering spectroscopy via gold nanostars**, *Journal of Raman Spectroscopy*, Volume 40, 86-91.
- 54-**Facchin M, Scarso A, Selva M, Perosa A, Riello P, (2017), **Towards life in hydrocarbons: aggregation behaviour of “reverse” surfactants in cyclohexane**, *RSC Advances*, Volume 7, 15337-15341.
- 55-**Fenn E Emily, Daryl B. Wong, M. D. Fayer, (2009), **Water dynamics at neutral and ionic interfaces**, *Proceeding of National Academy Sciences*, Volume 106 , Issue 36, 15243–15248.
- 56-**Flanagan W. Michael, Richard W. Wagner, Deborah Grant, Kuei-Ying Lin, Mark D. Matteucci, (1999), **Cellular penetration and antisense activity by a phenoxazine-substituted heptanucleotide**, *Nature Biotechnology*, Volume 17, 48-52.

- 57-**Freitas B.A. Avelar, V.G. Almeida, M.C.X. Pinto, F.A.G. Moura, A.R. Massensini, O.A. Martins-Filho, E. Rocha-Vieira, G.E.A. Brito-Melo, (2014), **Trypan blue exclusion assay by flow cytometry**, Brazilian Journal of Medical and Biological Research, Volume 47, Issue 4, 307-315.
- 58-**Fu-Heng Yang, Qing Zhang, Qian-Ying Liang, Sheng-Qi Wang, Bo-Xin Zhao, Ya-Tian Wang, Yun Cai, Guo-Feng Li, (2015), **Bioavailability enhancement of paclitaxel via a novel oral drug delivery system: paclitaxel-loaded glycyrrhizic acid micelles**, Molecules, Volume 20, 4337-4356.
- 59-**Gaurav Pratap Singh Jadaun, Shruti Dixit, Vandana Saklani, Sanjay Mendiratta, Renu Jain, Surinder Singh, (2016), **HPLC for peptides and proteins: principles, methods and applications**, Pharmaceutical Methods, Volume 8, Issue 1, 139-144.
- 60-**Gerothanassis I. P, Troganis Anastassios, Exarchou Vassiliki, Barbarossou Klimentini, (2012), **Nuclear magnetic resonance (NMR) spectroscopy: basic principles and phenomena, and their applications to chemistry, biology and medicine**, Chemistry Education Research and Practice, Volume 3, 229-252.
- 61-**Goon IY, Lai LMH, Lim M, Munroe P, Gooding JJ, Amal R, (2009), **Fabrication and dispersion of gold shell-protected magnetite nanoparticles: systematic control using Polyethylenimine**, Chemistry of Materials, Volume 21, 673-681.
- 62-**Grallert M Sibila, Carlota de Oliveira, Kerly M Pasqualoto, Leoberto C Tavares, (2012), **Polymeric micelles and molecular modeling applied to the development of radiopharmaceuticals**, Brazilian Journal of Pharmaceutical Sciences, Volume 48, Issue 1, 1-16.
- 63-**Grossen P, Witzigmann D, Sieber S, Huwyler J, (2017), **PEG-PCL-based nanomedicines: a biodegradable drug delivery system and its application**, Journal of Control Release, Volume 260, 46-60.
- 64-**Haddad P.R, Jackson P.E, (1990), **Ion chromatography. principles and applications**, Journal Chromatography Library, Volume 46.
- 65-**Hamaguchi T, Kato K, Yasui H, Morizane C, Ikeda M, Ueno H, Muro K, Yamada Y, Okusaka T, Shirao K, Shimada Y, Nakahama H, Matsumura Y, (2007), **A phase I and pharmacokinetic study of NK105, a paclitaxel-incorporating micellar nanoparticle formulation.**, British Journal of Cancer, Volume 97, 170-176.

- 66-Harmsen Stefan, Huang Ruimin, Matthew A. Wall, Hazem Karabeber, Jason M. Samii, Massimiliano Spaliviero, (2015), **Surface-enhanced resonance Raman scattering nanostars for high-precision cancer imaging**, *Science Translational Medicine*, Volume 7, Issue 271, 271-277.
- 67-Hatada Koichi, Kitayama Tatsuki, Masuda Eiji, (1986), **Studies on the radical polymerization methacrylate in bulk and benzene using totally deuterated monomer technique**, *Polymer journal*, Volume 18, Issue 5, 395-402.
- 68-Heinz Fissan, Simon Ristig, Heinz Kaminski, Christof Asbach, Matthias Apple, (2014), **Comparison of different characterization methods for nanoparticle dispersions before and after aerosolization**, *Analytical Methods*, Volume 6, 7324-7334.
- 69-Hema Sundaram, N Vijayalakshmi, KP Srilatha, (2009), **High performance liquid chromatography and its role in identification of mycobacteriae: an overview**, *NTI Bulletin*, Volume 45,1-4.
- 70-Heo Dong, Dae Hyeok Yang, Ho-Jin Moon, Jung Bok Lee, Min Soo Bae, Sang Cheon Lee, Won Jun Lee, In-Cheol Sun, I Keun Kwon, (2012), **Gold nanoparticles surface-functionalized with paclitaxel drug and biotin receptor as theranostic agents for cancer therapy**, *Biomaterials*, Volume 33, 856-866.
- 71-Holley C. Andrew, Ray G. Jacob, Wan Wenming, Savin A. Daniel, McCormick L. Charles, (2013), **Endolytic, pH-responsive HPMA-b-(L-Glu) copolymers synthesized via sequential aqueous RAFT and ring-opening polymerizations**, *Biomacromolecules*, Volume 14, Issue 10, 3793–3799.
- 72-Holmberg Krister, Jonsson Bo, Kronberg Bengt, Lindman Bjorn, (2002), **Surfactants and polymers in aqueous solution**, John Wiley & Sons, Ltd.
- 73-Honey Priya James, Rijo John, Anju Alex, Anoop K.R, (2014), **Smart polymers for the controlled delivery of drugs – a concise overview**, *Acta Pharmaceutica Sinica B*, Volume 4, Issue 2, 120-127.
- 74-Hoskins C, Papachristou A, Ho TMH, Hine J, Curtis ADM, (2016), **Investigation into drug solubilisation potential of sulfonated calix[4]resorcinarenes**, *Journal of Nanomedicine and Nanotechnology*, Volume 7, Issue 2, 370-377.
- 75-Hoskins Clare, Ouaiissi Mehdi, Lima Costa Sofia, Cheng Woei Ping, Loureiro Inês, Mas Eric, Lombardo Dominique, Cordeiro Anabela, Ouaiissi Ali, Lin Paul Kong Thoo, (2010), ***In vitro* and *in vivo* anticancer activity of a novel nano-**

- sized formulation based on self-assembling polymers against pancreatic cancer, *Pharmaceutical Research*, Volume 27, Issue 12, 2694-703.
- 76-Hoskins Clare, Paul Kong Thoo Lin, Laurence Tetley, Woei Ping Cheng, (2012), **The use of nano polymeric self-assemblies based on novel amphiphilic polymers for oral hydrophobic drug delivery**, *Pharmaceutical Research*, Volume 29, 782-794.
- 77-Hoskins Clare, Paul Kong Thoo Lin, Laurence Tetley, Woei Ping Cheng, (2012a), **Novel fluorescent amphiphilic poly(allylamine) and their supramacromolecular self-assemblies in aqueous media**, *Polymer for Advanced Technologies*, Volume 23, 71-719.
- 78-Hoskins Clare, Yue Min, Mariana Gueorguieva, Craig McDougall, Alexander Volovick, Paul Prentice, Zhigang Wang, Andreas Melzer, Alfred Cuschieri, Lijun Wang, (2012b), **Hybrid gold-iron oxide nanoparticles as a multifunctional platform for biomedical application**, *Journal of Nanobiotechnology*, Volume 10, Issue 27, 1-12.
- 79-Hoskins Clare, Lijun Wang, Woei Ping Cheng, Alfred Cuschieri, (2012c), **Dilemmas in the reliable estimation of the in-vitro cell viability in magnetic nanoparticle engineering: which tests and what protocols?**, *Nanoscale Research Letters*, Volume 7, Issue 1, 77.
- 80-Hui Wang, Kui Wang, Qingxin Mu, Zachary R. Stephen, Yanyan Yu, Shuiqin Zhou, Miqin Zhang, (2017), **Mesoporous carbon nanoshells for high hydrophobic drug loading, multimodal optical imaging, controlled drug release, and synergistic therapy**, *Nanoscale*, Volume 9, 1434-1442.
- 81-Ishihara Kazuhiko, Kobayashi Mineko, Ishimaru Naoshi, Shinohara Isao, (1984), **Glucose induced permeation control of insulin through a complex membrane consisting of immobilized glucose oxidase and a poly(amine)**, *Polymer Journal*, Volume 16, 625-631.
- 82-Ito D, Kubota K, (1997), **Solution properties and thermal-behaviour of poly(N-N-propylacrylamide) in water**, *Macromolecules*, Volume 30, Issue 25, 7828-7834.
- 83-Jäger Alessandro, Jäger Eliézer, Surman František, Höcherl Anita, Angelov Borislav, Ulbrich Karel, Drechsler Markus, Vasil M. Garamus, Cesar Rodriguez-Emmenegger, Frédéric Nallet, Petr Štěpánek, (2015), **Nanoparticles of the**

- poly([N-(2-hydroxypropyl)]methacrylamide)-b-poly[2-(diisopropylamino) ethyl methacrylate] diblock copolymer for pH-triggered release of paclitaxel**, Polymer Chemistry, Volume 6, 4946-4954.
- 84-**Jalili N A, Muscarello Madyson, Gaharwar A K., (2016), **Nanoengineered thermoresponsive magnetic hydrogels for biomedical applications**, Bioengineering & Translational Medicine, Volume 1, 297-305.
- 85-**James E. Polli, (2008), ***In Vitro* Studies are Sometimes Better than Conventional Human Pharmacokinetic *In Vivo* Studies in assessing bioequivalence of immediate-release solid oral dosage forms**, The AAPS Journal, Volume 10, Issue 2, 289-299.
- 86-**Jared L. Anderson, Alain Berthod, Verónica Pino Estévez, and Apryll M. Stalcup, (2015), **Analytical separation science**, 1st Edition, Wiley-VCH Verlag GmbH & Co. KGaA.
- 87-**Jhaveri A. M, Torchilin V. P, (2014), **Multifunctional polymeric micelles for delivery of drugs and siRNA**, Frontiers in Pharmacology, Volume 5, Article 77.
- 88-**Jianfeng Guo, Caitriona M. O'Driscoll, Justin D. Holmes, Kamil Rahme, (2016), **Bioconjugated gold nanoparticles enhance cellular uptake: a proof of concept study for siRNA delivery in prostate cancer cells**, International Journal of Pharmaceutics, Volume 509, Issues 1-2, 16-27.
- 89-**Jiang Jinqiang, Tong Xia, Zhao Yue, (2005), **A new design for light-breakable polymer micelles**, Journal of the American Chemical Society, Volume 127, Issue 23, 8290-8291.
- 90-**Jiang Jun, Klaus Tauer, Yun-Hao Qiu, Ya-Xu Zhong, Min-Rui Gao, Markus Antonietti, Shu-Hong Yu, (2017), **Thermosensitive polymer controlled morphogenesis and phase discrimination of calcium carbonate**, Chemical Communications, Volume 53, 6464-6467.
- 91-**Jie Shen, Kyulim Lee, Stephanie Choi, Wen Qu, Yan Wang, Diane J. Burgess, (2016), **A reproducible accelerated *in vitro* release testing method for PLGA microspheres**, International Journal of Pharmaceutics, Volume 498, 274-282.
- 92-**Jihong Han, Stanley S. Davis, Clive Washington, (2001), **Physical properties and stability of two emulsion formulations of propofol**, International Journal of Pharmaceutics, Volume 215, 207-220.

- 93-**Jin -Oh You, Dariela Almeda, George JC Ye, Debra T Auguste, (2010), **Bioresponsive matrices in drug delivery**, Journal Biological Engineering, Volume 4, 1-15.
- 94-** Jin X, Mo R, Ding Y, Zheng W, Zhang C, (2014), **Paclitaxel-loaded N-octyl-O-sulfate chitosan micelles for superior cancer therapeutic efficacy and overcoming drug resistance**, Molecular Pharmacy, Volume 11, Issue 1, 145-157.
- 95-**Jin Yongdong, Congxian Jia, Sheng-Wen Huang, Matthew O'Donnell, Xiaohu Gao, (2010), **Multifunctional nanoparticles as coupled contrast agents**, Nature Communications, Volume 1, Issue 41, 1-14.
- 96-**Jochum D. Florian, Theato Patrick, (2013), **Temperature- and light-responsive smart polymer materials**, Chemical Society Review, Volume 42, 7468-7483.
- 97-**John Kong, Kelsey Coolahan, Amos Mugweru, (2013), **Manganese based magnetic nanoparticles for heavy metal detection and environmental remediation**, Analytical Methods, Volume 5, 5128-5133.
- 98-**Johnson N. Russell, David S. H. Chu, Julie Shi, Joan G. Schellinger, Peter M. Carlson, Suzie H. Pun, (2011), **HPMA-oligolysine copolymers for gene delivery: optimization of peptide length and polymer molecular weight**, Journal Control Release, Volume 155, Issue 2, 303-311.
- 99-**Joyce J. Sung, Neha N. Pardeshi, Anke M. Mulder, Sean K. Mulligan, Joel Quispe, Kathy On, Bridget Carragher, Clinton S. Potter, John F. Carpenter , Anette Schneemann, (2015), **Transmission electron microscopy as an orthogonal method to characterize protein aggregates**, Journal of Pharmaceutical Science, Volume 104, Issue 2, 750-759.
- 100-** Judith K. Guy-Caffey, Veeraiah Bodepudi, Jeffrey S. Bishop, Krishna Jayaraman, and Nilabh Chaudhary, (1995), **Novel polyaminolipids enhance the cellular uptake of oligonucleotides**, Journal of Biological chemistry, Volume 270, Issue 52, 31391–31396.
- 101-** Jun Ge, Evgenios Neofytou, Thomas J. Cahill, Ramin E. Beygui, Richard N. Zare, (2012), **Drug release from electric field responsive nanoparticles**, ACS Nano, Volume 6, Issue 1, 227-233.
- 102-** Kadajji V Gowda, Betageri V. Guru, (2011), **Water soluble polymers for pharmaceutical applications**, Polymers, Volume 3, 1972-2009.

- 103-** Karayianni Maria, Pispas Stergios, (2016), **Self-Assembly of amphiphilic block copolymers in selective solvents**, Springer International Publishing Switzerland, 32-33.
- 104-** Karimi Mahdi, Zangabad Parham Sahandi, Ghasemi Amir, Michael R Hamblin, (2015), **Smart internal stimulus-responsive nanocarriers for drug and gene delivery**, Chapter 6, Morgan & Claypool Publishers.
- 105-** Karolewicz Bożena, (2016), **A review of polymers as multifunctional excipients in drug dosage form technology**, Saudi Pharmaceutical Journal, Volume 24, Issue 5, 525-536.
- 106-** Kashyap Smita, Jayakannan Manickam, (2014), **Thermo-responsive and shape transformable amphiphilic scaffolds for loading and delivering anticancer drugs**, Journal of Materials Chemistry B, Volume 2, 4142-4152.
- 107-** Kataoka Kazunori, Miyazaki Hiroaki, Bunya Masayuki, Okano Teruo, Sakurai Yasuhisa, (1998), **Totally synthetic polymer gels responding to external glucose concentration: their preparation and application to on-off regulation of insulin release**, Journal of The American Chemical Society, Volume 120, 12694-12695.
- 108-** Katrina L Schmid, Leisa M Schmid, (2000), **Ocular allergy: causes and therapeutic options**, Clinical and Experimental Optometry, Volume 83, Issue 5, 257-270.
- 109-** Kawatani Ryo, Nishiyama Yasuhiro, Kamikubo Hironari, Kakiuchi Kiyomi, Ajiro Hiroharu, (2017), **Aggregation control by multi-stimuli-responsive poly(N-vinylamide) derivatives in aqueous system**, Nanoscale Research Letters, Volume 12, 461.
- 110-** Kazuhiko Ishihara, (2015), **Highly lubricated polymer interfaces for advanced artificial hip joints through biomimetic design**, Polymer Journal, Volume 47, 585-597.
- 111-** Khadka Prakash, Jieun Ro, Hyeongmin Kim, Iksoo Kim, Jeong Tae Kim, Hyunil Kim, Jae Min Cho, Gyiae Yun, Jaehwi Lee, (2014), **Pharmaceutical particle technologies: an approach to improve drug solubility, dissolution and bioavailability**, Asian Journal of Pharmaceutical Sciences, Volume 9, Issue 6, 304-316.

- 112-** Kim Joo-Ho, Yim Dajeong, Jang Woo-Dong, (2016), **Thermo-responsive poly(2-isopropyl-2-oxazoline) and tetraphenylethene hybrids for stimuli-responsive photoluminescence control**, Chemical Communications, Volume 52, 4152-4155.
- 113-** Kim TY, Kim DW, Chung JY, Shin SG, Kim SC, Heo DS, Kim NK, Bang YJ, (2004), **Phase I and pharmacokinetic study of Genexol-PM, a cremophor-free, polymeric micelle-formulated paclitaxel, in patients with advanced malignancies**, Clinical Cancer Research, Volume 10, 3708-3716.
- 114-** Kirui K Dickson, Diego A Rey, Carl A Batt, (2010), **Gold hybrid nanoparticles for targeted phototherapy and cancer imaging**, Nanotechnology, Volume 21.
- 115-** Klaus Tauer, Daniel Gau, Susanne Schulze, Antje Völkel, Rumiana Dimova, (2009), **Thermal property changes of poly(N-isopropylacrylamide) microgel particles and block copolymers**, Colloid Polymer Science, Volume 287, 299-312.
- 116-** Kopeček Jindřich, Kopečková Pavla, (2010), **HPMA copolymers: origins, early developments, present, and future**, Advanced Drug Delivery Reviews, Volume 62, Issue 2, 122-149.
- 117-** Kshirsagar N A, (2000), **Drug delivery systems**, Indian Journal of Pharmacology, Volume 32, 54-61.
- 118-** Kulich D. M, Gaggar S. K, Lowry V, Stepien R, (2001), **Acrylonitrile-butadiene-styrene polymers**, Encyclopedia of Polymer Science and Technology, Wiley.
- 119-** Kumaravel R. S, Begum S. F, (2015), **Evaluation of cytotoxicity effect in drug coated intravascular catheter**, World Journal of Pharmacy and Pharmaceutical Sciences, Volume 4, Issue 11, 2023-2030.
- 120-** Lai Hengjie, Guangtao Chen, Peiyi Wu and Zichen Li, (2012), **Thermoresponsive behavior of an LCST-type polymer based on a pyrrolidone structure in aqueous solution**, Soft Matter, Volume 8, 2662-2670.
- 121-** Lee Jaehwi, Sang Cheon Lee, Ghanashyam Acharya, Ching-er Chang, Kinam Park, (2003), **Hydrotropic solubilization of paclitaxel: analysis of chemical structures for hydrotropic property**, Pharmaceutical Research, Volume 20, Issue 7, 1022-1030.

- 122-** Li Xinru, Zhuoli Yang, Kewei Yang, Yanxia Zhou, Xingwei Chen, Yanhui Zhang, Fei Wang, Yan Liu, Lijun Ren, (2009), **Self-assembled polymeric micellar nanoparticles as nanocarriers for poorly soluble anticancer drug ethaselen**, *Nanoscale Research Letters*, Volume 4, 1502-1511.
- 123-** Lin-Vien Daimay, Norman B. Colthup, William G. Fateley, Jeanette G. Grasselli, (1991), **The handbook of infrared and Raman characteristic frequencies of organic molecules**, Academic press, page 140.
- 124-** Lipeng Gao, Liefang Gao, Mingxue Fan, Qilong Li, Jiyu Jin, Jing Wang, Weiyue Lu, Lei Yu, Zhiqiang Yan, Yiting Wang, (2017), **Hydrotropic polymer-based paclitaxel-loaded self-assembled nanoparticles: preparation and biological evaluation**, *RSC Advances*, Volume 7, 33248-33256.
- 125-** Liu Gan, Rujiang Ma, Jie Ren, Zhong Li, Haixia Zhang, Zhenkun Zhang, Yingli An, Linqi Shi, (2013), **A glucose-responsive complex polymeric micelle enabling repeated on-off release and insulin protection**, *Soft Matter*, Volume 9, 1636-1644.
- 126-** Liu S.Q, Tong Y.W, Yang Yi-Yan, (2005), **Incorporation and in vitro release of doxorubicin in thermally sensitive micelles made from poly(*N*-isopropylacrylamide-*co*-*N,N*-dimethylacrylamide)-*b*-poly(*d,l*-lactide-*co*-glycolide) with varying compositions**, *Biomaterials*, Volume 26, Issue 24, 5064-5074.
- 127-** Liu X, Liu C, Zhou J, Chen C, Qu F, Rossi JJ, Rocchi P, Peng L, (2015), **Promoting siRNA delivery via enhanced cellular uptake using an arginine-decorated amphiphilic dendrimer**, *Nanoscale*, Volume 7, Issue 9, 3867-3875.
- 128-** Lobenhoffer J Martens, Meyer F.P (2001), **Prednisolone-containing ointment solid as traditional Chinese medicine**, *European Journal of Clinical Pharmacology*, Volume 57, 87-88.
- 129-** Lombardo Domenico, Kiselev A. Mikhail, Salvatore Magazù Pietro Calandra, (2015), **Amphiphiles self-assembly: basic concepts and future perspectives of supramolecular approaches**, *Advances in Condensed Matter Physics*, Volume 2015, 1-22.
- 130-** Lu Xiao-ju, Yang Xiang-yu, Meng Yuan, Li Shao-zhen, (2017), **Temperature and pH dually-responsive poly(β -amino ester) nanoparticles for drug delivery**, *Chinese Journal of Polymer Science*, Volume 35, Issue 4, 534-546

- 131-** Madaghiele Marta, Christian Demitri, Alessandro Sannino, Luigi Ambrosio, (2014), **Polymeric hydrogels for burn wound care: Advanced skin wound dressings and regenerative templates**, Burns & Trauma, Volume 2, Issue 4, 153-161.
- 132-** Maeda H, Brandon M, Sano A, (2003), **Design of controlled-release formulation for ivermectin using silicone**, International Journal of Pharmaceutics, Volume 261, 9-19.
- 133-** Mailänder V, Landfester K, (2009), **Interaction of Nanoparticles with cells**, Biomacromolecules, Volume 10, Issue 9, 2379-2400.
- 134-** Malekigorji Maryam, Alfahad Mohanad, Lin Paul Kong Thoo, Jones Stefanie, Curtis Anthony, Hoskins Clare, (2017), **Thermally triggered theranostics for pancreatic cancer therapy**, Nanoscale, Volume 9, 12735-12745.
- 135-** Mancin Fabrizio, Leonard J. Prins, Paolo Pengo, Lucia Pasquato, Paolo Tecilla, Paolo Scrimin, (2016), **Hydrolytic metallo-nanozymes: from micelles and vesicles to gold nanoparticles**, Molecules, Volume 21, 1014.
- 136-** Manourasa Theodore, Vamvakaki Maria, (2017), **Field responsive materials: photo-, electro-, magnetic- and ultrasound-sensitive polymers**, Polymer Chemistry, Volume 8, 74-96.
- 137-** Matsumoto Akira, Tanaka Miyako, Matsumoto Hiroko, Ochi Kozue, Morooka Yuki, Kuwata Hirohito, Yamada Hironori, Shirakawa Ibuki, Miyazawa Taiki, Ishii Hitoshi, Kataoka Kazunori, Ogawa Yoshihiro, Miyahara Yuji, Suganami Takayoshi, (2017), **Synthetic “smart gel” provides glucose-responsive insulin delivery in diabetic mice**, Science Advances, Volume 3, Issue 11.
- 138-** Matsumura Y, (2008), **Poly (amino acid) micelle nanocarriers in preclinical and clinical studies**, Advanced Drug Delivery Reviews, Volume 60, 899-914.
- 139-** Matsumura Y, (2008), **Polymeric micellar delivery systems in oncology**, Japanese Journal of Clinical Oncology, Volume 38, 793-802.
- 140-** Matsumura Y, Kataoka K, (2009), **Preclinical and clinical studies of anticancer agent-incorporating polymer micelles**, Cancer Science, Volume 100, 572-579.
- 141-** Matthew J, Julio Trevisan, Paul Bassan, Rohit Bhargava, Holly J Butler, Konrad M Dorling, Peter R Fielden, Simon W Fogarty, Nigel J Fullwood, Kelly

- A Heys, Caryn Hughes, Peter Lasch, Pierre L Martin-Hirsch, Blessing Obinaju, Ganesh D Sockalingum, Josep Sulé-Suso, Rebecca J Strong, Michael J Walsh, Bayden R Wood, Peter Gardner, Francis L Martin, (2014), **Using Fourier transform IR spectroscopy to analyze biological materials**, Nature Protocol, Volume 9, Issue 8, 1771-1791.
- 142-** Mayo R. Frank, Walling Cheves, (1950), **Copolymerization**, Chemical Reviews, Volume 46, Issue 2, 191-287.
- 143-** Mendonça V, Arménio C. Serra, Anatoliy V. Popov, Tamaz Guliashvili, Jorge F.J. Coelho, (2014), **Efficient RAFT polymerization of N-(3-aminopropyl)methacrylamide hydrochloride using unprotected “clickable” chain transfer agents**, Reactive & Functional Polymers, Volume 81, 1-7.
- 144-** Menglian Wei, Yongfeng Gao, Xue Li, Michael J. Serpe, (2017), **Stimuli-responsive polymers and their applications**, Polymer Chemistry, Volume 8, 127-143.
- 145-** Mihai Marcela, Stoica Iuliana, Schwarz Simona, (2011), **pH-sensitive nanostructured architectures based on synthetic and/or natural weak polyelectrolytes**, Colloid and Polymer Science, Volume 289, Issue 12, 1387-1396.
- 146-** Mikhail O Durymanov, Andrey A Rosenkranz, Alexander S Sobolev, (2015), **Current Approaches approaches for improving intratumoral accumulation and distribution of nanomedicines**, Theranostics, Volume 5, Issue 9, 1007-1020.
- 147-** Mingming Ding, Lijuan Zhou, Xiaoting Fu, Hong Tan, Jiehua Li, Qiang Fu, (2010), **Biodegradable gemini multiblock poly(ϵ -caprolactone urethane)s toward controllable micellization**, Soft Matter, Soft Matter, Volume 6, Issue 9, 2087-2092.
- 148-** Mitra Amoli-Diva, Kamyar Pourghazi, (2017), **Poly (methacrylic acid-co-acrylic acid)-grafted polyvinylpyrrolidone coated magnetic nanoparticles as a pH-responsive magnetic nano-carrier for controlled delivery of antibiotics**, Nanomedicine Journal, Volume 4, Issue 1, 25-36.
- 149-** Mitra K Ashim, Cholkar Kishore, Mandal Abhirup, (2017), **Emerging nanotechnologies for diagnostics, drug delivery and medical devices**, chapter 3, Elsevier Inc.

- 150-** Mo J, Eggers PK, Yuan ZX, Raston CL, Lim LY, (2016), **Paclitaxel-loaded phosphonated calixarene nanovesicles as a modular drug delivery platform**, Scientific Reports, Volume 6, article number 23489.
- 151-** Mochalova A. E, Zaborshchikova N. V, A. A. Knyazev, Smirnova L. A, V. A. Izvozchikova, Medvedeva V. V, Yu. D. Semchikov, (2006), **Graft polymerization of acrylamide on chitosan: copolymer structure and properties**, Polymer Science Series A, Volume 48, Issue 9, 918-923.
- 152-** Modugno Gloria , Cécilia Ménard-Moyon, Maurizio Prato, Alberto Bianco, (2015), **Carbon nanomaterials combined with metal nanoparticles for theranostic applications**, British Journal of Pharmacology, Volume 172, Issue 4, 975-991.
- 153-** Mohamed Anwar K Abdelhalim, Mohsen M. Mady, Magdy M. Ghannam, (2012), **Physical properties of different gold nanoparticles: ultraviolet-visible and fluorescence measurements**, Journal of Nanomedicine and Nanotechnology, Volume 3, Issue 3, 1-5.
- 154-** Morgan GE Jr., Mikhail M, Murray M, (2002), **The practice of anesthesia, Clinical Anesthesia**, 3rd ed. New York, 173-174.
- 155-** Mosmann T, (1983), **Rapid colorimetric assay for cellular growth and survival: application to proliferation and cytotoxicity assays**, Journal of Immunology Methods, Volume 65, Issue 1-2, 55-63.
- 156-** Mourya V.K, Nazma Inamdar, Nawale R.B, Kulthe S.S, (2011), **Polymeric micelles: general considerations and their applications**, Indian Journal of Pharmaceutical Education and Research, Volume 45, Issue 2.
- 157-** Movassaghian Sara, Olivia M. Merkel, Vladimir P. Torchilin, (2015), **Applications of polymer micelles for imaging and drug delivery**, WIREs Nanomedicine and Nanobiotechnology, Volume 7, Issue 5.
- 158-** Muhammad Rizwan, Rosiyah Yahya, Aziz Hassan, Muhammad Yar, Ahmad Danial Azzahari, Vidhya Selvanathan, Faridah Sonsudin, Cheyma Naceur Abouloula, (2017), **pH sensitive hydrogels in drug delivery: brief history, properties, swelling, and release mechanism, material selection and applications**, Polymers, Volume 9, 1-137.

- 159-** Murphy PG, Myers DS, Davies MJ, Webster NR, Jones JG, (1992), **The antioxidant potential of propofol (2,6-diisopropylphenol)**, British Journal of Anaesthesia, Volume 68, 613-618.
- 160-** Mutasim I. Khalil, (2015), **Co-precipitation in aqueous solution synthesis of magnetite nanoparticles using iron(III) salts as precursors**, Arabian Journal of Chemistry, Volume 8, 279-284.
- 161-** Nagavarma B V N, Hemant K.S, Ayaz A, Vasudha L.S, Shivakumar H.G, (2012), **Different techniques for preparation of polymeric nanoparticles- A review**, Asian Journal of Pharmaceutical and Clinical Research, Volume 5, Issue 3, 16-23.
- 162-** Neelam Seedher, Purshotam Sharma, (2007), **Solubility and stability enhancement of poorly-soluble drugs clarithromycin and prednisolone by combination with other drugs**, International Journal of Biological Chemistry, Volume 1, 229-236.
- 163-** Nekolla K, Kick K, Sellner S, Mildner K, Zahler S, Zeuschner D, Krombach F, Rehberg M, (2016), **Influence of surface modifications on the spatiotemporal microdistribution of quantum dots *in vivo***, Small, Volume 12, Issue 19, 2641-2651.
- 164-** Nicholas A. Peppas, Christie D. Bures, (2006), **Glucose-responsive hydrogels**, Encyclopaedia of Biomaterials and Biomedical Engineering.
- 165-** Nishiyama N, Kataoka K, (2006), **Current state, achievements, and future prospects of polymeric micelles as nanocarriers for drug and gene delivery**, Pharmacology Therapeutics, Volume 112, Issue 3, 630-48.
- 166-** Nori A, Kopecek J. (2005), **Intracellular targeting of polymer-bound drugs for cancer chemotherapy**, Advanced Drug Delivery Reviews, Volume 57, 609-636.
- 167-** Novich B. E, Ring T. A, (1984), **Colloid stability of clays using photon correlation spectroscopy**, Clays and Clay Minerals, Volume 32, Issue 5, 400-406.
- 168-** Oliveira Cleudaldo Soares de, Bruno Freitas Lira, José Maria Barbosa-Filho, Jorge Gonçalo Fernandez Lorenzo, Petrônio Filgueiras de Athayde-Filho, (2012), **Synthetic approaches and pharmacological activity of 1,3,4-oxadiazoles: a review of the literature from 2000-2012**, Molecules, Volume 17, 10192-10231.

- 169-** Ouadahi Karima, Kamal Sbargoud, Emmanuel Allard and Chantal Larpent, (2012), **FRET-mediated pH-responsive dual fluorescent nanoparticles prepared via click chemistry**, *Nanoscale*, Volume 4, 727-732.
- 170-** Park Wooram, Park Sin-jung, Shin Heejun, Na Kun, (2016), **Acidic tumour pH-responsive nanophotomedicine for targeted photodynamic cancer therapy**, *Journal of Nanomaterials*, Volume 2016, 1-8.
- 171-** Parvin Zakeri-Milani, Somayeh Hallaj Nezhadi, Mohammad Barzegar-Jalali, Leila Mohammadi, Ali Nokhodchi, Hadi Valizadeh, (2011), **Studies on dissolution enhancement of prednisolone, a poorly water-soluble drug by solid dispersion technique**, *Advanced Pharmaceutical Bulletin*, Volume 1, Issue 1, 48-53.
- 172-** Pasparakisa George, Vamvakaki Maria, (2011), **Multiresponsive polymers: nano-sized assemblies, stimuli-sensitive gels and smart surfaces**, *Polymer Chemistry*, Volume 2, 1234-1248.
- 173-** Pecora R, editor, (1985), **Dynamic light scattering: applications of photon correlation spectroscopy**, Plenum Press, New York.
- 174-** Popovtzer R, Agrawal A, Kotov NA, Popovtzer A, Balter J, Carey TE, Kopelman R, (2008), **Targeted gold nanoparticles enable molecular CT imaging of cancer**, *Nano Letters*, Volume 8, 4593-4596.
- 175-** Priya Bawa, Viness Pillay, Yahya E Choonara, Lisa C du Toit, (2009), **Stimuli-responsive polymers and their applications in drug delivery**, *Biomedical Materials*, Volume 4, 1-15.
- 176-** Purushotham S, Chang J, Rumpel H, Kee C, R T H Ng, Chow H, Tan K, Ramanujan V, (2009), **Thermoresponsive core-shell magnetic nanoparticles for combined modalities of cancer therapy**, *Nanotechnology*, Volume 20, Number 30.
- 177-** Qi Yang, Yimin Mao, Guangxian Li, Yajiang Huang, Ping Tang, Caihong Lei, (2004), **Study on the UCST behavior of polystyrene/poly(styrene-co-acrylonitrile) blend**, *Materials Letters*, Volume 58, Issue 30, 3939-3944.
- 178-** Qi Zhang, Lei Lei, Shiping Zhu, (2017), **Gas-responsive polymers**, *ACS Macro Letters*, Volume 6, Issue 5, 515-522.
- 179-** Qian Feng, Cui Fuying, Ding Jieying, Tang Cui, Yin Chunhua, (2006), **Chitosan graft copolymer nanoparticles for oral protein drug delivery:**

- preparation and characterization**, *Biomacromolecules*, Volume 7, Issue 10, 2722-2727.
- 180-** Qin Zhu, Wei Liu, Liang Guo, Xinsong Li, (2012), **Studies on guanidinated n-3-aminopropyl methacrylamide-n-2-hydroxypropyl methacrylamide copolymers as gene delivery carrier**, *Journal of Biomaterials Science*, Volume 23, 133-152.
- 181-** Radrigues M.R, (2005), **Synthesis and investigation of chitosan derivatives formed by reaction with acyl chlorides**, *Journal of Carbohydrate Chemistry*, Volume 24, 41-54.
- 182-** Rafat A Siddiqui, Mustapha Zerouga, Min Wu, Alicia Castillo, Kevin Harvey, Gary P Zaloga, William Stillwe, (2015), **Anticancer properties of propofol-docosahexaenoate and propofol-eicosapentaenoate on breast cancer cells**, *Breast Cancer Research*, Volume 7, R645-R654.
- 183-** Rahib Lola, Smith D. Benjamin, Aizenberg Rhonda, Rosenzweig B. Allison, Fleshman M. Julie, Matrisian M. Lynn, (2014), **Projecting cancer incidence and deaths to 2030: the unexpected burden of thyroid, liver, and pancreas cancers in the United States**, *Cancer Research*, Volume 74, Issue 11, 2913-2921.
- 184-** Rieger J, Dubois P, Jérôme R, Jérôme C, (2006), **Controlled synthesis and interface properties of new amphiphilic PCL-g-PEO copolymers**, *Langmuir*, Volume 22, Issue 18, 7471-7479.
- 185-** Roach Paul, David J. McGarvey, Martin R. Lees, Clare Hoskins, (2013), **Remotely triggered scaffolds for controlled release of pharmaceuticals**, *International Journal of Molecular Science*, Volume 14, 8585-8602.
- 186-** Robert Carlisle, James Choi, Miriam Bazan-Peregrino, Richard Laga, Vladimir Subr, Libor Kostka, Karel Ulbrich, Constantin-C. Coussios, Leonard W. Seymour, (2013), **Enhanced tumor uptake and penetration of virotherapy using polymer stealthing and focused ultrasound**, *Journal of the National Cancer Institute*, Volume 105, Issue 22, 1701-1710.
- 187-** Roberto F, Giuseppe A, Laura C, Eleonora M, Francesca Y. Russo, Giulia C, Alessia M, Eldorado C, (2013), **Long-term results of intratympanic prednisolone injection in patients with idiopathic sudden sensorineural hearing loss**, *Acta Oto-Laryngologica*, Volume 133, 900-904.

- 188-** Rodri'guez-Herna'ndez J, Che'cot, Gnanou Y, Lecommandoux S, (2005), **Toward 'smart' nano-objects by self-assembly of block copolymers in solution**, Progress in Polymer Science, Volume 30, Issue 7, 691-724.
- 189-** Ron ES, Bromberg LE, (1998), **Temperature-responsive gels and thermogelling polymer matrices for protein and peptide delivery**, Advanced Drug Delivery Review, Volume 31, Issue 3,197-221.
- 190-** Rongran Wei, Liang Cheng, Meng Zheng, Ru Cheng, Fenghua Meng, Chao Deng, Zhiyuan Zhong, (2012), **Reduction-responsive disassemblable core-cross-linked micelles based on poly(ethylene glycol)-b-poly(N-2-hydroxypropyl methacrylamide)-lipoic acid conjugates for triggered intracellular anticancer drug release**, Biomacromolecules, Volume 13, Issue 8, 2429-2438.
- 191-** Roy Debashish, Brooksb L. A. William, Sumerlin S. Brent, (2013), **New directions in thermoresponsive polymers**, Chemical Society Review, Volume 42, 7214-7243.
- 192-** Royal Pharmaceutical Society of Great Britain (2000), **Martindale, the extra pharmacopoeia**, 13th Ed., London, The Pharmaceutical Press.
- 193-** Rubinson, K.A, Rubinson, J.F, (2000), **Contemporary instrumental analysis**, 1st Ed, Upper Saddle River, NJ, Prentice Hall.
- 194-** Ryskulova Kanykei, Anupama Rao Gudur Srinivas, Thomas Kerr-Phillips, Hui Peng, David Barker, Jadranka Travas-Sejdic, Richard Hoogenboom, (2016), **Multiresponsive behavior of functional poly(p-phenylene vinylene)s in water**, Polymers, Volume 8, Issue 10.
- 195-** Sabina Tatur, Marco Maccarini, Robert Barker, Andrew Nelson, Giovanna Fragneto, (2013), **Effect of functionalized gold nanoparticles on floating lipid bilayers**, Langmuir, Volume 29, Issue 22, 6606-6614.
- 196-** Sadeghi Mohammad, Heidari Behrouz, (2011), **Crosslinked graft copolymer of methacrylic acid and gelatin as a novel hydrogel with pH-responsiveness properties**, Materials, Volume 4, 543-552.
- 197-** Saha Krishnendu, Sarit S. Agasti, Chaekyu Kim, Xiaoning Li, Vincent M. Rotello, (2012), **Gold nanoparticles in chemical and biological sensing**, Chemical Reviews, Volume 112, Issue 5, 2739-2779.

- 198-** Sailor MJ1, Park JH, (2012), **Hybrid nanoparticles for detection and treatment of cancer**, *Advanced Materials*, Volume 24, Issue 28, 3779-3802.
- 199-** Saimon Moraes Silva, Roya Tavallaie, Lydia Sandiford, Richard D. Tilley, J. Justin Gooding, (2016), **Gold coated magnetic nanoparticles: from preparation to surface modification for analytical and biomedical applications**, *Chemical Communications*, 2016, Volume 52, 7528-7540.
- 200-** Sandy Gim Ming Ong, Long Chiau Ming, Kah Seng Lee, Kah Hay Yuen, (2016), **Influence of the encapsulation efficiency and size of liposome on the oral bioavailability of griseofulvin-loaded liposomes**, *Pharmaceutics*, Volume 8, Issue 25, 1-17.
- 201-** Santos M. S, Tavares F. W, Biscaia Jr E. C, (2016), **Molecular thermodynamics of micellization: micelle size distributions and geometry transitions**, *Brazilian Journal of Chemical Engineering*, Volume 33, Issue 3, 515-523.
- 202-** Sebastian G. Roos, Axel H. E. Muller, (1999), **Copolymerization of n-butyl acrylate with methyl methacrylate and PMMA macromonomers: comparison of reactivity ratios in conventional and atom transfer radical copolymerization**, *Macromolecules*, Volume 32, 8331-8335.
- 203-** Sevimli S, Inci F, Zareie HM, Bulmus V, (2012), **Well-defined cholesterol polymers with pH-controlled membrane switching activity**, *Biomacromolecules*, Volume 13, Issue 10, 3064-3075.
- 204-** Shaikh N Tasnim, Agrawal S. A, (2014), **Qualitative and quantitative characterization of textile material by Fourier transform infra-red**, *International Journal of Innovative Research in Science, Engineering and Technology*, Volume 3, Issue 1, 8496-8502.
- 205-** Shalgunov V, Zaytseva-Zotova D, Zintchenko A, Levada T, Shilov Y, Andreyev D, Dzhumashev D, Metelkin E, Urusova A, Demin O, McDonnell K, Troiano G, Zale S, Safarova E, (2017), **Comprehensive study of the drug delivery properties of poly(l-lactide)-poly(ethylene glycol) nanoparticles in rats and tumor-bearing mice**, *Journal of Control Release*, Volume 261, 31-42.
- 206-** Sharp KW, Ross CB, Tillman VN, Dunn JF, (1989), **Common bile duct healing. Do different absorbable sutures affect stricture formation and tensile strength?**, *Arch Surgery*, Volume 124, Issue 4, 408-814.

- 207-** Shen J, Burgess DJ, (2012), **Accelerated in vitro release testing of implantable PLGA microsphere/PVA hydrogel composite coatings**, International Journal of Pharmaceutics, Volume 422, Issue 1-2, 341-348.
- 208-** Shirakura Teppei, Taylor J. Kelson, Aniruddha Ray, Antonina E. Malyarenko, Raoul Kopelman, (2014), **Hydrogel nanoparticles with thermally controlled drug release**, ACS Macro Letters, Volume 3, Issue 7, 602–606.
- 209-** Shoolery N. James, (2008), **A basic guide to NMR**, 3rd Edition, Stan's Library, Volume II.
- 210-** Singh P, Rathinasamy K, Mohan R, Panda D, (2008), **Microtubule assembly dynamics: an attractive target for anticancer drug**, IUBMB Life, Volume 60, Issue 6, 368-375.
- 211-** Škvarla Juraj, Rahul K. Raya, Mariusz Uchman, Jiří Zedník, Karel Procházka, Vasil M. Garamus, Anastasia Meristoudi, Stergios Pispas, Miroslav Štěpánek, (2017), **Thermoresponsive behavior of poly(N-isopropylacrylamide)s with dodecyl and carboxyl terminal groups in aqueous solution: pH-dependent cloud point temperature**, Colloid and Polymer Science, Volume 295, Issue 8, 1343-1349.
- 212-** SM. Wairkar, RS. Gaud, (2013), **Solid dispersions: solubility enhancement technique for poorly soluble drugs**, International Journal of Research in Pharmaceutical and Biomedical Sciences, Volume 4, Issue 3, 847- 854.
- 213-** Snyder, L.R., J.J. Kirkland, J.W. Dolan, (2011), **Introduction to modern liquid chromatography**, 3 Ed, John Wiley & Sons.
- 214-** So Young Kim, Hyun Jeong Kim, Kyung Eun Lee, Sung Sik Han, Youn Soo Sohn, Byeongmoon Jeong, (2007), **Reverse thermal gelling PEG–PTMC diblock copolymer aqueous solution**, Macromolecules, Volume 40, Issue 15, 5519-5525.
- 215-** Sonali K. Doke, Shashikant C. Dhawale, (2015), **Alternatives to animal testing: A review**, Saudi Pharmaceutical Journal, Volume 23, 223-229.
- 216-** Sonavane G, Tomoda K, Sano A, Ohshima H, Terada H, Makino K, (2008), **In vitro permeation of gold nanoparticles through rat skin and rat intestine: effect of particle size**, Colloids Surfaces B Biointerfaces, Volume 65, Issue 1, 1-10.

- 217-** Song Lichun, Sun Hui, Chen Xiaolu, Han Xia, Liu Honglai, (2015), **From multi-responsive tri- and diblock copolymers to diblock-copolymer-decorated gold nanoparticles: the effect of architecture on micellization behaviors in aqueous solutions**, *Soft Matter*, Volume 11, 4830-4839.
- 218-** Song-Bai Lin, Cong-Hui Yuan, Ai-Ru Ke, Zhi-Long Quan, (2008), **Electrical response characterization of PVA–P(AA/AMPS) IPN hydrogels in aqueous Na₂SO₄ solution**, *Sensors and Actuators B: Chemical*, Volume 134, Issue 1, 281-286.
- 219-** Stephanie Louguet, Berengere Rousseau, Romain Epherre, Nicolas Guidolin, Graziella Goglio, b Stephane Mornet, Etienne Duguet, Sebastien Lecommandoux, Christophe Schatz, (2012), **Thermoresponsive polymer brush-functionalized magnetic manganite nanoparticles for remotely triggered drug release**, *Polymer Chemistry*, Volume 3, 1408-1417.
- 220-** Stuart B, (2004), **Infrared Spectroscopy: Fundamentals and Applications**, John Wiley & Sons, Ltd, page 79-81.
- 221-** Sugimoto T, Matijevic, (1980), **Formation of uniform spherical magnetite particles by crystallization from ferrous hydroxide gels**, *Journal Colloid and Interface Science*, Volume 74, 227-243.
- 222-** Sun Feilong, Yuxia Wang, Yi Wei, Gang Cheng, Guanghui Ma, (2014), **Thermo-triggered drug delivery from polymeric micelles of poly(N-isopropylacrylamide-co-acrylamide)-b-poly(n-butyl methacrylate) for tumor targeting**, *Journal of Bioactive and Compatible Polymers*, Volume 29, Issue 4, 301-317.
- 223-** Sutton D, Nasongkla N, Blanco E, Gao J, (2007), **Functionalized micellar systems for cancer targeted drug delivery**, *Pharmaceutical Research*, Volume 24, 1029-1046.
- 224-** Svenson Sonke, Prud'homme K. Robert, (2012), **Multifunctional nanoparticles for drug delivery applications: imaging, targeting, and delivery**, Springer Science & Business Media.
- 225-** Talelli M, Rijcken C, Nostrum C, Storm G, Hennink W, (2010), **Micelles based on HEMA copolymers**, *Advanced Drug Delivery Reviews*, Volume 62, 231-239.

- 226-** Talelli M., C.J.F. Rijcken, C.F. van Nostrum, G. Storm, W.E. Hennink, (2010), **Micelles based on HPMA copolymers**, *Advanced Drug Delivery Reviews*, Volume 62, Issue 2, 231-239.
- 227-** Tang B, Cheng G, Gu JC, Xu CH, (2008), **Development of solid self-emulsifying drug delivery systems: preparation techniques and dosage forms**, *Drug Discovery Today*, Volume 13, 606-612.
- 228-** Tang Manling, Zhou Minglu, Huang Yuan, Zhong Jiaju, Zhou Zhou, Luo Kui, (2017), **Dual-sensitive and biodegradable core-crosslinked HPMA copolymer–doxorubicin conjugate-based nanoparticles for cancer therapy**, *Polymer Chemistry*, Volume 8, 2370-2380.
- 229-** Teja A. S, Koh P. Y, (2009), **Synthesis, properties, and applications of magnetic iron oxide nanoparticles**, *Progress in Crystal Growth and Characterization of Materials*, Volume 55, Issue 1, 22-45.
- 230-** Terry L Riss, Richard A Moravec, Andrew L Niles, Sarah Duellman, Hélène A Benink, Tracy J Worzella, Lisa Minor, (2013), **Assay Guidance Manual**, Chapter 12, Eli Lilly & Company and the National Center for Advancing Translational Sciences.
- 231-** Thakur Vijay Kumar, Thakur Manju Kumari, (2016), **Handbook of sustainable polymers: structure and chemistry**, Chapter 20, Page 784, Taylor & Francis Group, LLC.
- 232-** Tharmavaram Maithri , Rawtani Deepak , Pandey Gaurav , (2017), **Review fabrication routes for one-dimensional nanostructures via block copolymers**, *Nano Convergence*, Volume 4, Issue 12.
- 233-** Thomas S, Zaikov G, Valsaraj S, Meera A, (2010), **Recent advances in polymer nanocomposites: synthesis and characterisation**, Taylor & Francis Group LLC, P 11.
- 234-** Thompson C. J, Tetley L, Uchegbu I. F, Cheng W. p, (2009), **The complexation between novel comb shaped amphiphilic polyallylamine and insulin-towards oral insulin delivery**, *International Journal of Pharmaceutics*, Volume 376, Issue 1-2, 46-55.
- 235-** Tobias Miller, Gwenaëlle van Colen, Bjoern Sander, Mariola Monika Golas, Senta Uezguen, Markus Weigandt, Achim Goepferich, (2013), **Drug loading of polymeric micelles**, *Pharmaceutical Research*, Volume 30, Issue 2, 584-595.

- 236-** Tomohiro Konno, Junji Watanabe, Kazuhiko Ishihar, (2003), **Enhanced solubility of paclitaxel using water-soluble and biocompatible 2-methacryloyloxyethyl phosphorylcholine polymers**, Journal of Biomedical Materials Research, Volume 65A, Issue 2, 209-214.
- 237-** Torchilin V. P, (2006), **Nanoparticulates as drug carriers**, Imperial College press, 59.
- 238-** Townley, E.R. (1979), **Griseofulvin**, analytical profiles of drug substance, Volume 8, 219-249.
- 239-** Trivedi R, Kompella U, (2010), **Nanomicellar formulations for sustained drug delivery: strategies and underlying principles**, Nanomedicine (Lond), Volume 5, Issue 3, 485-505.
- 240-** Ulbrich Karel, Hola Katerina, Šubr Vladimír, Bakandritsos Aristides, Tucek Jiri, Zboril Radek, (2016), **Targeted drug delivery with polymers and magnetic nanoparticles: covalent and noncovalent approaches, release control, and clinical studies**, Chemical Reviews, Volume 116, 5338-5431.
- 241-** Uyama H, Kobayashi S, (1992), **A novel thermo-responsive polymer. Poly(2-isopropyl-2-oxazoline)**, Chemistry Letters, Volume 21, 1643-646.
- 242-** Van Durme K, Van Assche G, Nies E and Van Mele B, (2007), **Phase transformations in aqueous low molar mass poly(vinyl methyl ether) solutions: theoretical prediction and experimental validation of the peculiar solvent melting line, bimodal LCST, and (adjacent) UCST miscibility gaps**, Journal of physical chemistry B, Volume 111, Issue 6, 1288-1295.
- 243-** Verma Jyoti, Sumit Lal, Cornelis JF Van Noorden, (2014), **Nanoparticles for hyperthermic therapy: synthesis strategies and applications in glioblastoma**, International Journal of Nanomedicine, Volume 9, 2863-2877.
- 244-** Vo CD, Rosselgong J, Armes SP, Tirelli N. (2010), **Stimulus-responsive polymers based on 2-hydroxypropyl acrylate prepared by RAFT polymerisation**, Journal of Polymer Science A, Polymer Chemistry, 48, 2032-2043.
- 245-** Vogt M, Derendorf H, Krämer J, Junginger H.E, Midha K.K, Shah V.P, Stavchansky S, Dressman J.B, Barends D.M, (2007), **Biowaiver monographs for immediate release solid oral dosage forms: Prednisolone**, Journal of Pharmaceutical Sciences Volume 96, Issue 1, 27-37.

- 246-** Wang Huijuan, Xue Chenyang, Chen Rong, Zhang Wendong., (2010), **Fabrication and growth mechanism of star-shaped gold nanoparticles via seed-mediated growth method**, *Advanced Materials Research*, Volume 152-153, 600-604.
- 247-** Wang Z.T, Gong H.Y, Zheng F, Liu D.J, Dong T.L, (2015), **Propofol suppresses proliferation and invasion of pancreatic cancer cells by upregulating microRNA-133a expression**, *Genetics and Molecular Research*, Volume 14, Issue 3, 7529-7537.
- 248-** Wang. Z, Mohamed MB, Link S, EL-Sayed MA, (1999), **Crystallographic facets and shapes of gold nanorods of different aspect ratios**, *Surface science*, Volume 440, Issue 1, 809-814.
- 249-** Wanga Y, Lia J, Chena Y, Oupický D, (2015), **Balancing polymer hydrophobicity for ligand presentation and siRNA delivery in dual function CXCR4 inhibiting polyplexes**, *Biomaterials Sciences*, Volume 3, Issue 7, 1114-1123.
- 250-** Wanga Yong, Chyan-Ying Kea, Cyrus Weijie Beha, Shao-Qiong Liua, Suat-Hong Goh, Yi-Yan Yang, (2007), **The self-assembly of biodegradable cationic polymer micelles as vectors for gene transfection**, *Biomaterials*, Volume 28, 5358-5368.
- 251-** Warra A. A, Jimoh W. O, (2011), **Overview of an inductively coupled plasma (ICP) system**, *International Journal of Chemistry Research*, Volume 3, Issue 2, 41-48.
- 252-** Wei Wu, Quanguo He, Changzhong Jiang, (2008), **Magnetic Iron Oxide Nanoparticles: Synthesis and Surface Functionalization Strategies**, *Nanoscale Research Letters*, Volume 3, Issue 11, 397-415.
- 253-** Wen Wee Ma, Manuel Hidalgo, (2013), **The Winning formulation: The the development of paclitaxel in pancreatic cancer**, *Clinical Cancer Research*, Volume 19, Issue 20, 5572-5579.
- 254-** Wijaya C. Emmy, Separovic Frances, Drummond J. Calum, Greaves L. Tamar, (2016), **Micelle formation of a non-ionic surfactant in non-aqueous molecular solvents and protic ionic liquids (PILs)**, *Physical Chemistry Chemical Physics*, Volume 18, 24377-24386.

- 255-** Williams Dudley, Fleming Ian, (2008), **Spectroscopic methods in organic chemistry**, 6th edition, McGraw-Hill Education (UK) limited.
- 256-** Wilson RH, Plummer R, Adam J, Eatock M, Boddy AV, Griffin M, Miller R, Matsumura Y, Shimizu T, Calvert H, (2008), **Phase I and pharmacokinetic study of NC-6004, a new platinum entity of cisplatin-conjugated polymer forming micelles**, Journal of Clinical Oncology, Volume 26, 2573.
- 257-** Win L. Chiou, Shaw-Jen Chen, Narayan Athanikar, (1976), **Enhancement of dissolution rates of poorly water-soluble drugs by crystallization in aqueous surfactant solutions I: Sulfathiazole, prednisone, and chloramphenicol**, Journal of Pharmaceutical Sciences, Volume 65, Issue 11, 1702-1704.
- 258-** Xiaohua Huang, Mostafa A. El-Sayed, (2010), **Gold nanoparticles: Optical properties and implementations in cancer diagnosis and photothermal therapy**, Journal of Advanced Research, Volume 1, 13-28.
- 259-** Xioazhong Qu, Vitaliy V. Khutoryanskiy, Ailsa Stewart, Samina Rahman, Brigitte Papahadjopoulos-Sternberg, Christine Dufes, Dave McCarthy, Clive G. Wilson, Robert Lyons, Katharine C. Carter, Andreas Schaetzlein, Ijeoma F. Uchegbu, (2006), **Carbohydrate-based micelle clusters which enhance hydrophobic drug bioavailability by up to 1 order of magnitude**, Biomacromolecules, Volume 7, 3452-3459.
- 260-** Yan Jiatao, Zhang Xiaoqian, Li Wen, Zhang Xiuqiang, Liu Kun, Wu Peiyi, Zhang Afang, (2012), **Thermoresponsive supramolecular dendronized copolymers with tunable phase transition temperatures**, Soft Matter, Volume 8, 6371-6377.
- 261-** Yang Xi, Zhaojun Li, Ning Wang, Ling Li, Linjiang Song, Tao He, Lu Sun, Zhihan Wang, Qinjie Wu, Na Luo, Cheng Yi, Changyang Gong, (2015), **Curcumin-encapsulated polymeric micelles suppress the development of colon cancer *in vitro* and *in Vivo***, Scientific Reports 5, Article number: 10322.
- 262-** Yao Cuiping, Wu Ming, Zhang Cecheng, Lin Xinyi, Wei Zuwu, Zheng Youshi, Zhang Da, Zhang Zhenxi, Liu Xiaolong, (2017), **Photoresponsive lipid-polymer hybrid nanoparticles for controlled doxorubicin release**, Nanotechnology, Volume 28, Issue 25.
- 263-** Yogesh M. Choudhari, Sachin V. Detane, Sushant S. Kulthe, Chandrakant C. Godhani, Nazma N. Inamdar, Seema M. Shirolkar, Lalit C. Borde, Vishnukant K.

- Mourya, (2012), **Low molecular weight palmitoyl chitosan: Synthesis, characterization and nanoparticle preparation**, *Advanced Material Letters*, Volume 3, Issue 6, 487-492.
- 264-** Yokoyama M, (2011), **Clinical applications of polymeric micelle carrier systems in chemotherapy and image diagnosis of solid tumours**, *Journal of Experimental and Clinical Medicine*, Volume 3, Issue 4, 151-158.
- 265-** Yokoyama M, Okano T, Sakurai Y, Suwa S, Kataoka K, (1996), **Introduction of cisplatin into polymeric micelle**, *Journal of Control Release*, Volume 39, 351-356.
- 266-** Yua Hojeong, Huy M. Lea, Eliangiringa Kaale, Kenneth. D. Long, Thomas Layloff, Steven S. Lumettaa, Brian T. Cunningham, (2016), **Characterization of drug authenticity using thin-layer chromatography imaging with a mobile phone**, *Journal of Pharmaceutical and Biomedical Analysis*, Volume 125, 85-93.
- 267-** Yuan Weizhong, Tianxiang Shen, Jinju Wang, Hui Zou, (2014), **Formation–dissociation of glucose, pH and redox triply responsive micelles and controlled release of insulin**, *Polymer Chemistry*, Volume 5, 3968-3971.
- 268-** Yue Zheng, Ian W. Wyman, (2016), **Supramolecular nanostructures based on cyclodextrin and poly (ethylene oxide): syntheses, structural characterizations and applications for drug delivery**, *Polymers*, Volume 8, Issue 5, 1-18.
- 269-** Yunjie Cao, Yaojun Zhou, Qianfeng Zhuang, Li Cui, Xianlin Xu, Renfang Xu, and Xiaozhou He, (2015), **Anti-tumor effect of RGD modified PTX loaded liposome on prostatic cancer**, *International Journal of Clinical and Experimental Medicine*, Volume 8, Issue 8, 12182–12191.
- 270-** Yuting Li, Brad S. Lokitz, Charles L. McCormick, (2006), **Thermally responsive vesicles and their structural locking through polyelectrolyte complex formation**, *Angew Chemical International Edition*, Volume 45, 5792-5795.
- 271-** Zhang X, Zheng Y, Wang Z, Huang S, Chen Y, Jiang W, Zhang H, Ding M, Li Q, Xiao X, (2014), **Methotrexate-loaded PLGA nanobubbles for ultrasound imaging and synergistic targeted therapy of residual tumour during HIFU ablation**, *Biomaterials*, 35, 5148–5161.

- 272-** Zhang J, Post M, Veres T, Jakubek Z, Guan J, Wang D, Normandin F, Deslandes Y, Simard B, (2006), **Laser-assisted synthesis of superparamagnetic Fe@Au core-shell nanoparticles**, The Journal of Physics Chemistry B, Volume 110, Issue 14, 7122-7128.
- 273-** Zhang Liangshun, Lin Jiaping, Lin Shaoliang, (2007), **Aggregate morphologies of amphiphilic graft copolymers in dilute solution studied by self-consistent field theory**, Journal Physical Chemistry B, Volume 111, 9209-9217.
- 274-** Zhang Xiao-ying, Zhang Pei-ying, (2017), **Polymersomes in nanomedicine-a review**, Current Medical Chemistry, Volume 13, Issue 2, 124-129.
- 275-** Zheng Ronghua, Liu Guojun, Devlin Mark, Hux Karen, Jao Tze-chi, (2009), **Friction reduction of lubricant base oil by micelles and crosslinked micelles of block copolymers**, Tribology Transactions, Volume 53, Issue 1.
- 276-** Zheng Sijia, Xie Yanqi, Li Yuan, Li Ling, Tian Ning, Zhu Wenbo, Yan Guangmei, Wu Chuanbin, Hu Haiyan, (2014), **Development of high drug-loading nanomicelles targeting steroids to the brain**, International Journal of Nanomedicine, Volume 9, 55-66.
- 277-** Zhijun Liu, Fang Zhang, Gar Yee Koh, Xin Dong, Javoris Hollingsworth, Jian Zhang, Paul S. Russo, Peiyong Yang, Rhett W. Stout, (2015), **Cytotoxic and anti-angiogenic paclitaxel solubilized and permeation-enhanced by natural product nanoparticles**, Anticancer Drugs, Volume 26, Issue 2, 167-179.
- 278-** Zhou Weiqiang, Lu Wang, Feng Li, Weina Zhang, Wei Huang, Fengwei Huo, Huaping Xu, (2017), **Selenium-containing polymer@metal-organic frameworks nanocomposites as an efficient multi-responsive drug delivery system**, Advanced Functional Materials, Volume 27, 1605465.
- 279-** Zhou Yuxiang, Victoria A. Briand, Nitin Sharma, Suk-kyun Ahn, Rajeswari M. Kasi, (2009), **Polymers comprising cholesterol: synthesis, self-assembly, and applications**, Materials, Volume 2, Issue 2, 636-660.
- 280-** Zolnik BS, Leary PE, Burgess DJ, (2006), **Elevated temperature accelerated release testing of PLGA microspheres**, Journal of Controlled Release, Volume 112, Issue 3, 293-300.

Appendix

1.0- Determination of Propofol Solubility in (D-2)-b-(PEG) and (O-1)-b-(PEG)

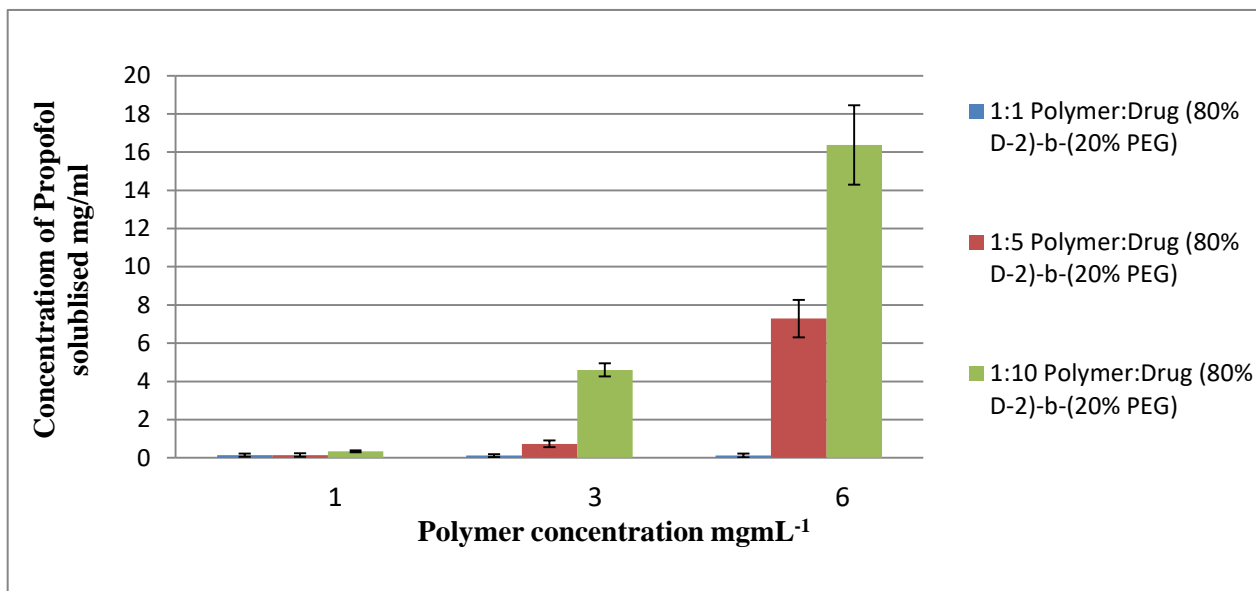


Figure 1- Drug loading of propofol onto (80% D-2)-b-(20% PEG) at different initial drug:polymer loading ratios (n=3, ave ± SD).

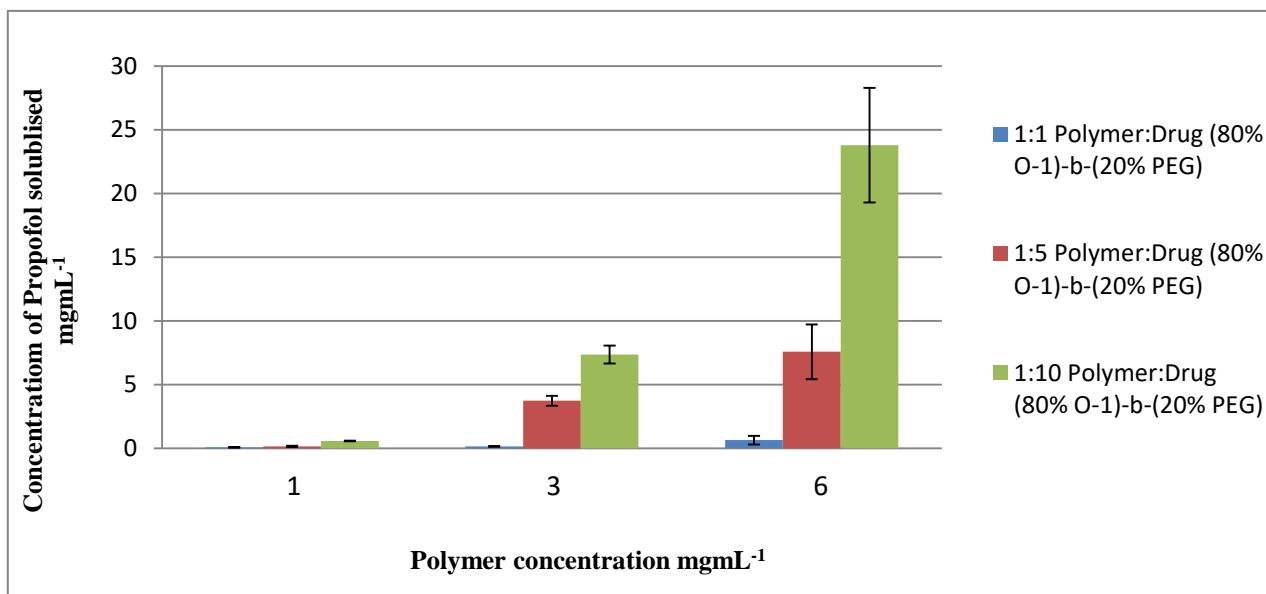


Figure 2- Drug loading of propofol onto (80% O-1)-b-(20% PEG) at different initial drug:polymer loading ratios (n=3, ave ± SD).

2.0- In vitro release of propofol from (D-2)-b-(PEG) and (O-1)-b-(PEG)

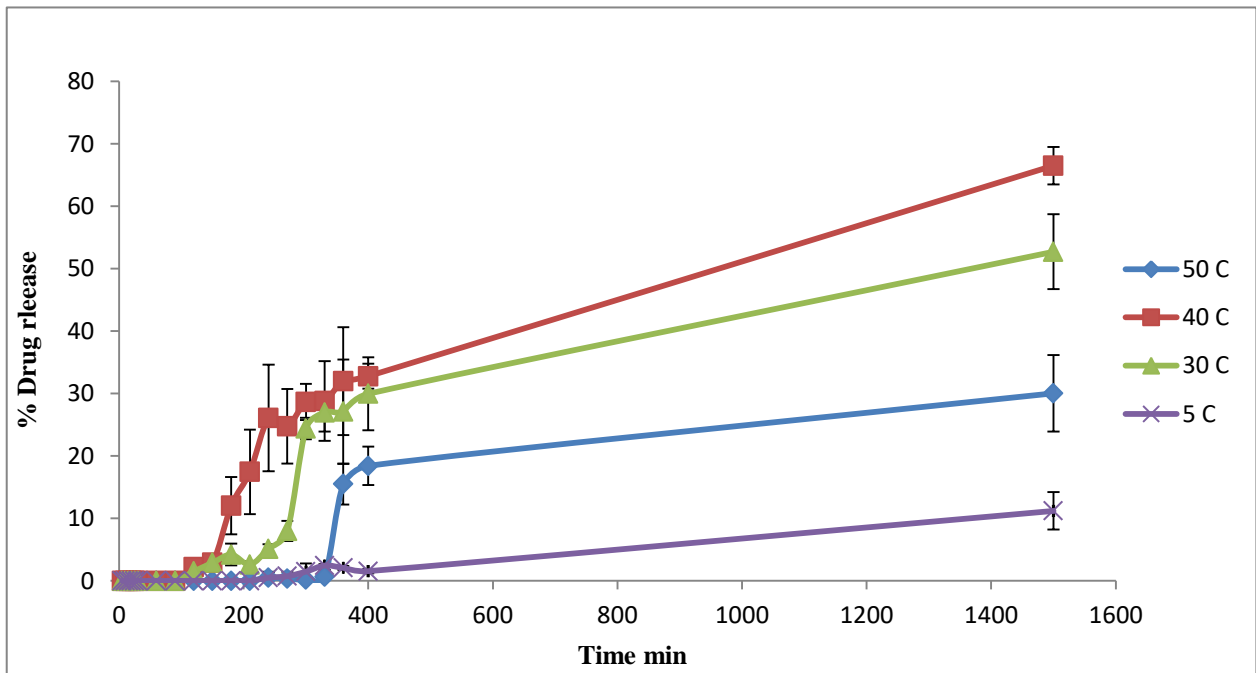


Figure 3- *In vitro* release of propofol from (80% D-2)-b-(20% PEG) formulation at different temperatures.

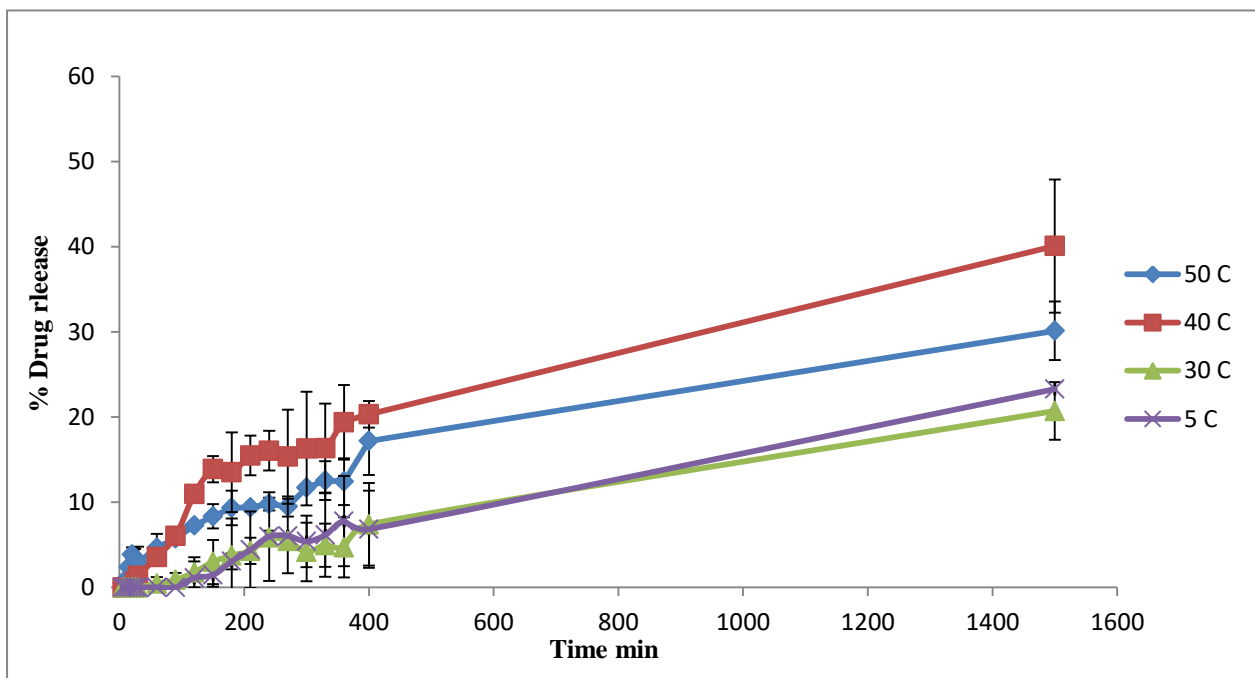


Figure 4- *In vitro* release of propofol from (80% O-1)-b-(20% PEG) formulation at different temperatures.